The Impact of Increased Penetration of Photovoltaic Generation on Smart Grids

By

Sara Eftekharnejad

A Dissertation Presented in Partial Fulfillment
of the Requirements for the Degree
Doctor of Philosophy

Approved November 2012 by the
Graduate Supervisory Committee:

Gerald Heydt, Co-Chair
Vijay Vittal, Co-Chair
Jennie Si
Daniel Tylavsky

ARIZONA STATE UNIVERSITY

December 2012

ABSTRACT

With the rapid growth of power systems and the concomitant technological advancements, the goal of achieving smart grids is no longer a vision but a foreseeable reality. Hence, the existing grids are undergoing infrastructural modifications to achieve the diverse characteristics of a smart grid. While there are many subjects associated with the operation of smart grids, this dissertation addresses two important aspects of smart grids: increased penetration of renewable resources, and increased reliance on sensor systems to improve reliability and performance of critical power system components. Present renewable portfolio standards are changing both structural and performance characteristics of power systems by replacing conventional generation with alternate energy resources such as photovoltaic (PV) systems. The present study investigates the impact of increased penetration of PV systems on steady state performance as well as transient stability of a large power system which is a portion of the Western U.S. interconnection. Utility scale and residential rooftop PVs are added to replace a portion of conventional generation resources. While steady state voltages are observed under various PV penetration levels, the impact of reduced inertia on transient stability performance is also examined. The simulation results obtained effectively identify both detrimental and beneficial impacts of increased PV penetration both for steady state stability and transient stability performance.

With increased penetration of the renewable energy resources, and with the current loading scenario, more transmission system components such as

transformers and circuit breakers are subject to increased stress and overloading. This research work explores the feasibility of increasing system reliability by applying condition monitoring systems to selected circuit breakers and transformers. A very important feature of smart grid technology is that this philosophy decreases maintenance costs by deploying condition monitoring systems that inform the operator of impending failures; or the approach can ameliorate problematic conditions. A method to identify the most critical transformers and circuit breakers with the aid of contingency ranking methods is presented in this study.

The work reported in this dissertation parallels an industry sponsored study in which a considerable level of industry input and industry reported concerns are reflected.

DEDICATION

To my family.

ACKNOWLEDGMENTS

I would like to express my sincere gratitude to my advisors, Prof. Vijay Vittal and Prof. Gerald Heydt, for their guidance, encouragement, and constant support throughout the course of this dissertation and for giving me the opportunity to work with them.

Special thanks to my committee members Prof. Daniel Tylavsky and Prof. Jennie Si for their time and considering being on my supervisory committee.

I would also like to thank my parents for their unconditional love and infinite support that have always motivated me throughout my life.

I wish to acknowledge the support provided by a local utility. My association with this utility for the high PV penetration project has provided valuable industrial input to this dissertation.

TABLE OF CONTENTS

Page

LIST OF TABLES viii

LIST OF FIGURES xi

NOMENCLATURE xvii

CHAPTER

1 INTRODUCTION 1

1.1 Overview 1

1.2 Motivation 2

1.3 Research Scope and Objectives 6

1.4 Dissertation Organization 6

2 IMPLICATIONS OF SMART GRID TECHNOLOGY ON TRANSMISSION SYSTEM RELIABILITY 9

2.1 The Smart Grid and its Implicaitons 9

2.2 Application of Smart Grid Technology on a Study System 12

2.3 Security Assessment Performance Indices 14

2.4 Identification of the Critical Transformers 20

2.5 *(N-1)-1* Contingency Analysis Results 34

2.6 Identification of the Critical Branches 38

2.7 Alleviating the Impact of Contingencies 41

2.8 Summary 54

3 IMPACT OF PHOTOVOLTAIC GENERATION ON STEADY STATE PERFORMANCE OF THE POWER SYSTEMS 55

CHAPTER Page

3.1 Integration of Photovoltaic Resources 55

3.2 Cases and Test-Beds Under Study 57

3.3 Modifications to the Base Case 59

3.4 Representation of the PV System for Power Flow Studies 61

3.5 Cases and Test-Beds Under Study 63

3.5 Analytical Explanation for Steady State Voltages 74

3.7 Summary 78

4 DYNAMIC ANALYSIS 79

4.1 Introductory Remarks Related to the Dynamic Response 79

4.2 A Dynamic Model of PV Resources 80

4.3 Loss of a conventional generator 87

4.4 Effect of double circuit outages 100

4.5 Effect of bus faults 112

4.6 Cloud cover: impact on bus voltages 121

4.7 Loss of distributed PV 123

4.8 Summary 125

5 SMALL SIGNAL STABILITY ASSESSMENT OF THE SYSTEMS WITH HIGH PV PENETRATION 126

5.1 Motivation for the Study 126

5.2 Small Signal Stability Analysis 129

5.3 Impacts on Power System Small Signal Stability 130

5.4 Transient Analysis 136

CHAPTER Page

5.5 Summary Relating to PV Penetration and System Stability .. 144

6 OPTIMAL SYSTEM DISPATCH RATIO FOR SYSTEMS WITH HIGH PV PENETRATION LEVELS 146

6.1 PV Penetration and Optimal Dispatch vs Gen. Displacement 146

6.2 Study Cases 148

6.3 Optimal Generation Dispatch with Regard to Frequency 151

6.4 Effect of Transients on Optimal Generation Dispatch 163

6.5 Small Signal Analysis Approach 166

6.6 ODR with Regard to Steady State Performance 176

6.7 Summary 189

7 SUMMARY, CONCLUSIONS AND FUTURE WORK 159

7.1 Summary 191

7.2 Conclusions 194

7.3 Future Work 199

REFERENCES 200

APPENDIX

A TRANSFORMER BRANCHES ABOVE 115 KV 208

B IN SERVICE GENERATORS IN THE BASE CASE 210

C PHOTOVOLTAIC SYSTEM BUS LOCATIONS 213

D LIST OF DISPLACED GENERATORS 216

E CATEGORY OF GENERATORS USED FOR VARIOUS DR .. 219

F PROGRAM TO CREATE POWER FLOW SCENARIOS 222

LIST OF TABLES

Table Page

2-1 Load case summary for summer peak case and summer SIL case of the study area 27

2-2 Power-based and voltage-based indices of transformer branches for normal summer peak case 29

2-3 Power-based and voltage-based indices for transformer branches while considering the SIL Case 30

2-4 List of Critical transformers for summer peak case 33

2-5 Critical transformer branches for the peak case while 659-660 (69 kV / 230 kV) transformer branch is out of service 36

2-6 Critical transformer branches for the peak case while the 1869-1870 (69 kV / 230 kV) transformer branch is out of service 36

2-7 Circuit breaker parameters for monitoring 39

2-8 Cost function coefficients for different generation types 48

2-9 List of effective loads in reducing overloading in case of transformer branch 659-660 outage 52

3-1 Summary of the studied area 57

3-2 Power export to the other areas 59

3-3 Summary of the PV penetration levels 64

3-4 Classification of bus voltage changes for 10% PV penetration 66

3-5 Classification of bus voltage changes for 20% PV penetration 68

3-6 Classification of bus voltage changes for 30% PV penetration 70

Table Page

3-7 Classification of bus voltage changes for 4% PV penetration.....71

3-8 Classification of bus voltage changes for 50% PV penetration.....72

5-1 Critical modes present in the case with no PV 132

5-2 Comparison of the dominant mode 3 under different PV levels 132

5-3 Comparison of the dominant mode 2 under different PV levels 133

5-4 Comparison of the dominant mode 5 under different PV levels 133

5-5 Comparison of the dominant mode 8 under different PV levels 133

5-6 Comparison of the dominant mode 13 under different PV levels 134

5-7 Eigenvalue sensitivity corresponding to the inertia of the displaced generators in the 20% PV penetration case (for mode 2) 136

5-8 Eigenvalue sensitivity corresponding to the inertia of the displaced generators in the 40% PV penetration case (for mode 2) 136

5-9 Prony analysis results of the generator 2104 speed for various PV penetration levels 142

6-1 Frequency metrics after two large unit outages.....157

6-2 Frequency metrics following the outage of two large units 162

6-3 Critical modes for zero dispatch ratios 169

6-4 Comparison of critical modes for various dispatch ratios (mode 1).....170

6-5 Comparison of critical modes for various dispatch ratios (mode 2).....170

6-6 Comparison of critical modes for various dispatch ratios (mode 3).....171

A-1 Transformer branches above 115 kV.....209

B-1 Base case in service generators.....211

Table Page

B-2 Base case in service generators (continued) 212

C-1 Residential rooftop buses 214

C-2 Residential rooftop buses (continued) 215

C-3 Utility scale PV buses 215

D-1 List of displaced generators for 10% PV penetration 217

D-2 List of displaced generators for 20% PV penetration 217

D-3 List of displaced generators for 30% PV penetration 217

D-4 List of displaced generators for 40% PV penetration 218

D-5 List of displaced generators for 50% PV penetration 218

E-1 Dispatched generators in the base case 220

E-2 Base generators in the base case 220

E-3 Displaced generators in the base case 221

LIST OF FIGURES

Figure Page

1.1 A conceptual picture of the smart grid.....5

2.1 Main characteristics of a smart grid.....11

2.2 Calculation of system performance indices.....13

2.3 Application of the smart grid in improving transmission system reliability ...21

2.4 Contingency ranking methods based on steady state bus voltages and line flows.....25

2.5 Flow chart of the ranking procedure.....26

2.6 Summer peak PI_{MVA} index versus PI_V index for all the 71 contingencies in the system 29

2.7 Summer peak PI_{MVA} index calculated for all the 71 contingencies in the system 32

2.8 PI_{MVA} index calculated for summer SIL case for all the 71 contingencies in the system.....33

2.9 PI_{MVA} versus contingencies number for the peak case while 659-660 (69 kV / 230 kV) transformer branch is out of service 35

2.10 PI_{MVA} versus contingencies number for the peak case while the 1869-1870 (69 kV/230 kV) transformer branch is out of service.....37

2.11 PI_{MVA} index calculated for summer peak case for candidate circuit breakers in the system 41

2.12 Corrective actions taken in a smart grid to alleviate the contingencies.....42

Figure Page

2.13 Overloaded branch loading versus PI_{MVA} for system loads above 30MW while reduced to half.....51

3.1 Power flow representation of rooftop photovoltaic systems.....62

3.2 Power flow representation of utility scale photovoltaic systems.....62

3.3 Steady state bus voltage deviations with varying PV penetration levels.....72

3.4 Reactive power flow summary of the studied area under various PV levels...74

3.5 Simplified two bus representation of a system with PV.....75

3.6 Variations of the load voltage versus the amount of solar generation for a two bus system.....77

4.1 A dynamic representation of a utility scale PV in PSLF.....81

4.2 PSLF Models used for representing utility scale PVs.....82

4.3 Converter model in PSLF.....83

4.4 Control block in PSLF.....85

4.5 The reactive power control model in PSLF used to represent a reactive power controller in utility scale PV simulation studies.....85

4.6 One line diagram of the system in vicinity of the bus 1489.....89

4.7 Relative rotor angle of the generator at bus 1488, BB1 for various penetration levels.....90

4.8 Relative rotor angle of the generator at bus 1566, G1 for various penetration levels.....91

4.9 Bus 1569 voltage for various penetration levels.....92

4.10 Bus 1569 frequency for various penetration levels.....92

Figure Page

4.11 Bus 2531 voltage for various penetration levels.....93

4.12 Real power generation of the generator at bus 1566, after loss of BB2 93

4.13 Reactive power generation of the generator at bus 1566, after loss of BB2..94

4.14 One line diagram of the system in vicinity of the bus 1969 96

4.15 Relative rotor angle and speed of the W14 generator located at bus 1967....97

4.16 Active and reactive power generation of the W14 generator at bus 1967 97

4.17 Bus 956 voltage and frequency.....98

4.18 Bus 1433 voltage and frequency.....98

4.19 Bus 1959 voltage and frequency.....99

4.20 Bus 1969 voltage following a generator loss at this bus.....99

4.21 Generator A11 relative rotor angle following the case A double line outage103

4.22 Generator A11 active and reactive power generation following the case A double line outage.....104

4.23 One line diagram of the system in vicinity of bus 1164 104

4.24 Generator G1 relative rotor angle following the case A double line outage105

4.25 Generator G1 active and reactive power generation following the case A double line outage.....105

4.26 Bus 1001 voltage and frequency following the case A double line outage .106

4.27 Bus 1569 voltage and frequency following the case A double line outage .106

4.28 One line diagram of the system in the neighborhood of bus 1569 107

4.29 Bus 1569 voltage and frequency following the case B double line outage .108

4.30 Bus 1886 voltage and frequency following the case B double line outage .108

Figure Page

4.31 Bus 1205 voltage and frequency following the case B double line outage .109

4.32 Bus 1164 voltage and frequency following the case B double line outage .109

4.33 Generator G1 relative rotor angle following the case B double line outage110

4.34 Generator G1 speed following the case B double line outage 110

4.35 One line diagram of the system near the faulted bus 113

4.36 Bus 1569 voltage and frequency following the case A bus fault.....114

4.37 Bus 1886 voltage and frequency following the case A bus fault.....115

4.38 Bus 1146 voltage and frequency following the case A bus fault.....115

4.39 Bus 1179 voltage and frequency following the case A bus fault.....116

4.40 Generator G1 relative rotor angle and speed following the case A bus fault116

4.41 Generator G1 active and reactive power generation following the case A bus fault 117

4.42 One line diagram of the system simulated for the case B bus fault.....118

4.43 Bus 2386 voltage and frequency following the case B bus fault.....119

4.44 Bus 2233 voltage and frequency following the case B bus fault.....119

4.45 Bus 1881 voltage and frequency following the case B bus fault.....120

4.46 Bus 2166 voltage and frequency following the case B bus fault.....120

4.47 Voltages of the 69 kV buses due to cloud cover.....121

4.48 Bus 1164 and 792 voltage magnitudes following loss of rooftop PVs.....124

4.49 Relative rotor angle of the generator 1567 following loss of rooftop PVs..124

4.50 Active and reactive power generation of the generator 1567 following loss of rooftop PVs 125

Figure Page

5.1 Participation factor of the machines participating in the critical mode detrimentally affected by high PV penetration 137

5.2 Single line diagram of the system near the generator at bus 2102.....138

5.3 Generator 2103 speed (p.u.) following a fault at bus 2104.....139

5.4 Generator 2103 relative rotor angle (deg) following a fault at bus 2104.....140

5.5 Active power output of the generator located at bus 2103 following a three phase fault at bus 2104.....141

5.6 Voltage of bus 844 following a three phase fault at bus 844.....143

5.7 Voltage of bus 810 E5 following a three phase fault at bus 844 143

5.8 Speed of the generator E5 following a three phase fault at bus 844.....144

6.1 Description of the performance metrics A_f, A_N, and A_t 153

6.2 Frequency response of various dispatch ratios for a loss of two major units 156

6.3 Frequency nadir of various dispatch ratios for loss of two major units.....156

6.4 Frequency settling value for loss of two major units.....158

6.5 System equivalent frequency for loss of rooftop PVs and two large units....160

6.6 Frequency nadir for loss of rooftop PVs and two major units.....160

6.7 Frequency settling value for loss of rooftop PVs and two large units.....161

6.8 Frequency settling value versus dispatch ratio 161

6.9 Voltage of the bus 1569 following a thee phase fault at 1569.....165

6.10 Voltage of the bus 2375 500 kV following a fault at 1569.....165

6.11 Frequency of the bus 1569, 500 kV following a fault at 1569 166

6.12 Frequency of the bus 2375, 500 kV following a fault at 1569 166

Figure Page

6.13 Voltage of the bus 1425 following the case 2 disturbance 172

6.14 Frequency of the bus 1425 following the case 2 disturbance 172

6.15 Voltage of the bus 810 following the case 2 disturbance 173

6.16 Speed of the generator 810 E5 following the case 2 disturbance 173

6.17 Voltage of the bus 1490 following the case 3 disturbance 175

6.18 Frequency of the bus 1487 following the case 3 disturbance 175

6.19 Speed of the generator 1490 following the case 3 disturbance.....176

6.20 $p_{critical}$ histogram.....185

6.21 Average bus voltages distribution.....183

6.22 Flow chart for calculating ODR.....184

6.23 Bus 108 voltage distribution 186

6.24 Regression coefficients for BCIs calculated based on (6.3) 186

6.25 Regression coefficients for BCIs calculated based on (6.7) 187

6.26 Regression coefficients for BCIs calculated based on (6.16) 189

NOMENCLAUTURE

AHP	Adaptive Hierarchy Process
BCI	Bus Criticality Index
CB	Circuit Breaker
CBM	Circuit Breaker Monitoring
DSA	Dynamic Security Assessment
DR	Dispatch Ratio
F	Frequency of the Oscillation in Hz
f_{sys}	The Center of Inertia Frequency Defined for the Entire System
Gen	Generator
H_i	Inertia of the i^{th} Generator
L	Number of Buses in the System
LP	Linear Programming
LCI	Line Criticality Index
MVAr	Megavolt Ampere Reactive
MW	Megawatt
n	Exponent of the Penalty Function
$n_{critical}$	Number of Times Bus Voltage is Outside the Tolerance Range
$n_{acceptable}$	Number of Times Bus Voltage is Within the Tolerance Range
nl	Number of the Lines
NLP	Nonlinear Programming
$n_{OverLimit}$	Number of Times Line Flows are Above the Line MVA Rating
$n_{UverLimit}$	Number of Times Line Flows are Below the Line MVA Rating
ODR	Optimal Dispatch Ratio
OPF	Optimal Power Flow
PCC	Point of Common Coupling
$p_{critical}$	Probability of Criticality

P_g	Generator Active Power Output
PI_{MW}	Power Performance Index
PI_V	Voltage Performance Index
PI_{VQ}	Combined Voltage and Reactive Power Performance Index
P_l	Load Active Power
P_l^{lim}	Maximum Allowable Power Flow of the Line
POI	Point of Interconnection
P_{pv}	Output Power of the Photovoltaic Source
PSAT	Power Flow and Short Circuit Analysis Toolbox
PSLF	Positive Sequence Load Flow
P_T	Transmission Line Active Power Drop
PV	Photovoltaic
Q_g	Generator Reactive Power Output
Q_l	Load Reactive Power
Q_T	Transmission Line Reactive Power Drop
RHP	Right Half Plane
RPS	Renewable Portfolio Standards
R_T	Transmission Line Equivalent Resistance
SCI	System Criticality Index
S_g	Generator Apparent Power Output
SIL	Simultaneous Import Limit
SSAT	Small Signal Analysis Tool
SVD	Singular Value Decomposition
TSAT	Transient Security Assessment Tool
V_i	Voltage Magnitude at Bus i
V_k	Voltage Magnitude at Bus k
V_k^{max}	Maximum Allowable Voltage at Bus k
V_k^{min}	Minimum Allowable Voltage at Bus k
V_l	Load Voltage

VO&M	Variable Operation and Maintenance
VSAT	Voltage Security Assessment Tool
WECC	Western Electricity Coordinating Council
W_k	Weighting Factor Corresponding to Bus k
W_{li}	Weighting Factor of Each Line
WLS	Weighted Least Squares
X_T	Transmission Line Equivalent Reactance
ZVRT	Zero Voltage Ride Through
Λ	i^{th} Eigenvalue of the State Matrix
E	Linear Regression Error
Φ	Right Eigenvector
Ψ	Left Eigenvector
ς	Damping Ratio
Ω	Vector of Regression Coefficients

Chapter 1

INTRODUCTION

1.1 Overview

The need for clean, renewable energy has resulted in new mandates to augment, and in some cases replace, conventional fossil based generation with renewable generation resources [1]. Solar and wind generation are among those resources that have been at the center of attention. These resources albeit currently more expensive (in $/MW installed comparison) are environmentally friendly, renewable, and they do not produce greenhouse gases. Therefore, replacing the conventional generation with large scale renewable units has been one of the major aspects characterizing *smart grids*.

With the extensive growth in the deployment of the photovoltaic resources, power system operators are expected to deal with a new generation of power system issues due to the different nature of the newly added power generation resources. The ability to reverse the flow of the power from the loads towards the transmission system and the reduced reactive power generation are some of the unique characteristics of the PV units that add to the complexity of power systems.

Ensuring system reliability in systems with high penetration of renewable energy resources is one of the most important challenges associated with the operation of smart grids. Maintaining a reliable power system that has the ability to respond to the customers' demands at all times is one major characteristic of smart grids. With the present consumer demand and with more complex

equipment being installed in power systems, the need for a grid with enhanced intelligence is more evident than before.

1.2 Motivation

The structural changes in power systems result in new concerns regarding the reliable and secure operation of the system with high penetration of renewable energy resources. While higher amounts of photovoltaic penetration levels are expected based on the established renewable portfolio standards (RPS), the exact effect of these resources are still to be fully identified. High PV penetration levels can significantly affect the steady state as well as the transient stability of the systems due to their distinct characteristics that differ from conventional generation resources. With high PV generation, a significant amount of conventional generation may be replaced with distributed PV resources. While a portion of this replaced generation is supplied by utility scale PVs, a majority of PV generation addition is expected to be provided by residential rooftop PVs that are located closer to the loads on the distribution system. Presently practiced standards, e.g., IEEE 1547 and UL 1741 [2] suggest that PV inverters should not actively regulate the voltage at the point of common coupling (PCC) [2]. Therefore, these units are mainly utilized as sources of active power and no reactive power is generated by these resources. Lack of reactive power support is an immediate concern at the systems with high PV penetration. Reduced system inertia is another by-product of utilizing higher amounts of PV generation resources.

Effects of photovoltaic systems on distribution systems have been the subject of many research investigations [3-6]. These studies largely focus on the behavior of the system while PV generation resources are connected to the grid, in terms of the location of the connection point and control strategies that could be considered for better system performance. Most of these research efforts are conducted for distribution systems since the level of PV installations is assumed to be small enough to have a less significant effect on the transmission system. With more PV installations, high PV penetration has been recently awarded more attention among researchers. Ongoing studies investigate the effect of these systems on the power distribution systems [7-9]. As these papers suggest, high PV penetration can affect the voltage profile depending on the loading conditions and amount of PV penetration. Study results of these works suggest that the presently available regulation equipment are not capable of mitigating the adverse effects of the PV system transients such as the effects of clouds. Therefore, power inverters should have some excess power capability to absorb or generate reactive power for voltage regulation [10]. The main theme in all these studies is the fact that high PV penetration levels can affect steady state voltage magnitudes and therefore more control options may be required.

Although many of the cited works are effective in identifying some of the problems associated with high PV penetration levels, they are mainly focused on distribution systems. However, these levels of PV penetration can directly affect the transmission systems during normal operating conditions as well as during various transients. Since this is a rather recent topic, there are a limited number of

topical research efforts reported in the literature, e.g., [11-13]. It has been shown in [11] that, depending on the amount of PV solar generation and the point of interconnection (POI), transient voltages could have better or worse behavior than the case without PV. Although most of these studies indicate that high PV penetration can have diverse effects on system transients, the cases considered for system studies are not actual representations of a larger, interconnected power system. The authors in [13] have analyzed the transmission system performance with high PV penetration on an IEEE 39 bus system, while various case studies have been conducted.

Unlike the aforementioned works, the present work investigates the effect of high PV penetration on a considerably larger system. Both utility scale and distributed rooftop PVs are modeled in this work to cover a broad range of PV systems. In addition to steady state analysis, the effect of transients on the system is investigated by utilizing software packages such as DSA^{Tools} and PSLF.

Although electric grids are facing more environmental, technological and infrastructural challenges due to the increased penetration of renewable resources, the technological advancements provide a mean to deal with these challenges. The emerging technologies in communication, control, sensing and computing all contribute to make the power grid smarter. Condition monitoring systems are one of these technologies that have found more applications in today's grids due to the increased system complexity. A very simplified concept of the smart grid is shown in Fig. 1.1.

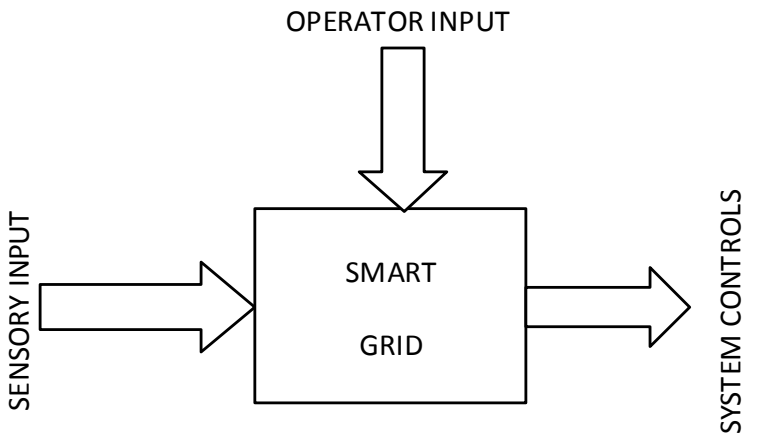

Fig. 1.1 A conceptual picture of the smart grid

The slower expansion rate of the transmission system infrastructure in comparison to the load growth has resulted in considerable increase in transformer deployment in recent years [14-15]. As a result of this increased usage more transformers are in need for maintenance due to excessive electrical and thermal stress. Although a need for maintenance is more evident than before, it is expensive and in some cases a hard task to implement, due to the fact that some of these components are located in remote areas. Therefore, maintaining all these transmission system components is not a practical solution for existing power systems. Condition monitoring of the circuit breakers and transformers optimizes the maintenance costs by providing information about the status of those elements and whether there is an impending failure in any of those system components. In this way, operators can decide on needed maintenance only if a transformer or circuit breaker is identified as nearing an impending failure.

1.3 Research Scope and Objectives

The objective of this work is to study various aspects of the smart grid with main focus on increasing the transmission system reliability and secure operation of smart grids. The specific objectives of the work are as follows:

Relating to transmission system component status and condition

- To study the effectiveness of various ranking methods in identifying the critical transmission system components.
- To propose an effective method for identifying the candidate transformer and circuit breakers for condition monitoring.

Relating to bulk power system operation

- To study the impact of various faults on the bulk power network with regard to voltage and angle stability with high penetration of PV systems.
- To study the steady state behavior of the power systems under different PV penetration levels.
- To study the small signal stability of the systems with high PV penetration.
- To introduce a method for identifying the optimal dispatch ratio of the conventional generators while PV systems are added to the power systems.

1.4 Dissertation Organization

This work has been organized into seven chapters.

Chapter 2 discusses the approach used in this work for condition monitoring of the transformers and circuit breakers and briefly introduces contingency ranking methods used in literature and the ranking methods used in this work. Contingency ranking study results along with the description of the system under study are presented in this chapter. Corrective actions that could be taken in case of each severe contingency are discussed at the end of Chapter 2.

Chapter 3 starts with a brief description of the studied system and presents the modeling aspects of the PV systems. This chapter mainly discusses the impacts associated with the high penetration of PV systems on power system steady state stability.

The analysis of transient stability is presented in Chapter 4. Investigating the impact of high PV penetration on the transient behavior of the power systems and comparison to the systems with no PV generation is the main objective of this chapter. Various fault scenarios are studied in Chapter 4 that include a broad range of power system events.

In Chapter 5 the impact of high PV penetration on small signal stability of the power system is investigated. Critical modes of the studied system are identified while their variations as more PV systems are added are compared. Transient stability studies are conducted to verify the results achieved by small signal stability analysis.

Chapter 6 studies the system under various dispatch or displacement ratios of the conventional generation resources. As more PV systems are added, the amount of reduction required in the output power of the thermal units could be

provided by displacing or rescheduling those units or combination of both. Chapter 6 identifies the optimal dispatch ratio (ODR) by simulation results followed by introduction of a method to identify ODR.

Chapter 7 summarizes the main findings of the research work related to impact of high penetration of PV systems on the transmission system and presents the scope and directions for further research in this area.

Chapter 2

IMPLICATIONS OF SMART GRID TECHNOLOGY ON TRANSMISSION SYSTEM RELIABILITY

2.1 The 'Smart Grid' and its Implications to Transmission and Distribution Systems

'Smart grid' is a general term for a series of infrastructural changes applied to the electric transmission, and distribution systems. To put it in simple words, the smart grid makes the traditional power systems smarter than what they are at the moment. According to the definition of the U.S. Department of Energy [17], 'smart grid' applies emerging technologies in order to bring more knowledge to power. With the growing increase in consumer demand and with more complex equipment being installed in power systems the need for a grid with enhanced intelligence is more evident than before. Although the load growth in the United States over the past two years is negative, it is anticipated that as the nation comes out of an economic slowdown, the load growth of the electric demand will again be significant and an important motivation for the application of smart grid technologies.

While there is no specific definition of a smart grid, its principal attributes can be represented by some important characteristics. The main features of a smart gird that could be found in different sources are intelligence, self-healing, adaptability, resiliency, sustainability, and digitalization [17]. Although all these features are important in the application of smart grid technology, intelligence seems to be the prominent aspect of the smart grid without which it is not possible

to address the emerging problems of the existing grids. All these characteristics are briefly introduced next. Figure 2.1 depicts these main characteristics of a smart grid.

Adaptability is the ability of the system to adapt to different operating conditions including geographical and climate fluctuations. Factors such as customers' load variability, unpredictable equipment failures, various faults, blackouts due to storms and similar natural events make the power system a highly unpredictable system. Techniques such as load forecasting and state estimation can help alleviate the effect of some of the unpredictable phenomena. However, these methods may not be applicable all of these cases. Conventional controllers installed in power system are based on previous experience and predicted operating conditions. Therefore, in the case of the unpredicted and unexpected operating conditions, they may fail to operate. Due to the aforementioned reasons, and in the view of the expansion of power systems, the need for an adaptive system with adaptive controllers is more critical than before. The smart grid, with the aid of adaptive controllers and learning capability, adapts itself to the new operating conditions to reduce the stress caused by unpredicted contingencies in the system.

Digitalization [17] is the factor that makes the application of smart technology feasible. Deploying fast and reliable computers, sensors and measurement and control techniques, facilitates the application of smart technology in power systems. One may say that the advances in computer

technology are the main reasons that have justified the application of smart technology in power systems.

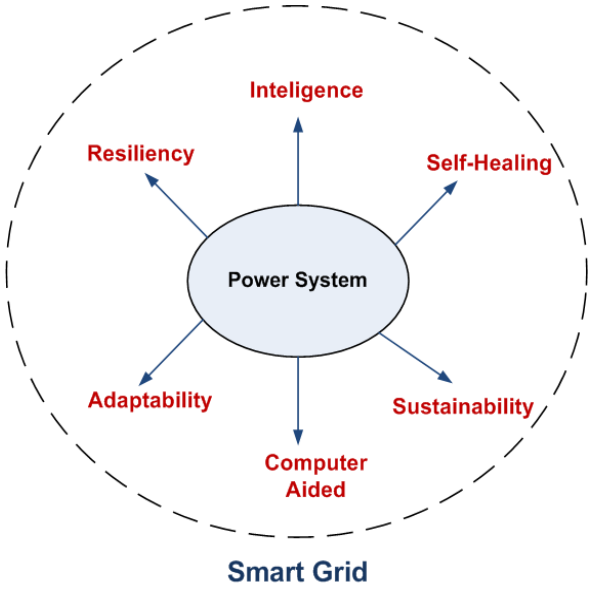

Fig. 2.1 Main characteristics of a smart grid

Self-healing and *resiliency* are often categorized in the same group while considering the characteristics of the smart grid. Self-healing is the ability of the power system to bring the system to a stable operating condition after a major disturbance has occurred in the system. In other words, the smart grid is capable of restoring the stable operating conditions by taking corrective actions fast enough to reduce the impact of the disturbance on the entire system and hence prevent cascading failures. Resiliency, is the ability of the system to maintain power delivery to the consumers in case of the disturbance. Therefore resiliency refers to the reliable and secure operation of the power system.

Sustainability can be described by the terms availability, efficiency and environmental friendliness [17]. The use of renewable energy resources which are more affordable can address both the environmental and customer demands.

2.2 Application of Smart Grid Technology on a Study System

With the rapid increase in the rate of transmission system transformer deployment, more transformers are in need for maintenance due to excessive electrical and thermal stress. Moreover, most of the transformers and circuit breakers are not designed for the prolonged duration of higher magnitudes of the power flows during peak load periods, resulting in fast aging of these transmission system components. Although a need for maintenance is more evident than before, maintenance is expensive and in some cases hard to implement due to the fact that some of these components are located in remote areas.

Condition monitoring of circuit breakers and transformers optimizes maintenance costs by providing information about the status of those elements and whether there is an impending failure in any of those system components. Therefore, operators can decide on needed maintenance only if a transformer or a circuit breaker is identified as approaching an impending failure. The information being provided by the smart condition monitoring systems is used to take corrective action that reduces the impact of the failure of transmission system components in case a contingency occurs in the system. A constrained optimal power flow (OPF) is used to re-dispatch the system in a way to reduce the effect of the failed system components and therefore provide the customers with a more

reliable service. In other words, condition monitoring entails constant monitoring of the system and in case there is a possible failure the smart module takes a corrective action which will be discussed in detail later in this chapter.

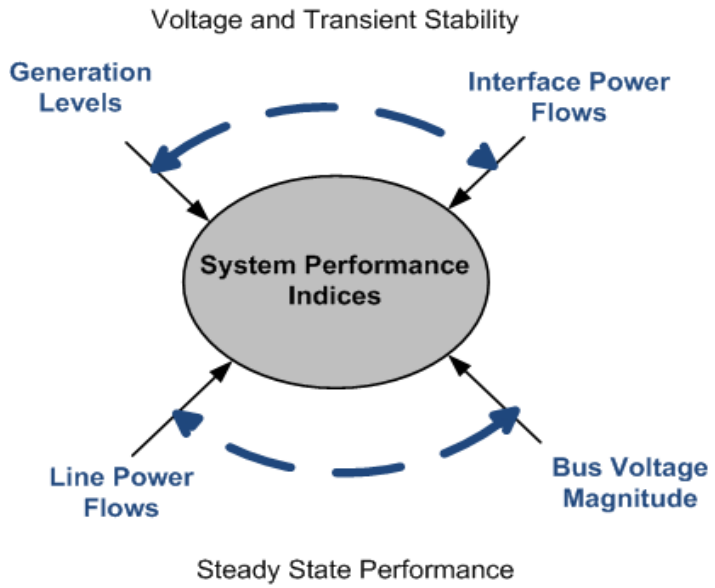

Fig. 2.2 Calculation of system performance indices

Monitoring all the transformers and circuit breakers not only is not cost effective but also requires a significant amount of data processing which in many cases might be unnecessary and redundant. Power flow data such as bus voltages and branch flows are used to calculate a series of performance indices that help determine the critical transformers or circuit breakers whose failure affects the system most. These critical elements are therefore best candidates for condition monitoring. Figure 2.2 shows the required information for calculating the performance indices. These data either assess the steady state performance or the transient stability of the system.

2.3 Security Assessment Performance Indices

Voltage stability is a critical cause of power system failures. Recent blackouts have shown the need for a more reliable and resilient power system. Therefore, it is vital to identify those elements whose failure affects the entire system the most. Contingency ranking is an approach introduced in many references [18-20] to pinpoint the critical elements of the power system such as circuit breakers and transformers whose failure can cause cascading outages.

Some contingency ranking methods are based on voltage violation at all system buses. In all these methods a performance index is defined and calculated for each bus in case of several contingencies. These methods vary based on the definition of the performance index and their effectiveness in identification of the critical elements. The purpose of the ranking procedure is to prevent the impending failures of critical elements and therefore, reduce the adverse effects of these failures on the entire system. In most cases the failure is not detected unless the system is stressed under specific operating conditions. In order to prevent this situation a model of the system should be utilized and several case studies should be studied on the system model. Hence, the computer simulation of the power system is essential in contingency ranking. With the developments in computer software for power system simulations, contingency ranking has found more application in power system operations and planning.

According to [21] voltage security assessment is defined as the ability of a given power system to maintain a desirable voltage range under normal operating conditions as well as all possible contingencies. Analyzing the system for all

possible contingencies is not a practical solution for a voltage security assessment problem. Therefore, contingency ranking is proposed to analyze the system only for the highest ranked contingencies, or in other words those which lead to voltage insecurity. As suggested in [21] most of the contingency ranking methods are not accurate since they neglect the nonlinearities of the reactive power equations as well as the effects of voltage regulators. Moreover, the loads are affected by the variations in the voltage, and hence this effect should be included in the ranking methods. The above mentioned inaccuracies which are mainly due to the modeling of the power system can lead to misranking of the contingencies. In order to deal with these problems the authors in [21] have suggested a new contingency ranking method which represents the effect of the voltage regulators and the sensitivity of the load to bus voltages. The nonlinearities due to the regulator tap positions and reactive power generation are included in the model for contingency ranking studies.

Contingencies in this study are divided into two different groups and each group is treated separately for ranking purposes. Therefore, the concept of *contingency stiffness* is introduced as a factor to categorize various contingencies. The first group of contingencies, which includes the majority of contingencies, is ranked based on the method proposed in [21] and other studies. However, the second group of contingencies which are mainly the most severe ones, should be ranked based on other, more complex methods such as *sub-network solution* [21]. The stiffness index is defined in [21] separately for a generating unit as well as a circuit outages. In case of a circuit outage this index is calculated for the

contingency and if this value is small the system states and power flow change linearly with respect to the circuit parameters. These equations should be linearized around the operating point. A high stiffness index determines that the contingency cannot be accurately ranked by performance index ranking methods. The same procedure is followed for generating unit outages and the corresponding stiffness indices are calculated. Similar to the circuit outage, a large value of stiffness index point outs the fact that the contingencies cannot be well predicted by performance index methods and thus alternate methods should be deployed.

The performance index ranking method is based on defining an index for contingencies and calculating the derivative of the performance index with respect to contingency parameters. Calculating the numeric values of these derivatives, ranks the severity of a specific contingency in terms of voltage violation. The performance index defined in [21] is as follows,

$$J=\sum_{k=1}^{N} W_k \left(\frac{2V_k - V_k^{max} - V_k^{min}}{V_k^{max} - V_k^{min}} \right)^{2n} \tag{2.1}$$

where,

W_k = Weighting factor corresponding to bus k

V_k = Voltage magnitude at bus k

V_k^{max} = Maximum allowable voltage at bus k

V_k^{min} = Minimum allowable voltage at bus k.

In (2.1), n is an arbitrary exponent which is usually selected to be equal to two. In order to account for the nonlinearities caused by reactive power limits and regulator tap limits authors in [21] have introduced different performance indices.

The same procedure of differentiation is followed to rank the contingencies. Although this method provides us with an accurate ranking method, it requires a considerable amount of complex calculations. Also, when the stiffness index is high this ranking method is not applicable and hence an alternate method is required.

In another work [22], Ejebe and Wollenberg have proposed an online security analysis method which analyses the contingencies based on the most recent operating condition. This method updates the list of the most severe contingency in an adaptive manner by ranking the contingencies and running the AC power flow to determine the set of problem causing contingencies in the system. The contingency ranking is again based on defining a set of performance indices for line and generator outage. These indices are defined in a way to treat the constraints of the load bus voltage and line flows as "soft" limits. In other words the violation of the limits imposed on the voltage and line flows are significantly penalized in the performance index.

In [22] three indices are defined for power flow and voltage analysis, which are referred to as PI_V, PI_{VQ}, and PI_{MW}. The first two indices are based on the voltage and the reactive power violations of the lines and the buses. These indices are defined [22] as,

$$PI_V = \sum_{i=1}^{l} \frac{W_i}{2n} \left(\frac{|V_i| - |V_i|^r}{\Delta V_i^{lim}} \right)^{2n} \tag{2.2}$$

In (2.2), V_i is the voltage magnitude at bus i and l is the number of buses in the system. The parameter n is the exponent of the penalty function which is usually

set to unity. The greater n may be, the more the penalty for violating the voltage limits. The weighting factors W_i are set arbitrarily for each bus. However, the more accurate and appropriate the weighting factors, the better the ranking of the contingencies. The term ΔV_i^{lim} represents the limit on the voltage deviation on each bus. In normal operating conditions this value is set to be ±5% of the rated voltage. The PI_{VQ} performance index is suggested in [22] to account for the violations of the reactive power in severe overvoltage conditions. This index is shown in (2.3),

$$PI_{VQ}=\sum_{i=1}^{l}\frac{W_{vi}}{2n}\left(\frac{|V_i|-|V_i|^r}{\Delta V_i^{lim}}\right)^{2n}+\sum_{i=1}^{m}\frac{W_{qi}}{2n}\left(\frac{Q_i}{Q_i^{max}}\right)^{2n} \tag{2.3}$$

In (2.3), Q_i is the reactive power at bus i while Q_i^{max} is the maximum allowable reactive power. The parameter m is the number of generating units in the system. The weighting factors in this case are W_{qi} and W_{vi}.

The authors in [22] have proposed a similar index for the line overload ranking. Therefore, the index involves the values of the real power flowing in each line [22],

$$PI_{MW}=\sum_{i=1}^{nl}\frac{W_{li}}{2n}\left(\frac{P_l}{P_l^{lim}}\right)^{2n} \tag{2.4}$$

As seen from (2.4), this index is based on the real power flow of the line P_l and maximum allowable power flow of the line P_l^{lim}. The parameter nl is the number of the lines while W_{li} is the weighting factor of each line.

The performance indices defined in [22] are simple to calculate and can effectively quantify the effect of each contingency on the entire system. One alternative to the definition of the performance indices shown in (2.3)-(2.4) is to combine PI_{MW} and PI_{VQ} and use the complex power instead of the real and reactive power separately. This could limit the system to the maximum allowable power flow in each line. While it is suggested in [22] to calculate the relative sensitivity of the performance indices to the outage in order to find the ordered list of contingencies, the simulation results of the AC power flow show that the calculation of the performance indices by itself is adequate to give reasonable ranking of the contingencies in the system. This adequacy is justified in a larger power system with a larger number of buses. The calculations of the indices are less complex than the sensitivity of the performance index.

In all the previous cases the indices are calculated based on weighting factors. These weights may not be definitive and conclusive work needs to be done in determining the optimal weights appropriate for accurate contingency ranking. In [23] the authors have proposed a method called the *adaptive hierarchy process (AHP)* to determine the weights which are used in calculation of the performance indices. In this method, depending on the importance of the transmission line or the bus in comparison to the rest of the system a value is assigned to the weighting factors subject to,

$$PI_{MW} = \sum_{i=1}^{nl} \frac{w_{ii}}{2n} \left(\frac{P_l}{P_l^{lim}} \right)^{2n} \tag{2.5}$$

$$\sum_i W_i = 1$$

The expert system will determine the importance of the voltage security at each bus and assigns a weight accordingly. The more important the bus, the higher the weighting factor and therefore the higher the penalty for violating the voltage or line flow limits. Although this method provides a better way of describing the performance indices used for ranking, the method used is more empirical rather than an approach based on actual system performance. An alternative to this method is the utilization of learning algorithms or methods such as neural networks which are based on the simulation results of the system. These methods can adjust the weights based on the results derived from the system model.

2.4 Identification of the Critical Transformers

Identifying the transformers or circuit breakers whose failure could result in loss of system components and hence decrease the system security is viable for improving the reliability of the transmission system. Once identified, these components that are referred to as *critical* system components, in this text, are equipped with condition monitoring systems to monitor their behavior and detect a probability of failure in these components.

One important aspect of the smart grid technology is to determine the correct action in case the system has encountered contingencies. The effectiveness of this task is more evident when there is a critical contingency in the system that could result in cascading failures. Alleviating the contingencies by a corrective action, which is determined by the smart module and is based on previous system

studies, is essential for system operation. However, studying all the system components and conducting *N*-1 and *N*-2 analysis on all the branches and transformers is not practical and in most of the cases might not be necessary. Based on these conclusions, the scope of this project is divided in to two tasks. The first part is to identify the critical elements of the system that require condition monitoring. As a result of identification, the system is further analyzed in the next section to find the corrective actions that could be taken in case a failure is detected in any of these critical system components. Figure 2.3 illustrates the process followed in this chapter along with the main objectives [24].

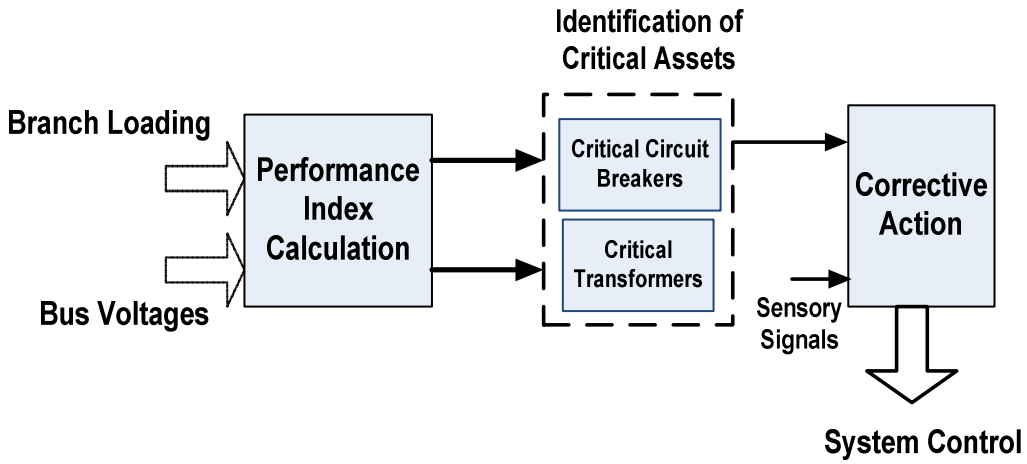

Fig. 2.3 Application of the smart grid in improving transmission system reliability

2.4.1 Ranking methods

Two different ranking methods are used in this thesis to identify the critical components of the system. The contingency ranking methods deployed in this chapter are inspired from the method discussed in [22]. These methods and their features are explained next.

The first method classifies each contingency based on the severity of the overloads caused on different branches. The second, however, utilizes the amount of voltage violations (over voltage or under voltage) of each bus as the basis for defining the performance indices. Combining these two methods could yield a third method that takes into effect both the branch overloads and the voltage violations of the busses. Although these methods are different in the variable used for identification, they all are based on the definition of a performance index. These indices associate the severity of each contingency and its effect on the entire system with a number so that it would be easier to compare and rank all the contingencies. In general, the *higher* the performance index, the *worse* is the contingency, and hence the more severe is the effect of that particular contingency on the rest of the system. It should be noted that what is meant by contingency is, in fact, failure of a transformer branch for the case of critical transformer monitoring; and outage of a branch equipped with circuit breakers for circuit breaker monitoring.

When considering solely the loading of the branches for the purpose of contingency ranking, a performance index is defined based on the weighted ratio of the apparent power of each branch to the MVA rating of that branch. This performance index is shown in (2.6). The terms w_{ij} are the weights associated with the *j*th branch while the *i*th contingency has occurred and n is the exponent factor that could in effect change the accuracy of the contingency ranking. Therefore, these two factors should be chosen accurately in order not to over rank or under rank any of the contingencies. The greater the value of n, the closer the

ranking gets to the definition of the infinity norm. However, large values of n can mask some of the contingencies and therefore do not show the severe cases in the ranking method. For the case at hand, a value of n equal to two has shown satisfactory results that are confirmed with the simulation results,

$$PI^{i}_{MW}=\sum_{j=1}^{nl}\frac{W_{ij}}{2n}\left(\frac{P_j}{P_j^{lim}}\right)^{2n} \tag{2.6}$$

In order to capture the effect of an overloading in the performance index, the weights are chosen to penalize any overloading while the branches with no power violation have the same lower weights. Therefore for the case of the overloading, the weights are set in way to change proportional to the amount of the overloading in the branch.

The second ranking method deploys the information related to the bus voltages in order to calculate the severity of the contingency. Similar to the previous method, a performance index is defined to convert the effect of each contingency to a numeric value. This performance index, which is shown in (2.7), calculates the weighted sum of the bus voltage violations over the voltage tolerance of that bus. The tolerance is usually ±5 percent of the rated voltage value,

$$PI_V=\sum_{i=1}^{l}\frac{W_i}{2n}\left(\frac{|V_i|-|V_i|^r}{\Delta V_i^{lim}}\right)^{2n} \tag{2.7}$$

Similar to the MVA ranking method, the voltage ranking weights are also set to highlight the effect of any violation in the performance index and reduce the effect of buses with voltages within the tolerance in the performance index.

Another method which is a combination of both rankings combines the above mentioned performance indices and calculates an index that takes into account both the bus voltages and the power flow of the lines. Depending on the system and the type of the system contingency either overloading or voltage violation might be the more important factor. Therefore, the selection of the ranking indices is contingent on the application. As discussed later in this chapter, the MVA ranking method is more applicable to the study system at hand; specifically when considering the summer peak cases. Figure 2.4 summarizes the aforementioned methods of contingency ranking.

The aforementioned contingency ranking methods rank the contingencies based on the value of the performance indices. As a result of this ranking, the transformers, which are the most critical components to the system, are identified so that they are monitored in order to prevent their permanent loss from the system. On the other hand, determining the critical branches creates a list of candidate circuit breakers that could enhance the system reliability if equipped with condition monitoring capabilities. In what follows, the contingency ranking results of a study system are presented and therefore the candidate transformers for condition monitoring are identified. The main software packages used for simulation are DSA^{Tools} and MATLAB. These packages have the capability to report the branch flows and bus voltages after each contingency. These values are then transformed to MATLAB to calculate the corresponding indices for each contingency. Figure 2.5 shows the basic structure of the contingency ranking program used for calculating the indices.

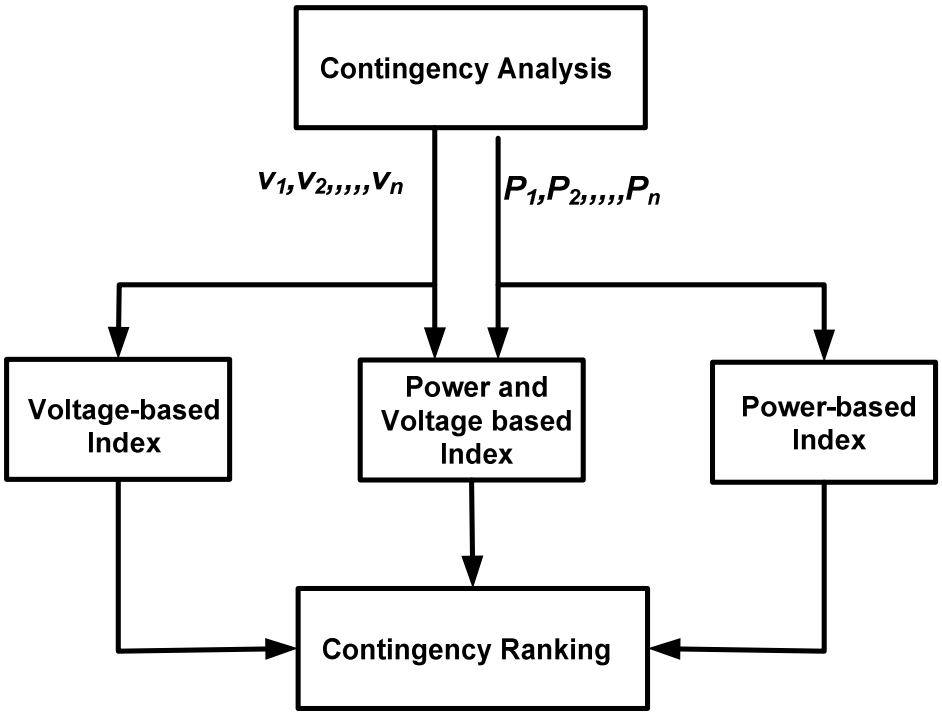

Fig. 2.4 Contingency ranking methods based on steady state bus voltages and line flows

Voltage Security Assessment Tool (VSAT) is part of the DSA[Tools] that can provide the user with the list of the busses that violate the voltage tolerance (5%). Also by defining the subsystem of interest, a comprehensive branch flow report is provided for each contingency case in the form of a text file which is then transferred to MATLAB for further analysis. Two different cases are studied in this work, which include the summer peak case as well as the summer simultaneous import limit (SIL). The first case is in fact the normal summer peak while the SIL case represents the maximum amount of load that can be served only with imports and therefore no local generation is included in this case.

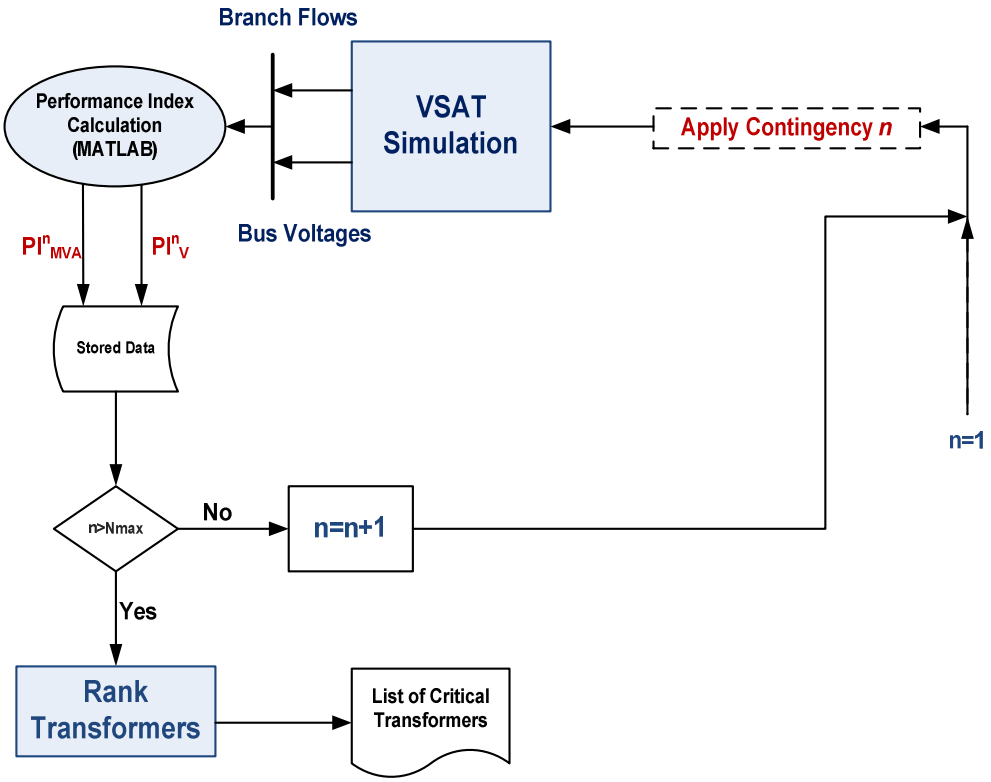

Fig. 2.5 Flow chart of the ranking procedure

2.4.2 Establishment of the concept via numerical simulation

In order to identify the best candidates for condition monitoring in the study area, transformers and circuit breakers of the system are ranked based on the method described in the previous sections. In the following sections, the studied system is described followed by ranking results of the transformers.

System description

The system under study is part of the U.S. Western Electricity Coordinating Council (WECC) with about 600 buses and 53 generators in the system. The total generation in this system is 8477 MW during the peak hours and the loads can vary from 7122 MW during summer peak hours to 5798 MW for the

summer Simultaneous Import Limit (SIL) case. Table 2-1 presents a summary of these two load cases for comparison purposes.

Table 2-1 Load case summary for summer peak case and summer SIL case of the study area

	Summer Peak Case	Summer SIL Case
Total Load (MW)	7122.06	5797.94
Total Generation (MW)	8476.92	5759.05
Total Export (MW)	1130.15	-246.24
Total Losses (MW)	223.25	205.94

At summer normal peak case, not all the generations are at maximum power or online. Also, some power is exported to the other neighboring areas. In the SIL case, however, the load is lower than the peak case and it is assumed that the load is served mostly with local generation, No exports are assumed to be present in this case. It should be noted that in all the contingency cases the total export and generation is assumed to be constant with no re-dispatch capability.

The list of contingencies that need to be considered consists of the loss of all transformer branches above the 115 kV level. Therefore a file is prepared in VSAT that automatically removes each one of these lines and calculates the power flows in each step**.** Appendix A lists all the candidate transformer branches. Each contingency number corresponds to the specific transformer branch that is removed as a result of a mis-operation or severe overloading. Since *N-1* contingencies are considered in this case, in each step only one branch is assumed to be out of service. Throughout this chapter, each contingency is referred to by

the individual transformer branch number. For instance, contingency number 71 translates to removing the 69 kV/230 kV transformer that connects bus 659 to bus 660, from the service. Next, the transformer ranking results including the procedure and list of the critical contingencies are presented for the above mentioned two loading cases.

Identification of critical transformers

One advantage of using VSAT over other available software packages is the ability of VSAT to automatically perform each contingency. Moreover, providing the user with the desired, custom defined information at each step is another motivation for using DSA^{Tools} in this work [25]. The contingency analysis results are transferred to MATLAB to calculate the power-based and voltage-based indices. The ranking results of the *N-1* contingency analysis for both summer peak case and the SIL case are presented in Tables 2-2 and 2-3 are obtained for the contingency performance indices. The first column calculates the MVA based indices and the second column calculates the voltage based indices for each contingency.

As seen from the results of the summer peak case shown in Table 2-2, the performance indices are close to each other in most of the contingencies and are different only for a few critical cases mentioned before. In order to provide a better comparison, these indices are plotted in Fig. 2.6. This figure illustrates the PI_{MVA} index versus PI_V index for each one of the 71 contingencies described for the summer peak case. Comparing these indices yields the decision of whether a transformer branch is critical or not.

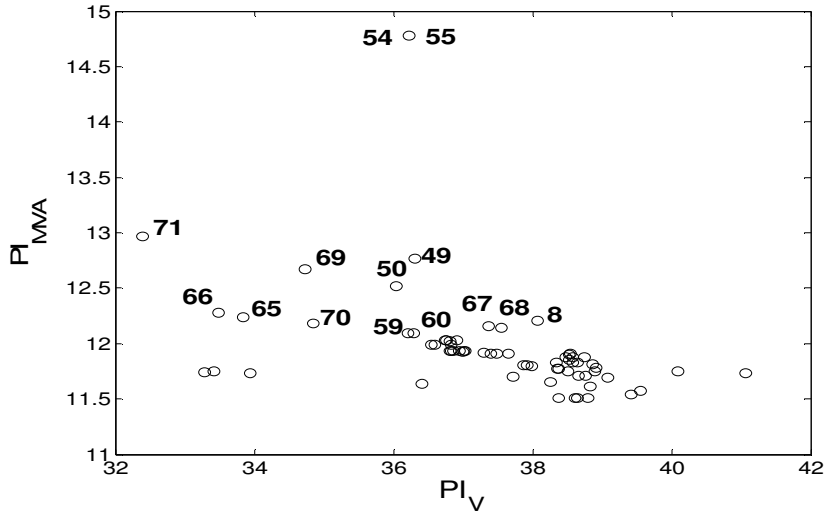

Fig. 2.6 Summer peak PI_{MVA} index versus PI_V index for all the 71 contingencies in the system

Table 2-2 Power-based and voltage-based indices of transformer branches for normal summer peak case

Cont. Number	PI_{MVA}	PI_V	Cont. Number	PI_{MVA}	PI_V	Cont. Number	PI_{MVA}	PI_V
1	11.51	38.60	19	11.78	38.92	58	11.75	33.42
2	11.51	38.64	20	11.82	38.86	59	12.098	36.21
3	11.51	38.80	21	11.75	38.52	60	12.096	36.30
4	11.54	39.43	22	11.69	39.085	61	12.026	36.76
5	11.57	39.55	23	11.71	38.65	62	12.028	36.74
6	11.73	41.06	24	11.71	38.76	63	12.025	36.82
7	11.75	38.90	25	11.70	37.73	64	12.027	36.91
8	12.20	38.06	26	11.86	38.53	65	12.23	33.85
9	11.88	38.74	27	11.87	38.58	66	12.28	33.49
10	11.51	38.38	28	11.83	38.64	67	12.14	37.55
11	11.51	38.38	29	11.83	38.59	68	12.16	37.37
12	10.12	37.90	30	11.83	38.34	69	12.67	34.73
13	11.78	38.38	31	11.91	37.65	70	12.18	34.85
14	11.78	38.35	32	11.93	36.95	71	12.97	32.39
15	11.66	38.26	33	11.93	37.04	40	11.80	37.98
16	11.64	36.40	34	11.93	36.99	41	11.88	38.48
17	11.62	38.83	35	11.99	36.83	42	11.88	38.47
18	11.75	40.10	36	11.99	36.60	43	11.91	38.55
37	11.10	36.55	55	14.78	36.23	44	11.90	38.54
38	11.80	37.88	56	11.74	33.28	45	11.93	36.82
39	11.80	37.92	57	11.73	33.94	46	11.93	37.02
47	11.93	36.84	49	12.76	36.30	51	11.91	37.30
48	11.93	36.86	50	12.52	36.03	52	11.91	37.48
53	11.91	37.40	54	14.78	36.23			

Table 2-3 Power-based and voltage-based indices for transformer branches while considering the SIL Case

Contingency Number	PI_{MVA}	PI_V	Contingency Number	PI_{MVA}	PI_V
1	13.33	26.23	19	13.73	26.023
2	13.33	26.19	20	13.73	26.02
3	13.34	26.22	21	13.73	26.22
4	13.46	25.66	22	13.73	26.22
5	13.52	25.69	23	13.73	26.22
6	13.72	26.43	24	13.73	26.22
7	13.73	26.24	25	13.73	26.22
8	14.99	26.50	26	13.97	26.23
9	14.01	26.70	27	14.07	26.19
10	13.73	26.21	28	14.16	25.95
11	13.73	26.22	29	14.22	25.97
12	13.73	26.22	30	14.54	26.58
13	13.66	26.04	31	14.52	26.53
14	13.73	26.22	32	14.08	28.05
15	13.60	26.16	33	14.07	27.86
16	13.46	26.03	34	14.07	27.84
17	13.46	26.03	35	14.32	29.35
18	13.18	25.92	36	14.30	29.14
37	14.31	29.28	55	13.85	26.23
38	14.07	26.44	56	13.87	26.07
39	14.07	26.48	57	13.87	26.11
40	13.80	26.25	58	13.88	26.09
41	13.80	26.20	59	13.87	26.06
42	13.81	26.26	60	14.25	27.24
43	13.90	26.51	61	14.26	27.30
44	14.25	28.20	62	13.94	26.35
45	14.25	28.15	63	13.94	26.28
46	13.89	26.06	64	13.94	26.34
47	13.89	26.08	65	13.95	26.33
48	13.88	26.10	66	14.039	26.27
49	13.91	27.62	67	14.05	26.31
50	13.91	27.68	68	15.25	33.61
51	13.90	27.76	69	14.97	38.38
52	13.83	26.27	70	15.60	64.16
53	13.84	26.27	71	13.73	26.22
54	13.86	26.28			

The results presented in Fig. 2.6 illustrate a few facts regarding the contingency cases. The first observation is that the cases with high MVA index are not necessarily the cases with high voltage index. In fact, in some severe cases in terms of branch loading, such as contingency number 71, the voltage index is low and hence no severe voltage violation is observed in these cases. Analyzing the cases in terms of voltage violations, it is observed that the worst contingency case and the least severe case are not significantly different than the base case. In the summer peak case, the PI_{MVA} index plays a more important role in ranking than the voltage based index. Consequently, PI_{MVA} is used for ranking purposes for the normal peak case rather than the PI_V index. Figure 2.7 illustrates the ranking results of the transformers by only considering the MVA index. From this figure, it is clearly observed that few contingency cases stand out as the severe cases while others have the PI_{MVA} index close to each other. As mentioned before, these transformers are the best candidates for condition monitoring. Table 2-4 summarizes the list of these critical transformers.

The same procedure is followed for the SIL case while it is expected to have less overloading since the total load and generation in this case is considerably less than the peak load case. As seen from the results summarized in Table 2-3, in contrast to the peak case, the MVA index does not vary as much in the SIL case. In other words, the difference between the PI_{MVA}^{MAX} and PI_{MVA}^{MIN} is small. The reason for this small difference is that the system is less loaded than the peak case and therefore the branches are not much overloaded even when the contingencies are present in the system.

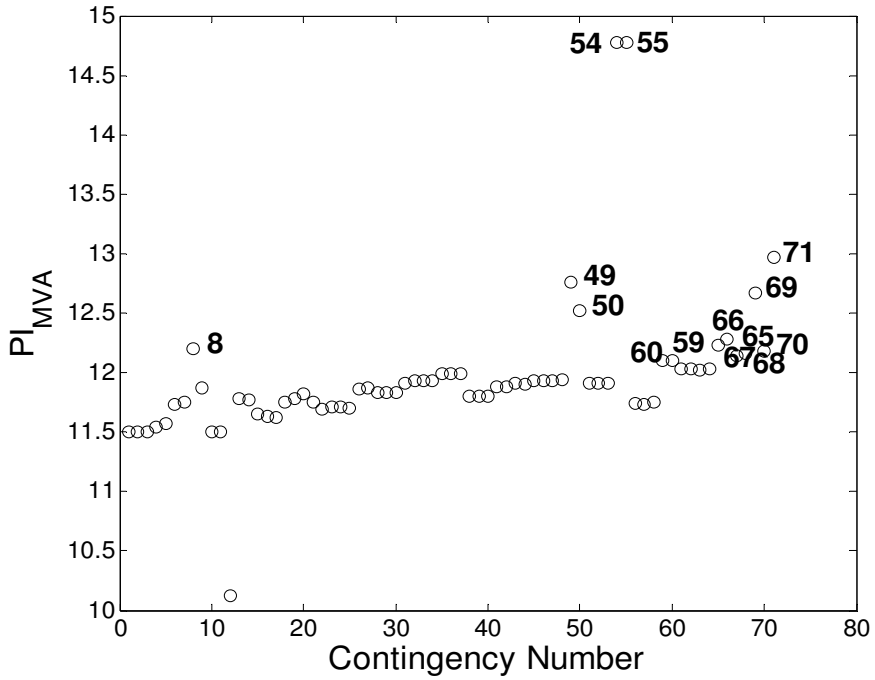

Fig. 2.7 Summer peak PI_{MVA} index calculated for all the 71 contingencies in the system

Similar to the peak load case it is observed that PI_{MVA} index is a better indication of the severe cases rather than the voltage based index. Figure 2.8 presents the ranking results for the SIL case considering only the MVA based index. As seen from these results, three cases, i.e. contingencies 70, 69, and 68, along with contingency number 8 are the severe contingencies in terms of the power based index. It should be noted that these transformers have already been identified as critical cases in the peak case and are listed in Table 2-4. From the aforementioned two cases, i.e. summer SIL case and summer normal peak case, it is concluded that the PI_{MVA} is a more fitting measure of the severity of the contingencies in the context of the critical transformer ranking. Another conclusion that could be derived from the simulation results is that the peak cases

are more preferred for identification purposes since they reflect the worst case contingencies and therefore can highlight the worst overloads in the system.

Table 2-4 List of Critical transformers of the studied system for summer peak case

Case Number	From Bus	To Bus	ID
71	659	660	1
54,55	1959	1968	1 or 2
69	1959	1968	2
49,50	1869	1870	2 or 4
65,66	2340	2339	1 or 2
67,68	2386	2387	1 or 3
59,60	1980	1981	1 or 3
8	1886	1885	4
70	315	316	4

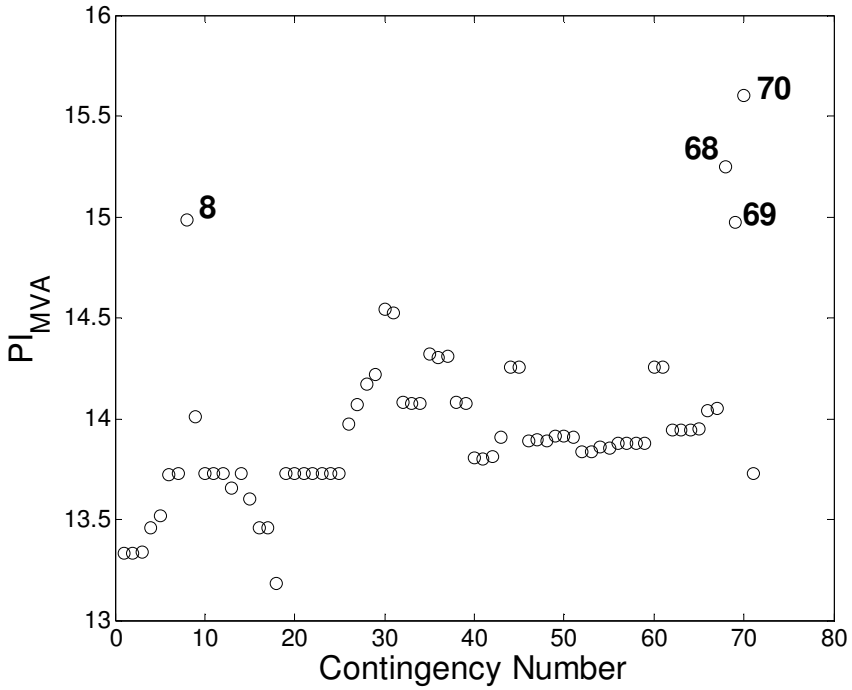

Fig. 2.8 PI_{MVA} index calculated for summer SIL case for all the 71 contingencies in the system.

2.5 *(N-1)-1* Contingency Analysis Results

Although it is important to find the critical transformers and circuit breakers, it is equally important to find the next subsequent contingency once the first critical contingency has occurred. If a severe contingency has occurred in the system, it is viable for the secure operation of the power system to prevent the next severe contingency by corrective actions, such as rescheduling. These actions can effectively prevent catastrophic events by mitigating the adverse effects of the second contingency. During the most severe *(N-1)-1,* i.e. the second outage after an outage has already occurred in the system, (or *N-2*) contingency cases, the system may not be able to recover by further rescheduling as there will be more overloaded lines and bus voltage violations than the case with one severe contingency.

Identifying these cases is handled through a *(N-1)-1* contingency analysis that starts from one of the most severe cases identified before and follows the same procedure to find the next severe contingency if the first contingency occurs in the system. Two cases of *(N-1)-1* contingencies are considered in this section with the first contingency being the loss of each one of the 659-660 (69 kV/230 kV), or 1869-1870 (69 kV/230 kV) transformers. Hence, for each case the other 70 cases mentioned in Appendix A are studied to find the most severe *(N-1)-1* contingency amongst them.

2.5.1 659-660 (69 kV / 230 kV) transformer branch out of service

The normal peak case is chosen as the basis of analysis since from the previous results it was shown that peak case is the best load case for ranking the

contingencies. Therefore, the PI_{MVA} index is calculated for all the remaining 70 cases. The same procedure as before is followed with modifications in the VSAT contingency file in order to account for the *(N-1)-1* contingency case. Figure 2.9 illustrates the calculated PI_{MVA} index versus contingency number for each contingency.

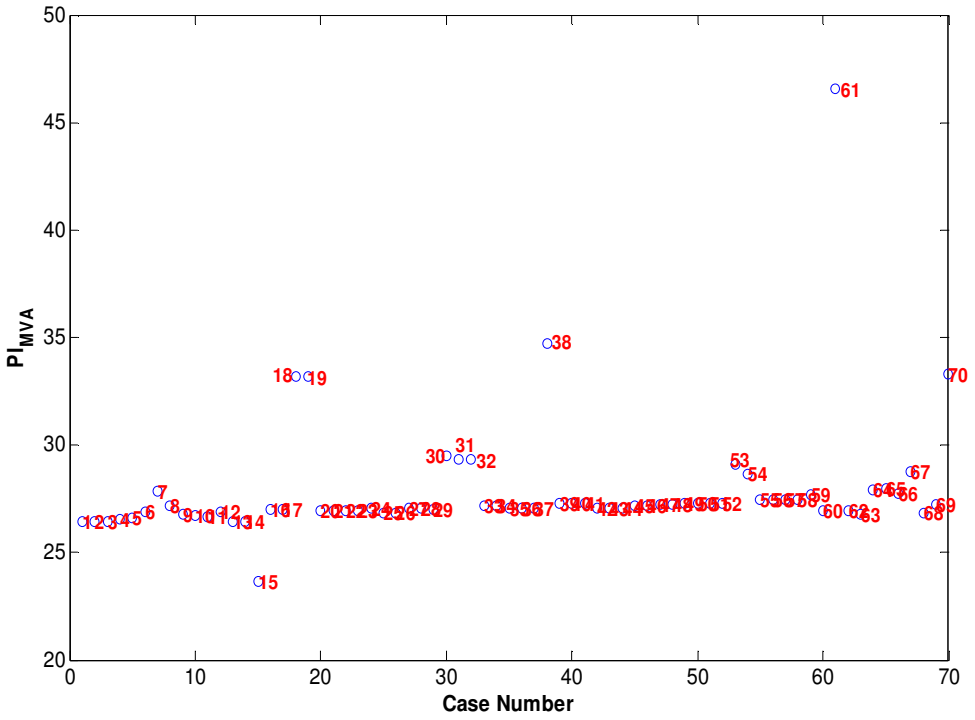

Fig. 2.9 PI_{MVA} versus contingencies number for the peak case while 659-660 (69 kV / 230 kV) transformer branch is out of service

Table 2-5 lists the worst contingencies while the other transformer branch is out of service. It is observed form the table that 315-316 (69 kV / 230 kV) transformer has the most severe effect on the rest of the system in terms of overloading. Although this branch is not among the critical transformers in the *N-*

1 analysis, loss of this transformer is a severe contingency in *(N-1)-1* contingency case. By comparing the results of Table 2-5 with those of Table 2-4 some similarities in terms of the critical transformers, such as the 1869-1870 (69 kV/230 kV) transformer branch, are found. Hence, by preventing overloading of these branches a more secure system is achieved and if for any reason one of the transformers is switched out of the service, the next severe contingency will not occur.

Table 2-5 Critical transformer branches for the peak case while 659-660 (69 kV / 230 kV) transformer branch is out of service

Case Number	From Bus	To Bus	ID
61	315	316	4
38, 70	1980	1981	3 or 1
18,19	1959	1968	1 or 2
30,31,32	1960	1959	3 or 4
53,54	1869	1870	2 or 4

2.5.2 1869-1870 (69 kV/230 kV) transformer branch out of service

The same procedure as the previous case is repeated while the contingency ranking results are presented in Fig. 2.10 and the critical branches are listed in Table 2-6.

Table 2-6 Critical transformer branches for the peak case while the 1869-1870 (69 kV / 230 kV) transformer branch is out of service

Case Number	From Bus	To Bus	ID
53,54,55,56	2231	2232	1,2, 3, 4
57	2386	2387	1
18,19	1959	1968	1 or 2

The results presented in Table 2-6 suggest that the 2231-2232 (69 kV/230 kV) transformer branch is a critical branch once the 1869-1870 (69 kV/230 kV) transformer is switched out of service. The two 2386-2387(69 kV/230 kV) and 1959-1968 (69 kV/230 kV) transformer branches are also critical branches while they were already expected to be critical based on the *N-1* contingency analysis results presented in Table 2-4. These observations, along with the results from the previous section suggest a few conclusions. First and foremost, the critical transformer branches identified based on the *N-1* contingency analysis can also cause a severe contingency in case of an *N-2* contingency. In other words, loss of any of the critical transformers can increase the chance of system failure as it might overload the other critical transformers.

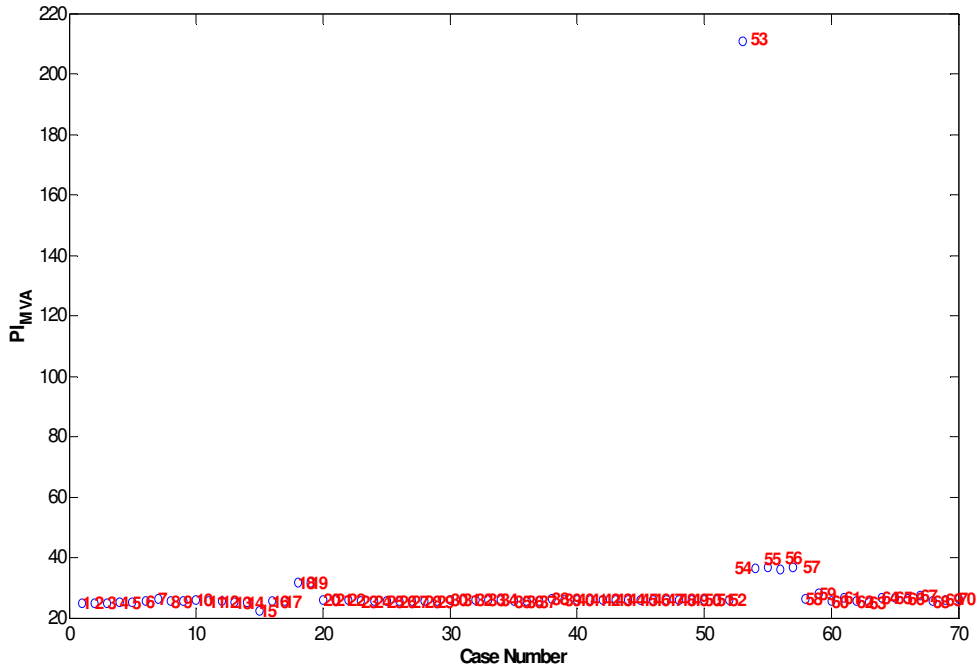

Fig. 2.10 PI_{MVA} versus contingencies number for the peak case while the 1869-1870 (69 kV/230 kV) transformer branch is out of service

2.6 Identification of the Critical Branches

Malfunction of the circuit breakers can cause permanent damage to system equipment, due to high fault currents. Moreover, it might also cause transients that have a potential of causing power outages. Circuit breaker (CB) maintenance is therefore an important part of CB operating strategy that should be done on a regular basis in order to prevent failure. However, CB maintenance might be expensive and it requires long repair times due to the fact that many of the breakers are located at remote and difficult to access areas. Remote and real time circuit breaker monitoring can be a solution to the aforementioned problem [26]. Monitoring breakers can inform the operators of the impending failures and their cause of occurrence. The operators can then decide on the proper maintenance and corrective actions to temporarily decrease the impact of the failed breaker on system operation. Moreover, circuit breaker monitoring optimizes the required maintenance while decreases the CB failure rates. Circuit breaker monitoring (CBM), however, has a complex nature since there are many parts associated with the circuit breaker operation. Hence, the monitoring system should monitor a variety of equipment ranging from the mechanical contacts to the signals received from circuit breaker control circuit. Table 2-7 lists some of the parameters that could be monitored in order to estimate status of a circuit breaker [26]. More information regarding the operation of the circuit breakers control circuit can be found in [27-28].

High costs of circuit breaker monitoring and the need for signal processing equipment are among the reasons limiting condition monitoring to only a selected

number of breakers. Therefore, an effective method that identifies a proper selection of the circuit breakers for monitoring ensures system reliability and yet reduces the cost of condition monitoring.

In order to find the critical circuit breakers, the same procedure as transformer identification is followed. However, only the PI_{MVA} index is calculated for each branch. The reason for only considering one index for calculations is the fact that circuit breaker operation depends on current interrupting capability. Hence, failure to interrupt currents above the circuit ratings may lead to damage to system components and consequently outage of the line equipped with the failed CB. As a result of this outage, excessive overloading might occur at other branches that could prevent opening of the CB contacts at those branches. Calculating the PI_{MVA} index for each contingency determines the severe cases and thus the critical circuit breakers in the system at hand.

Table 2-7 Circuit breaker parameters for monitoring

Parameter Type	Parameter
Control Circuit	Trip / Close timing
	Sequence of operation
	Auxiliary contact status
	Battery status
Operating Mechanism	Contact travel curve
	Contact velocity
	Heater status
	Friction
Main Contacts	Interrupter wear
	Contact erosion
	Interrupted current
	Circuit breaker status

Candidate circuit breakers are selected from the branches above 115 kV. This results in 122 contingencies in the studied case. The contingency in each case is outage of any of the described branches due to a circuit breaker failure. Simulation results of different load cases confirm that peak case is the better representation of the critical branches in terms of the severity of the effects caused by their outages. Figure 2.11 illustrates the plot of calculated PI_{MVA} index versus contingency number for the peak case.

As seen from these ranking results, there are three branches that seem to be more critical than the other branches in the study area, as they significantly differ in performance index in comparison with the rest of the branches. Further analysis of these critical branches shows that in fact severe overloading is caused as a result of their failure on the system. Therefore, monitoring circuit breakers available on these branches could notably increase system reliability while other circuit breakers are not as much important for monitoring purposes than these branches. These branches are referred to as branch number 42, 116, and 122 in the rest of this chapter.

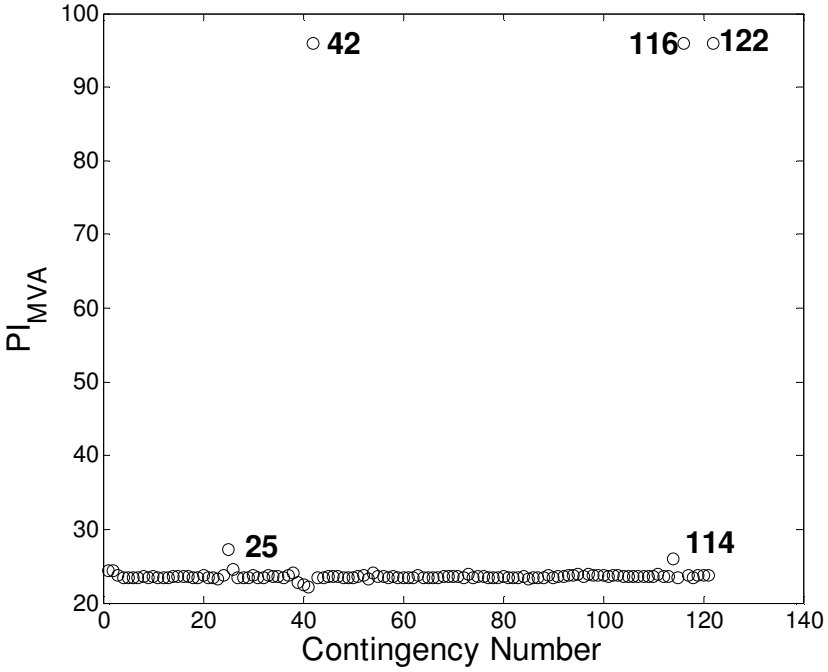

Fig. 2.11 PI_{MVA} index calculated for summer peak case for candidate circuit breakers in the system

2.7 Alleviating the Impact of Contingencies

Identifying critical transformers and circuit breakers has the advantage of locating the ideal location in the system for applying condition monitoring. Monitoring system components increases the reliability of the system by informing the operators of the impending failures. Upon receiving the data from the monitoring equipment, the operator decides on an action in order to reduce the effect of the failed circuit breaker or transformer on the rest of the system. Alleviating the consequences of the failure could be temporary or last until the failed transmission system component has been maintained.

2.7.1 Corrective actions

There are two sets of actions that could be taken in case of any contingency: corrective and preventive actions. Preventive actions, as suggested by their names, are taken in order to prevent occurrence of a failure in the future. Circuit breaker and transformer maintenance are among those actions, which are usually expensive and in most of the cases time consuming. Corrective actions, on the other hand, assume that a contingency has already occurred in the system and therefore the taken action compensates for the failed component in different ways that are shown in Fig. 2.12.

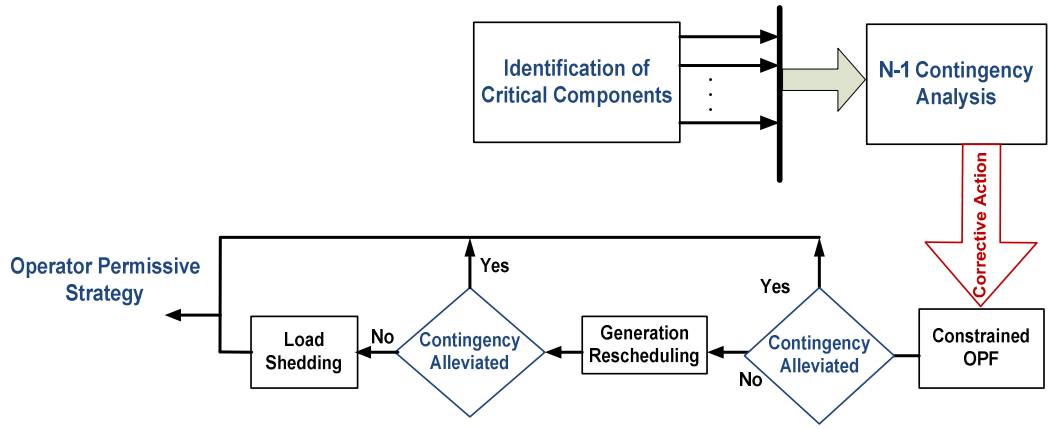

Fig. 2.12 Corrective actions taken in a smart grid in order to alleviate the contingencies

The objective of a corrective action is therefore to alleviate the effect of a system component failure by reducing or eliminating the effect of that power transmission component. As observed from Fig. 2.12 there are three sets of corrective actions that are taken in case of any critical contingency in the system. These actions are identified for each severe contingency based on offline studies

of the system at hand and once identified, are taken in case the contingency occurs in the future. However, these actions are prioritized based on their applicability to the system. In other words, actions such as load shedding are only applied to the system as a last resort, once other actions have failed to alleviate the consequences of a particular contingency.

Optimal power flow

Optimal power flow (that is, an 'optimal power flow study' or OPF) in its simplest form is a standard optimization problem that finds the optimal settings of the system while achieving a general objective. The objective of an OPF problem can vary depending on the application. Minimizing total generation cost, minimizing transmission loss, minimizing total reserve generation or minimizing slack bus generation or maximizing security margin index (SMI) are among the most important objectives mentioned in literature [29-30]. In order to solve an OPF problem, it is essential to first determine the objective function, which in case of this work it is assumed to be cost minimization. In addition to the performance index, system constraints in form of equalities and inequalities should be satisfied at all times. OPF can therefore be written in form of a general optimization problem as,

$$\begin{aligned} &Min\ F(u,x) \\ &Subject\ to:\ h(x,u) = 0 \ \text{ and } \ g(x,u) \leq 0 \end{aligned} \tag{2.8}$$

In (2.8), $F(x,u)$ is the objective function, which is a function of the control variable u and system dependent variable x, and is a scalar that is eventually minimized or

maximized depending on the problem definition. For the OPF problem an example of variable u could be generator bus voltages, generator active power output (except the slack bus), and transformer tap settings. System dependent variable x could be slack bus output power, load bus voltages, generator reactive power outputs [30].

Equality constraints are derived from power balance equations which in effect translate to active and reactive power balance equations. On the other hand, inequality constraints are the limits on control variables. Generator maximum and minimum capability, bus voltage limits, transmission line power flow limit are among the inequality constraints that should be satisfied in the optimization.

OPF problems have therefore a nonlinear nature and usually cannot be solved by conventional linear methods. Various techniques have been used to solve power system optimization problems. These methods differ in the approach taken to solve nonlinear problems and are categorized in seven major groups as follows [31]:

1. Nonlinear programming
2. Quadratic programming
3. Newton based solutions
4. Linear programming
5. Hybrid linear programming and integer programming
6. Interior point methods
7. Artificial intelligence based methods.

The first group of optimization techniques applied to solve OPF problems is nonlinear programming (NLP). These methods solve optimization problems with nonlinear objective functions and constraints. Lagrange multiplier based methods, and Kuhn-Tucker methods are examples of methods deployed to solve OPF problems in this category. In [32] Dommel and Tinney have used a NLP method to solve nonlinear OPF problem in which objective is to minimize the total fuel cost and active power loss. Concepts of penalty function are used to find the optimal solution while Lagrange multiplier approach is used to include nonlinear constraints in the optimization problem. This method was able to solve problems of power systems up to 500 busses and was the basis of the methods developed for OPF tools. The authors in [33-35] have extended the Dommel-Tinney work to improve the limitations associated with this method such as the inability to model components such as transformer taps that are not included in optimization problem [31]. The method presented in [32] is based on Newton's method in order to first find a feasible solution for the system without minimizing the objective function. Lagrange multipliers are used to include equality constraints. Equation (2.9) illustrates the Lagrangian function formulation for the OPF problem.

$$L(x,u,p)=f(x,u)+[\lambda]^T g(x,u,p) \tag{2.9}$$

In (2-9), $g(x,u,p) = 0$ is the vector of equality constraints in which p is the vector of fixed parameter. Also, $[\lambda]$ is the vector of Lagrange multipliers. In order to solve an OPF problem, the Lagrangian should be minimized. Necessary conditions of optimality are,

$$\left[\frac{\partial L}{\partial x}\right]=\left[\frac{\partial f}{\partial x}\right]+\left[\frac{\partial g}{\partial x}\right]^{T}.[\lambda]=0$$

$$\left[\frac{\partial L}{\partial u}\right]=\left[\frac{\partial f}{\partial u}\right]+\left[\frac{\partial g}{\partial u}\right]^{T}.[\lambda]=0$$

$$\left[\frac{\partial L}{\partial \lambda}\right]=[g(x,u,p)]=0 \qquad (2.10)$$

Dommel and Tinney have proposed the use of the *steepest descent* (or gradient) method to solve nonlinear equations presented in (2.10). The details of this method are presented in [36] and the idea is to start from a feasible solution to the above mentioned equations and move towards a negative gradient to reach another feasible solution with lower value of objective function. What is meant from gradient is in fact the value of the vector $\frac{\partial L}{\partial u}$. This iterative process is repeated until the gradient value is smaller than a tolerance. In each iteration control parameters *u* are changed and the whole process is repeated.

Quadratic programming relates to a category of OPF problems in which the objective function is approximated by a quadratic function while the constraints are assumed to be linear. Reid and Hasdorff have used concepts of simplex algorithm in [37] to solve the OPF problem without a need to include penalty factors or Lagrange multipliers. Instead Wolfe's algorithm is used to reduce the nonlinear system to a system with linear constraints solvable by simplex method. Other quadratic programming methods have been proposed in literature [38-40] but only a few of these methods have been applied to a real system and only with limited number of busses. One approach is essentially the

Kuhn-Tucker approach which incorporates the inequality constraints in the Lagrangian.

Newton based methods iteratively solve nonlinear equations that are derived from necessary conditions of optimality. Examples of these methods are presented in [41-42]. Linear programming (LP) techniques [43] are similar to quadratic programming in a sense that they both linearize the OPF problem and solve it with methods such as simplex. However, these two methods differ in their objective function as LP techniques also linearize the objective function. Mixed integer programming is a particular linear programming in which the variables are restricted to integers. A typical application of this method is in OPF problems with VAR planning. Interior point (IP) methods are more recent than the above described methods since they solve linear programming faster than the simplex method [31].

Since the total cost of generation is calculated in OPF problems, a cost function should be assigned to each generator in the studied area. This is due to the fact that in all rescheduling problems in this study it is assumed to be able to reschedule most of the generation resources within the studied area without a need to change power exchange between other areas. Different cost functions are defined for OPF problems [44-46]. These functions can be polynomial, exponential or a combination of polynomial and exponential functions. Also, linear cost functions have been used depending on the application. One of the most commonly used cost functions in literature is the cubic cost function. Equation (2.11) shows the cost of generation in each generator *i*,

$$C(P_i) = \left(A + BP_i + CP_i^2 + DP_i^3\right) \times FC + VO\&M \times P_i \quad (2.11)$$

FC : Fuel Cost

$VO\&M$: Variable Operations and Maintenance

Depending on the fuel type of generation, i.e. coal, natural gas, nuclear or hydro, the coefficients in the above equation can take different values. Table 2-8 shows the values for these coefficients for different generators that are used for this work. As seen from Table 2-8 coal fired systems are expected to have relatively higher generation costs than hydro or nuclear systems while hydro generation is assumed to be the cheapest among all available generation types. Therefore, it is expected to first deploy the hydro units rather than coal fired units. However, if there is any contingency in the system, more expensive units might be used in order to alleviate the contingency.

Table 2-8 Cost function coefficients for different generation types

Generation Type	A	B	C	D	Fuel Cost ($/Mbtu)	VO&M ($/MWh)
Coal fired	0	20	0.01	0	4.945	1.442
Nuclear	0	20	0.01	0	1.286	2.285
Natural Gas (Gas Turbine)	0	12.17	0.01	0	6.062	2.357
Natural Gas (Steam Turbine)	0	11.27	0.01	0	6.072	1.195
Natural Gas (Combined Cycle)	0	12.193	0.01	0	6.062	0.827
Hydro	0	10	0	0	1.00	1.287

Although OPF can be effective in alleviating over loadings caused by outages, in some severe contingencies there would not be any solution to the system with the new set of constraints. Therefore, other actions such as generation rescheduling are required to deal with the added contingency. Generation rescheduling is particularly effective if there is sufficient generation available in the neighborhood of the overloaded line. Consequently by using other generation resources, detrimental effects of the contingency could be alleviated. In the following section, some of the most stressed transformer branches are further analyzed to determine the corrective action that is effective in case these contingencies occur.

2.7.2 Study results

The most severe transformer branch outages were introduced in section 2.4. In this section the effect of those will be first investigated on the studied system followed by determining the proper actions that should be taken in case these contingencies occur in the future. Hence, the top severe transformer branch outages are analyzed in detail.

1) Transformer branch 659-660 out of service

The outage of this transformer is expected to have severe overloading effect on the other branches of the system. Summer normal peak is chosen as loading of the system. It is observed from simulation results that the outage of the aforementioned transformer will cause over loadings of up to 103% in the neighboring branches in comparison to the 14% loading of the base case. This

overloading needs to be decreased in order to ensure secure operation of the system.

As explained before, the system is analyzed to determine whether the above described overloading could be decreased by proper rescheduling. PowerWorld Simulator is used as a tool for solving a constrained OPF problem, while each generator in the study area is associated with a cost function defined based on the models available in this software. The objective function is hence to decrease the total generation cost while keeping the loading of all the branches in the studied system below 100%. Simulation results show that no possible rescheduling is able to eliminate the overloading of the aforementioned branch. In other words, this constraint is an *unenforceable* constraint in PowerWorld and consequently OPF cannot be solved. Therefore, even at the expense of increasing the generation cost, with the existing system topology, outage of the *659-660* transformer branch results in a subsequent branch overloading. This in turn could result in equipment damage, if it persists for a long period of time, and therefore cannot be permitted in the long term.

According to the above statements, the only action that could be taken in this case is to shed loads in order to be able to decrease the loading in the overloaded branch. In other words, load shedding will be the chosen action by the smart grid if the same contingency occurs in the future. As stated before, since load shedding will discontinue service to certain customers, it is chosen only as a last resort. It is also important to categorize the loads and shed the less important loads first before cutting service to more sensitive loads. However, not all the loads are

going to affect the overloading. Hence, a sensitivity analysis is carried out on the system to identify the loads that can affect the overloading, if they are shed. Therefore with the aid of a program that automatically calculates the MVA index discussed in Section 2.4 for each of the loads above 30 MW and the steady state information of the branch flows, the most effective loads are found. Figure 2.13 illustrates these study results. As seen from this figure, only three loads, marked as load numbers 28, 15, and 21, are capable of decreasing the loading of the aforementioned branch to below 100%.

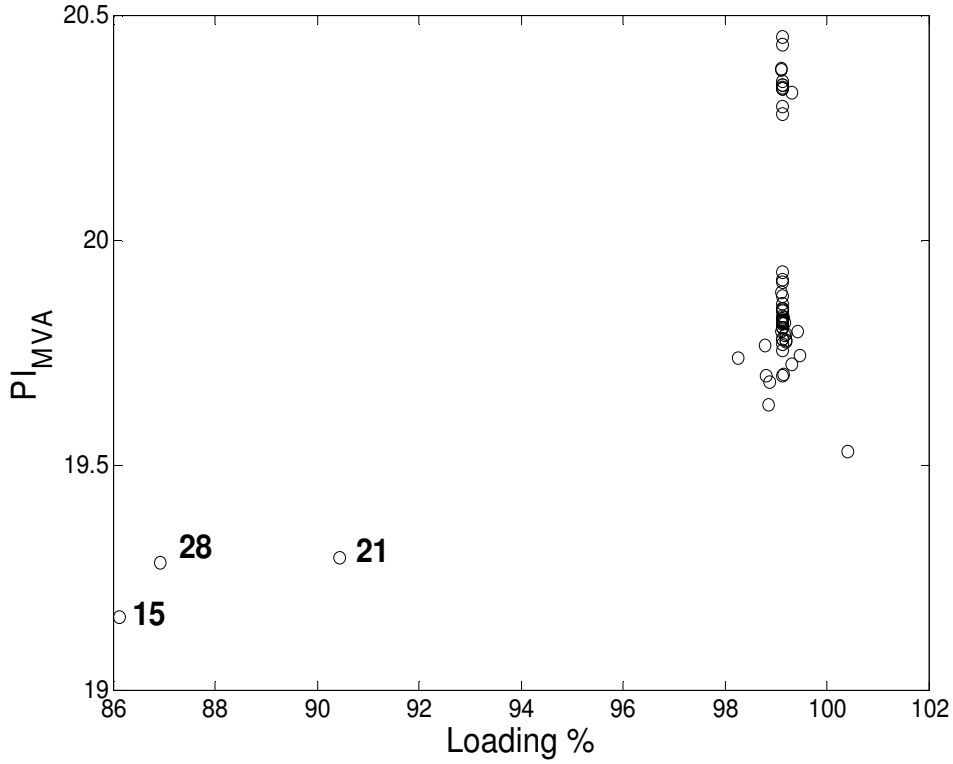

Fig. 2.13 Overloaded branch loading versus PI_{MVA} for system loads above 30MW while reduced to half

By including these loads in the previously applied OPF problem and assigning a high cost for load shedding, minimum required load shedding for any

of the three aforementioned loads is found. Table 2-9 presents these loads along with minimum shedding required from these loads. It should be noted that these values are only the minimum required to drop the overloading to just below 100%.

Table 2-9 List of effective loads in reducing overloading in case of transformer branch 659-660 outage

Load Number	Original Load (MW)	Minimum Shed (MW)
15	48	5.03
28	42.4	4.66
21	45.2	7.08

2) Transformer branch 1959-1968 out of service

Outage of this line has also shown to be a severe contingency since it overloads the parallel branch to 110% from the 55% in the base case. Therefore, a corrective action should decrease this loading to below 100%. As seen from the system map, there are quite a few generators around this transformer branch. This provides the system with more rescheduling capability than the other cases discussed before. A constrained OPF is the first action that is applied to the system analysis in order to decrease the overloading at the parallel transformer branch. With the objective of minimizing total generation cost, OPF decreases the overloading to 100%. However, it is desired to decrease this loading even further to below 100% which translates to increasing generation cost. By reducing the generation at the closest generation source to the aforementioned transformer, it is

expected to reduce the loading of this branch. Simulation results show that 40 MW decrease in generation of this source reduces loading of the aforementioned branch to 93%. With the generation cost functions defined, this generation reduction will translate to an additional 407 $/h in total generation cost as the generation reduction is compensated by another, more expensive, generation source.

3) Outage of branch number 42

As it was observed in contingency ranking results of section 2.5, outage of this branch creates a severe contingency on the rest of the system. Following the same procedure as the critical transformer branches, a solution to the contingency is sought through a constrained OPF problem. As it was expected from the ranking results, OPF is not able to find a solution to the problem while alleviating the contingencies in the system. OPF results in PowerWorld simulator indicate that there will be three branches with overloading of up to 116% as a result of outage of the aforementioned branch. Similar to the case with critical transformers, load shedding is the last resort in order to alleviate the contingency. However, sensitivity analysis results, reveal that even load shedding is not effective in decreasing the overloading caused by outage of this critical branch. It can be concluded that condition monitoring of the circuit breakers of this branch is extremely beneficial in ensuring the secure operation of the system.

2.8 Summary

This chapter discussed a method to increase power system reliability by providing more awareness to the operator of the impending failures of the system. Condition monitoring of the circuit breakers and transformers were introduced to monitor the status of these components and based on the collected data estimate the chance of a component failure.

Since it is not practical to apply condition monitoring to all the circuit breakers or transformers, contingency ranking is proposed in this work. This method is based on ranking outages of all the transformers and circuit breakers above 115 kV in order to find the most severe outages. Those components causing the most severe contingencies are referred to as critical CB or transformers which are the best candidates for condition monitoring. Performance indices based on MVA flow of the lines and bus voltages are introduced as tools for calculating the severity of each contingency.

Simulation results presented in this chapter identify the most stressed branches in the studied area. Having found the critical transformers and circuit breakers, Section 2.7 further studies the consequence of the most severe transformer branch outages. Corrective and preventive actions are suggested in this chapter in order to alleviate the effects of the contingencies and hence prevent cascading failures in the system.

Chapter 3

IMPACT OF PHOTOVOLTAIC GENERATION ON STEADY STATE PERFORMANCE OF THE POWER SYSTEMS

3.1 Integration of Photovoltaic Resources

PV resources are installed in the system and at a certain level of penetration could replace the conventional generators that are presently in use at various locations in the system. However, these resources are mostly located closer to the loads and at the lower voltage levels than the more distant conventional generation which is commonly located far from the loads and connected to them via the transmission grid. Consequently, depending on the PV penetration levels, a portion of the generation is transferred to the locations closer to the loads. This, in effect can also interrupt the amount of reactive power which is supplied to the loads due to the ratings of the lines and transmission system components such as transformers and circuit breakers. One immediate effect of this power flow interruption is changes in the bus voltages.

This chapter investigates the steady state effects of adding high penetration photovoltaic resources to the system. Steady state voltages are the main variables that are affected by the addition of the new photovoltaic resources to the system. Depending on how these voltages are altered, i.e. decreased or increased, under-voltages or over-voltages may occur across the system. Identifying the buses with high or low voltages and taking preventive actions could improve system reliability and concomitantly ensure that the system is operating within the permissible limits set by different standards.

In conducting the steady state analysis of the system it is assumed that the amount of power exchanged between the studied area and the neighboring areas is held fixed at the level being specified by the previous contracts. By adding PV resources to the system, no change in the tie-line flows is anticipated. Consequently it would be a valid assumption to assume that addition of PV resources will locally affect steady state voltages.

Although bus voltages are expected to have more variations once conventional generation is replaced by PV generation, generator rotor angles are also monitored for the purpose of comparison with the base case. It should be noted that depending on the level of photovoltaic generation, diverse effects might be observed on the system behavior. Various generation levels are studied in this chapter and the results are compared. Addition of various PV penetration levels yields different modifications to the base case in terms of the number of conventional generators that are displaced by photovoltaic generation and the amount of generation from the in service units.

This chapter describes the base case, i.e. the case with no PV systems, which is used for all of the studies performed for high PV penetration analysis. Modifications made to the base case are then presented, followed by the steady state analysis results. At the end of this chapter a simple mathematical analysis is conducted to explain the steady state behavior of the bus voltages due to the addition of the new generating resources closer to the loads. Computer simulations based on a simplified system model are carried out to compare the results with the numerical simulation results obtained earlier.

3.2 Cases and Test-Beds under Study

In order to better represent a case with high PV penetration a large power system is selected for study. The simulated case represents the entire WECC with transmission voltage levels ranging from 34.5 kV and 69 kV to, 345 kV and 500 kV. The PVs are only added to a portion of the system with a relatively large amount of conventional generation and export to other areas within the WECC. Table 3-1 presents a summary of the studied area with high concentration of utility scale and rooftop PVs. A list of all the in service generators available in the base case can be found in Appendix B. These units are later on compared to the case with solar generation available in the system.

Comparing Table 3-1 and Appendix B, it is seen that only half the generators are in service in the April case, and therefore a limited reactive support is available from the generators. Additionally, the reactive power export from the other areas is also limited which contributes to low reactive power support throughout the system.

Table 3-1 Summary of the studied area

Total Load	MW	13276
	MVAr	2188
Total Generation	MW	21571
	MVAr	2238.72
Total Export	MW	7651
	MVAr	63.4
Total Losses	MW	608
Total Number of Generators		226
Total Number of Buses		2419
Total Number of Lines		1861

The studied case is geographically located at an area that due to a relatively cooler weather conditions will experience light loading conditions around the month of April mainly due to the reduced number of the online air conditioning units. For the selected study area, these conditions are valid representations of a case with peak PV outputs and low loads.

By comparing the total load and generation given in Table 3-1, it is seen that approximately two third of the generation within the studied area is deployed to supply the local loads while the rest of the generation is exported to the neighboring areas. Table 3-2 presents a summary of the total exports to the other areas in the base case when there is no photovoltaic generation present in the system.

An important characteristic of the selected loading conditions is the fact that most of the in service loads in the April case are active loads and the reactive part of the loads is small. By further analyzing the loads it is seen that most of the loads have a reactive component less than 2 MVAr which is small in comparison to the loads during the summer peak.

Table 3-2 also reveals that the major part of the export is to Area6 and Area7, which are going to be held constant during the steady state simulations to solely examine the effect of solar generation on the studied area. This is done with the aid of the software tools that are used for steady-state analysis of the case under study. More details of the software utilized in this work will be given later in this chapter.

Table 3-2 Power export to the other areas

	MW	MVAr
Area1	416.83	-38.16
Area2	208.33	-1.7
Area3	499.98	269.95
Area4	52.8	-10.33
Area5	892.05	-108.32
Area6	2876.02	-42.27
Area7	2846.14	68.20
Area8	-60.53	-99.91
Area9	-81.70	27.15

3.3 Modifications to the Base Case

In this section the changes to the base case in order to account for the solar generation are listed. There are two projected kinds of photovoltaic systems that are expected to be installed within the study area: residential and commercial rooftop PVs and utility scale PVs. Based on the data given, the residential rooftop PVs are spread across the system at the 69 kV level buses. Depending on the amount of the PV generation that is studied, the output of these residential rooftop PVs will vary. However, the amount of these changes is relative to the installed capacity of the PV resources already available in various zones of the area under study.

As mentioned in the previous paragraph, the residential rooftop PVs are added to the existing base case based on the available data of the installed

capacity of the solar PVs within various zip codes of the studied area. Therefore the 69 kV buses selected as the location of the PV installations are chosen based on the available capacity of the installations and are then scaled up to accommodate the required amount of residential rooftops for the system , based on the level of PV penetration. Since this work is based on actual system data, a substation versus zip code map is utilized in addition to the available PV installation versus zip code data. By combining these two sets of data, a set of 69 kV buses, located in the study area, are acquired as the locations of the rooftop photovoltaic systems. The values of the installed capacity of the PVs are scaled up with the same ratio with respect to each other when increasing the amount of photovoltaic generation in different studies. Appendix C presents a list of 69 kV residential and commercial rooftop PV buses across the studied area along with their installed capacities. As seen from the data available in Appendix B, there are approximately 210, 69 kV level buses in this area that are selected as the possible locations for the rooftop PV installations. For this study, in order to keep the locations unchanged, only the bus capacities are increased for more PV generation while no additional PV installations are added to the system.

The data presented in Appendix C indicate the locations for residential and non-residential rooftop PVs that are installed in the study zones. However, for the system under study and under the RPS mandates, there is a requirement of a 200 MW utility scale photovoltaic generation for a selected number of the studied zones and 400 MW for the other half of the zones. The required utility scale solar generation plants are located within the mentioned areas in increments of 50 MW.

Therefore, there would be a total of 12 utility scale generation plants. These plants are located in the vicinity of the buses, presented in Table C-2 of Appendix C.

Since the photovoltaic generation resources are normally operated at lower voltages than the transmission system, transformers are used to step up the voltages from 480 kV to the interconnection bus voltages. These transformers should have the required reactive capability to accommodate for the active and reactive utility scale generation. The PV plants are sized at 50 MW generations with a power factor of 0.95 to comply with WECC guide [47] for photovoltaic system representation in large-scale power flow simulations.

3.4 Representation of the Photovoltaic System for Power Flow Studies

Residential rooftop photovoltaic systems, in general, generate small magnitudes of active power while characterizing no reactive capability and in contrast to conventional generators they lack inertia. Therefore, for the purpose of power flow studies, they are represented as P-Q buses or negative constant power loads with only active components. In other words, it is assumed that residential photovoltaic systems do not have any reactive power capability since no converters are assumed to be present for these sources. Consequently, depending on the level of PV generation being studied, these loads are added to the base case power flow file. Rooftop PVs are hence treated as loads in power flow equations. Figure 3.1 illustrates how the residential rooftop PV generation resources are represented for power flow studies.

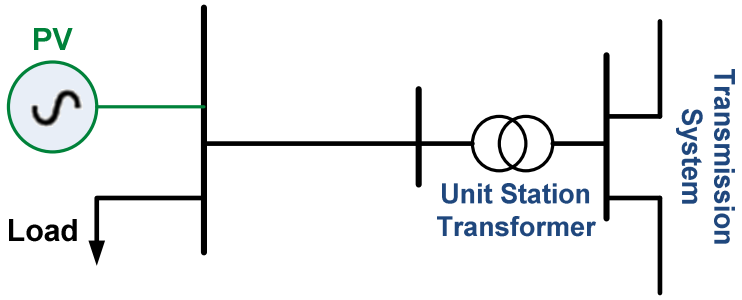

Fig. 3.1 Power flow representation of rooftop photovoltaic systems

Utility scale photovoltaic generation is equipped with converters which can be modeled in dynamic studies. Dynamic modeling of the full converters will be discussed in Chapter 4. For the purpose of steady state analysis these generation resources are modeled as conventional generators with active and reactive power generation capabilities. Additional P-V buses are added to the existing system in order to include the generators in the power flow file. Figure 3.2 illustrates the connection of the utility scale PV sources to the grid. Since these resources are treated as conventional generators, they would be included as P-V buses in power flow solutions.

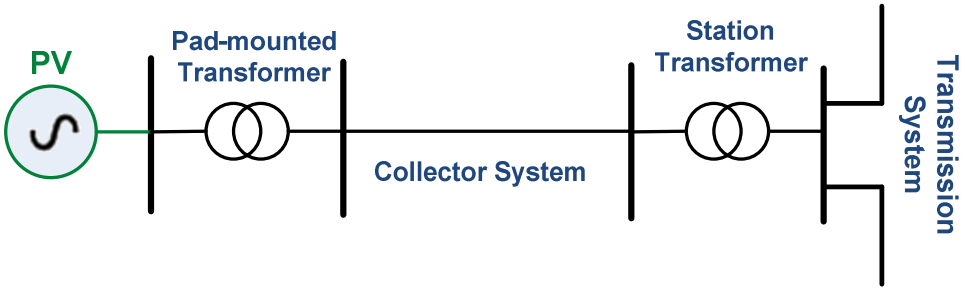

Fig. 3.2 Power flow representation of utility scale photovoltaic systems

3.5 Steady State Analysis of the System with High PV Penetration

3.5.1 Creation of the power flow study files

In the preceding section, steady state models for the photovoltaic systems were introduced and added to the base case. For the rest of this chapter, it is aimed to present the results of the steady state analysis, with increased PV penetration present at system. Although most of the focus would be on the steady state voltages, however, frequency and generator relative rotor angles will also be studied to thoroughly observe the steady-state behavior of the system.

Since only the steady state simulations are performed in this part, dynamic security assessment toolbox or DSA^{Tools} which is a software developed by PowerTech labs [25] is deployed in order to study the system. This software has different packages named, PSAT (Power flow and Short circuit Analysis Toolbox), VSAT (Voltage Security Assessment), SSAT (Small Signal Analysis) and TSAT (Transient Security Assessment Toolbox) which are powerful sources for study of large systems such as the system at hand.

In order to fully investigate the effect of PV penetration on steady state behavior of the studied system, different levels of PV generation are considered for this study. The results are compared to observe the steady state variations of the bus voltages as well as to investigate how the amounts of PV penetration is associated with those variations. It should be noted that the amount of utility scale PV generation is assumed unchanged in all the studied cases and only rooftop PVs are scaled up in order to accommodate various PV generation levels. Table 3-3 is a summary of the power generation based on the amount of PV penetration in

the system. A generic definition is used for the PV penetration levels that is provided bellow the Table. This definition is based on the total available generation within the studied area for the specific time of the year. Therefore, it is a specific type of a nameplate rating rather than an energy rating. The definition of the PV penetration used in this work is based on the available generation in the base case. While there are other methods for defining PV penetration levels, i.e. based on the system peak load [13] or by the amount of energy served, these methods are not adopted in this work. For comparison purposes, PV penetration levels are also defined based on the aforementioned methods in Table 3-3.

Table 3-3 Summary of the PV penetration levels

PV generation (MW)	2158	4316	6475	8633	10792
PV penetration level* (%)	10	20	30	40	50
PV penetration level (%) (load based)	11.2	22.5	34	45	56
PV penetration level (%) (by energy)	2.5	5	7.5	10	12.5

$$* \text{ PV Penetration}(\%) = \frac{\text{total PV generation(MW)}}{\text{total generation(MW)}} \times 100$$

A series of power flow study files are created to account for various PV penetration levels up to 50%. These power flow study files only differ in the amount of the residential rooftop PVs. As the amount of PV penetration increases, more conventional generators are required to be displaced by more PV generations. Since the system at hand is fairly large, changes like those mentioned would create a major deviation from the equilibrium point at which the power flow study converges. Therefore, a great amount of care and precision is required

in the creation of the power flow files in order to acquire a converged case. In order to do so, the PV sources are added to the system in increments and each time the power flow is solved. This is done for the case with 10% PV penetration first, and the solved case is used for the 20% penetration by increasing the amount of PV at each bus, again incrementally, and solving it in each step. The same procedure is followed for 30%, 40% and 50% penetration levels.

The addition of the sources along with the changes in their values is performed by a series of ".epc" files in PSLF which provide the capability to modify the power flow cases. The solved case can then be transferred to PSAT for further analysis. Appendix D lists the generators that have to be 'turned off' within the studied area for each penetration level. In the creation of the power flow files and thus turning off the conventional generators, a zone based strategy is taken. This translates to turning off the same amount of conventional generation in zones related to one utility as the amount of PV generation added to the system on those zones.

3.5.2 Steady state simulation results

Having created cases with different levels of PV penetration, the next step is to analyze the solved power flow cases in terms of bus voltages. These cases are transferred to PSAT where the buses of the studied area are selected and their power flow information such as the bus voltages, generators' active and reactive power generation are used to for the purpose of comparison with the base case. Since the main purpose of this work is to observe the effect of high penetration of PV systems on the transmission system, mainly buses with voltages above 69 kV

level are monitored. The following is a summary of the results achieved by steady state simulations of the system.

Starting with the case with 10% PV penetration, Table 3-4 lists the number of buses within the studied area that show more than 1% to 5% increase of their voltage magnitudes than the base case. As seen from this table, a 10% PV penetration creates some higher voltages in comparison to the base case. The maximum deviation of the bus voltages from the base case is 3% which is only observed at 8 buses. However, only a few buses show high voltage conditions that require any corrective actions.

Table 3-4 Classification of bus voltage changes for 10% PV penetration

		Bus Number	Voltage (p.u.)
Difference from the base case	1 %	Number of buses	
		1021	
	2%	296	
	3%	413	1.0404
		412	1.0538
		459	1.0353
		823	1.0500
		822	1.0372
		2401	1.0344
		2403	1.0508
		2404	1.0661
	4%	0	
	5%	0	

While these results indicated high voltage magnitudes within the entire system, most of the voltages remain within the range of ±5% tolerance. Therefore it can be concluded that a case with 10% PV penetration does not cause problematic high voltages within the studied area, although, in general, buses have higher voltages than the base case.

The same procedure is followed for the case with 20% PV penetration. The results are presented in Table 3-5 for buses with more than 1% to 5% voltage deviation from the base case. 20% PV penetration has caused more buses to deviate from their base values. Not only more buses are exhibiting more variations, but also some buses fall in the category of 4% and 5% increase in their steady state voltages. In fact, some of these high voltages can be treated as voltage violations since they violate the ±5% voltage tolerance.

One reason for these increased voltages is that increasing the amount of local, distributed generation, results in more local supply of the loads and replacing several distant generators with PV generation. Therefore, less sources of reactive power will be available at the system while the amount of inter area interchange is kept constant. This, in effect will result in limiting the amount of reactive power that can be flown through the transmission lines in order to satisfy the system requirements. Analytical explanations of the results are provided at the end of this chapter that once again confirm the results acquired in this part.

Table 3-5 Classification of bus voltage changes for 20% PV penetration

		Bus Number	Voltage (p.u.)
Difference from the base case	1 %	Number of buses	
		508	
	2%	618	
	3%	345	
	4%	36	
	5%	11	
		413	1.0649
		412	1.0780
		823	1.0739
		822	1.0600
		2112	1.0755
		2113	1.0737
		2123	1.0767
		2401	1.0570
		2402	1.0552
		2403	1.0742
		2404	1.0898

By increasing the PV penetration to 30% one may expect to see even more overvoltages occurring in the system. However, it is seen that the steady state voltage deviations from the base case are either slightly different than the 20% case or similar to it. These results are presented in Table 3-6. The first immediate explanation of this similarity is that most of the loads in the studied area, during the light loading conditions, are active loads and therefore less reactive power is

required from the generating resources. Therefore, the 20% penetration and 30% penetration levels are almost saturated in terms of the reactive power requirements of the system. As a result of this phenomenon, removing more generators from service will not create more overvoltages. Also, most of the conventional generators with higher reactive power generations have already been removed from service in the 20% case thus yielding no significant change from the 30% PV penetration case.

Although it is expected to observe the same steady state voltage behavior for the case with 40% and 50% PV penetration, which is in fact a considerable amount of PV addition to the system, it is seen that the voltage differences with the base case start to decrease. In other words, by further increasing the amount of PV penetration levels, there would be less over voltages across the system than the previous cases. This phenomenon can be observed from Table 3-7 and Table 3-8 for 40% and 50% PV penetration respectively.

To better observe the steady state behavior of the bus voltages under different PV penetration levels, the most severe bus voltages in terms of over voltages caused are plotted versus the amount of PV penetration. Simulation results presented in Fig. 3.3 reveal the behavior of the steady state bus voltages with the increase of PV generation. The results shown typify the results seen in a wide range of simulation studies. Although only few of the bus voltage magnitudes are shown, the same quadratic type behavior is observed in all the buses of the studied area.

Table 3-6 Classification of bus voltage changes for 30% PV penetration

		Bus Number	Voltage (p.u.)
Difference from the base case	1 %	Number of buses	
		522	
	2%	578	
	3%	289	
	4%	88	
	5%	23	
		413	1.0757
		412	1.0886
		60	1.0755
		126	1.0226
		125	1.0116
		820	1.0386
		823	1.0871
		822	1.0727
		1445	1.0648
		1446	1.0542
		1647	1.0826
		1841	1.0802
		2112	1.0824
		2113	1.0807
		2123	1.0836
		2330	1.0402
		2399	1.0053
		2400	1.0052
		2401	1.0695
		2402	1.0673
		2403	1.0873
		2404	1.1030
		2496	1.0358

Table 3-7 Classification of bus voltage changes for 40% PV penetration

		Bus Number	Voltage (p.u.)
Difference from the base case	1 %	Number of buses	
		560	
	2%	156	
	3%	23	
	4%	13	
	5%	16	
		126	1.0325
		125	1.0208
		211	1.0458
		210	0.9897
		413	1.0634
		412	1.0765
		823	1.0848
		822	1.0705
		1647	1.0761
		1841	1.0726
		2399	1.0149
		2400	1.0145
		2401	1.0674
		2402	1.0645
		2403	1.0850
		2404	1.1007

A simple explanation for this voltage behavior would be the fact that more loads are supplied locally and there are no more reactive power requirements than the previous cases due to the fact that most of the loads only require active power. In the later parts of this chapter, steady state voltages of some of the buses are plotted in order to better observe the steady state behavior of the bus voltages.

Steady state voltages of the system increase with the increase of up to 30% in PV penetration, although for a few buses the peak value occurs at 20% PV

generation. As more PV generation is added to the system, steady state voltage magnitudes drop until they reach closer to their base case values.

Table 3-8 Classification of bus voltage changes for 50% PV penetration

		Bus Number	Voltage (p.u.)
Difference from the base case	1 %	Number of buses	
		50	
	2%	14	
	3%	11	
	4%	5	
	5%	11	
		126	1.0320
		125	1.0204
		211	1.0440
		210	0.9879
		823	1.0712
		822	1.0574
		2399	1.0144
		2400	1.0141
		2401	1.0544
		2403	1.0716
		2404	1.0871

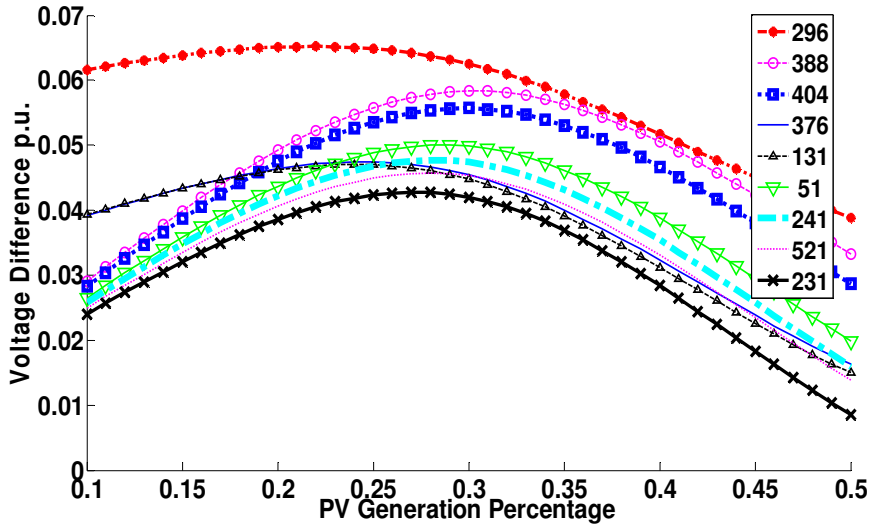

Fig. 3.3 Steady state voltage deviation of the system buses with varying PV penetration levels

Overvoltages caused by high PV penetration attain a peak of up to +10% increase in some buses within the study area. Thus, corrective actions are required to prevent these buses reaching their peak values as more PV systems are added. Switching off the capacitive shunts or adjusting the conventional generator voltages are examples of the preventive measures that are taken to mitigate the adverse effects of high PV penetration.

Reactive power flows of the system with different scenarios are illustrated in Fig. 3.4. Due to their dependency, variation of the reactive power generation is consistent with the voltage magnitude changes across the system. The power flow study results presented in Fig. 3.4 show that reactive power losses tend to decrease while PV penetration is increased to 30%. The reactive power export is at its maximum value during this time period. With the addition of more PV generation, reactive power export decreases while the reactive power generated by the synchronous generators tend to increase with a slower rate than the increase in the reactive power losses. Additional required reactive power is imported from other areas. This import results in the reversal of the reactive power flow in parts of the system.

The reason for more reactive power generation after 30% penetration of PV generation is the fact that at this point the rooftop PV systems can contribute to the active power flow within the system and hence result in reversal of the active power flow from the loads towards the transmission system. Conventional generators are provided with greater latitude for reactive power generation. Improved voltage magnitudes at PV generation levels higher than 30% result

from this behavior of the reactive power flows due to the reversal of the active power from the load to the transmission system.

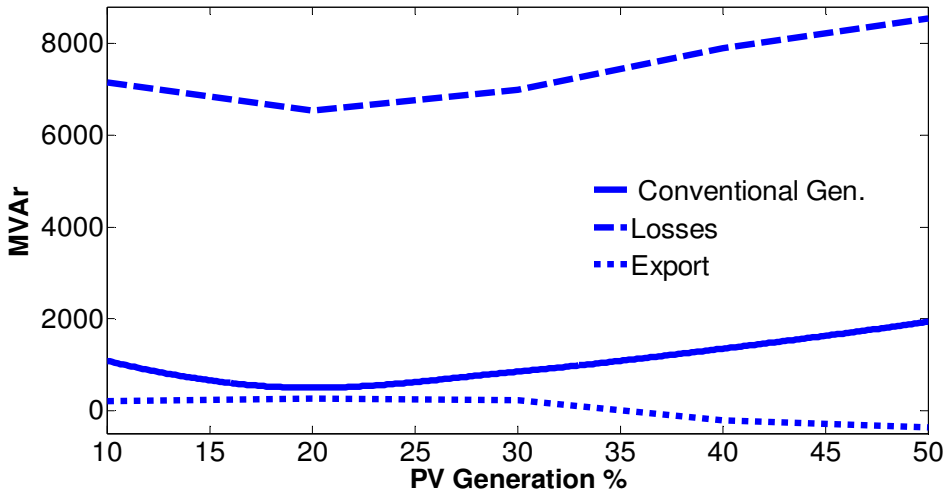

Fig. 3.4 Reactive power flow summary of the studied area under various PV penetration levels

3.6 Analytical Explanation for Steady State Behavior of Bus Voltages

Quadratic type behavior of the steady state voltages observed in the preceding section suggests an analytical study of a representative simplified system. It is useful to analytically corroborate the observed behavior. An analytical explanation of the results is sought by deriving the steady state equations of a simplified two bus system. Figure 3.5 presents the schematic of a simplified two-bus system used for studies carried out in this section.

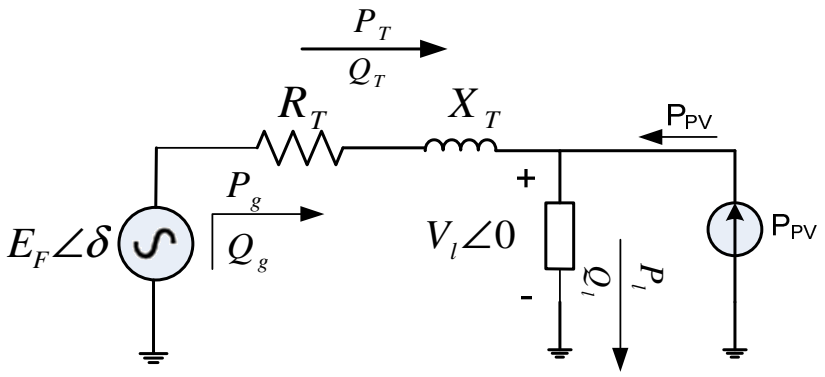

Fig. 3.5 Simplified two bus representation of a system with PV

Conventional generation is represented by its Thévenin equivalent and the PV source is assumed to be at the load side. Also, it is assumed that the PV source is only providing active power and therefore the conventional generator is the only source of the reactive power available to the load. It is also assumed that the load has a constant power factor. The transmission line is represented by an equivalent resistance R_T and inductance X_T. Steady state equations are written for the above mentioned system and the steady state load voltage, V_l, is found in term of the amount of PV generation, P_{pv}. Steady state equations of the system presented in Fig. 3.5 are solved in order to represent the load voltage V_l, in terms of the amount of PV generation, P_{pv}.

$$S_g = \left(E_F\angle\delta\right)I^* = \frac{\left|E_F\right|\left(\cos\delta + j\sin\delta\right)\left(\left|E_F\right|\left(\cos\delta - j\sin\delta\right) - \left|V_l\right|\right)}{R_l - jX_T} \tag{3.1}$$

$$P_g = \mathrm{Re}\left\{S_g\right\} = \frac{|E_F|}{{R_l}^2 + {X_T}^2}\left(R_l|E_F| + |V_l|\left(X_T\sin\delta - R_l\cos\delta\right)\right) \tag{3.2}$$

$$Q_g = \mathrm{Im}\{S_g\} = \frac{|E_F|\left(X_T|E_F| - |V_l|R_l \sin\delta - |V_l|X_T \cos\delta\right)}{R_l{}^2 + X_T{}^2} \tag{3.3}$$

$$S_T = V_T I^* = \frac{\left[|E_F|(\cos\delta + j\sin\delta) - |V_l|\right]\left[|E_F|(\cos\delta - j\sin\delta) - |V_l|\right]}{R_l - jX_T} \tag{3.4}$$

$$P_T = \mathrm{Re}\{S_T\} = \frac{|E_F|^2 R_l - 2|E_F||V_l|R_l \cos\delta + |V_l|^2 R_l}{R_l{}^2 + X_T{}^2} \tag{3.5}$$

$$Q_T = \mathrm{Im}\{S_T\} = \frac{|E_F|^2 X_T - 2|E_F||V_l|X_T \cos\delta + |V_l|^2 X_T}{R_l{}^2 + X_T{}^2} \tag{3.6}$$

$$Q_g = Q_T + Q_l \quad \text{assumption: } Q_l = kP_l \tag{3.7}$$

Further simplification yields,

$$|E_F||V_l|\left(X_T \cos\delta - R_l \sin\delta\right) = kP_l\left(R_l^2 + X_T^2\right) + |V_l|^2 X_T \tag{3.8}$$

$$P_l = P_{Pv} + P_g - P_T \tag{3.9}$$

Combining (3.2), (3.5) and (3.9) gives,

$$\rightarrow |V_l||E_F|(X_T \cos\delta - R_l \sin\delta) = kP_l\left(R_l{}^2 + X_T{}^2\right) + |V_l|^2 X_T$$

$$|E_F||V_l|\left(-X_T \sin\delta - R_l \cos\delta\right) = \left(P_{PV} - P_l\right)\left(R_l^2 + X_T^2\right) - |V_l|^2 R_l \tag{3.10}$$

Equations (3.8) and (3.10) are combined revealing a quadratic characteristic for load voltage V_l in terms of PV generation, P_{PV},

$$\left|V_l\right|^4+\left(P_{PV}-P_l\right)^2\left(R_l^2+X_T^2\right)+k^2P_l^2\left(R_l^2+X_T^2\right)-2\left|V_l\right|^2R_l\left(P_{PV}-P_l\right)$$
$$+2kP_lX_T\left|V_l\right|^2-\left|V_l\right|^2\left|E_F\right|^2=0 \tag{3.11}$$

Equation (3.11) is quadratic, representing the relationship between the load voltage magnitude $|V_l|$ (the 'open circuit solution') and the amount of solar generation P_{PV}. Solving this equation yields four solutions from which only one is a feasible solution for the bus voltage magnitude. This voltage magnitude is plotted versus the amount of PV generation in p.u. for two sets of system parameters which is illustrated in Fig. 3.6.

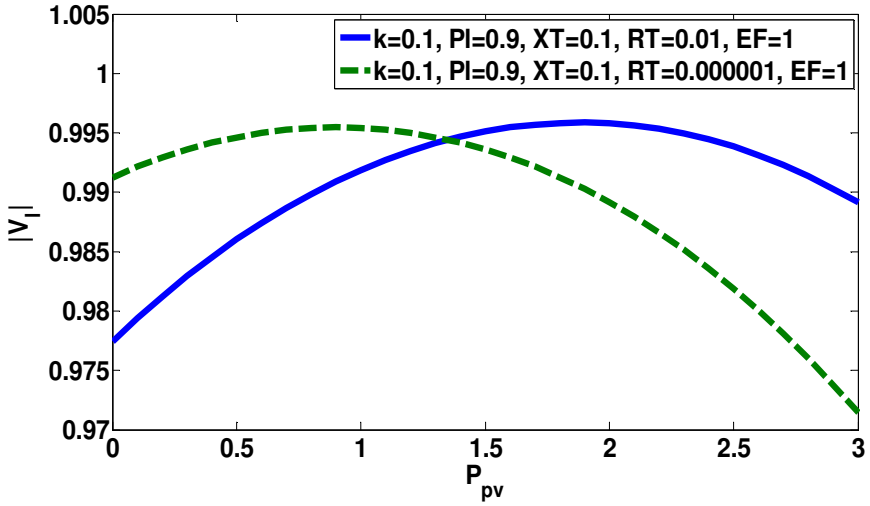

Fig. 3.6 Variations of the load voltage versus the amount of solar generation for a two bus system

By comparing the voltage magnitudes plotted in Fig. 3.6 and the simulation results of Fig. 3.3 it is observed that the voltages exhibit a similar behavior in both cases as PV generation increases. Hence, the analytical results corroborate the results obtained from the simulation. In this figure, two sets of parameters which differ in line resistance are plotted, which shows the effect of resistance on the amount of PV generation required to peak the voltage. In other

words, the more the resistance and line losses, the more the amount of PV generation is required to pass the peak point of the steady state voltage.

3.7 Summary

This chapter investigated the impact of high PV penetration on static stability of the system. Steady state analysis was conducted to observe voltage levels at various buses while different PV generation levels were present in the system. Simulations were performed using DSA^{Tools} which is a software package mainly utilized for power flow studies. Simulation results revealed that steady state voltages tend to increase at higher PV generation levels of up to 30%. As generation levels increase further, voltages move closer to their original values. Analytical calculations of a simplified two-bus system confirm the simulation results.

Chapter 4

DYNAMIC ANALYSIS

4.1 Introductory Remarks Related to the Dynamic Response of a Power System

The *steady state* behavior of voltages in an interconnected power system were observed and analyzed in the previous chapter. The objective of this chapter is to study the *dynamic* behavior of the system dealing with various disturbances in the system. In a large interconnected system such as the WECC, a small change in one area will also affect the other neighboring areas. This will consequently change the amount of inter area interchanges which is normally required to be kept constant. As stated in the previous chapter, the addition of new PV resources and the replacement of conventional generators results in less sources of reactive power since most of the PV units are residential and are assumed to be mainly sources of active power. These characteristics of the PV systems might affect the dynamic performance of the system specifically when reactive power supply to the loads is interrupted for any reason.

Replacing conventional generation resources will also result in less inertia in the system which might be a reason for potential angle stability problems. These problems mainly occur during various disturbances in the system ranging from bus faults to the loss of a generating unit and line removals. It is vital to monitor generator relative rotor angles during diverse disturbances to ensure that the system is not prone to instability while these new PV resources are added to

the system. One direct advantage of this study is that it helps to locate the most critical generating stations and also most vulnerable locations of the system. This information is later taken into account with the addition of the new PV resources. In light of these studies, power system planners will identify the best locations to add the PV resources. These locations are selected based on the severity of the adverse dynamic effects on the system as well as the potential beneficial impacts. Both PSLF and DSA^{Tools} are deployed for the studies carried throughout this chapter. However, a major part of the studies is carried using PSLF due to the availability of the models for utility scale PVs. These models will be introduced in detail in the next section.

In the subsequent sections of this chapter, different scenarios are studied and their dynamic effects on the system are examined. The aim is to cover a wide range of disturbances such as loss of a generator, line removal, and bus faults. The results of these studies will help identify the challenges associated with the systems equipped with high levels of PV generation.

4.2 A Dynamic Model of PV Resources

Steady state models of the residential rooftop PVs were provided in Chapter 3. For dynamic studies, residential rooftop PVs are modeled as in the power flow studies, i.e., as constant loads at the load buses. However, the utility scale photovoltaic resources will differ in their model from the power flow studies. This is due to the fact that these units are equipped with converters that need to be modeled in order to better represent their dynamic behavior.

As suggested in [48], General Electric type 4 wind turbine full converter models that are available in PSLF can approximately represent the full converter models for the PV units. Figure 4.1 shows the schematic of the model used in PSLF. Components that contribute to the dynamic behavior of these models are as follows:

- *converter model* -- a full converter model is provided to fully represent the dynamic behavior of the utility scale PVs while due to the fast operation of the converters DC side dynamics are neglected;
- *control model* -- controllers are included in this model to control active and reactive power as well as the current of the converter;

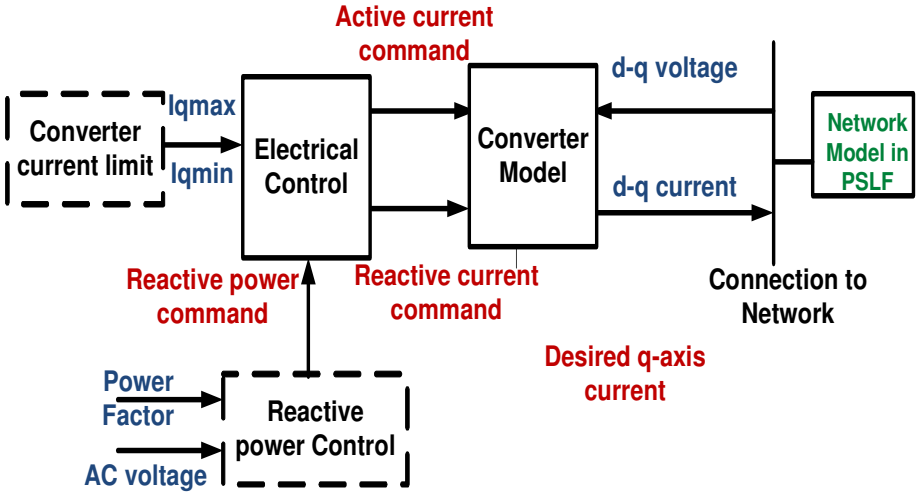

Fig. 4.1 A dynamic representation of a utility scale PV in PSLF

As seen from Fig. 4.1 the suggested model has control capabilities which include reactive power and current control capabilities. In fact, two models are required from the PSLF model library in order to fully represent the converter and its control aspects: the control model (ewtgfc) and the converter model (gewtge).

Figure 4.2 is a block diagram representation of the models used in PSLF [48]. A detailed description of these models can be found in [49].

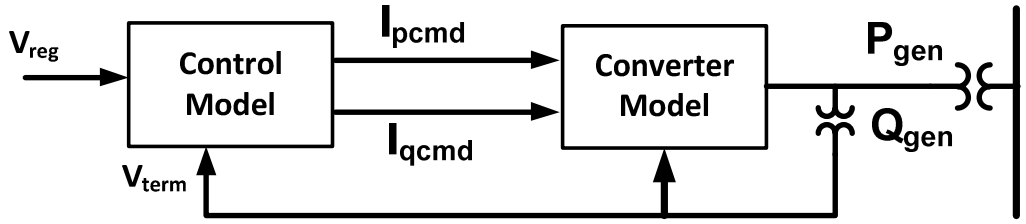

Fig. 4.2 PSLF Models used for representing utility scale PVs

4.2.1 Converter model

The converter model shown in Fig. 4.2 provides the interface between the solar plant and the network. This model is a current source that algebraically calculates the injected current into the network based on the active and reactive current commands being provided by the control model. Figure 4.3 illustrates the converter model with default values for the control blocks [49]. This model assumes a constant value for the active current command which is derived from the power flow solutions of the network. However, if it is desired to have a time varying active current due to solar cell characteristics and parameters such as variations in the amount of irradiance, a user-written solar model should be used to represent these variations.

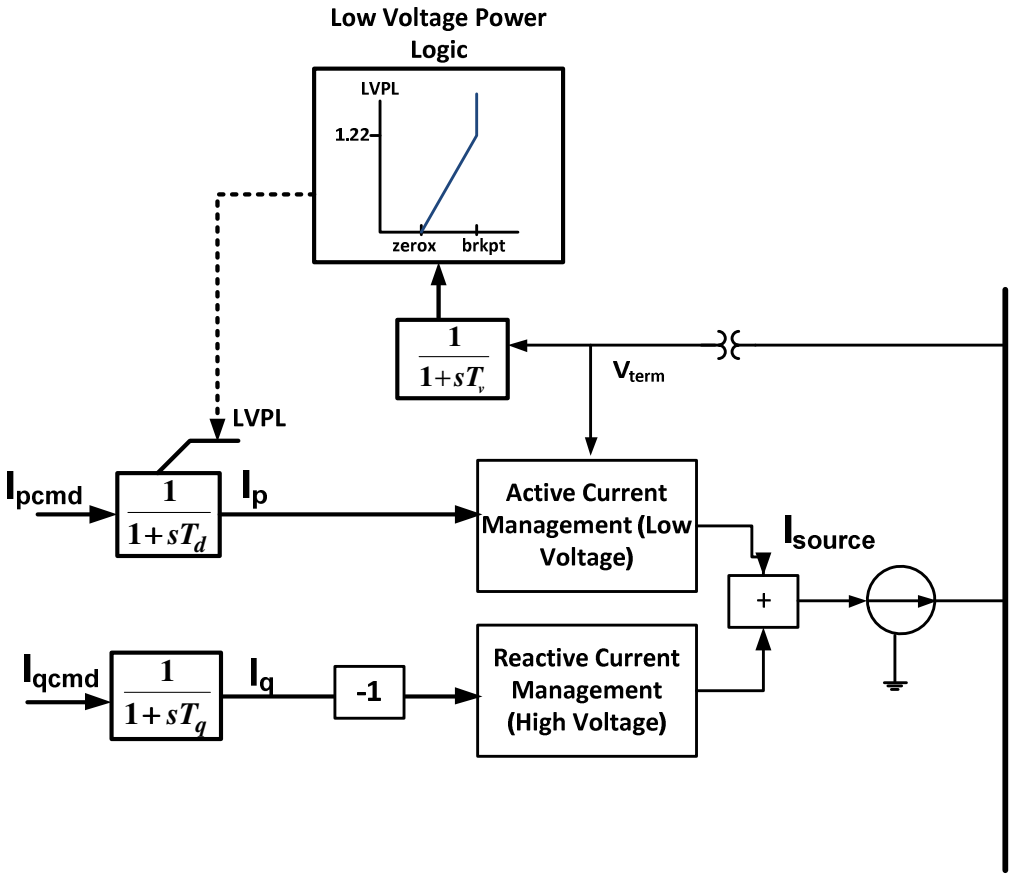

Fig. 4.3 Converter model in PSLF

The low voltage power logic (LVPL) included in the model is meant to decrease the system stress following a fault in the system. This control block is not active under normal operating conditions. A fault that results in an abnormal low voltage conditions, namely the breakpoint, will limit the active current command by providing an upper limit on its value. This limit is set to zero for the zero-crossing point. It should be mentioned that all the values related to the zero-crossing point and breakpoint are user-defined. The two additional blocks of the "High voltage reactive current management" and "Low voltage active current management" are algebraic models rather than control blocks that are intended to

limit the current for extraordinary voltage conditions. The converter model is also equipped with zero voltage ride through (ZVRT) capability that requires the plant not to trip for less severe events. The severity of the events and hence the associated parameters, such as the low voltage level and time duration of the event, for ZVRT are defined contingent on the application.

4.2.2 Control model

The control block consists of three major parts that control the active and reactive power current injections. These units are shown in Fig. 4.4 and are as follows [49]:

- Electrical controller: This model is equipped with converter current limiter that prevents a combination of the real and reactive currents to exceed the converter capability. This combination is determined by assigning a priority to real or reactive power. The current limiter is an algebraic control while the details of this model can be found in [51].
- Power factor regulator: Figure 4.5 presents the block diagram of this model as used in PSLF. This option is activated by setting the appropriate flag (pfaflg) to 1.
- SolarCONTROL emulator: The SolarCONTROL model is in fact a voltage controller that monitors a specific bus voltage and compares it with a reference bus voltage. Figure 4.5 also presents a schematic of this controller in PSLF [49]. The parameter f_N is used to represent the wind plant, and therefore is set to 1 for solar plant representation.

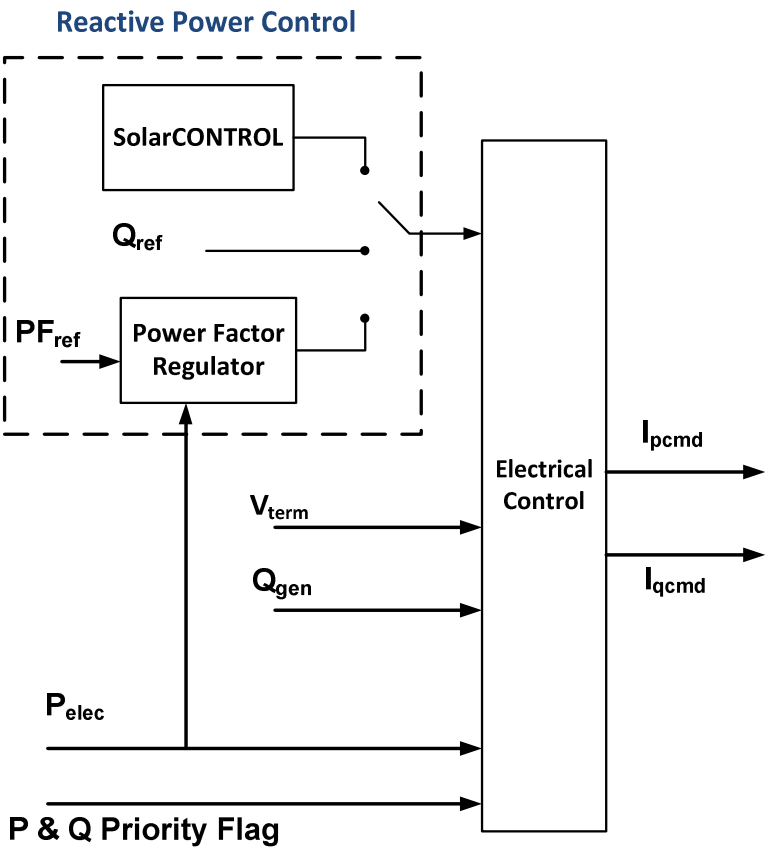

Fig. 4.4 Control block in PSLF [49]

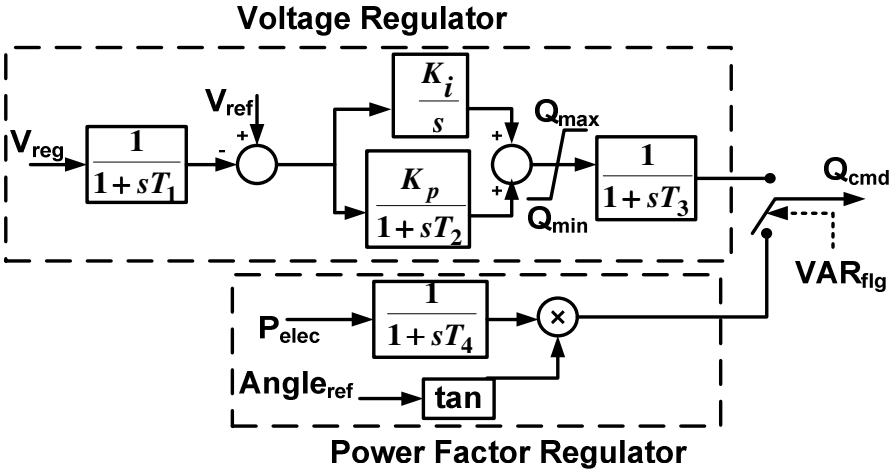

Fig. 4.5 The reactive power control model in PSLF used to represent a reactive power controller in utility scale PV simulation studies

Transient stability is the ability of the power system to maintain synchronism during *large* disturbances. These disturbances range from equipment and line outages to bus faults or even a cloud cover in case of the photovoltaic generation. The time frame of interest is generally 3 - 5 s following a disturbance and depending on the system, the time frame might extend to 10 - 20 s [50].

Generator – turbine inertia generally plays a key role in providing synchronizing capability to the synchronous generators whenever a disturbance results in a mismatch between the mechanical power input and electrical power output of the generator. Since in a system with high PV penetration, some of the synchronous generators are replaced with PV units, the overall system inertia is dramatically decreased which can lead to potential system problems during various disturbances.

The synchronizing power capability of the systems can also be affected by the angle differences of the bus voltages. Large injection of power from PV resources will cause the voltage angles across the ac system to adjust to accommodate the injection of power from such resources. As a result, the angle differences between the ac bus voltages will increase, reducing the synchronizing power capability.

The effect of high PV penetration on system dynamic behavior is also impacted by other parameters such as the type of the disturbance and its location with respect to the PV systems and the large scale generating units. These effects will be studied in the subsequent sections by simulation studies being carried on the system described in Chapter 3. The objective of these simulations is to

examine if various system disturbances affect the system in a different way with high PV penetration levels present in the system. Simulations are conducted for disturbances that range from three phase faults at several buses to double line outages. Interruption of the output of the PV systems is simulated in terms of a cloud cover scenario. These simulations are classified in the following sections. Several cases has been simulated for the purpose of this study, however, only few candidate cases are reported in this chapter.

4.3 Loss of a conventional generator

Loss of a conventional generator during normal operation of the system can cause angle instability or voltage oscillations depending on the output of the generating unit and its location with respect to the PV resources. This is due to the fact that with high penetration levels power systems are highly dependent on the reactive support being supplied from the non-displaced conventional generators. A major loss or reduction in the output of these units, which can occur due to a maintenance or system fault, can lead to subsequent problems in the system, varying by the amount of PV penetration.

The loading conditions of the system can also alleviate or worsen the effect of a generation loss across the system. Since we are considering the light spring loading conditions, as it will be observed from the simulation results, we might not observe major instability problems which are directly caused by the addition of the PV resources. However, these cases might be problematic when

considering the peak cases rather than the April case. For the case of this research, only the light loading conditions are studied.

For all the simulations conducted in this chapter the cases with 20% and 40% PV penetration are considered. Details of these cases can be found in Chapter 3 as well as the Appendix D. The only required modification is the addition of utility scale PV models to the existing dynamic models. Two different cases are studied in this part, which are mainly related to loss of a large generating facility. The reason these two are selected is their high contribution to the reactive power generation in the studied system. Also, it is important to investigate how the system with distributed PVs would respond to a major loss of active power generation. In all the simulations carried throughout this chapter, the results are compared with the case with no PV in the system to solely investigate the improvements or adverse effects of the PV installations. In addition to comparison to the base case, this study will identify whether there would be a critical penetration level in which the system with be at the threshold of instability. Next, case study descriptions along with the PSLF simulation results are presented.

Case A: Loss of large gas unit

The three generating units shown in the one line diagram of Figure 4.6 have significant contribution to the total generation in the studied area. In this case it is assumed that one of the generating units, i.e. the BB2 generator located at bus 1489, is switched off the service during normal operation of the system at simulation time 1 s. This translates to loss of 803 MW of active power and 53

MVAr of reactive power from the power generation of the system. The other two units have the same level of power generation in comparison to the unit removed from the service.

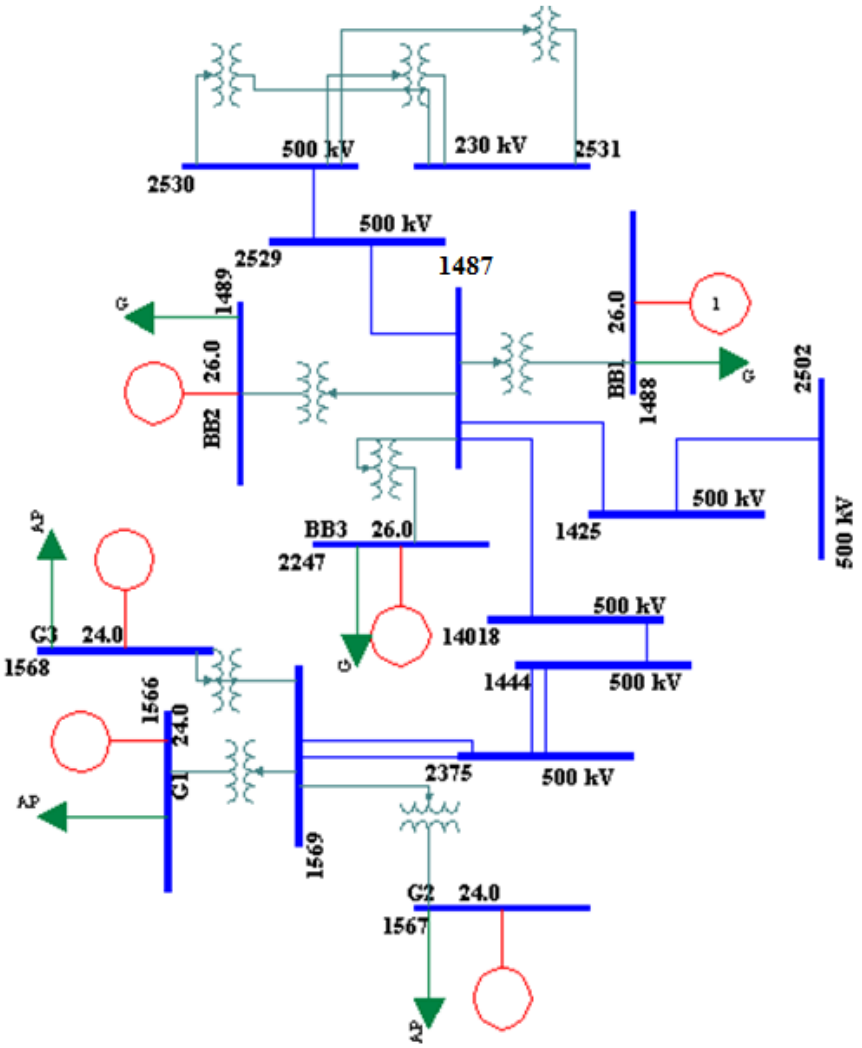

Fig. 4.6 One line diagram of the system in vicinity of the bus 1489

As seen from the diagram, the system is located close to the 500 kV level buses within the transmission system. Therefore, any voltage variations in these buses could propagate farther along the transmission system. The location of this

generator is also in vicinity of the other three major generating units, i.e. G1-G3. Hence, monitoring these units following any disturbance is also vital in identifying the crucial outages within the system.

Simulation results are presented in Fig. 4.7-4.11. The solid lines represent the case with no PVs present in the system while the dashed lines correspond to the cases with various PV penetration levels.

Simulation results show that loss of this generating unit does not cause any noticeable oscillations in the relative rotor angles at the neighboring large generating units. However, the steady state values of the rotor angles tend to be higher in the systems with higher values of PV penetration in comparison to the base case.

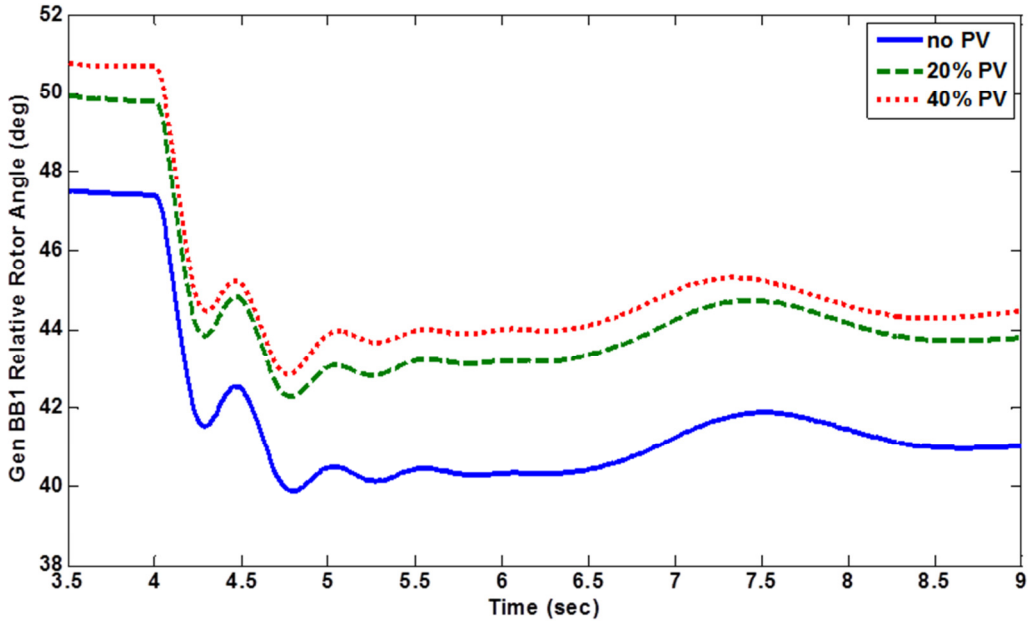

Fig. 4.7 Relative rotor angle of the generator at bus 1488, BB1 for various penetration levels

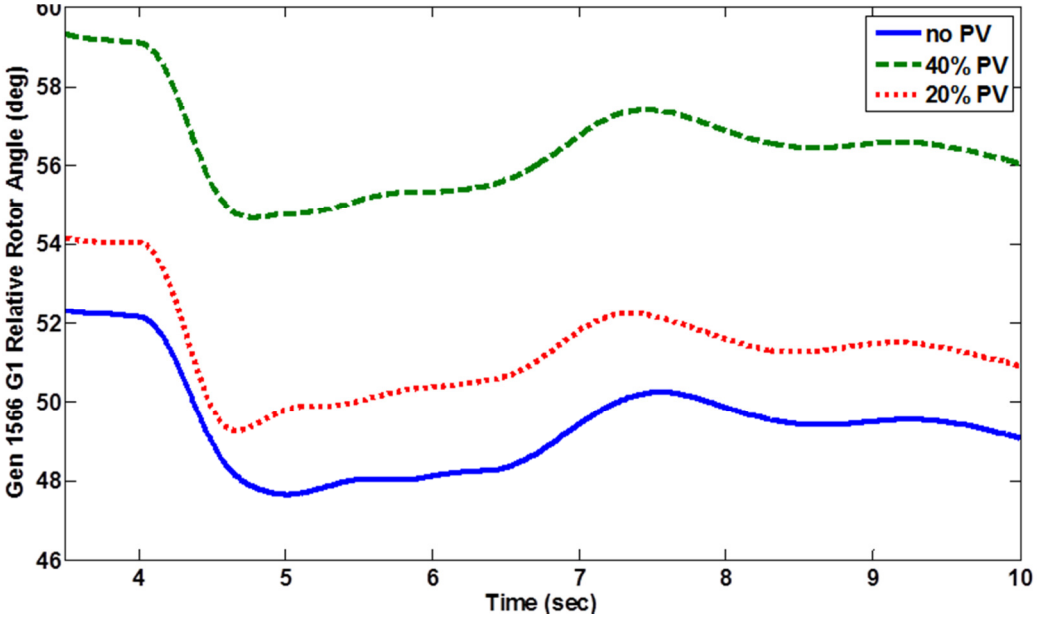

Fig. 4.8 Relative rotor angle of the generator at bus 1566, G1 for various penetration levels

It is observed that this generation loss does not cause any voltage problems in the system, while it will result in frequency drop at the buses. Although, the frequency drop and voltage oscillations caused by the disturbance is the same in the 20% PV case and the case with no PV, as the level of PV penetration is increased to 40% more oscillations are observed in both the parameters.

Having installed PVs during light loading conditions does not result in a significant change in the voltage or frequency. It should be noted that having dropped the BB2 generating unit will initially cause significant oscillations in the neighboring generators' outputs, as illustrated in Fig. 4.12. This is due to the fact

that originally the generators closer to the point of disturbance will pick up the needed generation.

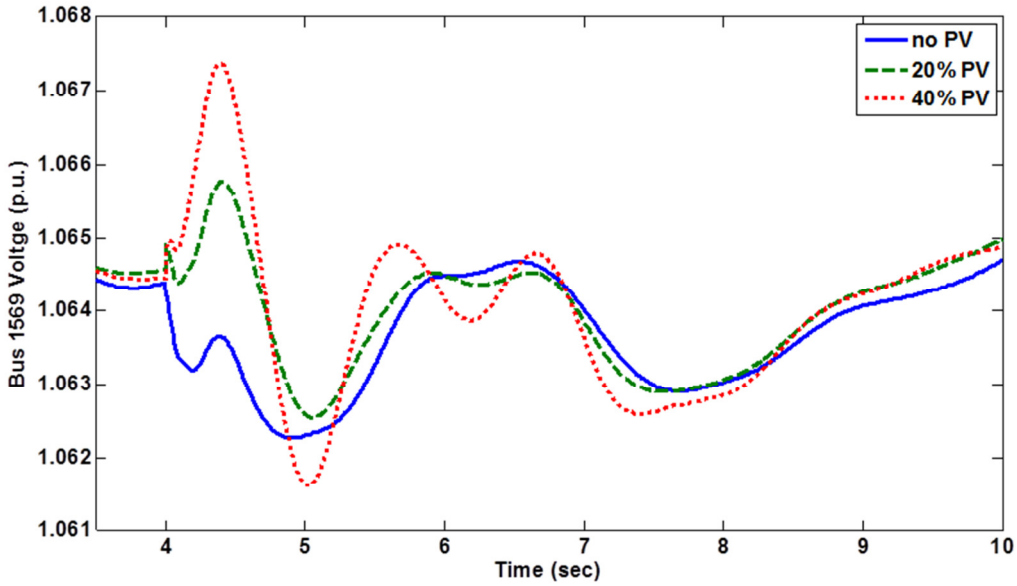

Fig. 4.9 Bus 1569 voltage for various penetration levels

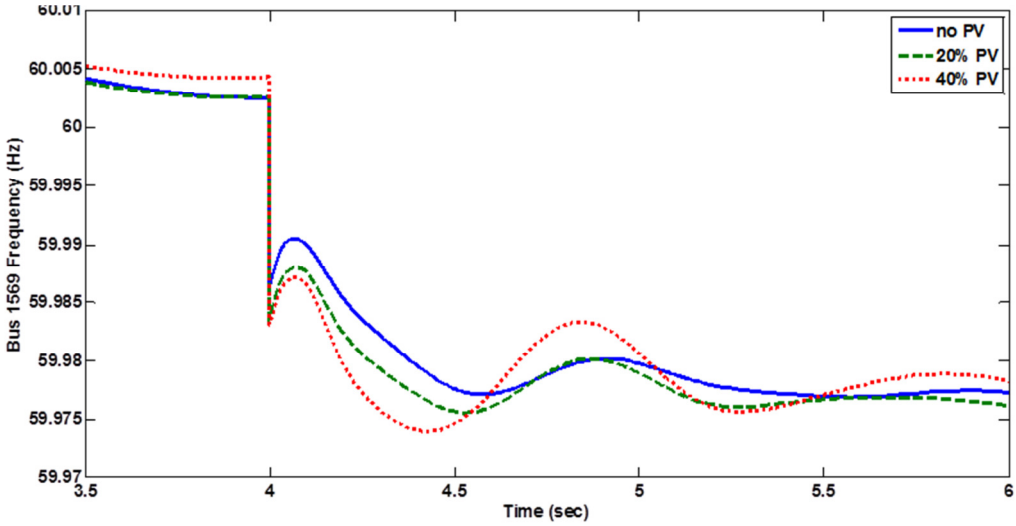

Fig. 4.10 Bus 1569 frequency for various penetration levels

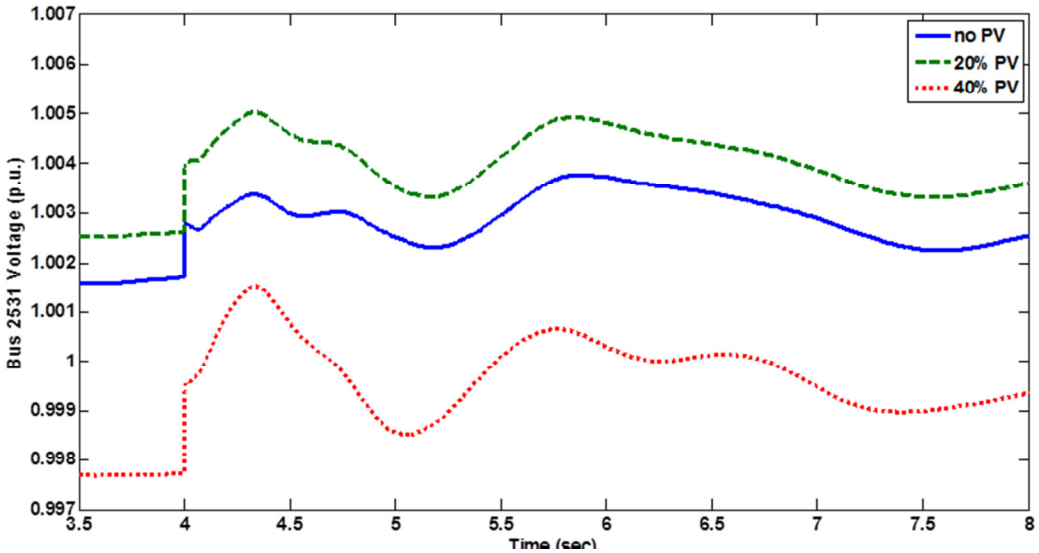

Fig. 4.11 Bus 2531 voltage for various penetration levels

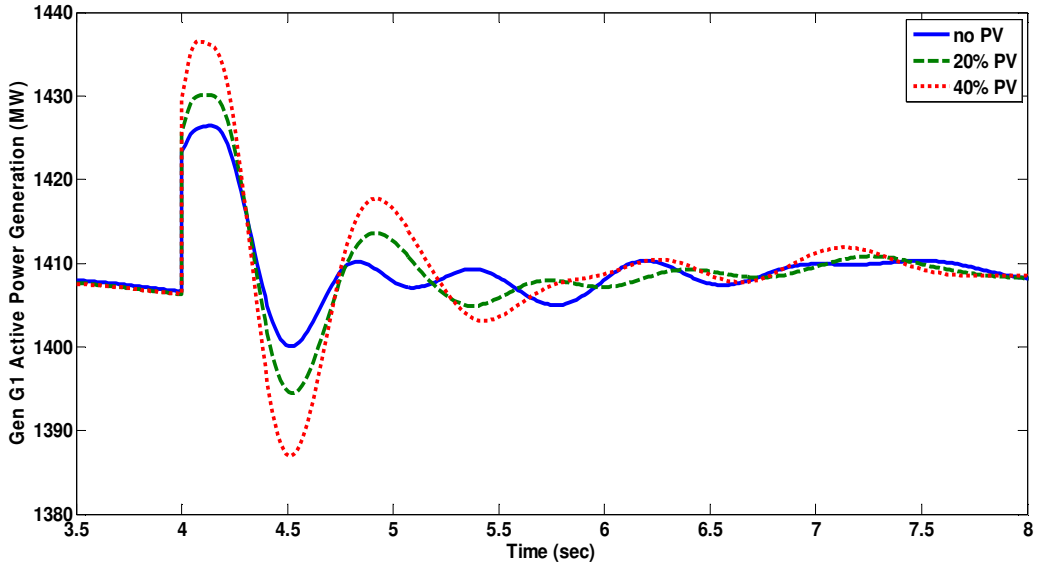

Fig. 4.12 Real power generation of the generator located at bus 1566, G1 after loss of BB2 unit

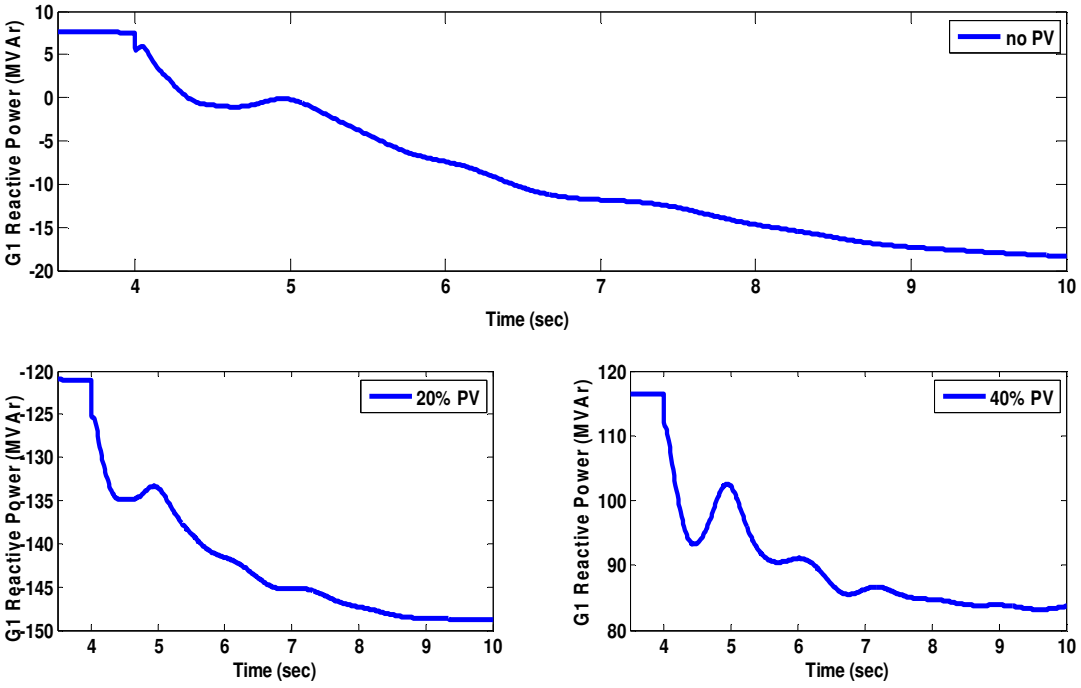

Fig. 4.13 Reactive power generation of the generator located at bus 1566, G1 after loss of BB2 unit

As the point of consideration is moved farther from the time of disturbance, the required generation is provided by reduction in the flows to the other areas. Consequently, the amount of generation in the other unit will stabilize to the initial, pre-disturbance value. These oscillations tend to increase as the level of PV generation increases in the system.

The voltage and frequency of the 500 kV level bus of 1569, which are presented in Fig. 4.9 and Fig. 4.10, show that this disturbance has caused more voltage as well as frequency oscillations in this bus. Therefore, it could be said that lack reactive power support has resulted in more widespread effect of the disturbance across the transmission system.

Case B: Loss of a gas unit in vicinity of residential PVs

In this generation loss scenario a large gas unit, i.e., W15, with about 160 MW of active power and 60 MVAr of reactive power generation is switched off. The reason this generating unit is selected is the fact that there are quite a few PVs present in the vicinity of the unit located at bus 1969, i.e. W15. Therefore, it would be a good case to study the impact of PV generation on the system behavior. This case will in effect illustrate the role of distributed generation on the stability of the system. Figure 4.14 shows the one line diagram of the system for the case with 20% PV Penetration.

As seen from Fig. 4.14, some of the generators are already switched off for the case with 20% PV generation in comparison with the base case. The same applies to the case with 40% PV penetration, with the difference that even more units are displaced with PV in this case. Simulation results of the bus voltages and frequencies, as well as the generator's relative rotor angles are presented in Fig. 4.15-4.20. Various bus voltages ranging from 500 kV to 69 kV are plotted for the purpose of comparison.

From the simulation results it is observed that the system is stable following the interruption of the W15 generating unit, which in effect means a loss of 160 MW and 47 MVAr power generation. The relative rotor angles and speed of the neighboring generators do not show any severe oscillations and they are relatively close in different penetration levels. As expected, with higher penetration levels the neighboring generators exhibit higher reactive power generation. This higher generation is the result of replacing some of the

generators in the study area with rooftop PVs. However, variations of the active and reactive power generation following the disturbance are negligible and independent of the amount of PV generation.

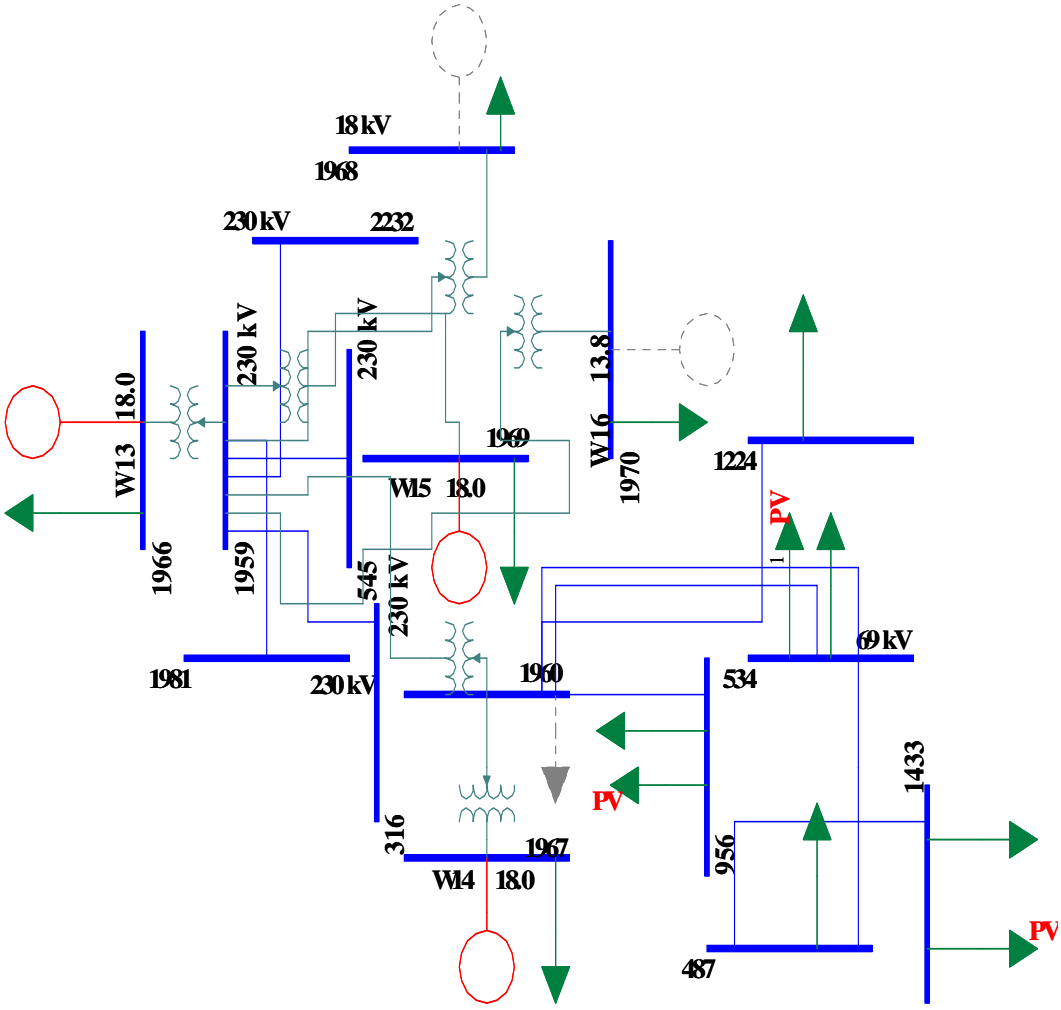

Fig. 4.14 One line diagram of the system in vicinity of the bus 1969

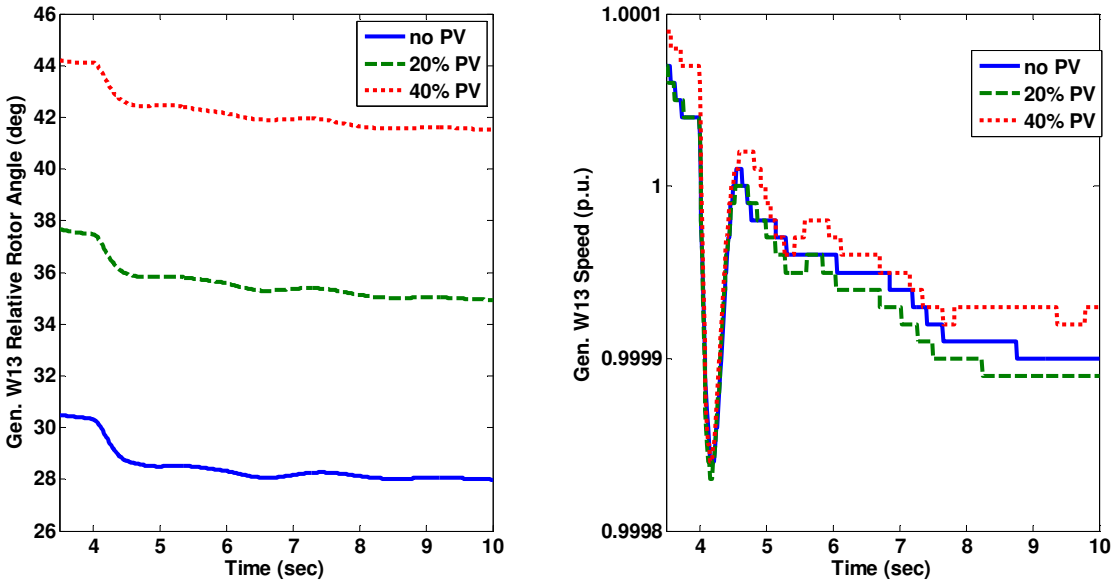

Fig. 4.15 Relative rotor angle and speed of the W14 generator located at bus 1967

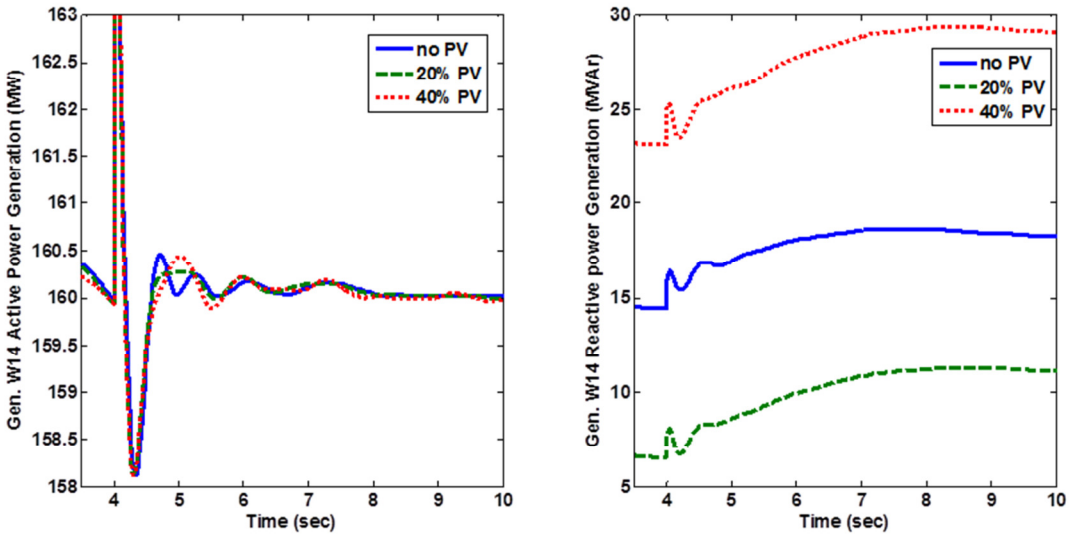

Fig. 4.16 Active and reactive power generation of the W14 generator located at bus 1967

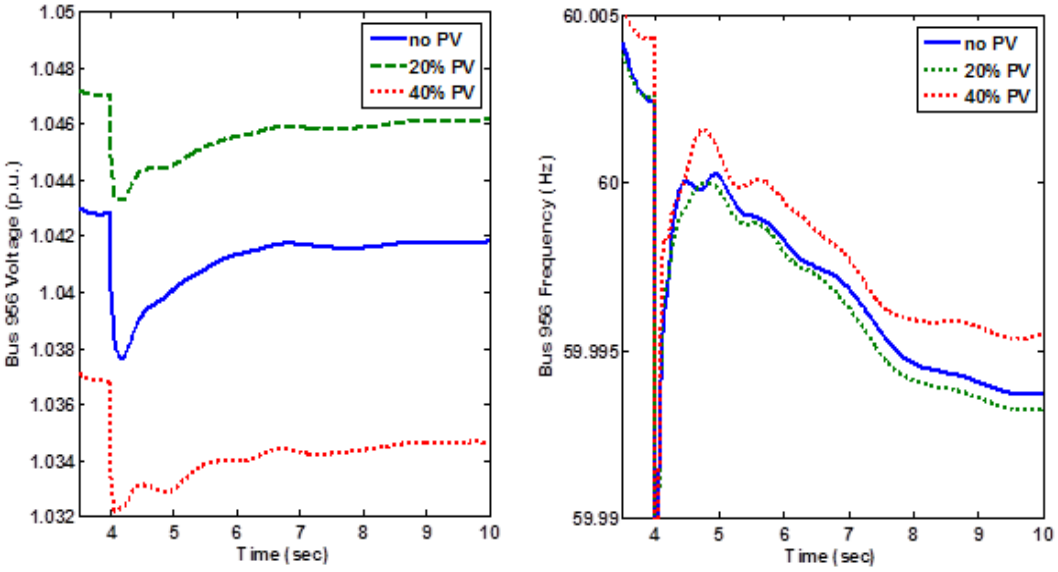

Fig. 4.17 Bus 956 voltage and frequency

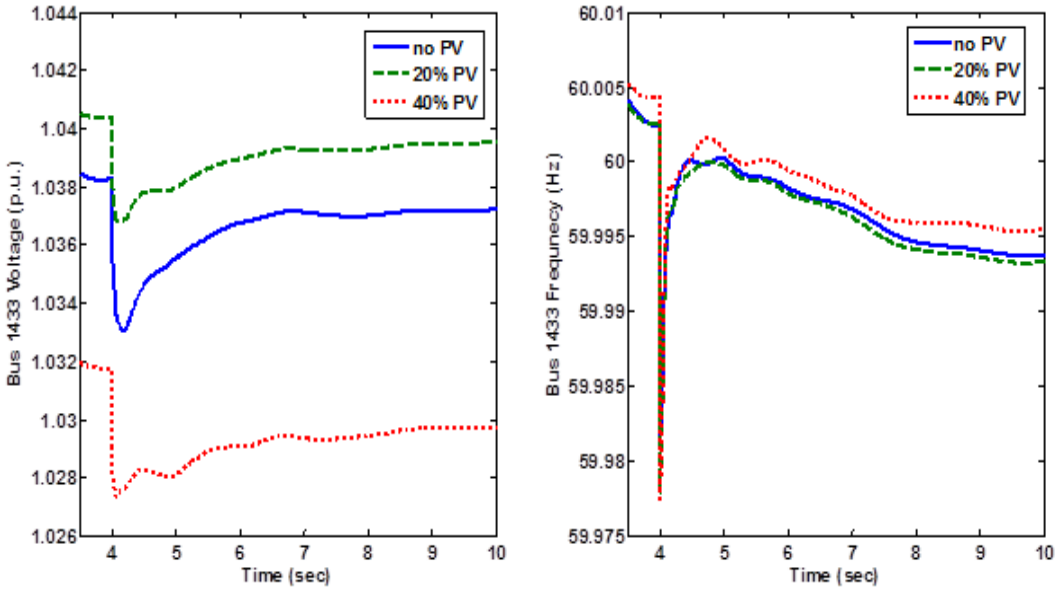

Fig. 4.18 Bus 1433 voltage and frequency

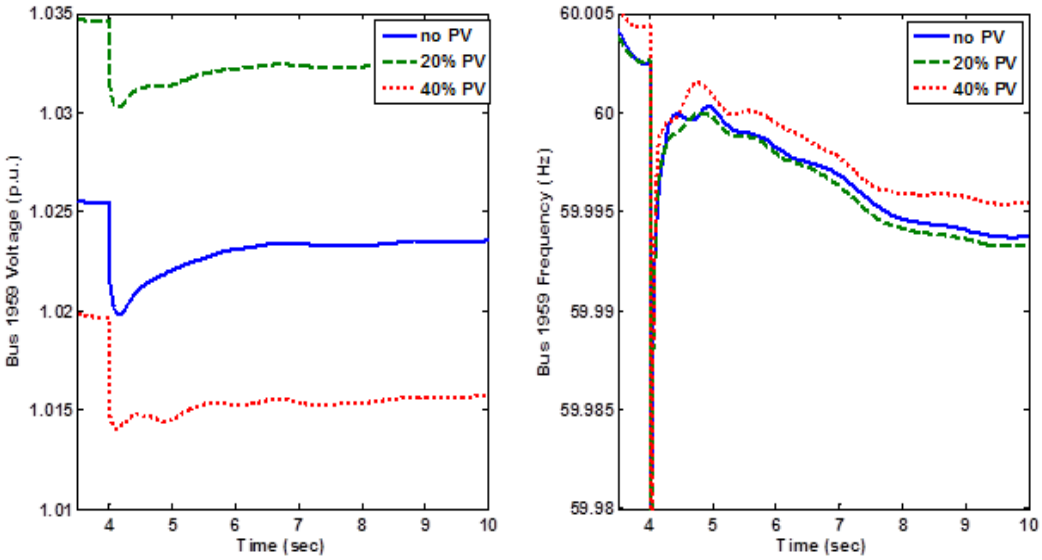

Fig. 4.19 Bus 1959 voltage and frequency

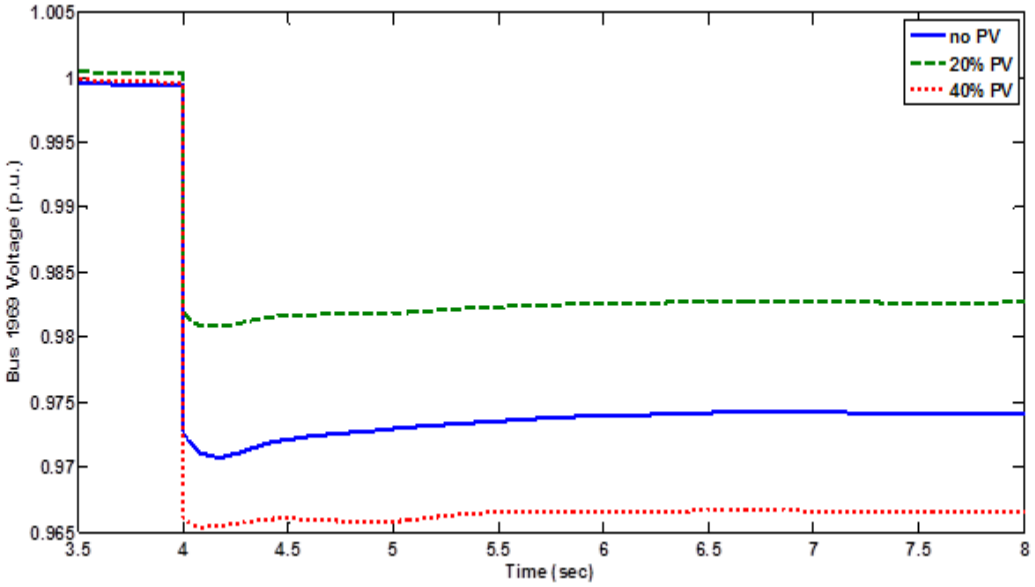

Fig. 4.20 Bus 1969 voltage following a generator loss at this bus

Although the bus frequencies drop significantly for a short period of time, there would be no significant frequency drop eventually. As seen from Fig 4.18-4.19, voltages in the case with PV and without PV will defer in their steady state

values. In this particular case, it can be said that 20% PV generation has resulted in about 1% higher voltages than the system with no PVs present. On the contrary, as it was observed in Chapter 3, 40% PV generation has dropped the steady state voltage values from the base case. Slightly higher oscillations are observed in bus voltages at 230 kV and 69 kV levels following the generation loss in the studied area.

The most prominent difference in various cases is delayed voltage recovery for the load buses with PV installations and the 230 kV buses. This is particularly important since the voltages in some buses do not restore back to the pre-disturbance value and therefore they might violate the voltage tolerance allowed under normal operating conditions. In all other aspects, all three cases have the same behavior dealing with this disturbance.

4.4 Effect of double circuit outages

Double circuit outages can cause severe oscillations in the system and might eventually lead to system instability. Since it was observed in the previous part and from other simulation results that (*N*-1) contingencies were not causing severe problems in the case at hand, double circuit outages are studied which will be categorized among the (*N*-2) contingencies. In order to identify the most severe (*N*-2) contingencies steady state behavior of the system following any (*N*-2) contingency is chosen to select the possible study cases for transient studies. Hence, there would be a need to study all different scenarios within the system that is resulted from any combination of generator or transmission line outages.

However, for a large system such as the one at hand, these would translate to thousands of cases studies which require the most advanced computational capabilities and memory requirements. As a result of that, studying all the contingency cases within the system is not feasible.

To address the dimensionality problem associated with the steady state contingency analysis problem, a contingency analysis package, named SSTools, in PSLF is deployed. This program first runs a set of *(N-1)* contingency analysis in order to identify the most severe contingencies. A ranking method is used in the identification process that uses the steady state information such as the bus voltages and line flows and their post-disturbance values as the comparison parameters. As any other ranking procedure, ranking parameters are user-defined and will determine the final value for the number of severe contingencies.

Once the severe *(N-1)* contingencies are identified, these contingencies can be used for further analysis, i.e. *(N-2)* or *(N-1)-1* contingency analysis. The ranking procedure utilized in the aforementioned software, significantly reduces the number of the cases being analyzed in *(N-2)* contingency analysis. The following are the cases that have shown to be severe *(N-2)* contingencies in terms of steady state analysis.

Two different cases which have shown to be severe outages in terms of the subsequent voltage and frequency oscillations are studied and reported next. It should be noted that among double circuit outages that were simulated, many of them have shown the same behavior with and without PV systems. Therefore only two cases that differ in this behavior have been reported here.

Case A: 1164-913 double line outage

This contingency is the outage of the two parallel 500 kV lines connecting the bus 1164 to the bus 913. The neighboring generators are the A1-A13 generating stations, at which some generators are switched off in the 20% and 40% PV penetration cases. Figure 4.23 shows the one line diagram of the studied area.

It is assumed that the system is operating at the normal conditions when the two parallel lines are removed from the service. Figure 4.21-4.27 present the simulation results after the occurrence of the disturbance. Simulation results show that the bus voltage and frequency oscillations in the studied area are well damped for the case with PVs present in the system. On the contrary, the case with no PVs shows poor damped oscillation of the voltages in addition to the frequency instability. Therefore it can be concluded that the existence of distributed PV systems instead of having conventional generators concentrated at one location, can improve system stability while dealing with a severe contingency.

One reason for the improved behavior of the system with PVs, in this particular case, is that the double circuit outages will separate the generators from a major part of the system. In other words bus 912, which is a 230 kV bus, is the only remaining path for flow of the power being generated by the units present at this location. This will contribute to the system instability following the outages. On the other hand, in the system with 20% and 40% PV generation, most of these units are already replaced with distributed generators and therefore the outage of

these two lines will have less effect on the system since it will cause less interruption in the flow of the power. The same justification could be used to explain the improved behavior of the system with 40% PV generation over the system with 20% PV generation.

Comparing the active and reactive power generated by the neighboring generators, such as A11 and G1, it is observed that the double line outage has caused severe oscillations in the output of these units in the base case. However, as the amount of PV generation increases, fewer oscillations are observed in the output of these units. This observation once again confirms the beneficial impact of the distributed PV on the stability of the system.

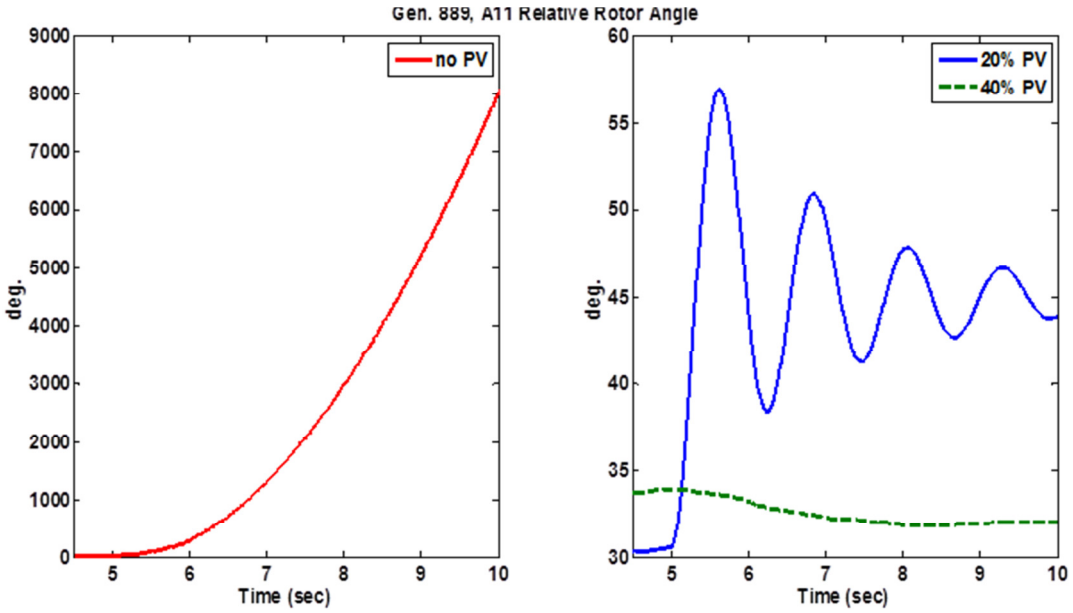

Fig. 4.21 Generator A11 relative rotor angle following the case A double line outage

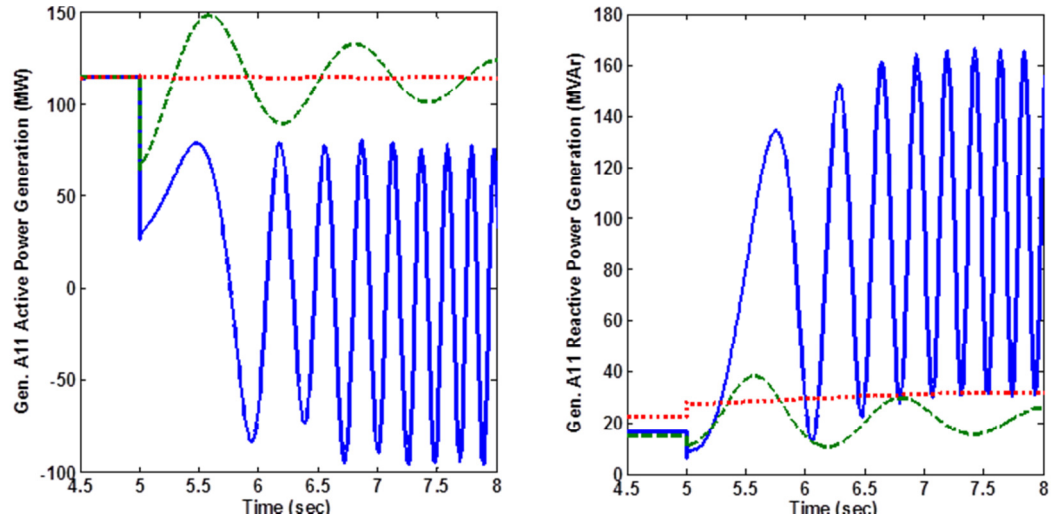

Fig. 4.22 Generator A11 active and reactive power generation following the case A double line outage

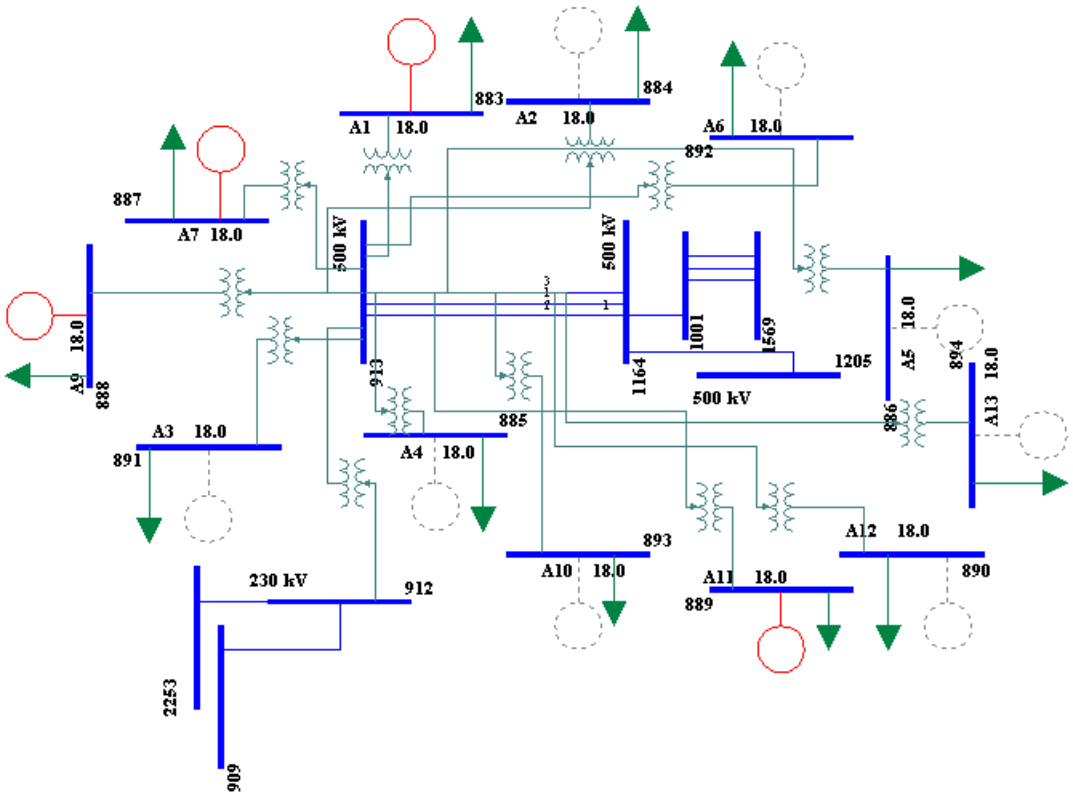

Fig. 4.23 One line diagram of the system in vicinity of bus 1164

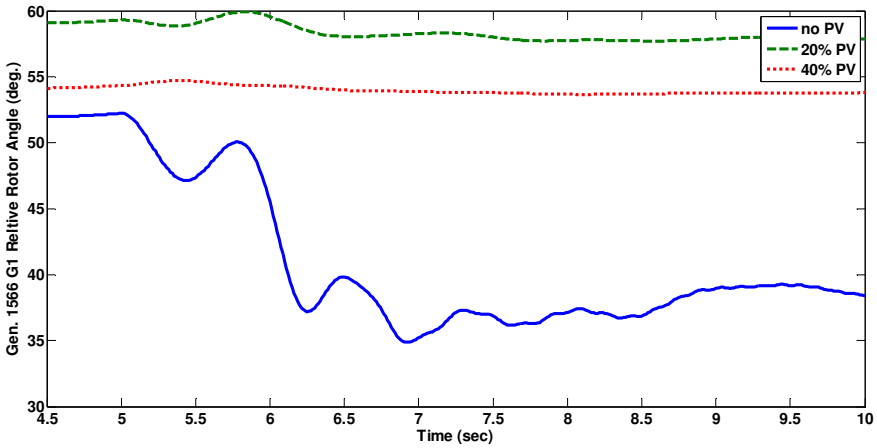

Fig. 4.24 Generator G1 relative rotor angle following the case A double line outage

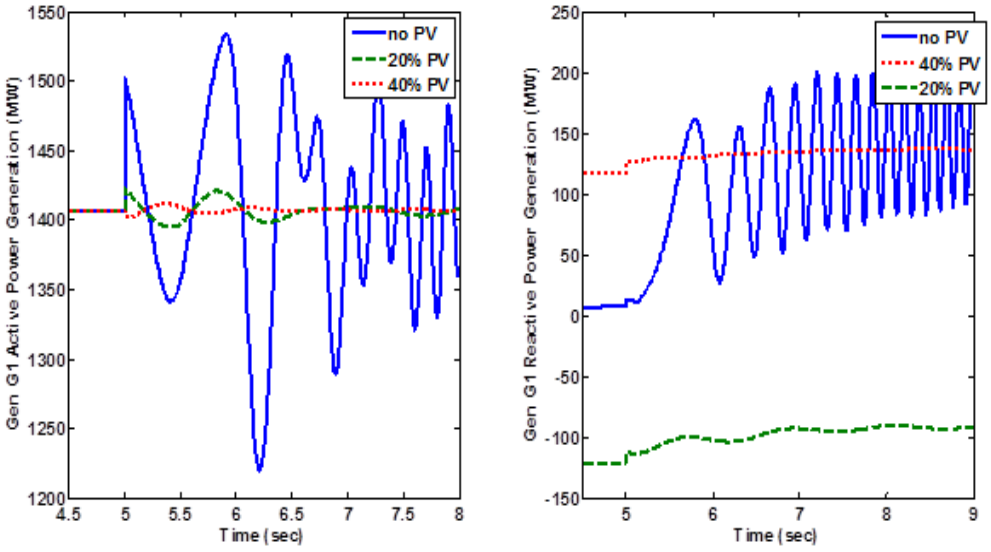

Fig. 4.25 Generator G1 active and reactive power generation following the case A double line outage

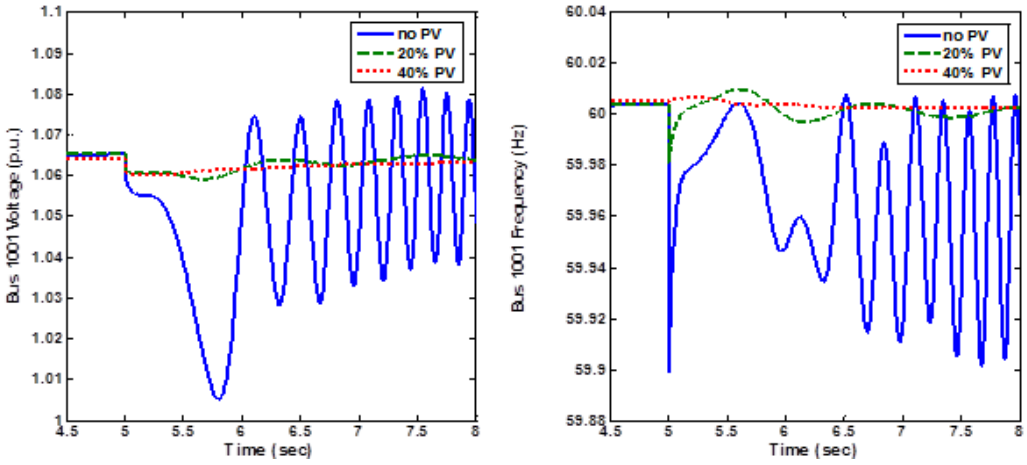

Fig. 4.26 Bus 1001 voltage and frequency following the case A double line outage

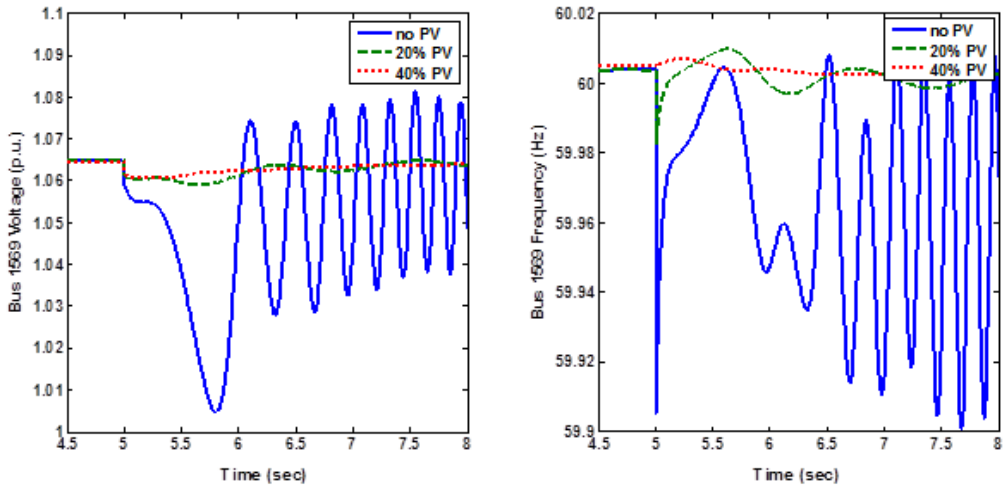

Fig. 4.27 Bus 1569 voltage and frequency following the case A double line outage

Case B: 1164- 1205 and 1569-1886 double circuit outage

The simulated double circuit outage in this part includes outage of two adjacent lines that do not cause instability in the base case but rather result in damped voltage and frequency oscillations. This outage occurs at two 500 kV

lines, i.e. 1164- 1205 and 1569-1886. Figure 4.28 shows the one line diagram of the area in which the double line outage occurs.

The simulated outage has shown to be severe in terms of the steady state voltages that it will cause. Therefore, it is a reasonable candidate for dynamic studies. Simulation results are presented in Fig. 4.29-4.34 for some of the buses in this area. Other buses in the vicinity of this area have shown similar behavior dealing with this disturbance. Also, the response of the nearby generators has been investigated.

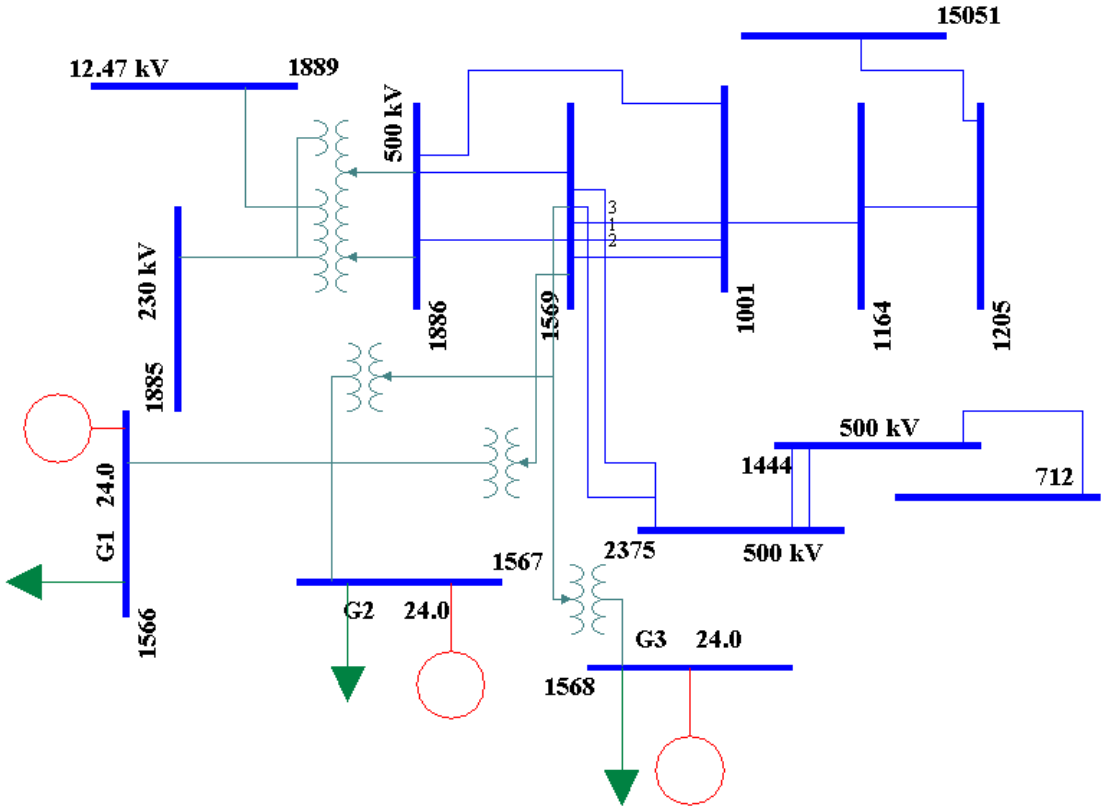

Fig. 4.28 One line diagram of the system in the neighborhood of bus 1569

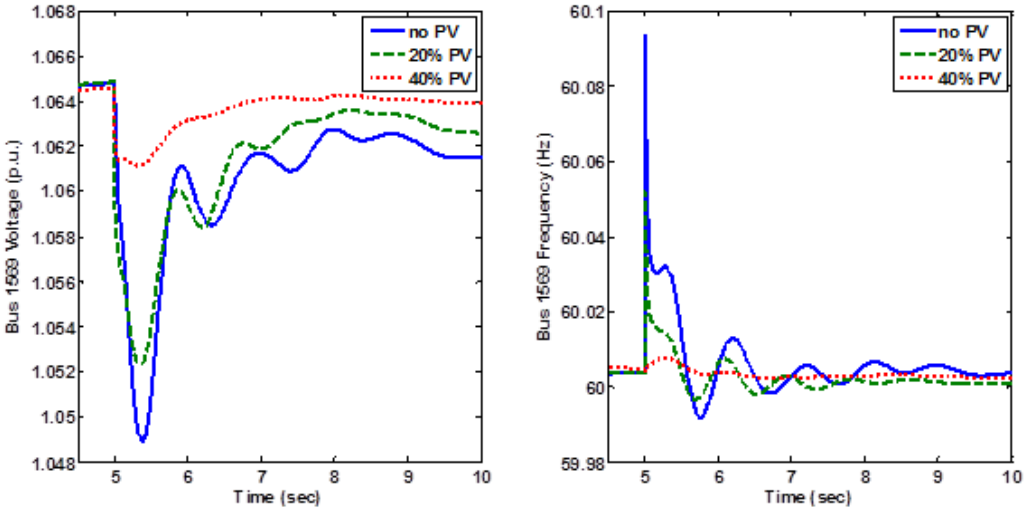

Fig. 4.29 Bus 1569 voltage and frequency following the case B double line outage

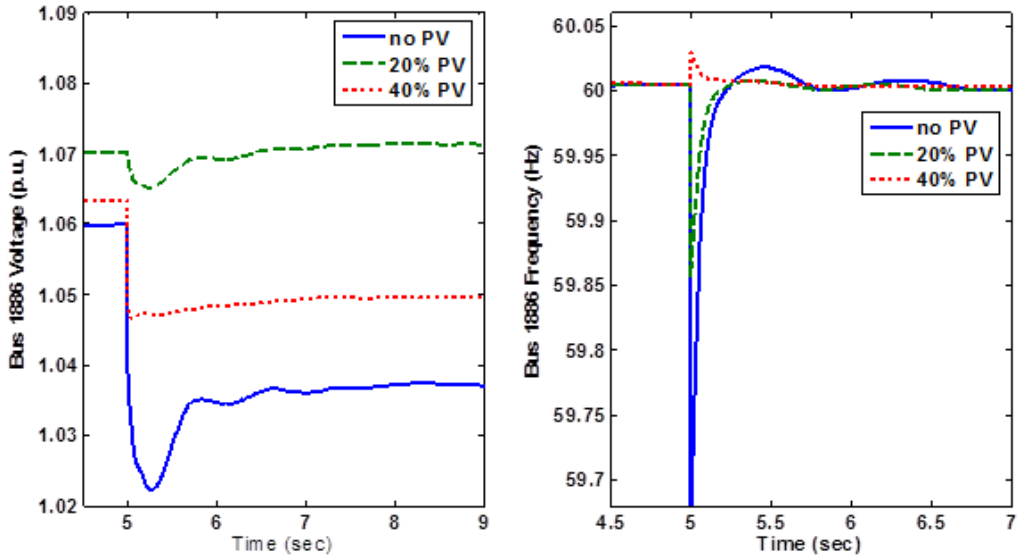

Fig. 4.30 Bus 1886 voltage and frequency following the case B double line outage

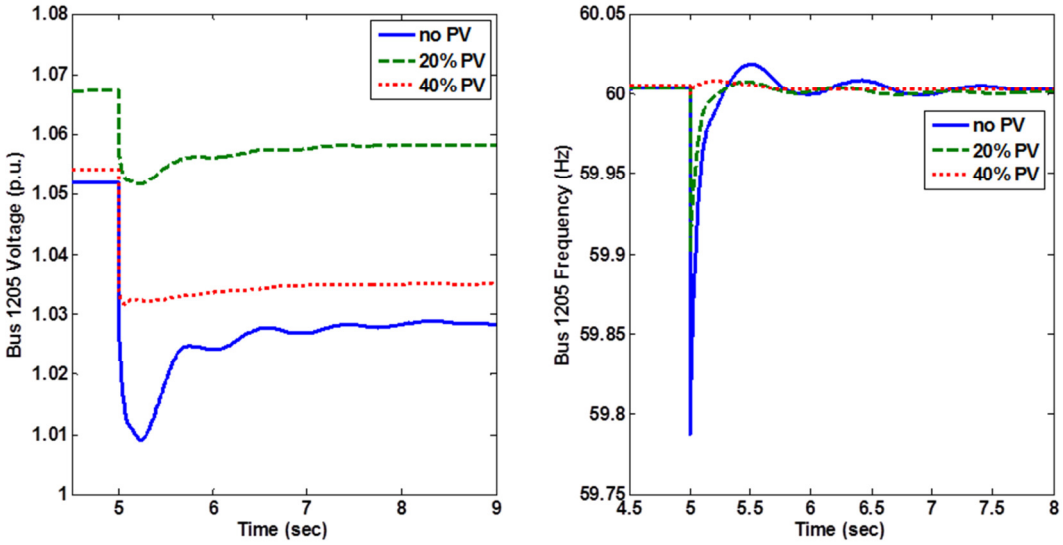

Fig. 4.31 Bus 1205 voltage and frequency following the case B double line outage

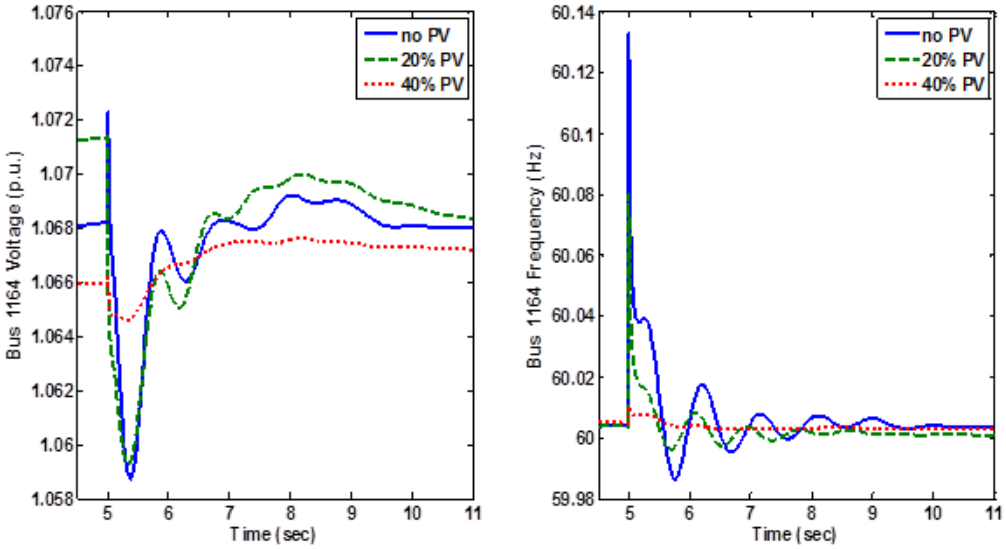

Fig. 4.32 Bus 1164 voltage and frequency following the case B double line outage

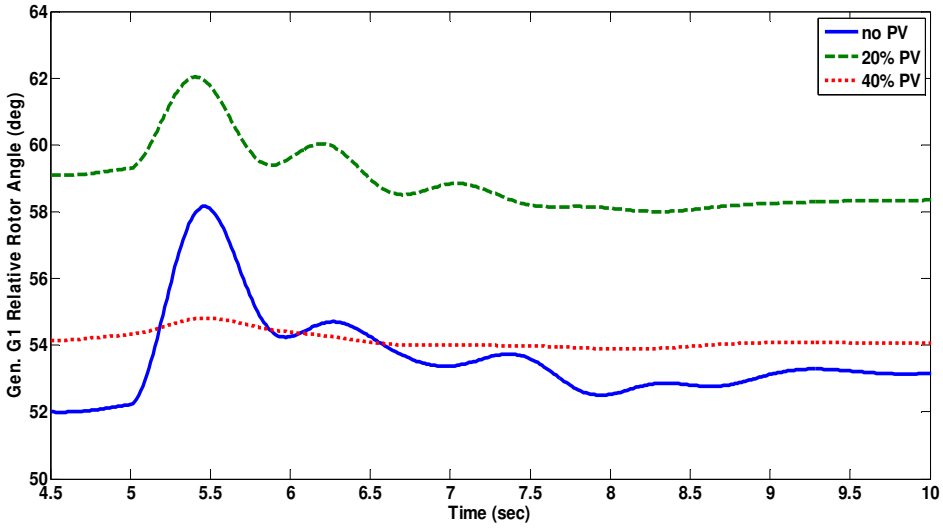

Fig. 4.33 Generator G1 relative rotor angle following the case B double line outage

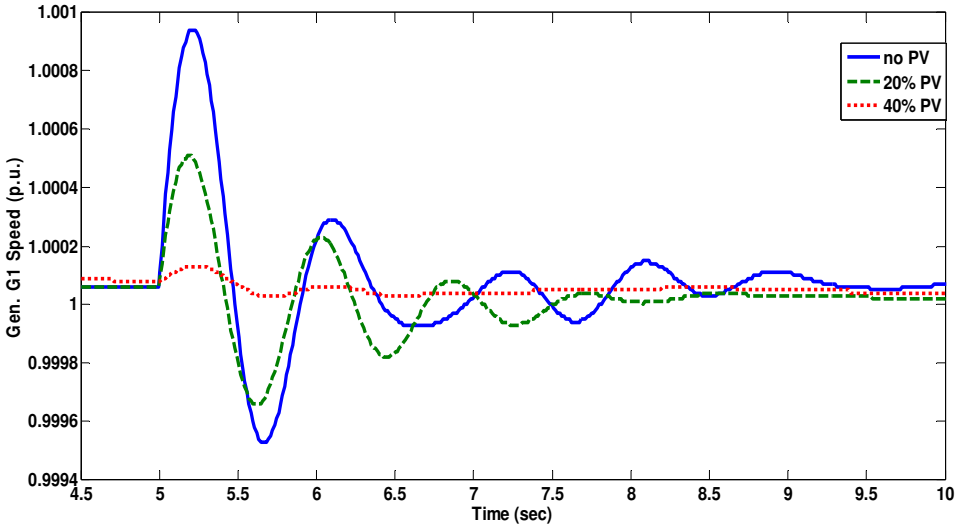

Fig. 4.34 Generator G1 speed following the case B double line outage

By observing the simulation results, it is concluded that the existence of the PV systems in this particular case of the double circuit outage improves bus

frequencies in all the buses that are in the neighboring of the outaged lines. This improvement is more evident as the level of PV penetration increases to 40%. As seen in Fig. 4.31-4.32 with 40% PV penetration, the frequency oscillations following the disturbance become almost nonexistent.

In addition, by increasing the PV penetration, the behavior of the bus voltages is significantly improved since less voltage oscillations are observed as the PV generation levels increase in the system. What is meant by improvement is less frequency dips and oscillations following the disturbance. For example at bus 1886, for the case with 20% PV, frequency has 0.2 Hz less dip than the case with no PVs in the system. Similar effect is observed at the bus 1205.

Relative rotor angles and the speed of the neighboring generators shown in Fig. 4.33-4.34 show the same behavior observed in bus voltages and frequencies. For instance the oscillations in speed of the generator G1 is better damped in the 20% PV case than the base case. The same applies to the case with 40% PV generation in comparison to the case with 20% PV generation.

As a result of the observations from the previous two contingency cases, it could be said that the existence of the distributed PV resources can overall improve the system performance dealing with line outages. On the other hand, addition of the PV units decreases the voltage deviation from its initial value. For instance, at the bus 1205 voltage settles down at a value which is 5% lower than the initial value in the base case while this value is about 2% for the case with PV.

4.5 Effect of bus faults

As one of the prominent reasons for system instability, bus faults are studied in this section. The objective is to compare the response of the system with and without PV systems while a bus fault occurs at the system. Since the system is under light loading conditions, the base case itself is well behaved with the occurrence of bus faults. However, if the existence of PVs adversely affects the behavior of the system, it can be an indication of instability in more critical cases such as the peak case. It is believed that at higher PV penetration levels, the transmission system may exhibit a different behavior than the system with no PV. Therefore, the fault scenarios considered in this part are located at higher voltage levels, i.e. 500 kV and 345 kV for the purpose of transmission system studies.

Fault scenario A: fault at a 500 kV level bus

A three phase fault is simulated on a 500 kV level bus while it is cleared after 4 cycles which is a suitable time for this voltage level. The bus structure near the faulted bus is shown in Fig. 4.36. This fault is followed by outage of a 500 kV transmission line connecting the faulted bus, i.e. bus 1569, and the bus number 1886. Simulation results are shown in Fig. 4.36-4.38 for the bus voltage and frequencies. In addition, the speed and relative rotor angles, as well as active and reactive power generation of the generators in vicinity of the faulted bus are observed in the time domain.

Simulation results show that, in most aspects, this fault scenario has an adverse impact on the system with respect to the increased PV penetration. This impact is observed by comparing the behavior of the system with no PVs and the

system with 20% and 40% PV penetration present as sources of power generation. Generator relative rotor angles tend to achieve higher peaks during the post fault transients when 20% PV generation is present. However, as the penetration level increases, relative rotor angles and speed of the generators, follow the same behavior as the base case. The relative rotor angles of the G1 generating station shows about 10 degrees of difference between the rotor angles of the cases with 20% PV penetration and without PV systems. Although, the steady states values of the relative rotor angles are different in both cases, the oscillations of the rotor angles for the case with PV exceed those of the base case following the disturbance. This in effect reveals that the system is more perturbed once it is subject to the aforementioned disturbance. It could be said that lack of system inertia has led to these higher oscillations in this case.

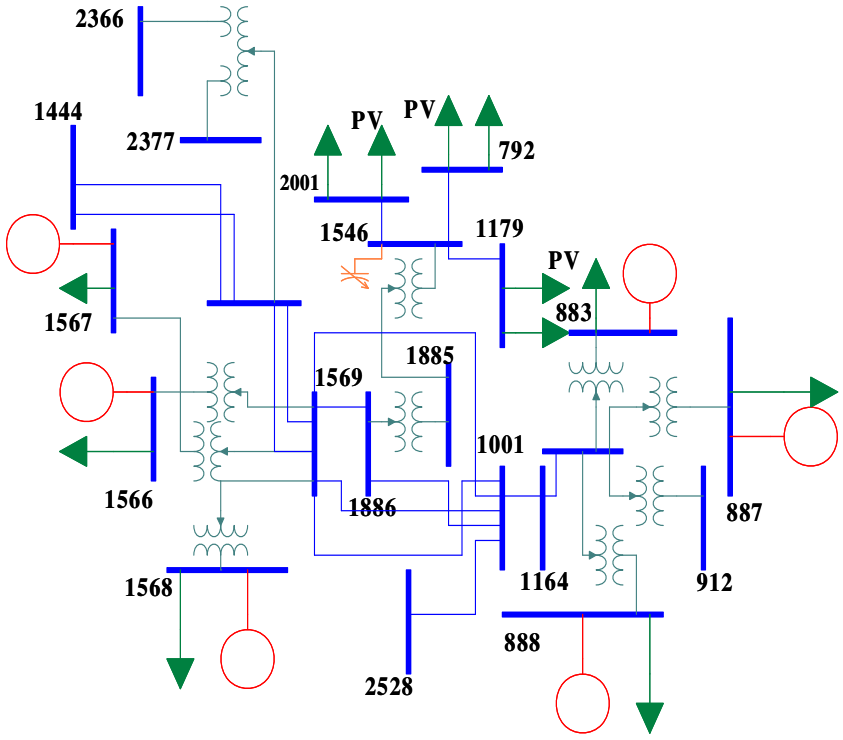

Fig. 4.35 One line diagram of the system near the faulted bus

Plots of the bus voltages show that existence of the PV systems has caused higher oscillation peak values at the faulted bus due to the disturbance. For instance at bus 1569 the voltage peaks to about 4% with the existence of the PV systems while this value is 2% in the absence of these systems. A similar effect is observed at the bus 1886. Consequently, it could be said that PV systems have caused higher voltage oscillations due to the above mentioned fault. Although, the voltage magnitudes have similar behavior in terms of the settling time and their peak values, the system equipped with photovoltaic systems shows increased voltage dips during the transients. The difference between the voltage dips can in some cases reach a value of 5%.

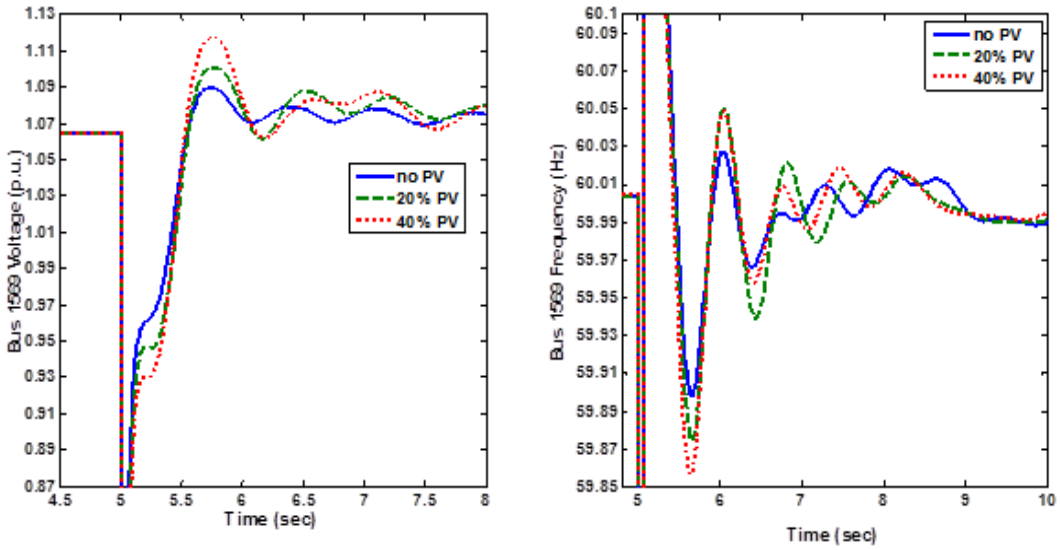

Fig. 4.36 Bus 1569 voltage and frequency following the case A bus fault

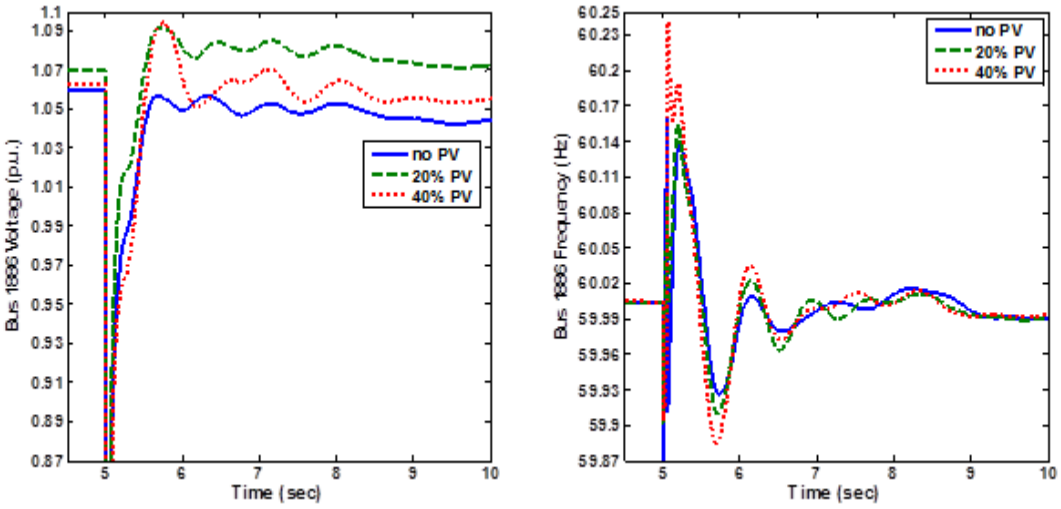

Fig. 4.37 Bus 1886 voltage and frequency following the case A bus fault

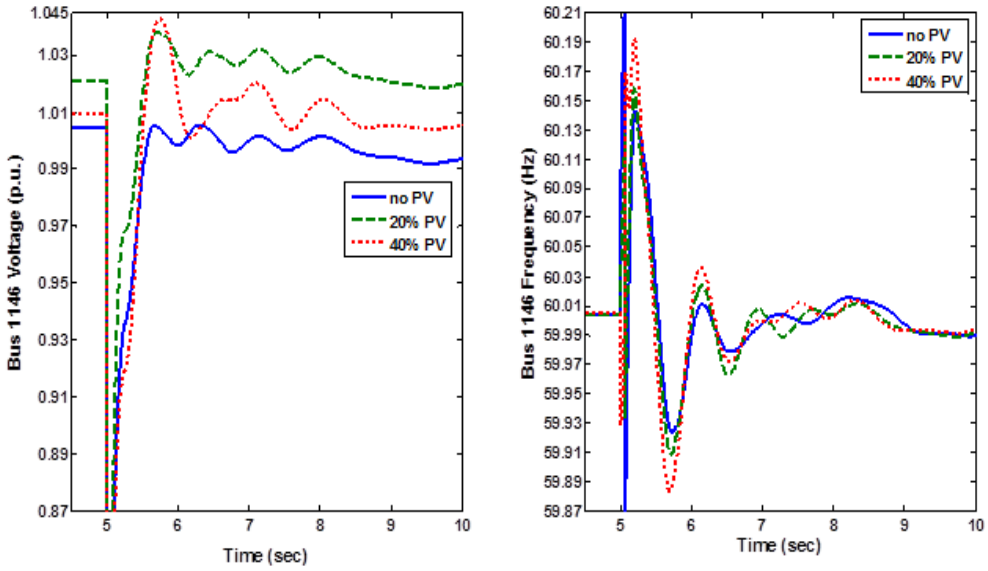

Fig. 4.38 Bus 1146 voltage and frequency following the case A bus fault

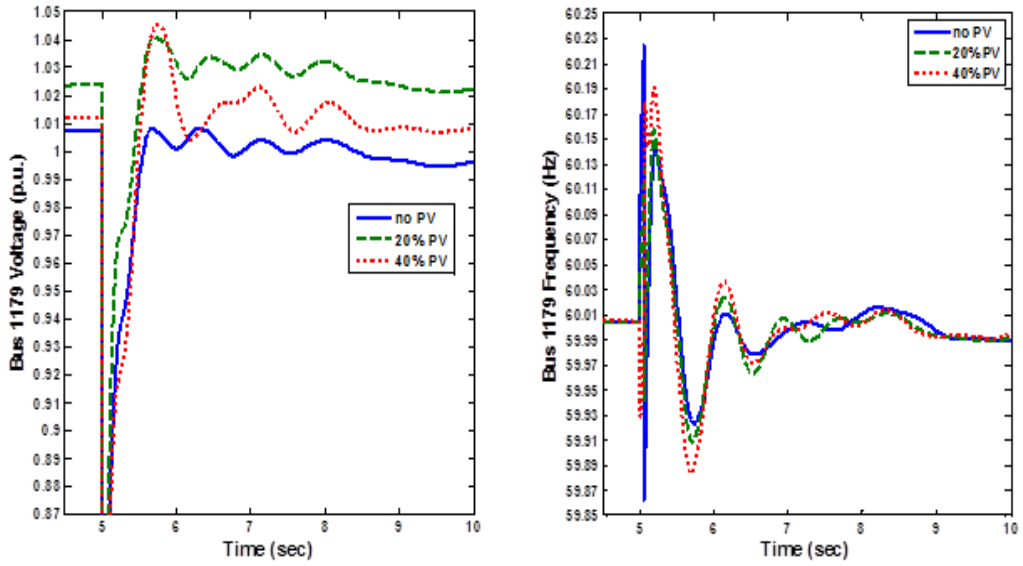

Fig. 4.39 Bus 1179 voltage and frequency following the case A bus fault

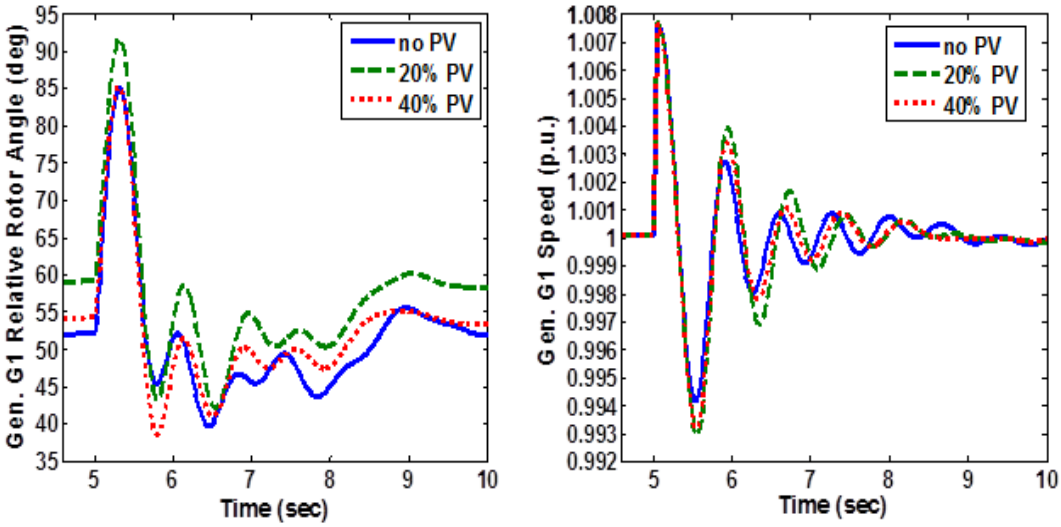

Fig. 4.40 Generator G1 relative rotor angle and speed following the case A bus fault

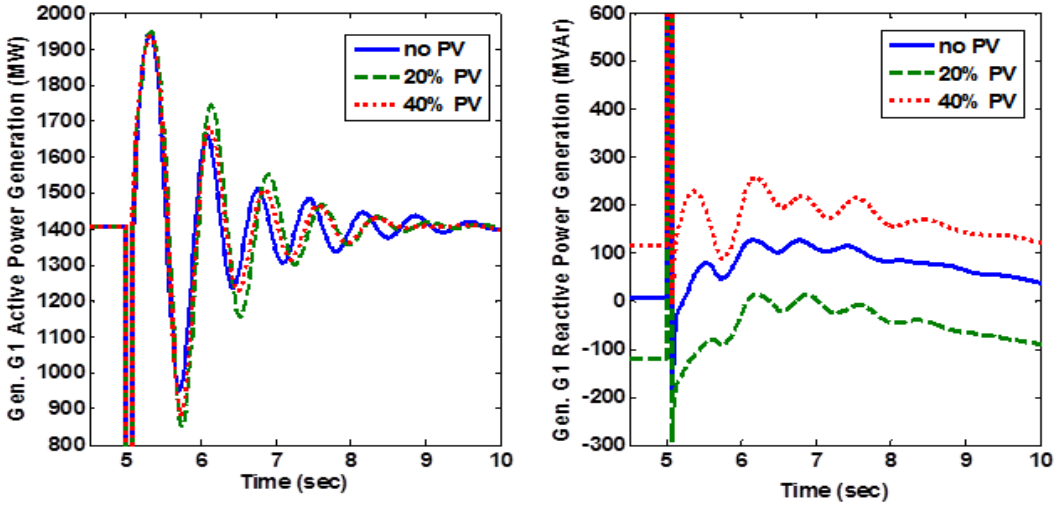

Fig. 4.41Generator G1 active and reactive power generation following the case A bus fault

Bus frequencies have also been adversely impacted by the PV penetration level following the simulated bus fault. For instance 40% PV penetration can cause severe frequency fluctuations in transmission system buses. Overall, unlike the double line outage scenarios, addition of the PV systems has adversely impacted the system dealing with a bus fault at 500 kV bus.

Fault scenario B: fault at a 69 kV level bus

A three phase fault is simulated at a 69 kV level bus, 2386. The fault is cleared after 8 cycles followed by the outage of the adjacent 69 kV line, i.e. 2386-2233 line following the fault clearance. The one line diagram of the system is presented in Fig. 4.42 while the simulation results proceed next. As seen from the one line diagram, the simulated bus fault is in vicinity of many residential rooftop PVs as well as a utility scale PV unit, i.e. PV5. Hence, the location of this fault will be a good candidate to observe the direct impact of the PV systems on transmission system transient stability.

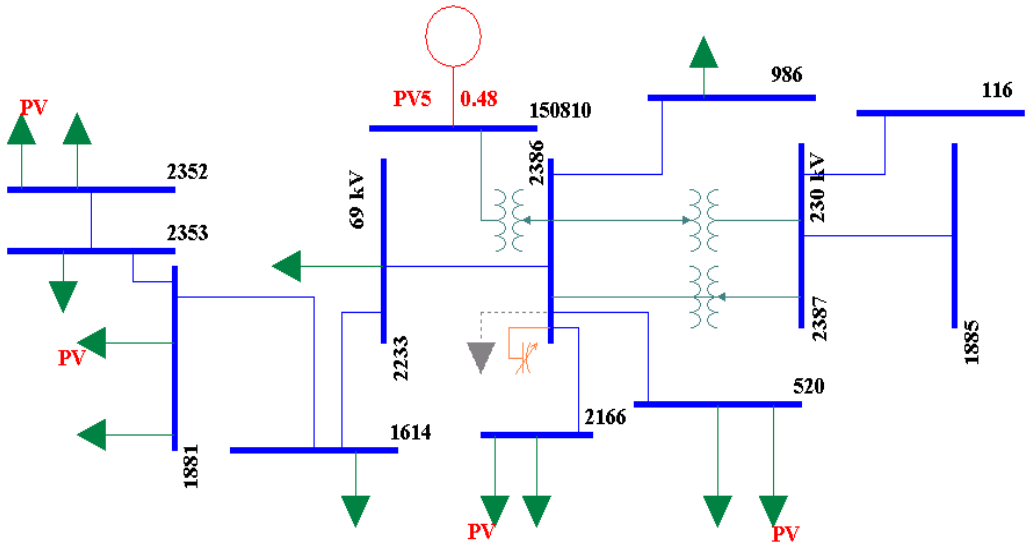

Fig. 4.42 One line diagram of the system simulated for the case B bus fault

Simulation results presented in Fig. 4.43-4.46 illustrate the bus voltages and frequencies following the second bus fault scenario. As observed from these results, bus voltages tend to have higher peaks immediately following the fault clearance. These peaks are more evident at the 69 kV load buses which are also the location of some residential rooftop PV installations. Although different in steady state voltage magnitudes, 20% PV penetration and 40% PV penetration cases exhibit the same transient behavior in terms of the transient voltage oscillations and its settling time.

At buses farther from the point of fault such as 1569 bus voltages have higher voltage dips in existence of PV systems than the base case. This once again confirms the fact that in general, PV systems cause deeper voltage dips during the fault.

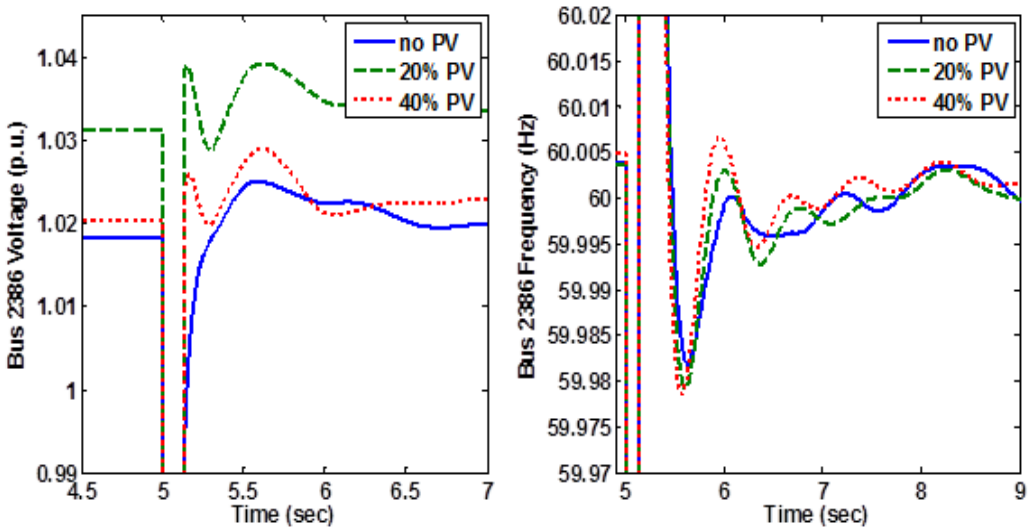

Fig. 4.43 Bus 2386 voltage and frequency following the case B bus fault

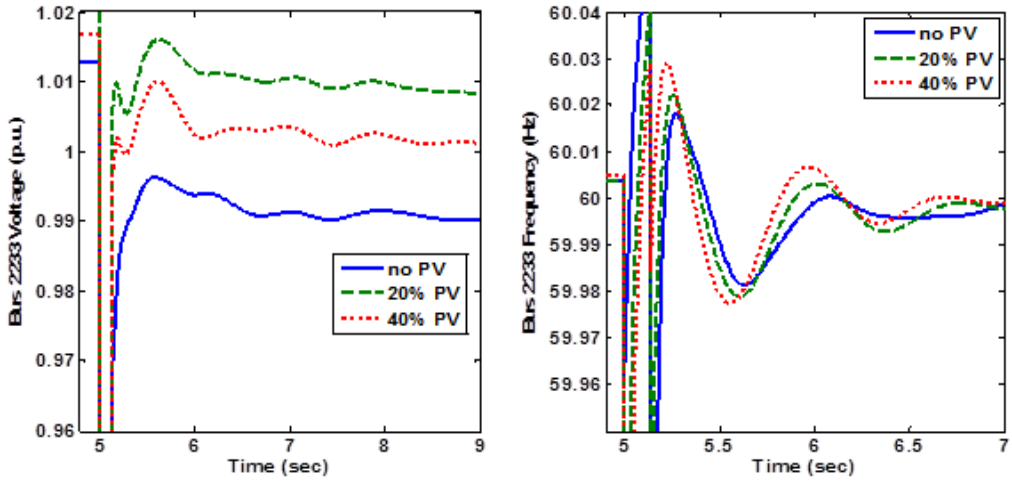

Fig. 4.44 Bus 2233 voltage and frequency following the case B bus fault

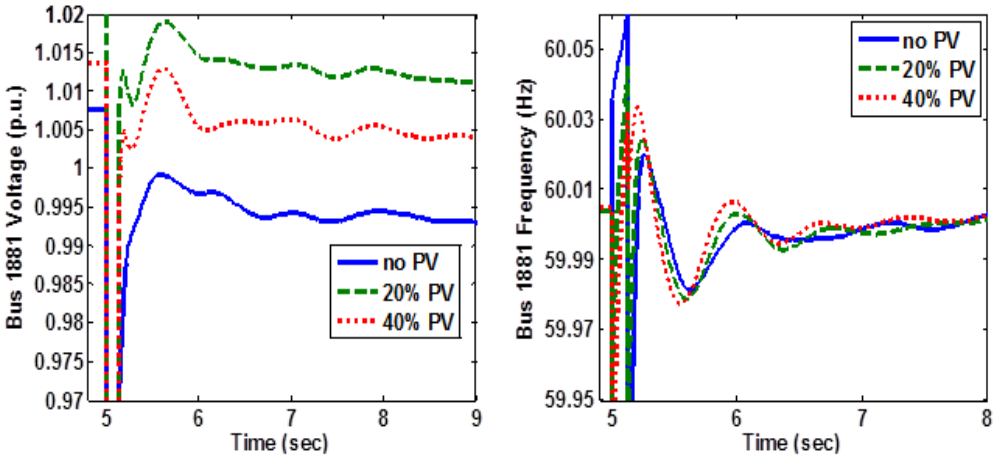

Fig. 4.45 Bus 1881 voltage and frequency following the case B bus fault

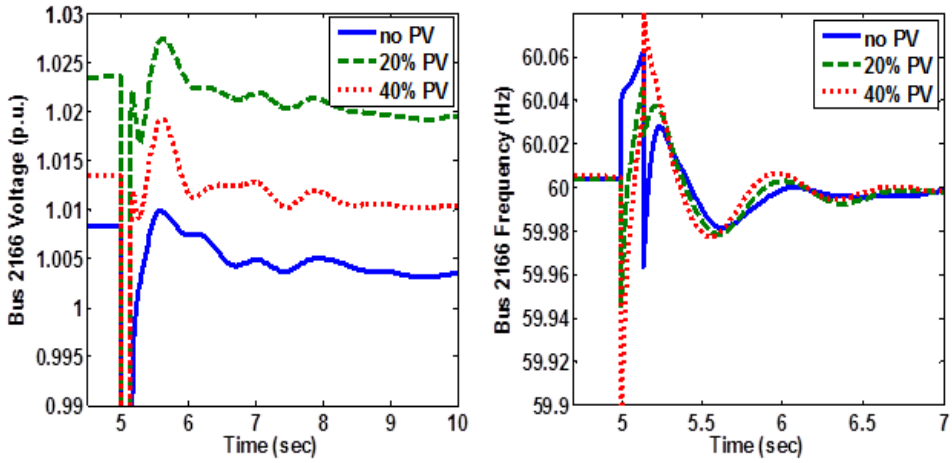

Fig. 4.46 Bus 2166 voltage and frequency following the case B bus fault

The bus frequency peaks up to about 67 Hz at the faulted bus following the disturbance which indicates the severity of the fault. However, after the fault clears, the peak values of the oscillations are higher in cases with PV rather than the base case. In general, as the level of PV penetration increases, the bus frequencies achieve higher peaks immediately after the fault clearance.

Based on the bus fault simulation results, being presented during the last two study cases, it can be concluded that the addition of the PV systems, in general, is expected to have a detrimental impact on the transmission system. This impact is more evident at bus voltages, in terms of the voltage dips and peak values following a fault, as well as the magnitudes of the frequency oscillations after the fault clearance.

4.6 Cloud cover: impact on bus voltages

Being highly dependent on weather conditions, the output power delivered by photovoltaic systems can fluctuate due to climate variations such as a cloud cover. These output fluctuations can lead to variations in bus voltages. Depending on the cloud characteristics and the loading of the system, voltages may violate the allowable operating limits. In order to illustrate cloud cover effects on the transmission system voltage magnitudes, a moving cloud scenario is simulated in this section. This illustrates the bus voltage magnitude changes as the cloud moves across the studied system. The area studied is about 1600 square miles which is divided into four sections. It is assumed that the cloud is large enough to cover each section in each time interval of the simulation.

It is assumed that the output of the PV units drop to 50% of their original values while they are covered by a cloud, in each time interval. For the purpose of simplification and due to software limitations, the study is carried out for a period of 100 seconds instead of a longer time. Since simulation results are well stabilized before next time interval, this scenario can be a valid example of a real

cloud cover case. Fig. 4.47 shows the voltage magnitudes of few 69 kV buses as the cloud moves across the system.

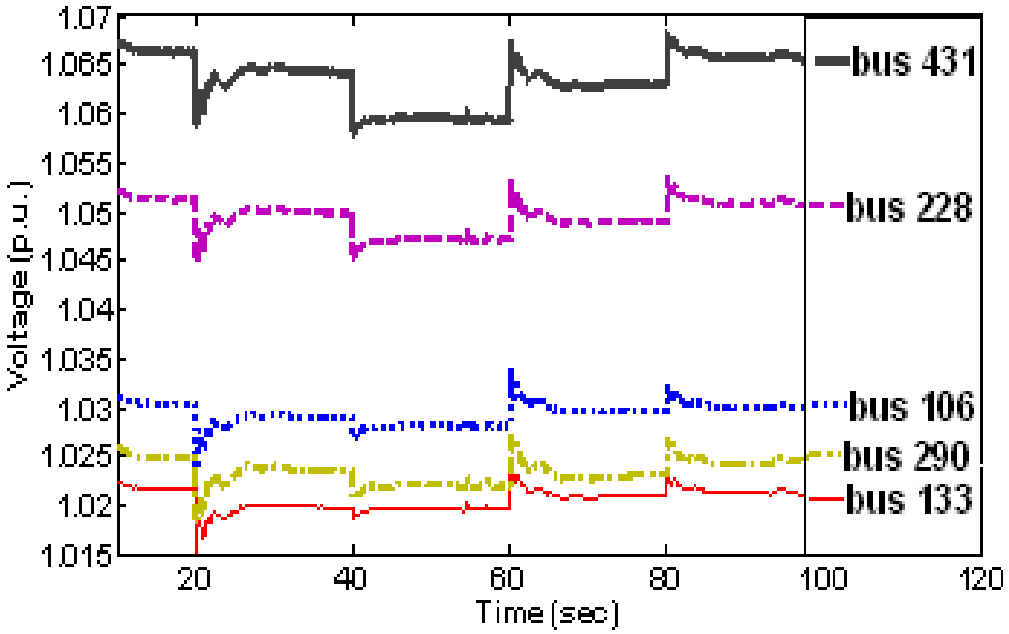

Fig. 4.47 Voltages of the 69 kV buses due to cloud cover

Simulation results reveal that depending on the amount of photovoltaic systems that are affected due to the cloud cover, bus voltages fluctuate over a range of magnitudes. For instance, during the 40-60 s time interval the highest amount of voltage drop from the original value is observed. This is due to the fact that more PV systems are affected as a result of cloud cover during this time frame. The fact that these buses are located in a portion of the system which has relatively small voltage control capability, in terms of tap changing transformers or shunt capacitors, designates more importance to these voltage fluctuations.

4.7 Loss of distributed PV

The fluctuations in the amount of power being generated by the PV units, in the worst case, can lead to loss of a large portion of the distributed PV generation. Additionally, the distributed PV systems can all trip simultaneously due to a single system event such as an extreme voltage dip condition [6]. This effect introduces one of the most important challenges associated with the systems with high PV penetration. In order to study the behavior of the transmission system in occurrence of the aforementioned fault scenario, a large portion of the residential rooftop PVs, which are located in the same neighboring area, are tripped for the case of 20% as well as 40% PV penetration. Figure 4.48 illustrates the voltage magnitudes of a few transmission system buses, which are located at various locations of the studied area, following the loss of the PV units. Relative rotor angles of a neighboring generator as well as the active and reactive power generated by this unit is presented in Fig. 4.49-4.50.

Simulation results presented in Fig. 4.48-4.50 indicate the fact that loss of a major portion of distributed PV systems, can lead to voltage fluctuations as well as deviations in the relative rotor angles of the neighboring synchronous generators. As the amount of PV penetration increases, these voltage fluctuations tend to be higher and they require a longer settling time.

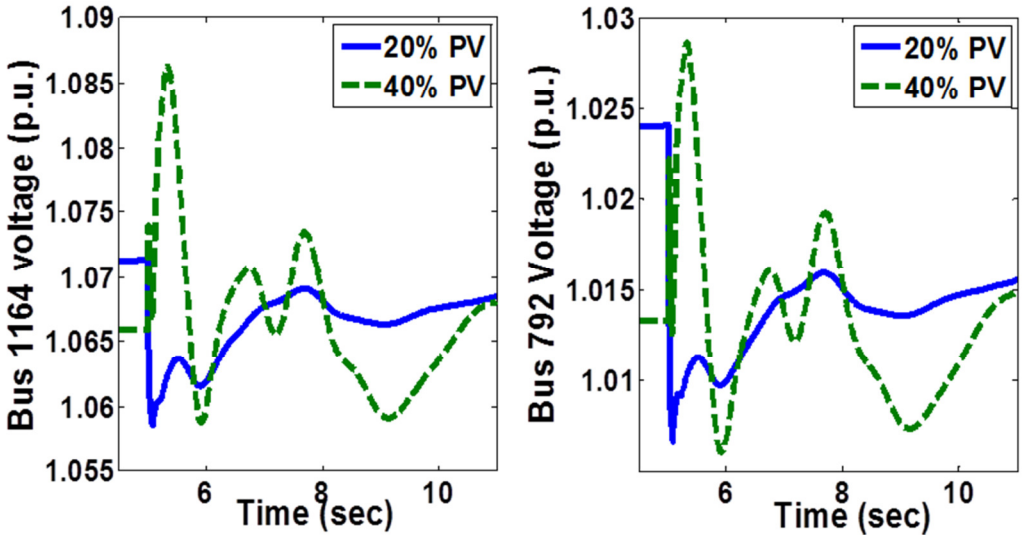

Fig. 4.48 Bus 1164 and 792 voltage magnitudes following loss of a major portion of rooftop PVs

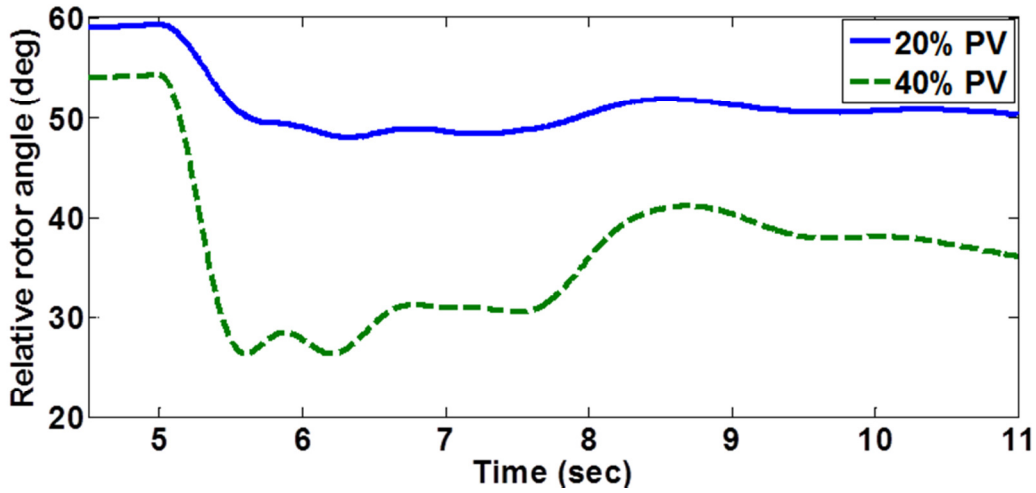

Fig. 4.49 Relative rotor angle of the generator 1567 following loss of a major portion of rooftop PVs

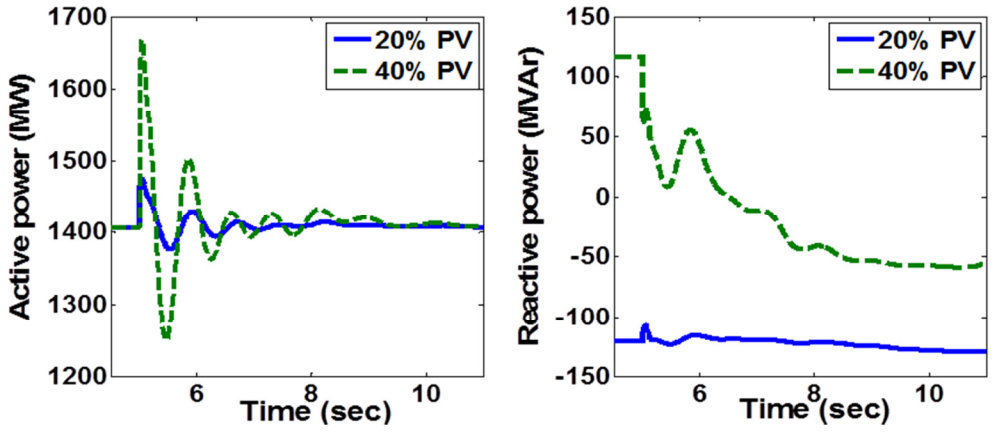

Fig. 4.50 Active and reactive power generation of the generator 1567 following loss of a major portion of rooftop PVs

4.8 Summary

This chapter studied the effect of high PV generation on system transient stability. Simulations with 20% PV penetration were performed while utility scale PV units were modeled in PSLF. Different case studies such as generator outages and bus faults were studied to compare the results with the system not equipped with PV systems. Simulation results show that effect of PV systems is highly dependent on parameters such as type of the disturbance, point of the disturbance as well as the loading conditions in the system.

Overall, it was observed that during stable transients, PV systems will cause higher voltage dips and rises while to some extent worsening frequency oscillations. Also, a case study in which PV systems have prevented system instability was presented in this chapter.

Chapter 5

SMALL SIGNAL STABILITY ASSESSMENT OF THE SYSTEMS WITH HIGH PV PENETRATION

5.1 Motivation for the Study

In a given power system, displacing part of the conventional generators with more PV resources translates to less rotating mass within the system, hence decreasing overall system inertia. Although this phenomenon will not create a major concern in terms of the steady state behavior of the power systems, it can jeopardize the system stability during transients. The ability of the system to adjust the system operating conditions in response to various disturbances, and performing the required tasks in a timely manner is essential for a reliable system operation.

Small signal stability is defined as the ability of the system to maintain synchronism when it is subjected to small disturbances [50]. In this context, there are two types of instability that can occur: the steady state rotor angle increase due to lack of synchronizing torque and the increasing rotor oscillations due to insufficient damping torque are the two major types of small signal instability [52]. Generator – turbine inertia generally plays a key role in providing synchronizing capability to the synchronous generators whenever a disturbance results in a mismatch between the mechanical power input and the electrical power output of a generator. In a system with high PV penetration, some of the synchronous generators are replaced with PV units. Authors in [53] have proposed a general approach for integration of variable energy resources. The

method suggests that for every 3 MW addition of renewable generation to the system, there would be a 2 MW reduction in conventional generators' commitment and 1 MW reduction in their dispatch. While the choice of the '1/3-2/3 rule' could be quite arbitrary, the overall system inertia is decreased, which can lead to potential small signal stability problems. Consequently, with displacing/rescheduling of the conventional units as a result of the addition of PV generation, it would be advantageous to determine if a particular generation station's inertia has significant impact on a particular inertial oscillation mode. This could be determined by performing sensitivity analysis with respect to inertia and performing de-commitment/rescheduling using the sensitivity to inertia as a constraint.

Small signal stability of the power systems has been studied in detail in many research efforts [54-55]. Although considerable work has been done with regards to the small signal analysis of the power systems, the examination of the impact of high PV penetration on small signal stability of power systems has been studied to a limited extent in the literature. In [56] small signal stability of a two area power system under increased PV generation is investigated to observe both the detrimental as well as the beneficial impacts of PV generation on the inter-area modes of the system. The authors in [58] study the voltage stability as well as angle stability of an IEEE 14 bus system while equipped with utility scale PV systems. The effect of PV units on inter-area mode oscillations is also investigated in this work. In another work [57] the effect of PV systems on a power system represented as a single machine and an infinite bus is investigated.

This work derives a mathematical model based on the V-I characteristics of the PV systems which is better suited for the distribution system rather than a large scale transmission system. It is also not apparent that considering the V-I characteristics significantly impacts electro-mechanical oscillations. Shah et al. [59] investigate the effect of PV systems with capacitors on inter area modes of oscillations.

The objective of this chapter is to investigate whether the critical modes of the system are detrimentally or beneficially affected by increased PV penetration. The following steps are taken in the proposed approach:

- Identify the most critical, i.e. poorly damped, modes of the system by performing eigenvalue analysis on the base case with no PV generation.
- Perform eigenvalue analysis for the cases after introducing various levels of residential rooftop and utility scale PVs.
- Compare the results of the eigenvalue analysis under different PV penetration levels to investigate the impact of high PV penetration on small signal stability of the system under study.
- Perform eigenvalue sensitivity analysis with respect to the displaced generators' inertia to validate the results achieved from the eigenvalue analysis.
- Analyze the transient stability performance of the system and examine whether the identified critical modes can be excited by a large disturbance and substantiate the results obtained by eigenvalue analysis.

This chapter first starts with description of the theory utilized throughout this chapter for small signal stability analysis. The results of the eigenvalue analysis of the system under various PV penetration levels are presented followed by the transient analysis results to compare the behavior of the critical modes of the system as affected by a large disturbance.

5.2 Small Signal Stability Analysis

Small signal stability analysis is based on deriving a linear model of the non-linear system model around a certain operating condition. While the system deviation from the equilibrium point is small, the system states can be modeled as linear system as follows,

$$\dot{X} = AX + BU \tag{5.1}$$

where X is the state vector of the system, U is the input vector, and A is referred to as the state matrix. The state vector of the system includes the states of the system such as the speed and relative rotor angles of the machines.

The stability of the linearized system is determined by the eigenvalues (λ) of the state matrix A while the participation of each system state in a specific eigenvalue is determined by the right eigenvector (ϕ) and the left eigenvector (ψ). The ith eigenvalue of the system matrix A and its corresponding eigenvectors are defined as

$$A\phi_i = \lambda_i \phi_i \tag{5.2}$$

$$\psi_i A = \lambda_i \psi_i \tag{5.3}$$

For a complex eigenvalue that corresponds to an oscillatory mode of the system, the mode frequency in Hz (*f*) and the damping ratio (ς) are expressed as,

$$\lambda_i = \sigma_i \pm j\omega_i \tag{5.4}$$

$$f_i = \frac{\omega_i}{2\pi} \tag{5.5}$$

$$\varsigma_i = -\frac{\sigma_i}{\sqrt{\sigma_i^2 + \omega_i^2}} \tag{5.6}$$

The damping ratio shown in (5.6), which is related to the real part of the eigenvalues, in fact determines the rate at which the amplitude of the oscillations decreases [60]. Hence, a positive real part corresponds to oscillations with increased amplitudes while a negative real part corresponds to a damped oscillation. As the complex mode moves towards the right half plane (RHP), the damping of the system worsens.

The critical modes of the system are defined based on the damping and frequency of the oscillations of the modes with low frequency and poor damping. Throughout this chapter, the modes of interest are defined within the frequency range of [0.01-2.00] Hz with a damping ratio below 20%.

5.3 Impacts on Power System Small Signal Stability

In order to study the impact of high PV penetration on the small signal stability of the systems the first step is to identify the critical modes of the system in the base case where no PV systems are present. The critical modes of the system assess the small signal stability of the base case and locate the machines participating in the critical modes of the system. In order to locate the critical

modes of the system, an eigenvalue analysis is conducted for the modes within the frequency range of 0.01 Hz to 2.00 Hz and damping of less than 10%.

This analysis is performed utilizing the small signal analysis toolbox (SSAT) which is part of the DSA^{Tools} software package [25]. SSAT has the capability to also determine the modes shapes and identify the amount of the participation of each machine in the modes of the system. By comparing the values of the participation factors, it is feasible to determine whether the eigenvalue of interest is a local or an inter area mode of oscillation. The analysis is conducted for various PV penetration levels defined in Chapter 3. The selected critical modes of the base case are presented in Table 5-1. This table only lists the critical modes of oscillation that are only related to the machine speeds and relative rotor angles.

To compare the variations of the modes presented in Table 5-1 with respect to the level of PV penetration the same procedure is followed for the system with PV penetration varying from 10% to 50%. The selected eigenvalue analysis of the systems with high PV penetration identifies the critical modes of each scenario. Next, each of the modes presented in Table 5-1 are compared under different PV penetration levels. The results of comparison are presented in Tables 5-2 through 5-6 for few of the critical modes that illustrate a change in the variations of the critical mode.

Table 5-1 Critical modes present in the case with no PV

Mode Number	Real Part (1/s)	Imaginary Part (rad/s)	Frequency (Hz)	Damping Ratio (%)
1	-0.4229	12.5101	1.991	3.38
2	-1.0926	11.2221	1.786	9.69
3	-0.7454	9.5445	1.5191	7.79
4	-0.7428	7.4016	1.178	9.99
5	-0.92	10.83	1.72	8.43
6	-0.148	5.331	0.8485	2.78
7	-0.3291	2.494	0.3969	13.08
8	-1.4142	9.1328	1.4535	15.3
9	-0.5837	10.0481	1.5992	5.8
10	-0.8295	9.1963	1.4636	8.98
11	-0.8773	9.6678	1.5387	9.04
12	-0.9283	9.3887	1.4943	9.84
13	-1.7235	11.2838	1.7959	15.1

Table 5-2 Comparison of the dominant mode 3 under different PV levels

PV Penetration (%)	Real Part (1/s)	Imaginary Part (rad/s)	Frequency (Hz)	Damping Ratio (%)
0%	-0.7454	9.5445	1.5191	7.79
20%	-0.7218	9.3608	1.4898	7.69
30%	-0.7319	9.4402	1.5024	7.73
40%	-0.7578	9.6499	1.5358	7.83
50%	-0.7741	9.8403	1.5661	7.84

Table 5-3 Comparison of the dominant mode 2 under different PV levels

PV Penetration (%)	Real Part (1/s)	Imaginary Part (rad/s)	Frequency (Hz)	Damping Ratio (%)
0%	-1.0926	11.2221	1.786	9.69
20%	-0.9135	11.1828	1.7798	8.14
30%	-0.9423	11.1346	1.7721	8.43
40%	-0.5173	11.0029	1.7512	4.7
50%	-0.4876	10.9947	1.7499	4.43

Table 5-4 Comparison of the dominant mode 5 under different PV levels

PV Penetration (%)	Real Part (1/s)	Imaginary Part (rad/s)	Frequency (Hz)	Damping Ratio (%)
0%	-0.9162	10.8252	1.7229	8.43
20%	-0.9329	10.8293	1.7235	8.58
30%	-0.8414	10.6211	1.6904	7.9
40%	-0.8378	10.5162	1.6737	7.94
50%	-0.7944	10.4007	1.6553	7.62

Table 5-5 Comparison of the dominant mode 8 under different PV levels

PV Penetration (%)	Real Part (1/s)	Imaginary Part (rad/s)	Frequency (Hz)	Damping Ratio (%)
0%	-1.4142	9.1328	1.4535	15.3
20%	-1.0841	8.1806	1.302	13.14
30%	-1.0503	8.2224	1.3086	12.67
40%	-1.0466	8.2745	1.3169	12.55
50%	N/A	N/A	N/A	N/A

Table 5-6 Comparison of the dominant mode 13 under different PV levels

PV Penetration (%)	Real Part (1/s)	Imaginary Part (rad/s)	Frequency (Hz)	Damping Ratio (%)
0%	-1.7235	11.2838	1.7959	15.1
20%	-1.7503	11.3161	1.801	15.29
30%	-1.7445	11.3188	1.8014	15.23
40%	-1.7217	11.2746	1.7944	15.1
50%	-1.6622	11.2258	1.7866	14.65

Comparing the critical modes of the base case that are also present in higher PV penetration levels, it is observed that the low frequency and low damped modes of the system in general attain the same or slightly poor damping as the level of PV penetration increases in the system. However, in two modes that are presented in Table 5-1, i.e. mode 2 and mode 8, the damping ratio of the critical mode shows a more significant reduction. Therefore, in order to better study the impact of the PV levels on the system behavior, transient analysis is conducted in the proceeding section to further study the system.

In order to substantiate the results observed by the eigenvalue analysis, a sensitivity analysis is carried out corresponding to the mode which is detrimentally impacted with increased PV penetration. As more conventional generators are displaced with distributed PV resources the overall system inertia is reduced. Hence, sensitivity assessment of the critical modes of the system, with respect to inertia, is a means of explaining the detrimental impacts of the PV

generation on small signal stability of the power systems. The eigenvalue sensitivity with respect to inertia (H_j) of the *j*th generator is expressed as [61],

$$\frac{\partial \lambda_i}{\partial H_j} = \frac{\psi_i \frac{\partial A}{\partial H_j}}{\psi_i^T \phi_i} \tag{5.7}$$

The sensitivity of the detrimentally impacted critical modes of the system with respect to the inertia of the system generators that are being displaced in the higher PV penetration levels is computed. These computations are performed with the aid of SSAT software that calculates sensitivity of a particular mode to variations of a system parameter. Inertia of the conventional generators is the perturbed system parameter in this case.

Tables 5-7 and 5-8 present a summary of the sensitivity of the critical mode number 2 to inertia variations of the conventional generators being displaced by rooftop PVs in the 20% and 40% penetration levels, respectively. Considering the fact that the damping of the system modes is determined by the real part of the eigenvalues, the real part sensitivity of the critical mode is presented in the aforementioned tables.

The negative real part sensitivities of the eigenvalues shown in Tables 5-7 and 5-8 illustrate the detrimental impact of high PV penetration on system damping. By displacing the conventional generators listed in those tables with rooftop PVs, the real part of the studied mode moves closer to the RHP. The sensitivity analysis results corroborate the results derived from the full eigenvalue analysis of the system under various PV penetration levels.

Table 5-7 Eigenvalue sensitivity corresponding to the inertia of the displaced generators in the 20% PV penetration case (for mode 2)

Generator Bus Number	Base Value of Inertia (s)	Real Part Sensitivity ($1/s^2$)
469	3.54	-0.0129
471	3.54	-0.015
555	2.59	-0.0486
556	2.59	-0.048
809	1.3106	-0.0013
184	2.93	-0.0007

Table 5-8 Eigenvalue sensitivity corresponding to the inertia of the displaced generators in the 40% PV penetration case (for mode 2)

Generator Bus Number	Base Value of Inertia (s)	Real Part Sensitivity ($1/s^2$)
806	3.13	-0.0062
807	3.13	-0.0062
164	2.3	-0.0023
165	2.3	-0.0023
2164	4.3	-0.0023

5.4 Transient Analysis

The results of the modal analysis presented in the previous section point out the fact that reduced system inertia, which is a side effect of increasing the

distributed rooftop PVs, could result in decreased system damping. To illustrate the adverse effects of increased PV generation on small signal stability of the systems, the detrimentally impacted critical modes are scrutinized in time domain. A large disturbance that excites the most detrimentally impacted critical mode with respect to the PV penetration level is simulated. The purpose of this study is to illustrate the scope of the system impact of decreased system inertia under various PV generation levels.

In order to identify the transient case that would excite a detrimentally impacted critical mode, the dominant machine with the highest participation factor in that mode needs to be identified. The participation factors of various machines participating in the first studied mode, i.e. $-1.09 \pm j11.21$, are presented in Fig. 5.1.

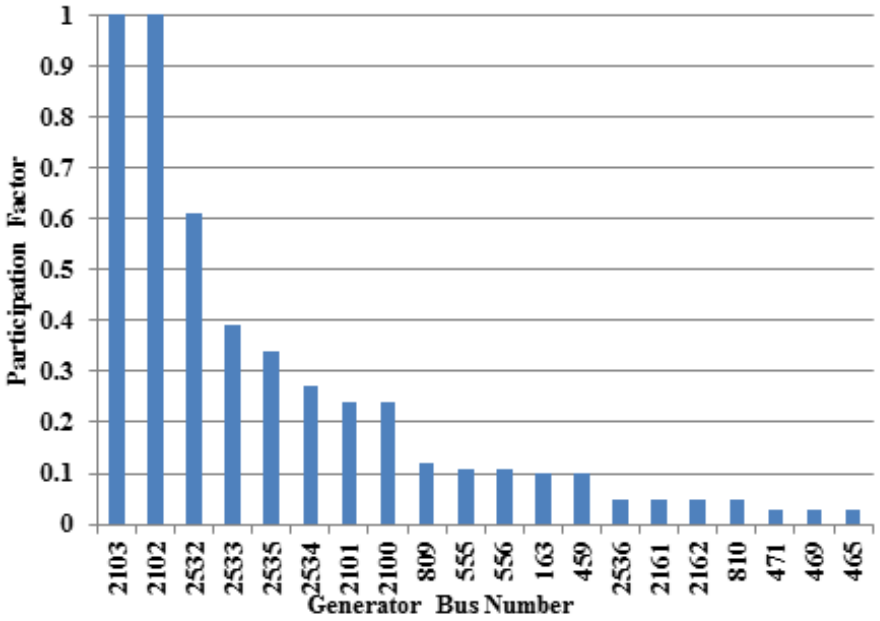

Fig. 5.1 Participation factor of the machines participating in the critical mode detrimentally affected by high PV penetration

As seen from these results, the generators located at bus 2103 and 2102 have the highest participation factors in this mode. In view of the fact that this mode is related to the speed of the aforementioned generators, the speed of either of these generators is monitored during the transients. The one line diagram of the system in vicinity of the two participating generators is presented in Fig. 5.2.

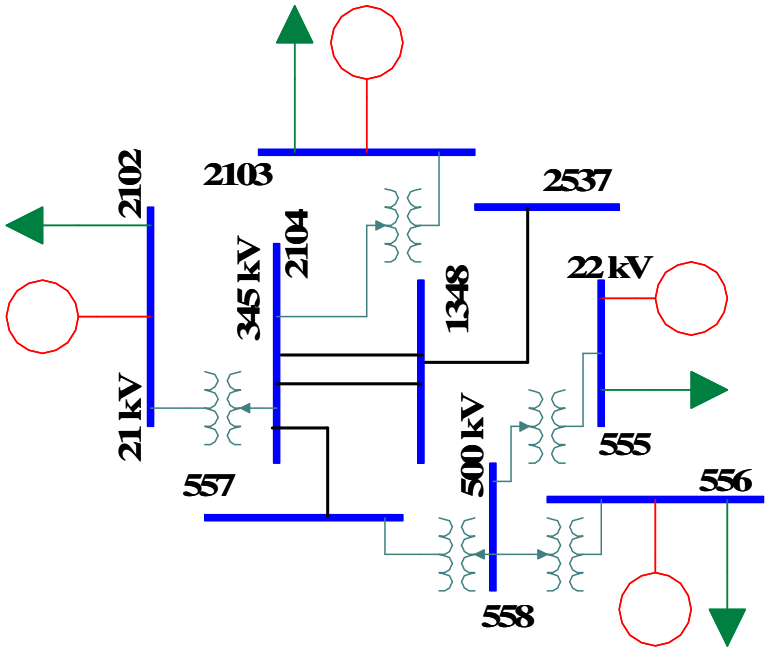

Fig. 5.2 Single line diagram of the system near the generator at bus number 2102.

The two participating generators are located in the same area and are connected to a 345 kV level bus with a step-up transformer. To identify the location of the disturbance that excites the detrimentally affected critical mode, various faults are simulated in the vicinity of the generator located at bus number 2103. Among the simulated fault scenarios, a three phase fault at the 345 kV bus of 2104, which is cleared after 4 cycles, has shown to excite the mode observed in

eigenvalue analysis results. Later in this chapter, the validity of the studied transient case is verified with the aid of Prony analysis [62].

Figure 5.6 illustrates the speed of the generator located at bus 2103 following the aforementioned three phase fault. As observed from Fig. 5.2, at higher PV penetration levels more oscillations are observed in speed of the aforementioned generator. In other words, the decreased damping observed in modal analysis is verified by the transient analysis results.

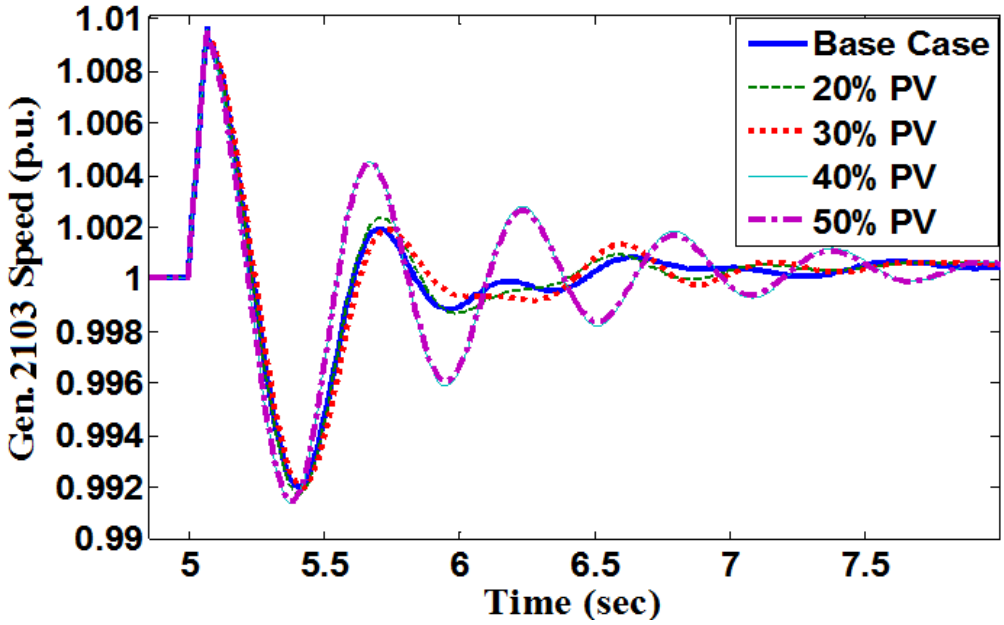

Fig. 5.3 Generator 2103 speed (p.u.) following a three phase fault at bus 2104

At a PV penetration level of 40% and above the generator speeds attain higher peaks and deeper voltage dips. Higher oscillations are also observed in the relative rotor angle of the generator located at bus 2103, under various photovoltaic penetration levels. Variations of the relative rotor angles are presented in Fig. 5.4. Detrimental impact of the PV penetration levels, which

result in increased generator speeds, is also evident in the active power output of the generator located at bus 2103. Variations of the generator active power output are shown in Fig. 5.5.

Transient simulation results presented so far corroborate the results achieved by the small signal stability analysis. However, to reassert the premise of these simulations, a measure is required to ascertain that the simulated disturbance in fact excites the detrimentally impacted mode. Prony analysis is carried out to ensure the presence of the studied mode in the transient response of the generator 2103 speed. This method is an extension to Fourier analysis that directly estimates the frequencies, damping, amplitude and relative phase of the modes presents in a given signal [62].

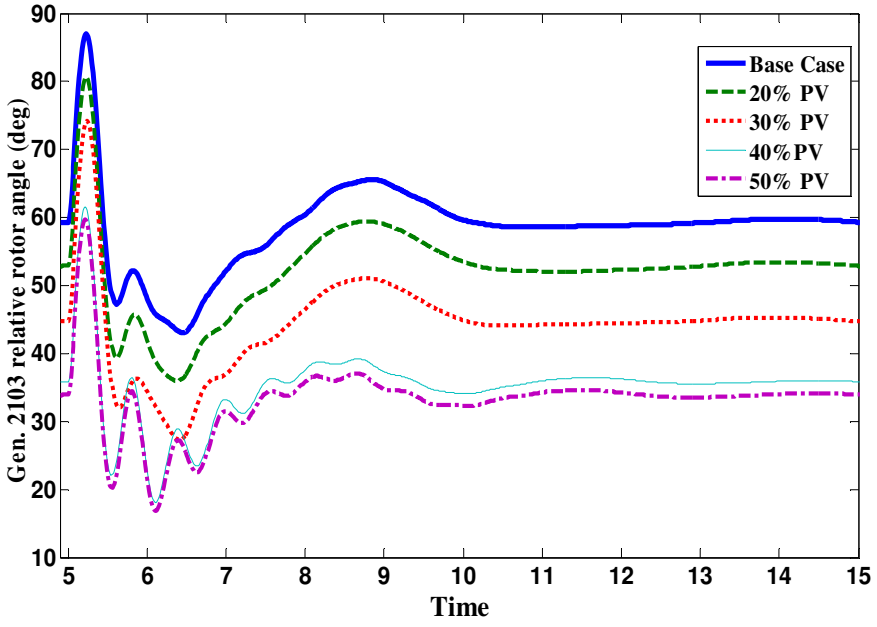

Fig. 5.4 Generator 2103 relative rotor angle (deg) following a three phase fault at bus 2104

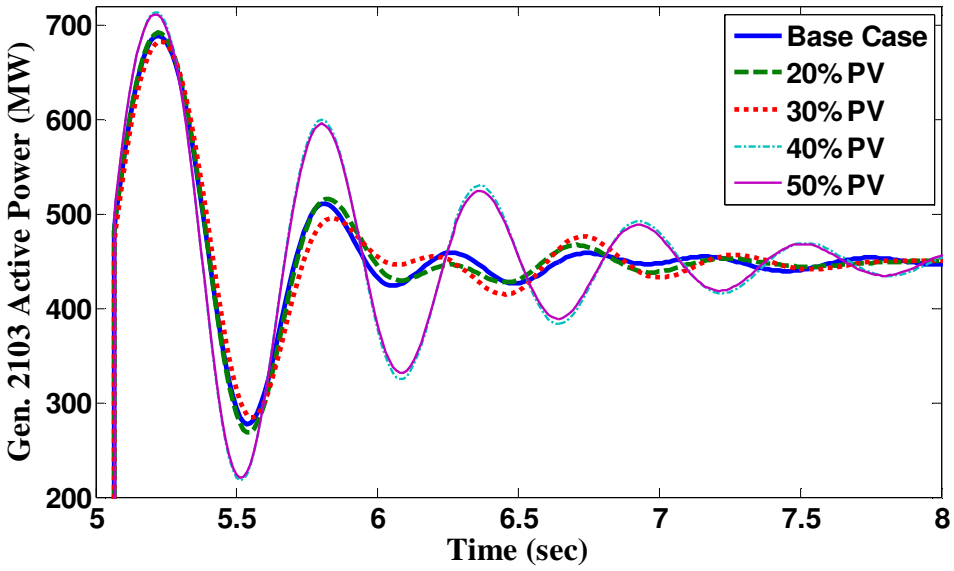

Fig. 5.5 Active power output of the generator located at bus 2103 following a three phase fault at bus 2104

The result of the Prony analysis following a three phase fault at bus 2104 is presented in Table 5-9. As presented in this Table, the same mode is observed in generator speed as was observed in the eigenvalue analysis. The difference between the results presented in Table 5-1 and Table 5-9 is related to the inaccuracy of the discrete models used in the Prony analysis method. As expected, with an increase in PV penetration levels, the damping of the studied mode is reduced.

In another case study, the second detrimentally affected critical mode, i.e. mode 8 in Table 5-1, which involves the generator E5 located at bus 810, is studied. A three phase fault occurring at the 500 kV bus number 844, which is cleared after 5 cycles, is simulated in this section. The transmission line connecting the two buses of 1425 – 810 is cleared following the fault clearance.

Fig. 5.6 illustrates the voltage of the bus 844 while Fig. 5.7 presents the voltage of the bus 810.

The speed of the E5 generator is presented in Fig. 5.8. By comparing the simulation results presented in Fig. 5.6-5.7 it is observed that bus voltages attain higher peaks and more oscillations as the level of PV penetration increases. In other words, higher PV penetrations correspond to poor damped oscillations which were expected by the results of the eigenvalue analysis. The bus voltages are more affected by the aforementioned three phase fault than the speed of the generator.

Table 5-9 Prony analysis results of the generator 2103 speed for various PV penetration levels

PV Level (%)	Magnitude	Frequency (Hz)	Damping (%)
Base Case	0.06	1.76	6.6
20%	0.06	1.76	6.4
30%	0.126	1.75	6.9
40%	0.42	1.75	4.8
50%	0.45	1.75	4.8

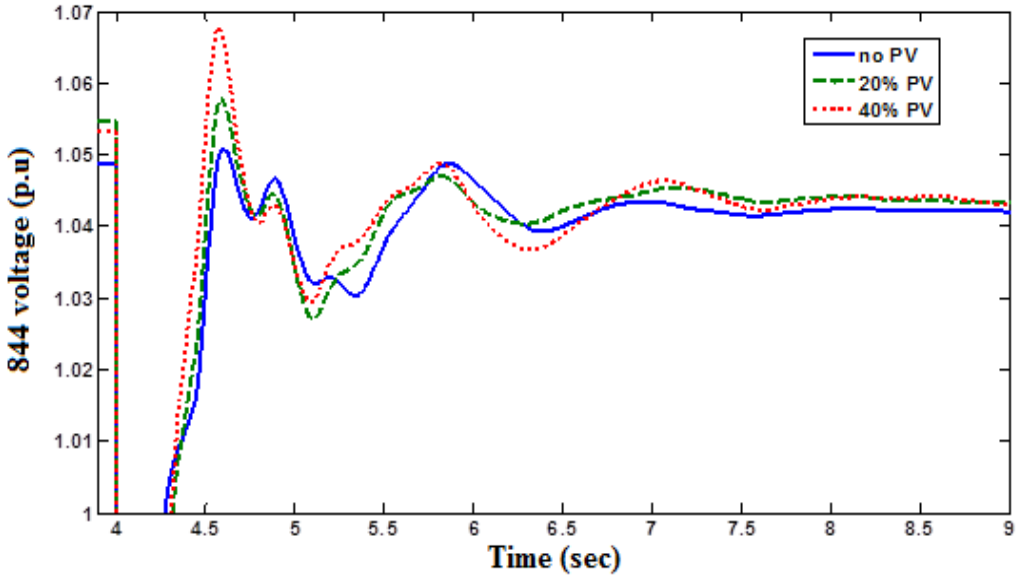

Fig. 5.6 Voltage of bus 844 following a three phase fault at bus 844

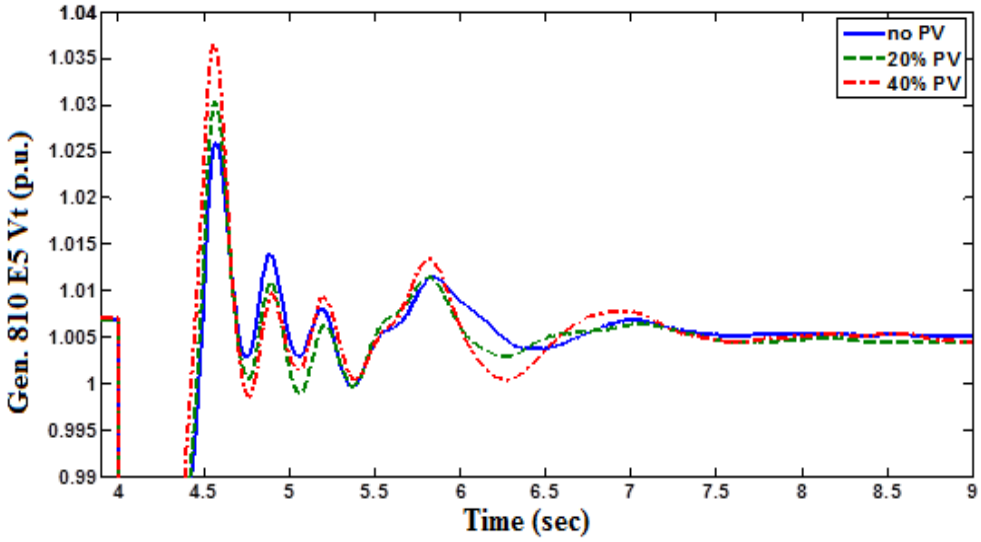

Fig. 5.7 Voltage of bus 810 E5 following a three phase fault at bus 844

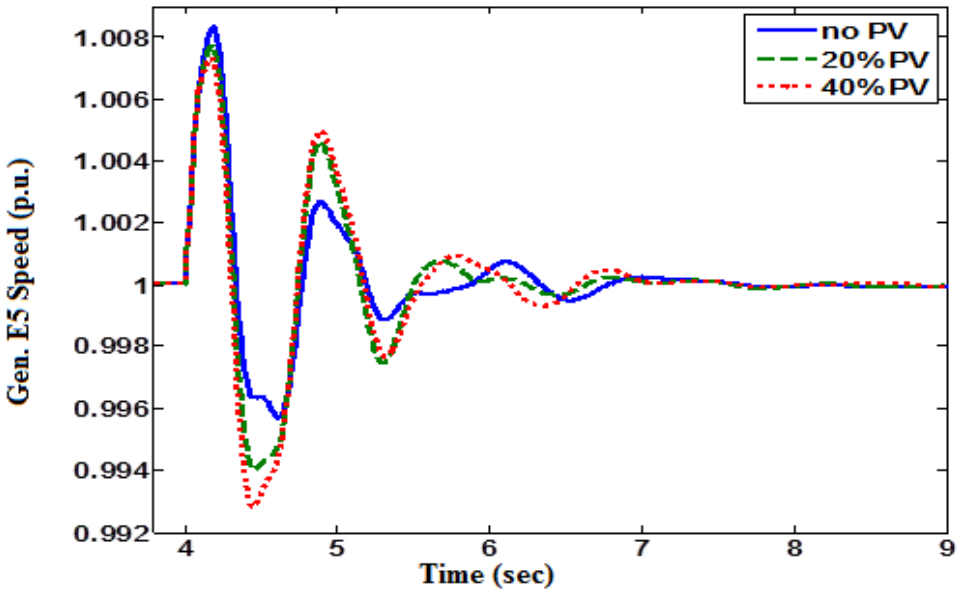

Fig. 5.8 Speed of the generator E5 following a three phase fault at bus 844

5.5 Summary Relating to PV Penetration and System Stability

In this chapter the impact of high PV penetration on power system small signal stability was investigated. Various levels of PV penetration were examined for their effect on system small signal stability. Modal analysis was conducted on the system with no PVs as well as the cases after different PV levels were introduced.

Eigenvalue analysis performed on the studied system identified the locations of the critical modes of the system. These modes are searched in the frequency range of 0.01 Hz to 2.00 Hz with a damping ratio of less than 20%. Reduced system inertia as a result of displacing conventional generators with distributed rooftop PVs may result in a reduction in the damping torques of the system modes. In order to illustrate this effect, results of the modal analysis were

compared to cases with PV penetration levels of up to 50%. The results of these comparisons identified the detrimental impacts of high PV penetration on deceasing the damping of the critical modes of the system.

Time domain analysis was performed to examine the detrimental impacts of high PV penetration during the system transients. Using the concept of participation factors and by utilizing Prony analysis, a transient case that excites a detrimentally impacted critical mode was identified. Transient studies carried out for various PV penetration levels substantiate the results of small signal analysis together with eigenvalue sensitivity analysis.

Chapter 6

OPTIMAL SYSTEM DISPATCH RATIO FOR SYSTEMS WITH HIGH PV PENETRATION LEVELS

6.1 PV Penetration and Optimal Dispatch vs. Generation Displacement

Studies carried out so far on the system with high PV penetration illustrate the fact that the impact of high PV penetration on the existing systems can be impacted by a spectrum of factors. The locations as well as the type of the transients, availability of adequate reserves within the system, the generators displaced by PV generation resources, and the generators being dispatched as a result of high PV penetration are among the factors that can change the severity of the impacts of high PV penetration on the system behavior. While all these factors to some extent contribute to the nature of the PV impacts, some will overshadow the rest of the factors due to the extent of their impact on the system behavior. While higher penetration of photovoltaic resources are added to the systems, the strategy used to displace or reschedule the conventional generators is one example of the most prominent factors involving power system operation with high PV penetration levels.

Presently practiced standards such as IEEE 1547 [2] limit the rooftop PV systems to be operated at unity power factor. Operating the rooftop PVs mainly as sources of active power, results in characteristics such as low inertia and insufficient reactive power reserves in the systems with high PV penetration. With these characteristics, power systems encounter increased need for reactive power as well as active power reserves than before. In addition, the ability to respond to

various system transients will increasingly transfer the burden on the non-displaced conventional generators. An appropriate choice of the displaced generators as well as the generators whose outputs are only backed down rather than entirely displaced by PV units is essential for mitigating the adverse effects of the photovoltaic systems on the rest of the power grid.

While more PV units are added to the existing grids, the output power generated from the other units should be reduced in order to maintain a generation and load balance. However, in practice, it would not be economically and environmentally justifiable to retain the more expensive units and all the fossil based units in service. Therefore, displacing a portion of the conventional generators with the PV systems is an inevitable consequence of high PV penetration. As mentioned previously, to ensure system reliability and in order to decrease the adverse effects of these unprecedented changes to the existing grids, there is an imminent need to identify the optimal dispatch or displace ratio of the conventional generators that lead to reliable system operation. It is critical to analyze the system to calculate for each MW addition of PV generation, the percentage of generation compensated by displacing conventional units and the percentage of generation compensated by a reduction in the generated output of the in-service units.

The objective of this chapter is to thoroughly study the system described in Chapter 3 in order to identify the optimal displace/dispatch ratio of the conventional generators while more PV generation is added to the system. Various parameters are taken into account when studying the system. Frequency

of operation, bus voltages, generator speed and relative rotor angles are among the parameters monitored during the studies carried in this chapter.

This chapter first describes the procedure followed for creating the power flow study cases. These cases are then subjected to a major generation loss within the system and the frequency response of the system is examined. The cases studied are inspired from a similar work for wind and solar integration study [63]. Optimal system dispatch is then studied by taking into account various system performance metrics that affect other parameters such as bus voltage magnitudes and generator speeds. The results of the simulations for various dispatch/displace ratios are then compared to find the optimal ratio for the system at hand. Conclusions based on the observations of the simulation results are presented at the end of this chapter.

6.2 Study Cases

The cases that have been studied in the previous chapter relate to a fixed method of displacing the conventional generators while various PV penetration levels were added to the system. However, the goal of this chapter is to compare various dispatch ratios and therefore power flow files are modified and created for various ratios. During this chapter a 40% PV penetration case, based on the levels defined in Chapter 3 is utilized for studies.

To create the aforementioned power flow files the first step required is to identify the base case (no PV units) generators that are expected to be displaced by the PV units as well as those that are being dispatched. Also the third category of generators relates to the base generation which is not impacted by the addition

of the PV units. Therefore, conventional generators are listed in to three main categories of "dispatched", "displaced", and "base" generators. Appendix E lists the base case generators of the study area belonging to each aforementioned category.

A C++ program is developed to create a list of generator outputs depending on the displace/dispatch ratio. For a 40% PV penetration case, 8033 MW of active power is supplied from the residential rooftop and commercial PVs. This additional active power is compensated by a reduction in conventional generators' outputs with various scenarios of dispatch /displace ratios. The program creates a total of 21 study cases starting from the case with all the power reduction supplied from displacing the conventional generators to case 21 in which the conventional generators are rescheduled to reduce their cumulative output by 8033 MW. The rest of the cases have various dispatch/displace ratios defined as follows for case *i*,

$$
\begin{aligned}
&delta = 0.05 \\
&ratio = 1 - delta \times i \\
&0 \le i \le 20 \\
&\text{displace (MW)} = ratio \times \mathrm{PV_{MW}} \\
&\text{dispatch (MW)} = \mathrm{PV_{MW}} - \text{displace (MW)} = (1 - ratio) \times \mathrm{PV_{MW}} \qquad (6.1)
\end{aligned}
$$

As observed from (6.1) in each interval the displace ratio is decreased by 5% and hence the dispatch ratio is increased by the same amount. The aforementioned program will then identify the generators that are turned off in each scenario as well as the output power of the redispatched generators. It should be mentioned that the output power of the redispatched generators is reduced based on their

contribution to the total output power of the dispatched generators. Therefore, the same ratio is retained while decreasing their output power. Once the output power of the conventional generators as well as their status (on or off) is determined for each study scenario, a program is written to create a set of power flow files in *PSAT*. The details of the aforementioned program is provided in Appendix E.

Due to the complexity and size of the system, the modifications to base case needs to be performed in steps in order to attain a converged power flow case. The following procedure has shown to be a proper method for creating converged power flow files for each scenario:

- Start with a converged power flow file for the base case with no PV generation present in the system
- Start with the case with all the generators being re-dispatched and none displaced
- Add the 40% PV generation (8033 MW) rooftop PVs in increments and in each increment adjust the same amount of the conventional generation based on the created macrofiles
- Solve the power flow in each increment and continue until all the modifications to the base case are performed and all the PV units are added
- Save the converged power flow file of that specific scenario
- Start from the power flow file created from the previous scenario and compare the two cases in terms of their adjustments and only modify the power flow file based on their differences. The two cases should only

differ in 5% displace ratio and therefore small modifications to the previous case are required

- Solve the power flow and move to the next scenario until all the scenarios are solved and power flow files are created for each case

6.3 Optimal Generation Dispatch with Regard to Frequency of Operation

Identifying the optimal dispatch ratio for the conventional generators is essential for ensuring the system reliability with high penetration of photovoltaic systems. Adequate resources at all times are essential for a frequency response that complies with various standards such as NERC performance criteria [64]. However, due to weather conditions, constant availability of the PV resources is an issue dealing with the systems with high PV penetration. Therefore, retaining adequate power resources within the system to account for those variations is vital for secure system operation.

This section studies the system described in Chapter 3 with 40% PV penetration under various displace ratios. The behavior of the system is solely monitored based on the frequency of operation following a major power loss within the system. The objective is to calculate the optimal dispatch ratio that meets the reserve requirements of the system and exhibits an acceptable frequency behavior dealing with the type of aforementioned disturbances.

Two different scenarios are studied in this section. The first scenario compares the frequency response of the system for all different dispatch ratio scenarios developed in the previous section, following a loss of two major units in the study area [63]. The second scenario, not only entails loss of the two major

units, but also assumes a major loss in the output power of the PV units due weather fluctuations. The variations could be as a result of a cloud cover, single system event or other unpredictable weather conditions that commonly occur in systems with high PV solar based generation. The two cases are then compared to draw conclusion as the optimal dispatch ratio with regards to adequate system reserves. The active power exchange to the other areas is maintained constant within this study to only study the local effects of PV systems on the studied area.

6.3.1 Frequency metrics

In determining the frequency response of the entire system, various performance metrics are taken into consideration for comparison purposes. These metrics are mainly adopted from [65] and are explained subsequently.

- *Frequency Nadir:* The nadir of a given frequency signal is the *lowest point* of a frequency response in response to an event in the system. This point is shown as the point A_N in Fig. 6.1. This metric is particularly important for system operation due to the fact that low values of frequency nadir might not be in compliance with various performance standards and also trip the under frequency load shedding relays.
- *Frequency Nadir Time:* This parameter determines the time it will take for the system frequency to reach its nadir. Nadir time is shown in Fig. 6.1 as point A_t.
- *Settling Frequency:* This metric determines the frequency at which the response will settle after a certain amount of time. This time is taken to be 50 s following a disturbance throughout this text as it is an adequate time

for the frequency to settle to its steady state value following a transient. Point A_f in Fig. 6.1 shows the settling frequency for a given signal.

The three metrics mentioned above will be used throughout this section to compare various scenarios in order to find the optimal dispatch ratio in terms of the frequency response. However, frequency needs to be checked at all points of the system to determine the overall frequency behavior rather than a specific point within the system. This could result in inaccurate comparisons due to the computing requirements of the large system at hand.

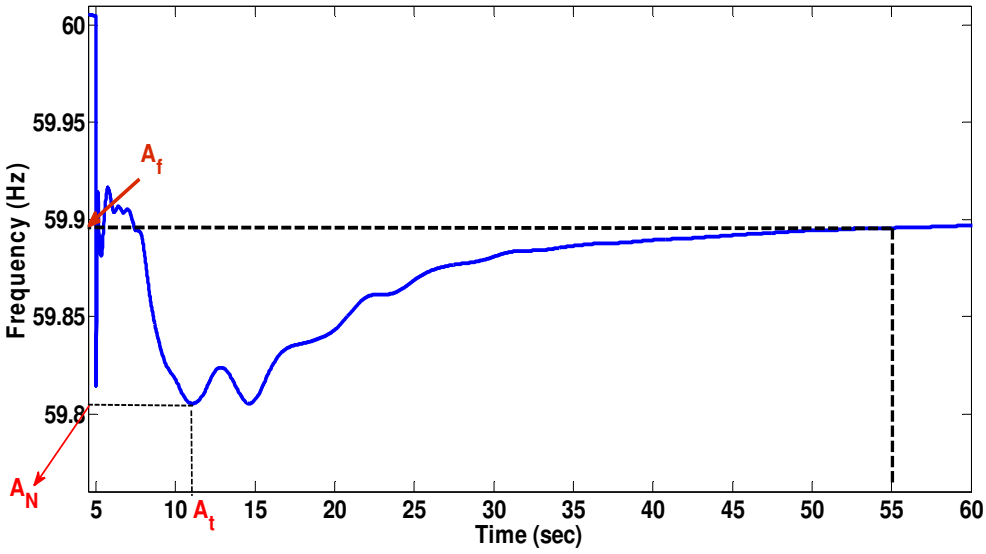

Fig. 6.1 Description of the performance metrics A_f, A_N, and A_t

To better represent the frequency of the system following a disturbance, a system based frequency is defined [65] that measures the frequency of operation at various machines and averages these frequencies based on the size of the machine. Hence, the contribution of each frequency to the overall frequency of the system will be based on the size of the individual machines. This system

equivalent frequency can be referred to as the center of inertia speed of the conventional synchronous machines. For the purpose of this study the system equivalent frequency is calculated for the studied area following the two aforementioned disturbances in the system. Based on the aforementioned descriptions, the system based frequency is defined as follows [65],

$$f_{sys} = \frac{\sum_{i=1}^{N} MVA_i \times f_i}{\sum_{i=1}^{N} MVA_i} \tag{6.2}$$

where,

f_{sys} is the center of inertia frequency defined for the entire system

MVA_i is the rating of generator i

f_i is the frequency of generator i

N is the total number of the synchronous generators in the system.

One advantage of using the metric shown in (6.2) over the nodal frequency values is that the local swings will be filtered out. Therefore the frequency response is filtered in way to better represent the frequency of the entire system. In addition, since the overall system is considered in the system based frequency, the system based frequency provides a better tool for comparing various dispatch and commitment scenarios. This is the case since comparing the frequencies at each and every point within the system will be a rather difficult task due to the size of the system at hand.

6.3.2 Case study 1: loss of two major units

In the first study case considered in this section, the effect of the loss of a significant portion of conventional generation on the system frequency is observed. To account for a considerably large disturbance an outage of 2820 MW of active power loss from the overall system generation is assumed. Therefore, the system frequency is expected to settle at a lower value than the normal operating frequency, i.e. 60 Hz. All the 21 cases generated in the previous section with various dispatch or de-commitment ratios are utilized for simulation of the case described. The simulations carried in this part are conducted in PSLF.

It is assumed the two units are switched off at $t=5\ s$ of the simulation time while the system is operating under normal operating conditions before that time. For each study scenario, the time responses of the frequencies of the conventional generators are simulated and their values are transferred to MATLAB for further analysis. With the aid of a MATLAB code these values are utilized to calculate the system equivalent frequency shown in (6.2).

To compare various aspects of the frequency response for different studied scenarios, the simulation results are shown in separate figures. While each figure is meant to focus on a certain aspect of the response, such as the frequency nadir, settling time, and signal damping, all the figures combined will present a better idea of the system behavior under various dispatch or de-commitment ratios. Figures 6.2-6.4 present a summary of the simulation results for various ratios. For comparison purposes various parameters of the frequency response are also summarized in Table 6-1.

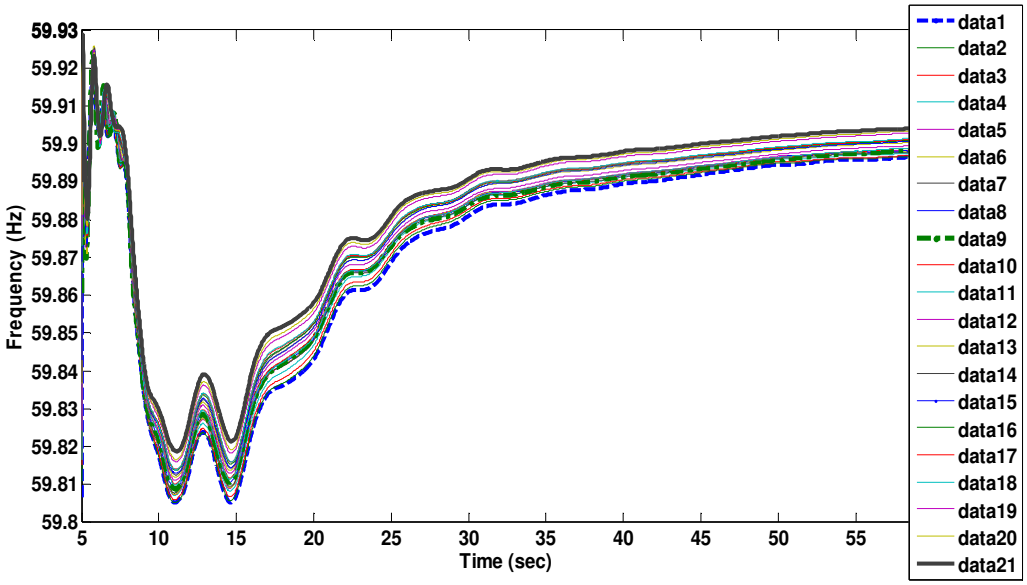

Fig. 6.2 Frequency response of various dispatch ratios for a loss of two major units

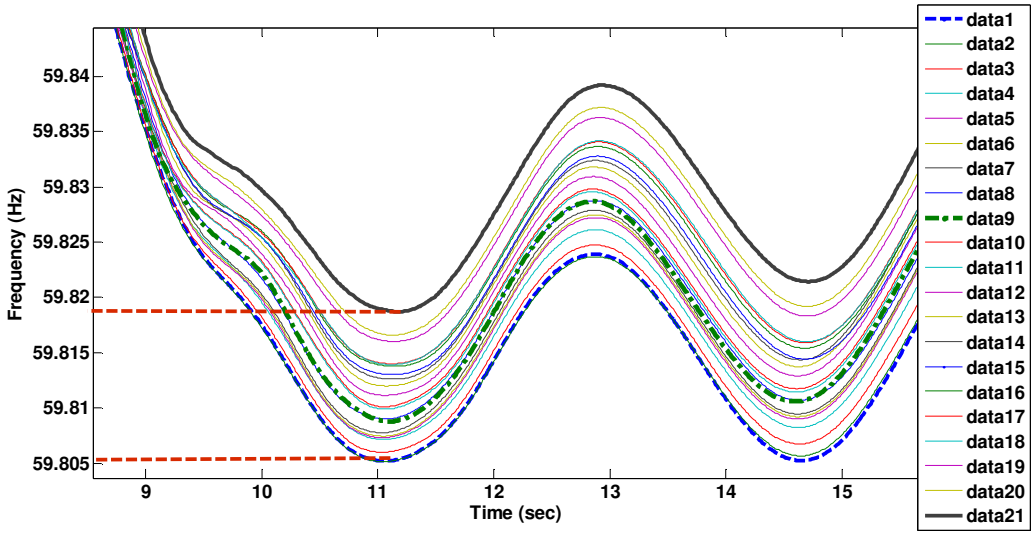

Fig. 6.3 Frequency nadir of various dispatch ratios for a loss of two major units

Figure 6.2 shows the frequency response of the system following an outage of the two major units. Various dispatch/de-commitment ratios are simulated, ranging from zero dispatch ratio in the first set of data to 100%

dispatch ratio in the 21st scenario. The two extreme cases are shown with solid and dashed lines in the aforementioned figure. As seen from this figure the overall frequency response of the system is slightly improved as more generators are re-dispatched than de-committed. This behavior is more evident in Figs. 6.3-6.4 that compare the frequency nadir and settling frequency respectively.

Table 6-1 Frequency metrics for various scenarios after two large unit outages

Scenario Number	Dispatch Ratio (%)	Frequency Nadir (Hz)	Nadir Time (s)	Settling Frequency (Hz)
1	0	59.8052	11.05	59.8977
2	5	59.8051	11.05	59.8977
3	10	59.806	11.05	59.8977
4	15	59.8071	11.05	59.8986
5	20	59.8073	11.04	59.8994
6	25	59.8075	11.04	59.8992
7	30	59.8078	11.025	59.899
8	35	59.809	11.063	59.8992
9	40	59.8088	11.114	59.8992
10	45	59.8101	11.063	59.8994
11	50	59.8099	11.063	59.8993
12	55	59.8112	11.05	59.90
13	60	59.812	11.076	59.901
14	65	59.8126	11.126	59.902
15	70	59.813	11.126	59.9016
16	75	59.8138	11.126	59.9019
17	80	59.814	11.126	59.9021
18	85	59.8139	11.1135	59.9024
19	90	59.816	11.138	59.9039
20	95	59.8166	11.138	59.904
21	100	59.8187	11.188	59.905

Various scenarios differ more in terms of the frequency nadir than the settling frequency. The difference between the frequency nadirs are as a result of the reduced inertia in the lower dispatch ratio cases. However, the steady state

values of the frequencies are relatively close due to the assumption that PV units are all available during the simulation and are operating at their nameplate values.

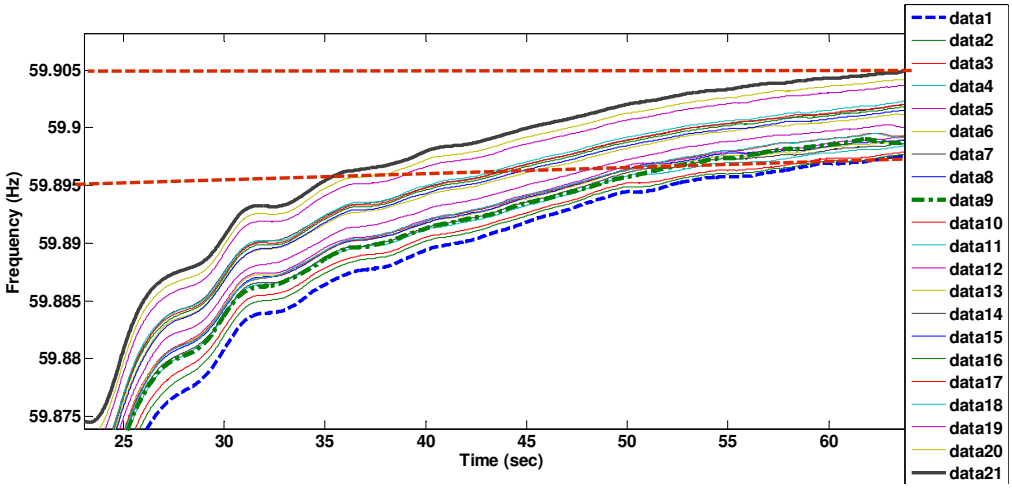

Fig. 6.4 Frequency settling value of various dispatch ratios for a loss of two major units

6.3.3 Case study 2: loss of two large units in addition to loss of PV units

Unlike the previous case, the case studied in this section does not assume that the PV units are constantly available at all times. In fact, the same outage scenario simulated in the previous section is studied in this case in addition to the assumption of a cloud cover that could impact the output power of the PV units. Similar to the previous case, a penetration level of 40% is assumed for the case studied.

The simulation carried out in this section assumes that the output power of the rooftop PV units in a certain geographical area is lost due to a single system event. This translates to 2400 MW of power loss from the total system PV generation. A cloud cover could be an example of those scenarios that can lead to such power outages. It is assumed that this outage occurs after 4 sec of the start of

the simulation and will continue until 15 sec. At t=15 sec the two outaged units will also trip that will add to the outage of the PV units. The simulation is continued until t=70 sec in order to observe the settling frequency of each scenario studied. Simulation results are presented in Fig. 6.5-6.7. For comparison purposes settling frequencies as well as the frequency nadir of the cases are also summarized in Table 6-2.

As observed from Fig. 6.7 the system equivalent frequency in the first two dispatch scenarios, i.e. dispatch ratios of up to 5%, is significantly lower than the other studied cases. In other words the frequency response of the system improves after 10% dispatch ratio. The frequency nadir improves proportional to the increase in the dispatch ratio. Therefore, the settling frequency would be a better identifier for determining the optimal dispatch ratio in the system. Figure 6.8 plots the settling frequency values for all the cases studied versus the case number. By observing the results plotted in Fig. 6.8 it is seen that the frequency values are significantly different above 5% dispatch ratios than at any setting before that. Therefore, the value of 10% dispatch ratio can be the cut-off value for the optimal dispatch ratio selection while only considering the frequency as the parameter of interest. As it will be explained in the following section, other parameters such as the bus voltages are also affected by various dispatch ratios. The optimal dispatch ratio is also determined by bus voltages in response to various system transients.

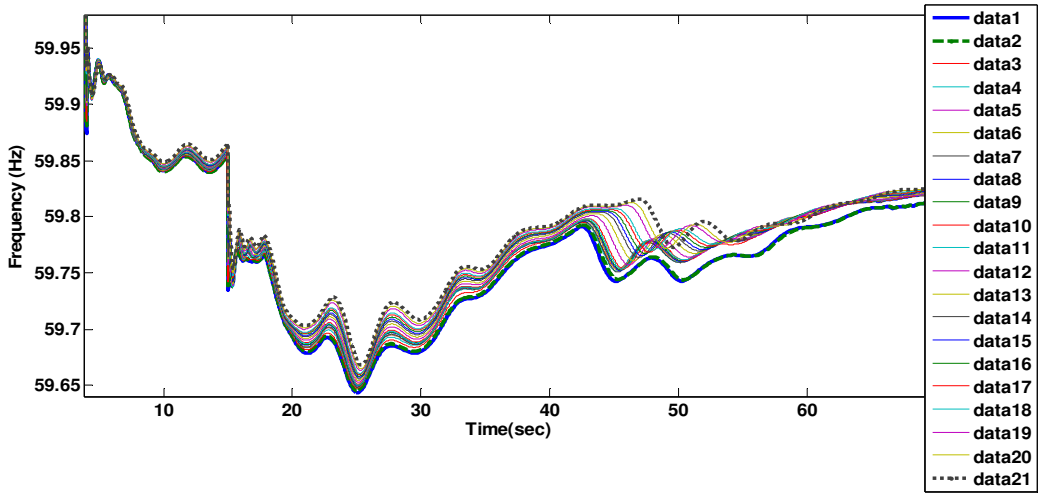

Fig. 6.5 System equivalent frequency for various dispatch ratios for loss of rooftop PVs and two large units

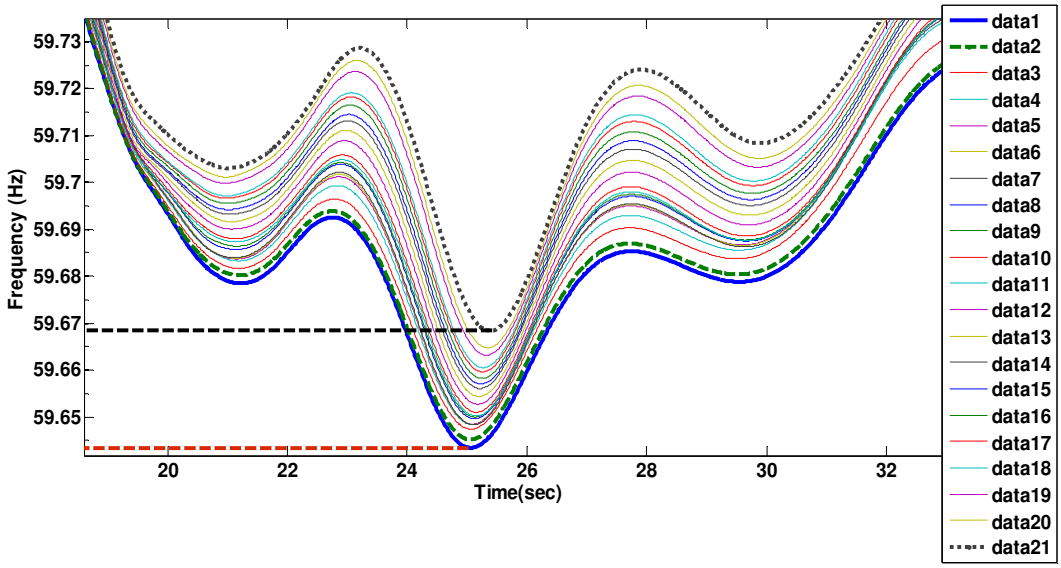

Fig. 6.6 Frequency nadir of various dispatch ratios for loss of rooftop PVs and two major units

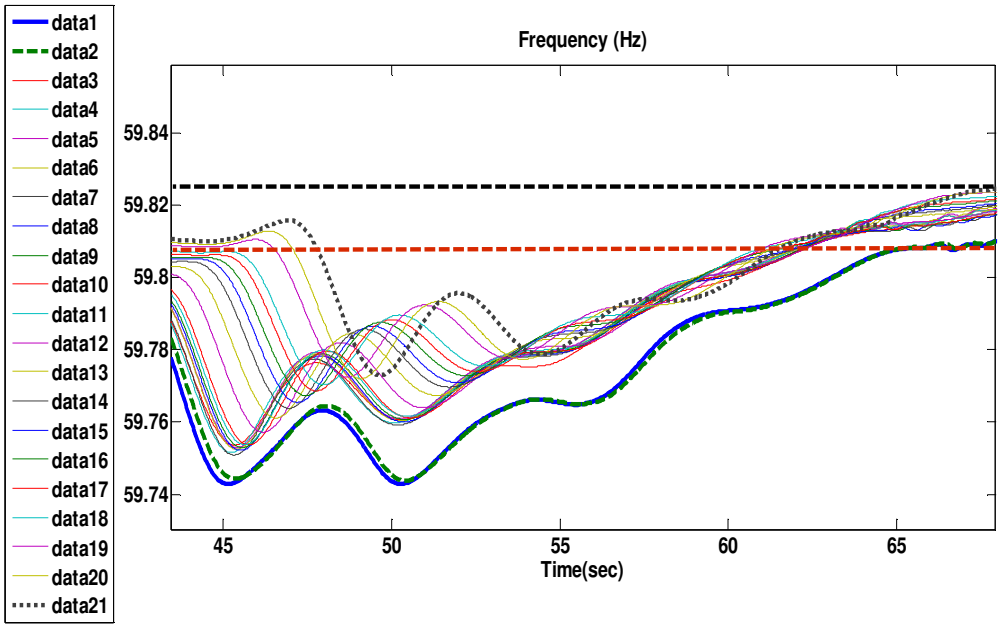

Fig. 6.7 Frequency settling value of various dispatch ratios for loss of rooftop PVs and two large units

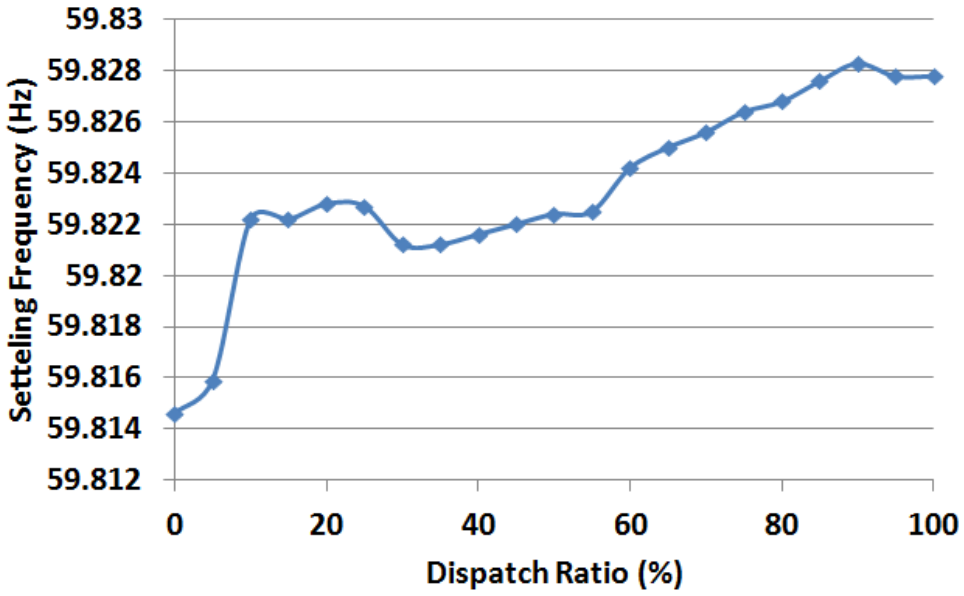

Fig. 6.8 Frequency settling value versus dispatch ratio

Table 6-2 Frequency metrics for various scenarios following the outage of two large units

Scenario Number	Dispatch Ratio (%)	Frequency Nadir (Hz)	Nadir Time (s)	Settling Frequency (Hz)
1	0	59.6435	25.057	59.8146
2	5	59.6452	25.058	59.8159
3	10	59.6474	25.06	59.8222
4	15	59.6484	25.095	59.8222
5	20	59.6485	25.095	59.8228
6	25	59.6484	25.095	59.8227
7	30	59.6484	25.107	59.8212
8	35	59.6496	25.1203	59.8212
9	40	59.65	25.1324	59.8216
10	45	59.651	25.158	59.822
11	50	59.6502	25.1454	59.8224
12	55	59.6527	25.170	59.8225
13	60	59.6544	25.2085	59.8242
14	65	59.6561	25.2212	59.825
15	70	59.6571	25.2337	59.8256
16	75	59.6582	25.2464	59.8264
17	80	59.6597	25.2489	59.8268
18	85	59.6605	25.2715	59.8276
19	90	59.6632	25.3219	59.8283
20	95	59.6648	25.3471	59.8278
21	100	59.6648	25.3849	59.8278

The results presented in this section points out the fact that the higher the dispatch ratio, the better the frequency performance of the system would be. There would not be a significant difference between the worst frequency response (0% dispatch ratio) and the best frequency response (100% dispatch ratio). The main reason for the similarity of these responses is the fact that the generation and load balance is similar in all the cases. In other words the availability of the active

power is almost similar in all the cases due to the fact that the retained conventional generators have the capability to adjust their output power to react to the loss of the PV resources. If a summer peak case was selected for the study, the results could be different in terms of the active power availability due to the fact that most of the generators are already at their maximum value in the peak case.

6.4 Effect of Transients on Optimal Generation Dispatch

As mentioned in the previous section, during the light loading conditions, the system frequency will not serve as the best identifier for determining the optimal dispatch ratio at high PV penetration levels. In this section, system behavior is analyzed in terms of the other parameters such as bus voltages and generator speed as well as the relative rotor angles. Three phase faults, line outages or a combination of both are the type of the disturbances studied. The disturbances are selected based on the previous simulations in order to select the cases that have shown to have significant impact on the system mainly due to the fault location and its impact on the rest of the system. The objective is to identify the *minimum dispatch ratio* while achieving an acceptable system behavior in terms of the bus voltages, generator speeds and etc. The reason the minimal dispatch ratio is selected is mainly due to the fact that with more conventional generation units decommitted from the service, cost of generation will be reduced. In addition, some more expensive units as well as the less environment friendly generating units can be decommitted from the service.

Two cases, that have shown to be among the severe cases, are presented in this section. The fact that these two cases are selected for this study is solely

based on the previous simulation results of the system which has identified the more severe transients in the system.

Case study 1: Three phase fault with line removal

The case study presented in this chapter is related to a three phase fault at the 500 kV level bus 1569. The faulted bus is close to three main generating stations. Therefore, a fault at this location can disturb a significant amount of the generated power from these three generating units. It is assumed that the fault is cleared after 5 cycles and the connecting transmission line 1569-2375 is removed from the service following the fault clearance. Similar to the previous cases studied in this chapter a 40% PV penetration case is simulated for all the various dispatch ratio cases studied.

The simulation is carried out for all the 21 cases that have been explained at the beginning of this chapter. The simulation results are presented in Figs. 6.9-6.12. Voltage of the faulted bus, i.e. bus 15021, is presented in Fig. 6.9 while Fig. 6.10 shows the voltage of the bus 2375 following the disturbance for all the 21 cases considered for the study. The frequency of the bus 1569 is also presented in Fig. 6.11.

As seen from the bus frequencies and the voltage magnitudes, the system goes unstable following the aforementioned bus fault for certain dispatch ratios. The system becomes stable as the dispatch ratio is increased and therefore less conventional generators are de-committed from the service. The minimum dispatch ratio that makes the system stable is found to be related to the 10^{th} studied scenario. This scenario corresponds to a dispatch ratio of 45%. This

dispatch ratio means for every 100 MW of PV power added to the system, 45 MW of power generated by the conventional generating units is reduced by redispatching those units and 55 MW of the required power reduction is provided by displacing the conventional units.

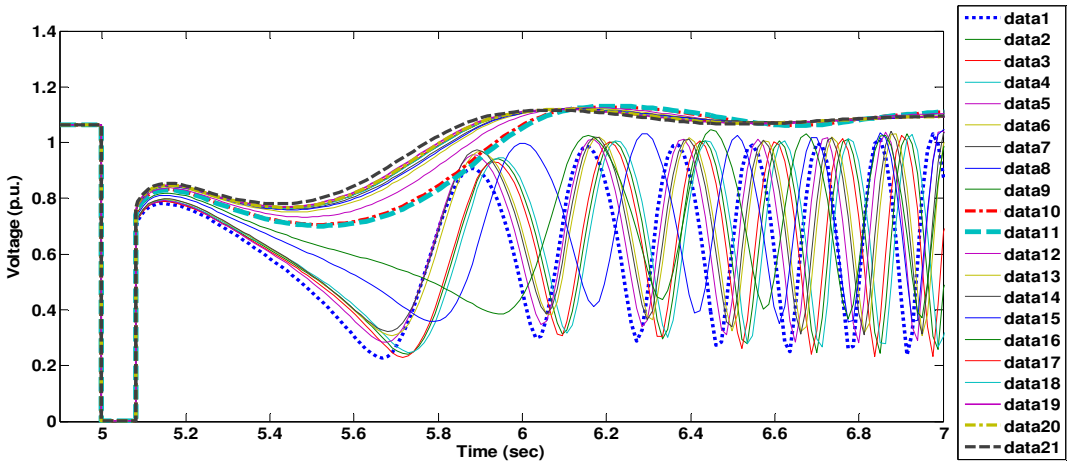

Fig. 6.9 Voltage of the bus 1569 following a thee phase fault at 1569

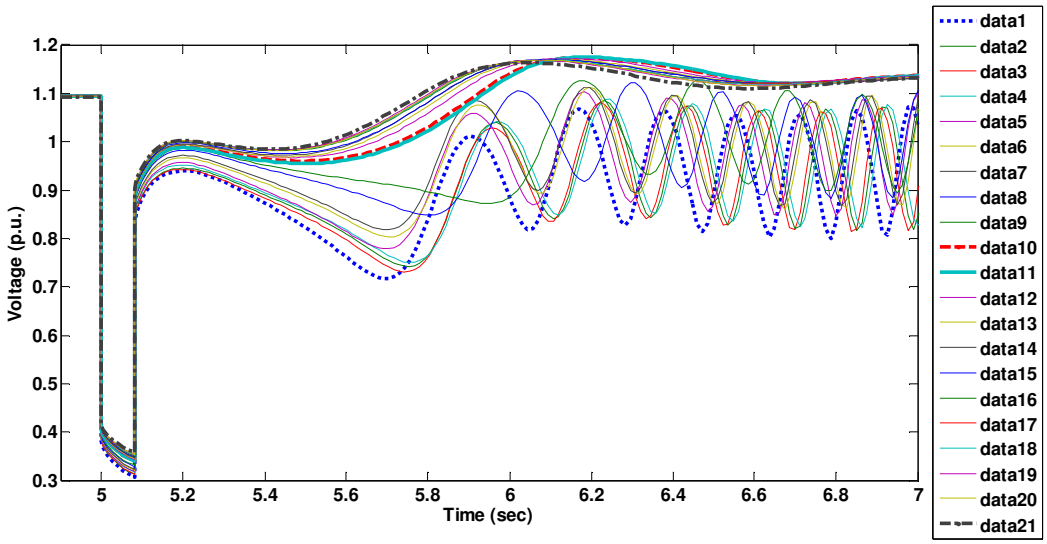

Fig. 6.10 Voltage of the bus 2375 500 kV following a thee phase fault at 1569

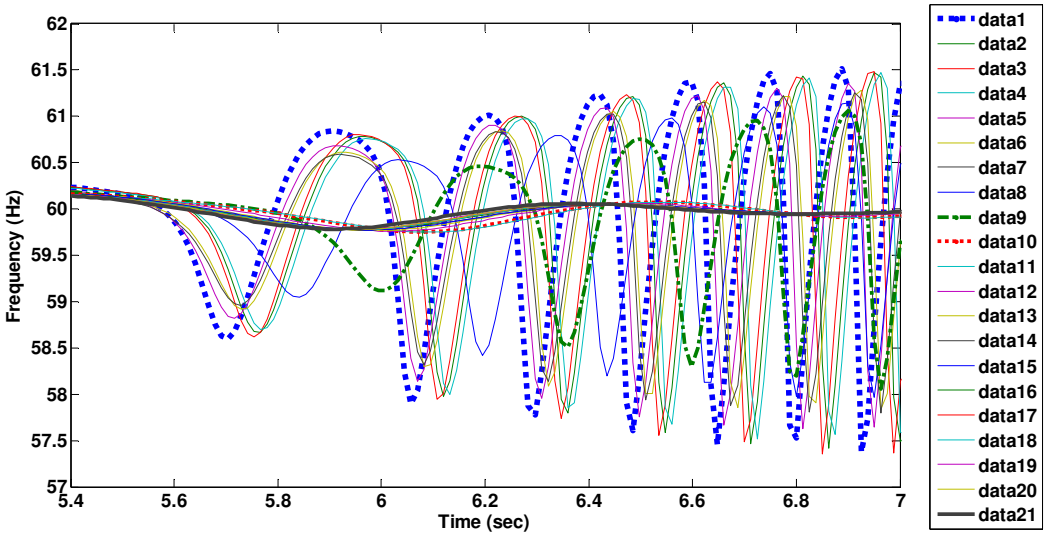

Fig. 6.11 Frequency of the bus 1569, 500 kV following a thee phase fault at 1569

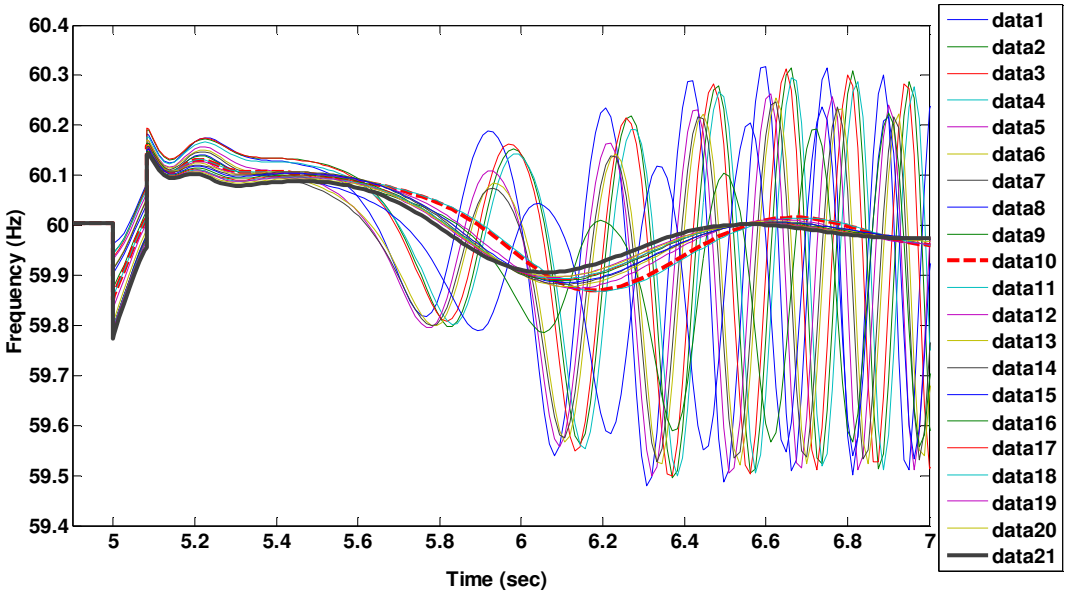

Fig. 6.12 Frequency of the bus 2375, 500 kV following a thee phase fault at 1569

6.5 Small Signal Analysis Approach to Optimal Generation Dispatch

The studied cases presented in the previous section showed that an appropriate dispatch ratio can in fact determine the unstable and stable behavior following a large disturbance. However, in order to better identify the cases that

might trigger the same characteristics, a similar approach as Chapter 5 is followed in this section.

Small signal analysis is conducted on the system with 40% PV penetration level under the 21 various conventional generation dispatch ratios in order to compare different modes of the system with regards to the dispatch ratios. A selected eigenvalue analysis can identify the critical modes of the system, i.e. the modes with low damping and low frequency, under various dispatch ratios. Hence, comparing these modes would be an appropriate tool to assess the small signal stability of the system in different scenarios. Once the more critical modes that also differ in terms of their impact with various dispatch ratios are identified, a transient analysis is conducted to compare the transient behavior of the system. These cases will then identify the optimal conventional generation dispatch ratios by following the same procedure presented in the previous section.

A summary of the results of the selected eigenvalue analysis is presented in Table 6-3 that only presents the *critical modes* of the system for the case with zero dispatch ratio. The rest of the eigenvalues are not shown due to the fact that they would not lead to any major stability concern in the system. The small signal analysis is performed in SSAT. The frequency of interest for full eigenvalue analysis is [0.01 Hz-1.2 Hz] while the modes with the damping of less than 20% are considered for study.

Among the eigenvalues presented in Table 6-3, there are a few modes that have a different damping while the dispatch ratio of the conventional generators is increased. For better comparison, these modes are presented in Tables 6-4 through

6-6 for various dispatch ratios. Although the results presented do not exhibit a significant change in the damping ratios, the simulation studies presented later in this section will show that when dealing with a large disturbance these differences are expected to become larger.

Table 6-3 Critical modes for zero dispatch ratios

Real	Imaginary	Frequency (Hz)	Damping (%)	Dominant State
-0.4477	12.5097	1.991	3.58	2103 : SS4 : Speed
-0.6998	9.1514	1.4565	7.62	1567 : G2 :Speed
-0.6987	9.1367	1.4542	7.62	1568 : G3 : Speed
-1.2915	10.4389	1.6614	12.28	2164 : DD1 : Speed
-1.369	10.6416	1.6937	12.76	184 : P3 : Speed
-0.333	2.5037	0.3985	13.19	808 : E3 :Speed
-0.3321	2.3119	0.3679	14.22	808 : E3: Speed
-1.6645	11.228	1.787	14.66	2247 : BB3 :Angle
-1.4637	9.1478	1.4559	15.8	810 : E5 : Angle
-2.1446	10.5689	1.6821	19.89	2164 : DD1 :Speed
-2.852	12.1256	1.9298	22.9	473 : D4 :Angle
-2.4163	8.9645	1.4267	26.03	183 : P2 :Speed
-2.832	7.0097	1.1156	37.46	2100: SS1 :Speed

The results presented in Table 6-3 to Table 6-6 confirm the fact that the small signal stability of the system will be improved once the conventional generators' dispatch ratio is increased. However, as seen from these tables, the eigenvalues of the system in most of the cases move farther towards the left half plane until a certain dispatch ratio and then begin to move closer to the right half plane (RHP) afterwards.

Table 6-4 Comparison of critical modes for various dispatch ratios (mode 1)

Run Number	Mode			Damping (%)
	Real	Imaginary	Frequency (Hz)	
0	-0.333	2.5037	0.3985	13.19
1	-0.3464	2.501	0.3981	13.72
2	-0.3592	2.4953	0.3971	14.25
3	-0.3692	2.4868	0.3958	14.69
4	-0.3807	2.4748	0.3939	15.21
5	-0.3514	2.2988	0.3659	15.11
6	-0.3974	2.4367	0.3878	16.1
7	-0.4012	2.412	0.3839	16.41
8	-0.3951	2.3855	0.3797	16.34
9	-0.3843	2.3691	0.377	16.01
10	-0.3749	2.3603	0.3757	15.69
11	-0.3727	2.3542	0.3747	15.64
12	-0.3705	2.3478	0.3737	15.59
13	-0.3726	2.3402	0.3725	15.72
14	-0.3737	2.3299	0.3708	15.83
15	-0.373	2.3299	0.3708	15.81
16	-0.3756	2.3288	0.3706	15.92
17	-0.3749	2.3276	0.3704	15.9
18	-0.3732	2.3245	0.37	15.85
19	-0.3748	2.3246	0.37	15.92
20	-0.3734	2.3222	0.3696	15.87

Table 6-5 Comparison of critical modes for various dispatch ratios (mode 2)

Run Number	Mode			Damping (%)
	Real	Imaginary	Frequency (Hz)	
0	-1.6645	11.228	1.787	14.66
1	-1.6869	11.2404	1.789	14.84
2	-1.6976	11.2365	1.7884	14.94
3	-1.7206	11.2395	1.7888	15.13
4	-1.7464	11.2402	1.7889	15.35
5	-1.7772	11.2341	1.788	15.63
6	-1.8041	11.2129	1.7846	15.89
7	-1.8282	11.1813	1.7796	16.14
8	-1.8431	11.1374	1.7726	16.33
9	-1.8603	11.0555	1.7595	16.59
10	-1.8449	10.9861	1.7485	16.56
11	-1.8358	10.9262	1.739	16.57
12	-1.7934	10.8548	1.7276	16.3
13	-1.7335	10.7894	1.7172	15.86
14	-1.6518	10.7268	1.7072	15.22
15	-1.6579	10.7113	1.7048	15.3
16	-1.6613	10.7133	1.7051	15.32
17	-1.6642	10.7151	1.7054	15.35
18	-1.6631	10.7267	1.7072	15.32
19	-1.6556	10.7261	1.7071	15.26
20	-1.654	10.7257	1.7071	15.24

To better illustrate this behavior and also in order to find the ODR for the system at hand the methodology used in this work is to study the transient behavior of the system under various disturbances. The disturbances selected are those that will excite the above discussed modes. Two different disturbances corresponding to each eigenvalue presented in Table 6-4 to Table 6-6 are studied next.

Table 6-6 Comparison of critical modes for various dispatch ratios (mode 3)

Run Number	Mode			Damping (%)
	Real	Imaginary	Frequency (Hz)	
0	-0.4477	12.5097	1.991	3.58
1	-0.4921	12.489	1.9877	3.94
2	-0.5424	12.4627	1.9835	4.35
3	-0.5962	12.4315	1.9785	4.79
4	-0.6426	12.3943	1.9726	5.18
5	-0.7057	12.3494	1.9655	5.7
6	-0.7899	12.295	1.9568	6.41
7	-0.8828	12.2339	1.9471	7.2
8	-0.9885	12.1649	1.9361	8.1
9	-1.1044	12.0911	1.9244	9.1
10	-1.2248	12.0128	1.9119	10.14
11	-1.3443	11.9305	1.8988	11.2
12	-1.4553	11.8565	1.887	12.18
13	-1.5486	11.7904	1.8765	13.02
14	-1.6173	11.7349	1.8677	13.65
15	-1.6079	11.398	1.814	13.97
16	-1.6078	11.3981	1.8141	13.97
17	-1.6079	11.398	1.8141	13.97
18	-1.604	11.3967	1.8138	13.94
19	-1.6893	11.7154	1.8646	14.27
20	-1.693	11.7118	1.864	14.31

Case study 2: Three phase fault at bus 844 with line removal

The case studied in this section is a three phase fault at the 500 kV bus of 844 which is cleared after 5 cycles. The transmission line connecting the two buses of 1425 and 844 is removed following the fault clearance. The faulted bus is in the vicinity of the generator E5 located at bus 810 to which the mode presented in Table 6-4 belongs. Voltage and frequency of the bus 1425 is

presented in Figs. 6.13-6.14 respectively. For comparison purposes the voltage of the bus 810 is also presented in Fig. 6.15. The eigenvalue presented in Table 6-4 corresponds to the speed of the generator 810. Therefore, the speed of this generator under various dispatch ratios is shown in Fig. 6.16.

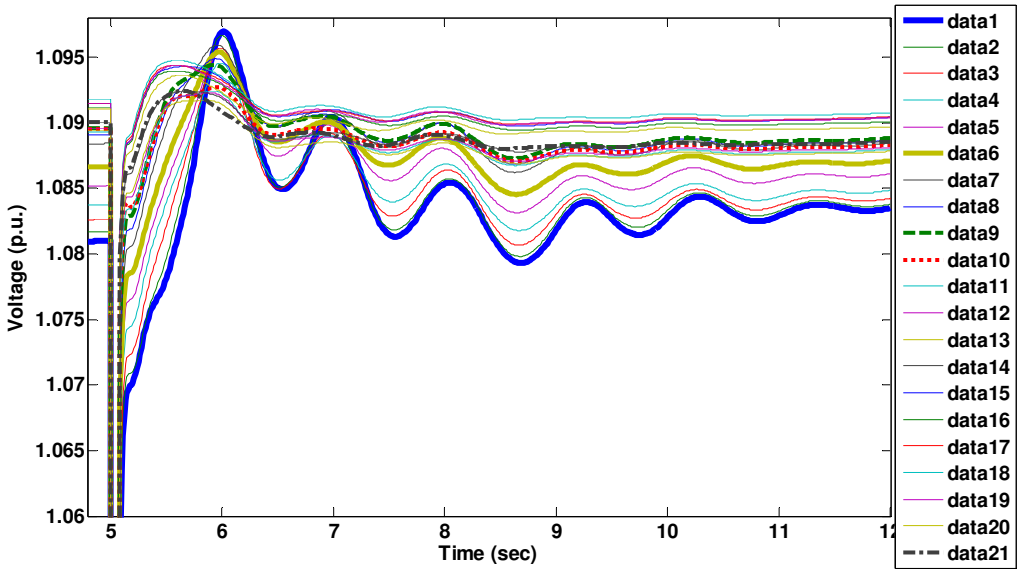

Fig. 6.13 Voltage of the bus 1425 following the case 2 disturbance

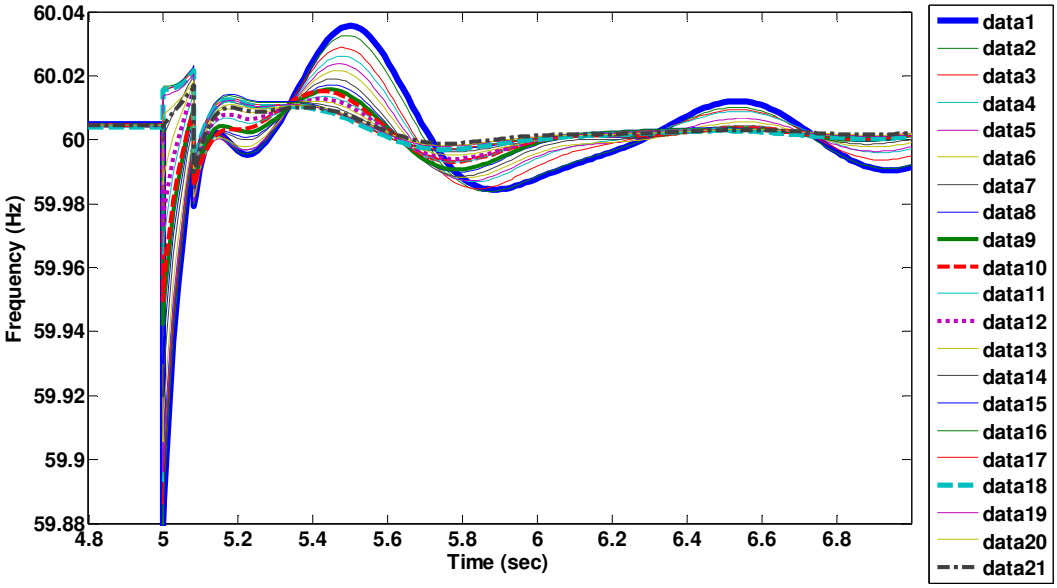

Fig. 6.14 Frequency of the bus 1425 following the case 2 disturbance

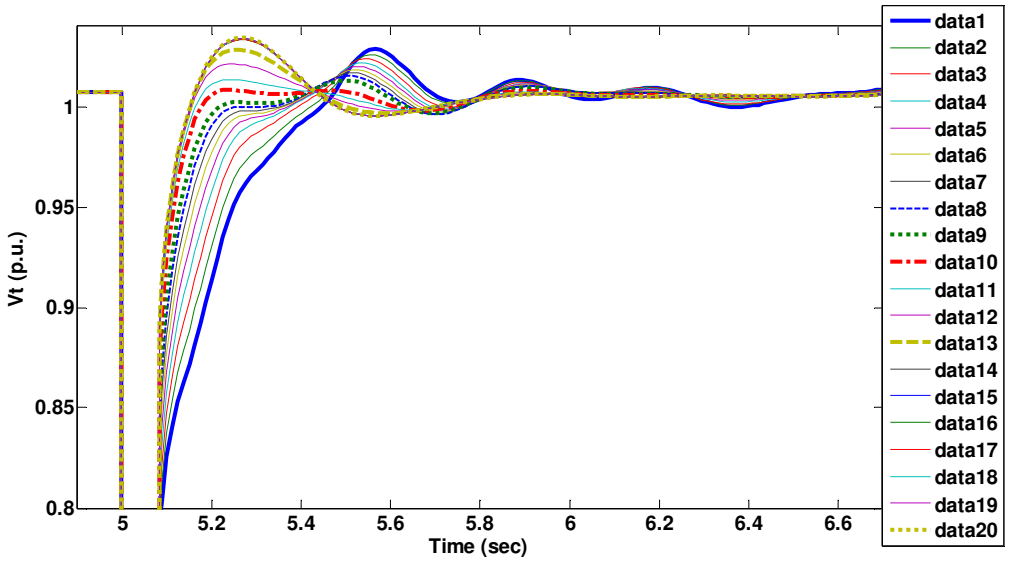

Fig. 6.15 Voltage of the bus 810 following the case 2 disturbance

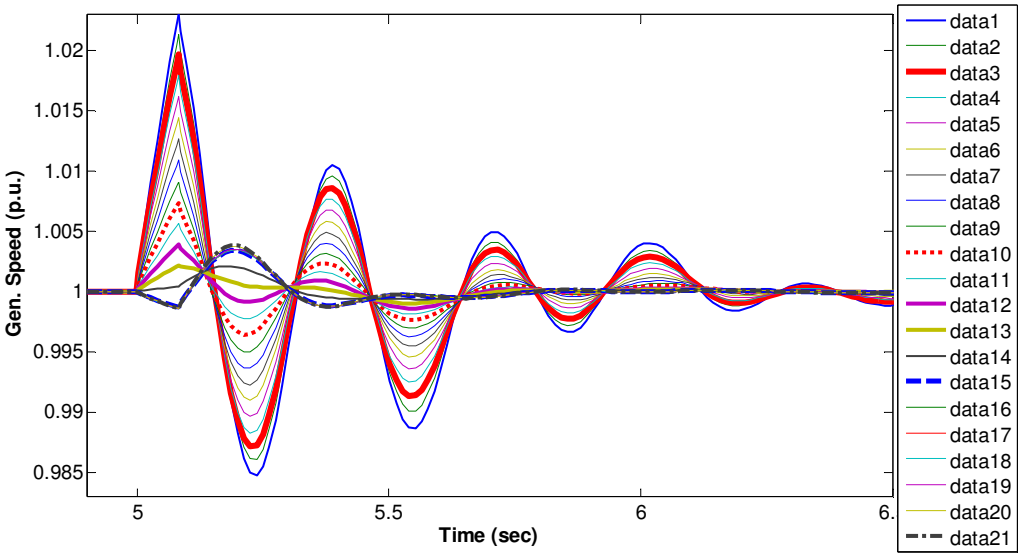

Fig. 6.16 Speed of the generator 810 E5 following the case 2 disturbance

By comparing the simulation results presented in Figs. 6.13-6.16, a few conclusions are drawn with regards to system operation with different dispatch ratios. The bus frequencies illustrate a better performance as the dispatch ratios

are increased in the system. However, after a certain dispatch ratio, the responses are very close that the differences could be neglected. Other factors such as the bus voltages could be used to determine the optimal dispatch ratio in this case. The voltage of the bus 1425 shows a significant improvement at the 10^{th} study scenario. This scenario corresponds to a 45% conventional generation dispatch ratio or in other words, 55% of the generators are de-committed from the service as PV generation is added to the system. This dispatch ratio also corresponds to oscillations of less than 1% in magnitude for the speed of the 810 generator. The 45% dispatch ratio also leads to the best voltage behavior for the bus 810 as shown in Fig. 6.15. The voltage of this bus attains the smallest peak under the 45% dispatch ratio following the case 2 disturbance.

Case study 3: Three phase fault at bus 15021 with line removal

Similar to the previous case studied, this section studies the effect of a large disturbance associated with an eigenvalue presented in Table 6-5. A three phase fault is simulated on the bus 1487 which is cleared after 5 cycles. The transmission line connecting the two 500 kV buses of 1487 and 2529 is removed following the fault clearance. The same procedure as the previous section is followed in this part. Simulation results are presented in Fig. 6.17-6.19.

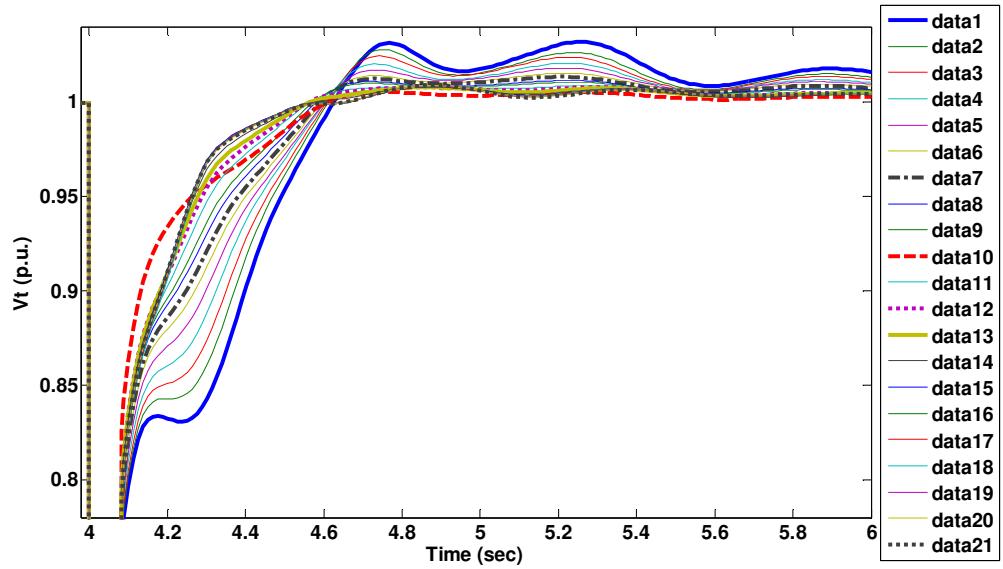

Fig. 6.17 Voltage of the bus 1490 following the case 3 disturbance

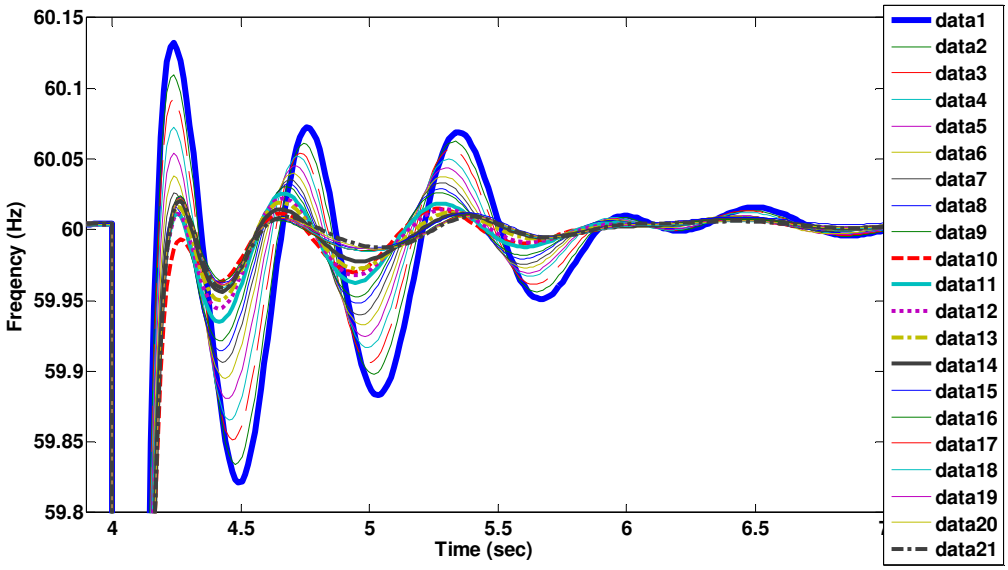

Fig. 6.18 Frequency of the bus 1487 following the case 3 disturbance

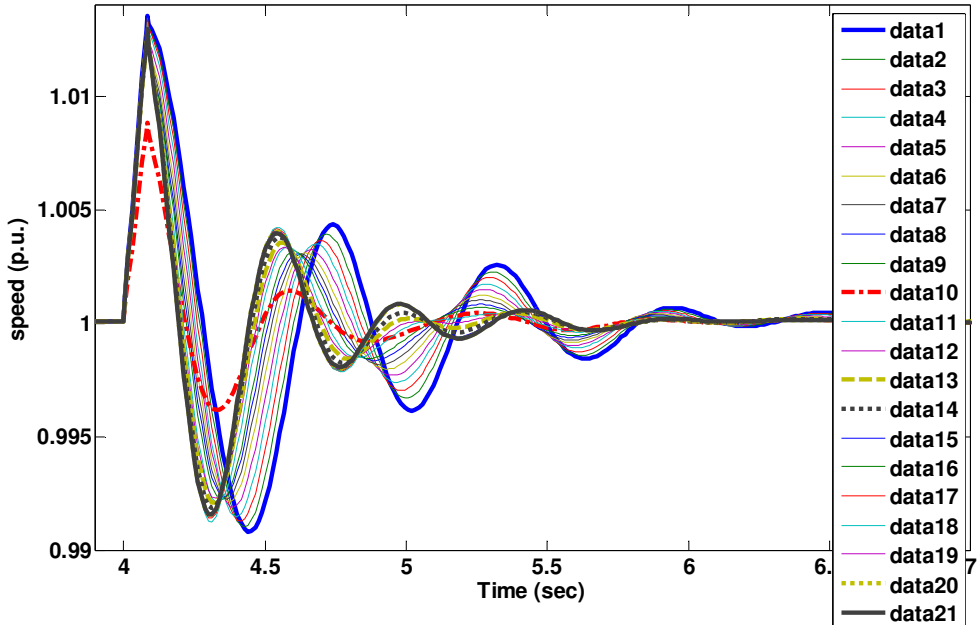

Fig. 6.19 Speed of the generator 1490 following the case 3 disturbance

The results presented following the case 3 disturbance also confirm that the 45% dispatch ratio, that corresponds to the 10th scenario, illustrates the best voltage as well as frequency response for the buses surrounding the faulted bus. In addition, the speed of the generator located at bus 2247 has smaller oscillations in terms of their magnitudes with a 45% dispatch ratio.

6.6 Optimal Dispatch Ratio with Regards to Steady State Performance

Various dispatch ratios, translate to different number of generators that are online. The difference in the total number of the generators online, results in variations of the power flown through the transmission lines. As the dispatch ratio as defined in the previous section decreases, or in other words displacement ratio increases, reactive power flows may travel longer distances to serve the loads. Hence, the bus voltages and the line flows may be affected differently with the addition of the PV units while under different dispatch ratios.

This section aims to identify the ODR value for the system described in the previous section in order to maintain acceptable steady state performance. What is meant by the acceptable performance is bus voltages within ±5% of the rated value and the line flows bellow the ratings. Although the method for calculating ODR values are based on the simulation results achieved from the system described in Chapter 3, the method is general and can be applied to any system for determining the ODR values.

The method introduced in this chapter estimates the ODR value as a function of the 'bus criticality index'. The bus criticality index (BCI) is a measure introduced in this dissertation that quantifies the voltage violations and their distance from the tolerance in order to show whether the system buses are operating under critical conditions. The BCI index for the bus voltages are defined as follows,

$$BCI = \frac{1}{e}\int_{1}^{|v-1|+1} e^{x-1}dx \times \left(1+\left(1-p_{critical}\right)g\right) \tag{6.3}$$

$$p_{critical} = \frac{n_{critical}}{n_{critical}+n_{acceptable}} \tag{6.4}$$

$$g = \begin{cases} 0 & ; \text{if} \quad 0.95 \le |v| \le 1.05 \\ 1 & ; \qquad \text{otherwise} \end{cases} \tag{6.5}$$

where,

v=bus voltage

$n_{critical}$= number of times bus voltage is outside the tolerance range for all the historical data

$n_{acceptable}$= number of times bus voltage is within the acceptable range for all the historical data

As seen from (6.3) the BCI is defined based on the voltage of each bus and consists of two terms. Since the objective of the BCI is to determine the criticality of a bus voltage, the two terms are defined in a manner to increase the BCI value as the voltages move farther from the acceptable tolerance. The tolerance throughout this text is defined as a voltage between 0.95 to 1.05 pu. Therefore, the first term in (6.3) will serve as an exponential penalty factor as the voltages deviate from 1 (p.u.). The second term of (6.3) is intended to serve as penalty factor for the bus voltage if it is operating in the critical range. Therefore, the function *g(v)* in only non-zero outside the acceptable voltage range. The function $p_{critical}$ is calculated based on the numerous simulations of the study system and represents the probability of criticality based on the test data. The objective of including the second term in (6.3) is to significantly increase the BCI if the criticality is caused less frequently, as a result of a severe contingency. On the other hand, if a particular bus holds a critical voltage value at all times, including the no contingency case, the BCI would be less affected by this particular bus voltage.

The test data utilized to calculate $p_{critical}$ include the bus voltages for the entire system, under various dispatch ratios, following various contingencies as well as the case with no contingency.

For the purpose of this study, a total of 536, *(N-1)* contingencies are simulated for the 21 study cases described in the previous section, which sum to a

total of 11084 datasets (for the cases with converged solution), including the cases with no contingencies. VSAT software package is utilized for the purpose of contingency analysis in this section.

To compare the accuracy of the results achieved based on the BCI defined in (6.3) the term $p_{critical}$ is also calculated based on the *Chebyshev's inequality* [66]. Chebyshev's theorem states that for every random variable x with any probability distribution function and finite expected value μ and non-zero variance σ^2,

$$p\left(\left|X-\mu\right| \geq k\sigma\right) \leq \frac{1}{k^2} \tag{6.6}$$

Equation (6.6) determines the upper bound for the probability of a random variable to be k standard deviations away from the mean value μ. Based on *Chebyshev's* theorem, the modified BCI function is calculated as,

$$BCI = \frac{1}{e}\int_1^{|v-1|+1} e^{x-1}dx \times \left(1+\left(1-p_v\right)g\right) \tag{6.7}$$

$$p_v = \frac{1}{k^2}$$
$$k = \frac{v-\mu}{\sigma} \tag{6.8}$$

where μ is the mean value of the test data while σ is the standard deviation of the test data that are collected by the contingency analysis. The term k shows how far, in terms of the standard deviation of the data, a particular bus voltage is from the mean value of the historical data of that bus voltage. The BCI values calculated based on (6.7) are more conservative than those calculated by (6.3) as

they are defined based on the upperbound probability of criticality. Hence, the ODR values found based on the second method would be smaller due to the fact that the probability of criticality is higher most of the times.

A *regression* method is used in this work to estimate the ODR of the system as a function of the bus BCIs, which in turn are functions of system bus voltages. Regression is a tool to predict a real value, such as the dispatch ratio, for a given data set, such as the bus voltage magnitudes. Regression techniques estimate the relation between a dependent variable, y, and the independent variables, x_i,

$$y \approx F\left(x_1, x_2, ..., x_n\right) \tag{6.9}$$

Among various regression techniques, *linear regression* in its simplest form represents the output variable y or label, as a linear function of the input variables set X or regressors as follows,

$$y = X\omega + \varepsilon \tag{6.10}$$

where ω is the vector of regression coefficients and ε is the error of the linear regression. The objective of each regression method is to estimate ω and ε using the test data which are often called the learning data set. Various methods are applied to solve the regression problems [67], among which *weighted least squares (WLS)* is a widely used method. The objective of this method is to minimize the difference between Y and the estimated value as follows,

$$\min \left\| Y - XW \right\|^2 \tag{6.11}$$

$$\frac{\partial}{\partial W}\|Y - XW\|^2 = 0$$
$$\frac{\partial}{\partial W}(Y - XW)^T (Y - XW) = 0$$
$$\frac{\partial}{\partial W}\left(Y^T - W^T X^T\right)(Y - XW) = 0$$
$$\frac{\partial}{\partial W}\left(Y^T Y - Y^T XW - W^T X^T Y + W^T X^T XW\right) = 0$$
$$-2X^T Y + 2X^T XW = 0$$
$$2X^T XW = 2X^T Y$$
$$W = \left(X^T X\right)^{-1} X^T Y \tag{6.12}$$

The weighting matrix W calculated from (6.12) derives the relation between the output variable, which is dispatch ratio (DR) in this case, and the regressors, i.e. the BCI values. As seen from (6.12) calculation of W requires calculation of the inverse of the matrix (X^TX) which often requires extensive calculations. To avoid calculation of the aforementioned matrix inversion, the matrix X can be represented as multiplication of three matrices U, V^T, and the diagonal matrix Σ using the singular value decomposition (SVD) technique as shown in (6.13).

$$X = U\Sigma V^T$$
$$W = \left(X^T X\right)^{-1} X^T Y = \left(V\Sigma U^T U\Sigma V^T\right)^{-1} V\Sigma U^T Y$$
$$\rightarrow W = \left(V\Sigma^2 V^T\right)^{-1} V\Sigma U^T Y = V\Sigma^{-2} V^T V\Sigma U^T Y$$
$$\xrightarrow{VV^T = I} W = V\Sigma^{-1} U^T Y \tag{6.13}$$

Based on the aforementioned methods of calculating the BCI values, for each set of test data, the corresponding BCI values are calculated for each bus. These calculated values serve as the regressors for estimating the DR for the studied system. By calculating the estimate of the DR as a function of the bus

voltages, the ODR could be found. The ODR ensures that the system criticality index (SCI), which is shown in (6.14) is minimized. The parameter n is the number of the buses in (6.14),

$$SCI = \sum_{i=1}^{n} BCI_i \tag{6.14}$$

As shown later in this section, the buses might hold high voltages most of the time and therefore the ODR will ensure that their magnitudes do not fall into the most severe range of the bus voltages. Consequently, by calculating the minimum value of the system criticality index and estimating the DR based on the BCIs of a test case that yields the minimum SCI, the optimal dispatch ratio of the system will be obtained as shown in (6.15). The parameter j is the index of the test case that yields the minimum SCI value among all the test cases.

$$ODR = (BCI_1, BCI_2, ..., BCI_n)^j \times W \tag{6.15}$$

A summary of the method proposed to calculate the ODR of the system is shown in Fig. 6.22. To illustrate the effectiveness of the proposed method a numerical example is presented in the following section for the system described in the beginning of this chapter and the corresponding dispatch ratio scenarios. As explained before, a total of 11084 data sets are used as the regressors and for calculation of the BCI values. The corresponding BCI values are calculated for each bus, of the 2418 bus within the studied system. To better understand the characteristics of the system studied, the histogram of the $p_{critical}$ values of the system buses are plotted in Fig. 6.20 for the historical data derived from the contingency analysis.

As seen from Fig. 6.20 the probability of criticality for the 2418 buses considered in the studied system is mostly distributed between the [0-0.1] and the [0.9-1] range. To illustrate the voltages of the system buses, the histogram of the average bus voltages is presented in Fig. 6.21 while the bus voltage distribution of a single bus is presented in Fig. 6.23. As seen from Fig. 6.21, due to the fact that the system is operating at 40% PV penetration, many system buses are operating at higher voltage values which are rather high during some contingencies.

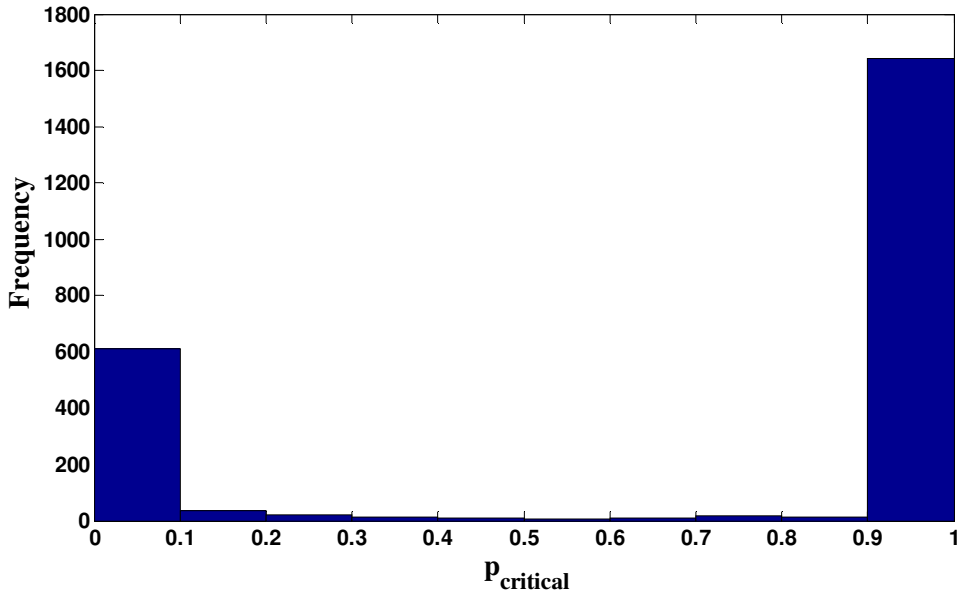

Fig. 6.21 $p_{critical}$ histogram

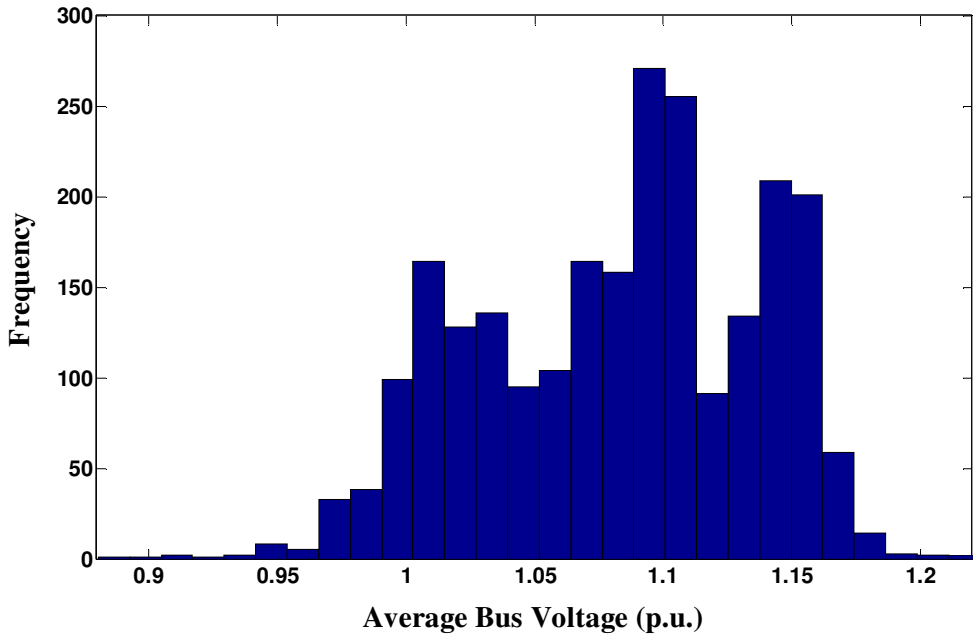

Fig. 6.22 Average bus voltages distribution

Comparing Figs. 6.20 and 6.22-6.23 yields the conclusion that the system is does not have voltage magnitude violations only for a certain number of test cases and does have significant voltage magnitude violations for other cases. This conclusion confirms the results of the transient analysis presented in the previous section that there exists a dispatch ratio at which the system exhibits a more desirable behavior.

Next, the steps shown in Fig. 6.21 are followed to calculate the ODR value for the system. The weight matrix W is calculated for two different methods of calculating BCIs and the DR is estimated based on the bus BCI values. Due to large number of components, the elements of W are only presented in Fig. 6.24 and 6.25 for two different definitions of BCIs presented in (6.3) and (6.7) respectively.

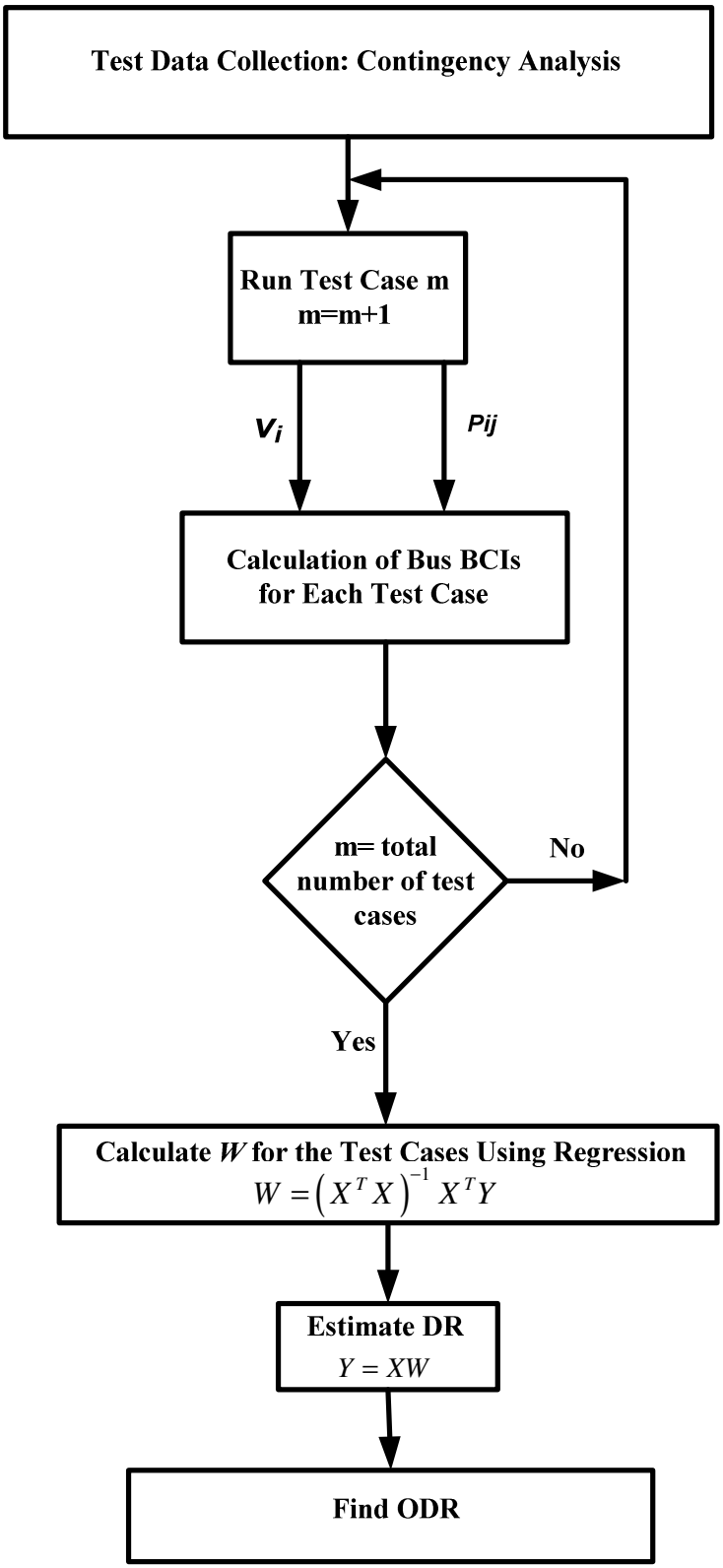

Fig. 6.20 Flow chart for calculating ODR

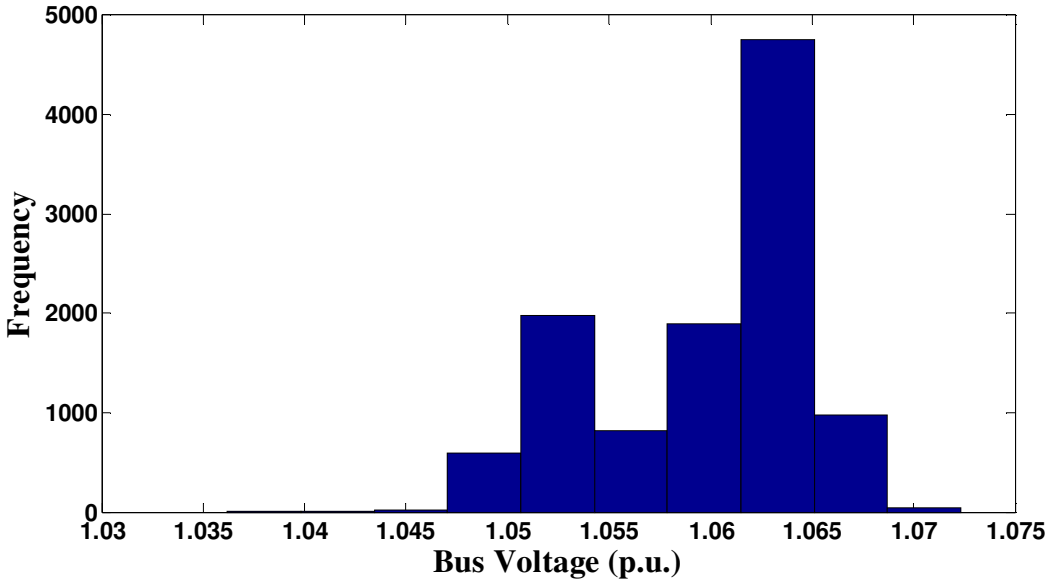

Fig. 6.23 Bus 108 voltage distribution

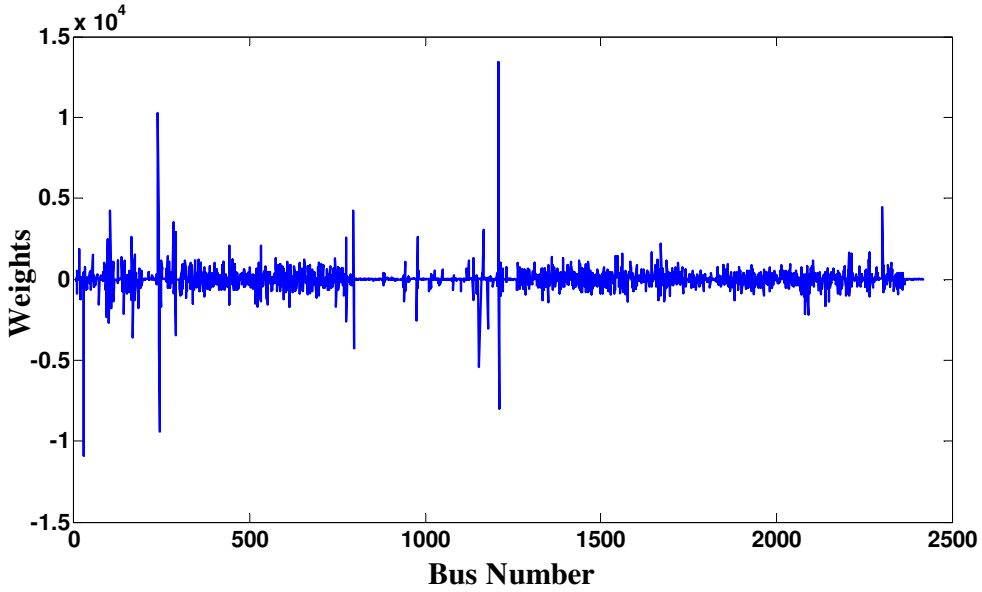

Fig. 6.24 Regression coefficients for BCIs calculated based on (6.3)

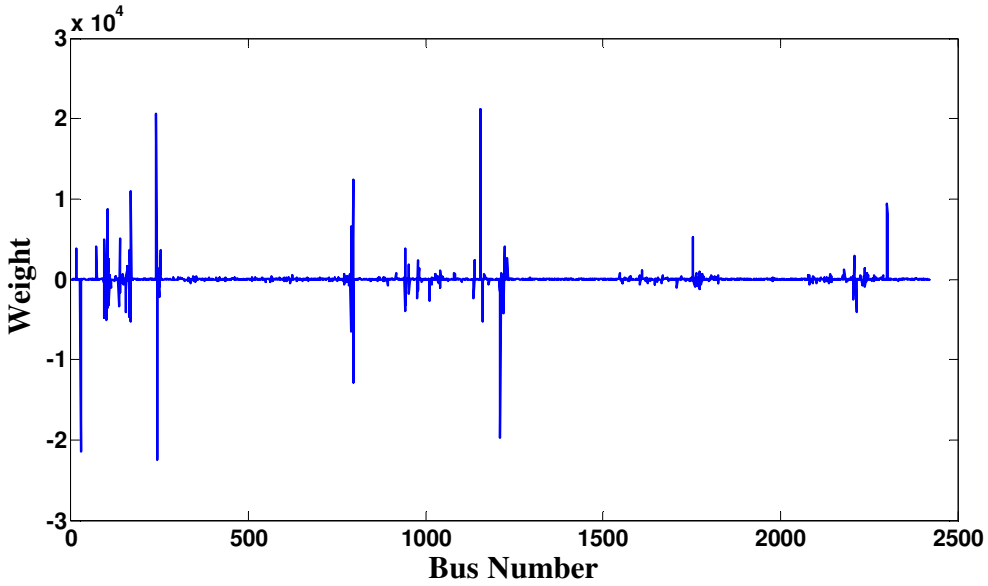

Fig. 6.25 Regression coefficients for BCIs calculated based on (6.7)

The regression coefficients presented in Fig. 6.24 and 6.25 show that the output variable, i.e. DR, is more dependent on few BCIs rather than all the buses within the system. This phenomenon in effect, filters out the buses that are not affected under various dispatch ratios. As explained previously, to optimize the dispatch ratio, the SCI values are calculated for all the aforementioned test cases and the case that yields the minimum SCI value is identified. The ODR is then calculated. Based on the regression coefficients derived from the test data, the ODR value is calculated to be 89.77% and 75.33% for the two different methods of calculating BCI values, i.e. (6.3) and (6.7) respectively.

The method introduced in the previous section, calculated the ODR value only based on the steady state bus voltages. Similar to the contingency ranking methods presented in Chapter 2 of this dissertation, the criticality index can also be defined based on the steady state power flows of the system transmission lines.

Equation (6.3) is modified to define the line criticality index (LCI) of each transmission line based on the line flows as shown in (6.16).

$$LCI = 3\int_0^p x^2 dx \times \left(1 + \left(1 - p_{OverLimit}\right) g \right. \tag{6.16}$$

$$p_{OverLimit} = \frac{n_{OverLimit}}{n_{OverLimit} + n_{UnderLimit}} \tag{6.17}$$

$$g = u(p - P_{\lim}) \tag{6.18}$$

where,

p=line flows

$n_{OverLimit}$= number of times line flows are above the line MVA limit

$n_{UnderLimit}$= number of times line flows are below the line MVA limit

Function $u(p\text{-}P_{lim})$ in (6.18) is a step function that attains a value of one if $p \geq P_{lim}$ and is zero otherwise. Similar to (6.7), the LCI values can also be defined based on *Chebyshev's* theorem.

The same procedure introduced for the bus voltages can be applied to the calculation of ODR values based on the line flows. The same set of test data and contingencies are selected for this section as well. The regression coefficients for the LCI values calculated based on (6.16) are presented in Fig. 6.26.

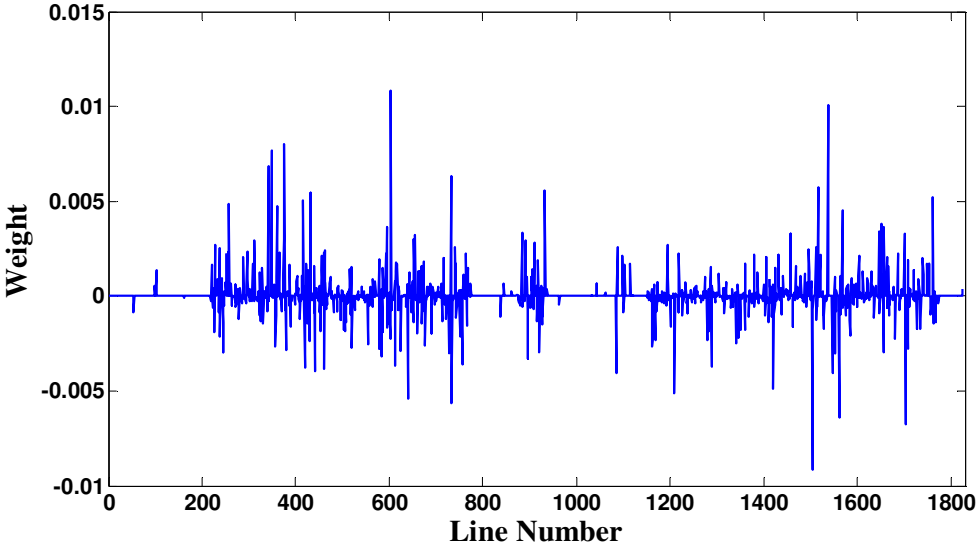

Fig. 6.26 Regression coefficients for LCIs calculated based on (6.16)

Following the same procedure as the bus voltages and calculating the ODR values for the test case that minimizes the system SCI, the optimal dispatch ratio is found to be 71.64% based on (6.16) and 71.39% based on *Chebyshev's* theorem, which is very similar in both cases.

6.7 Summary

This chapter studied a power system to determine the optimal dispatch ratio that ensures the stability of the system under various disturbances and outages. Among the cases studied, faults accompanied with line outages have shown to impose a more severe contingency on the system and therefore were the identifying cases for the ODR. A case with 45% dispatch ratio that also corresponds to 55% de-commitment ratio, illustrated the most desirable response following various disturbances. The results of the full eigenvalue analysis of the

system reveal that the critical modes of the system have different damping ratios under various dispatch ratios. The damping ratios improve at higher dispatch ratios. The critical modes of the system can further be studied under large disturbances that excite the aforementioned modes. These cases can reveal the behavior of the system under various disturbances and therefore could identify the optimal dispatch ratio for the system studied.

A method for calculating the optimal dispatch ratio was introduced in this chapter, which is mainly based on the steady state behavior of the power systems. Using regression techniques, this method utilizes a collection of test data in order to estimate the dispatch ratio of the system as a function of bus criticality indices that were also introduced in this chapter. Simulation results derived from contingency analysis identified the optimal dispatch ratio with regards to steady state bus voltages as well as line power flows.

Chapter 7

SUMMARY, CONCLUSIONS AND FUTURE WORK

7.1 Summary

This chapter summarizes the studies presented in this thesis which have addressed two important aspects of smart grids. The main conclusions derived from these two avenues of investigation along with the future work follow the summaries.

With increased deployment of renewable energy resources, providing a more reliable and resilient power system is of more concern with the addition of these resources. The ability to meet the increased demands of the customers and the fluctuating outputs of the renewable resources such as wind and solar is one important challenge that the future smart grids would face and need to be addressed. Therefore, a method to increase power system reliability by providing more awareness to the operator of the impending failures in the system is discussed. Condition monitoring of the circuit breakers and transformers were introduced in this work to monitor the status of these components and based on the collected data estimate the chance of a component failure.

Since it is not practical to apply condition monitoring to all circuit breakers or transformers, contingency ranking is proposed in this work. The contingency ranking approach is based on ranking outages of all the transformers and circuit breakers above 115 kV in order to find the most severe outages. Those components causing the most severe contingencies are referred to as critical CB or transformers which are the best candidates for condition monitoring.

Performance indices based on MVA flow of the lines and bus voltages were introduced as tools for calculating the severity of each contingency.

As one other important feature of smart grids, this dissertation also investigated the impact of high penetration of photovoltaic systems on a large interconnected system. Photovoltaic generation is added to the studied system with both residential rooftop PVs and utility scale PVs. Both steady state and dynamic behavior of the system with and without the existence of these generation resources are studied and compared to identify improvements or adverse effects of photovoltaic systems on the power transmission systems. Various PV penetration levels up to 50% are considered for the steady state analysis, while conventional generators are replaced with PV systems in each step. For dynamic analysis, 20% PV penetration is deemed to be a valid representation of a case with high PV penetration.

For power flow studies, residential rooftop PVs were regarded as negative loads that were added at 69 kV P-Q buses. Utility scale PVs however, were treated as conventional generators with reactive power generation capability. Dynamic studies required more detailed models for the utility scale PV systems. A Generic model similar to the type 4 wind turbine converter model, which is presently available in the PSLF model library, is deployed in this work in order to represent the aforementioned systems. While adding the PV system models to the existing power flow files, a certain number of generators were displaced by PV systems in order to keep the swing generation and inter area interchanges fixed, and at values equal to the base case.

Small signal stability of the power systems with high PV penetration is also investigated in this work. Critical modes of the system are identified by eigenvalue analysis while the variations of these modes are compared under various PV penetration levels of up to 50%. The results of the eigenvalue analysis point out the most adversely affected modes of the system while the PV penetration increases. To highlight the adverse effects of reduced inertia on electromechanical modes of oscillation, eigenvalue sensitivities to inertia of the displaced generators are calculated. Time domain analysis is performed to examine the detrimental impacts of high PV penetration during system transients. Using the concept of participation factors and by utilizing Prony analysis, a transient case that excites a detrimentally impacted critical mode was identified in an example test bed.

The addition of the PV generation resources to the system will result in rescheduling the conventional generating units in order to maintain the load and generation balance within the system. The reduction of these resources can be in a form of displacing the conventional units or rescheduling their output values, or a combination of both. This dissertation investigates the impact of various dispatch or displacement ratios of the conventional generating units on the power system steady state as well as transient stability. A method to calculate the optimal dispatch ratio based on the steady state behavior of the studied system is also introduced in this dissertation that is based on the historical data achieved from the contingency analysis.

7.2 Conclusions

Simulation results presented in Chapter 2, result in the conclusion that sensory signals can be used to increase power system reliability. If the signals received from condition monitoring of circuit breakers and transformers indicate an increased chance of component failure, the operator is guided with a corrective action to be taken in order to prevent the effect of possible outages in the future.

Contingency ranking methods presented in this study are shown to be effective in identifying the most stressed transformers and circuit breakers. Simulation results of the system under these stressed circumstances confirm the result of the contingency ranking methods. In most of the contingencies, severe overloading is created in the other branches as a result of a branch outage.

One of the advantages of this study is to bring more awareness of the system stressed points and the ability to prevent any outages in the future. This goal is achieved by knowing the corrective actions that needs to be taken if any of the studied failures happens in the future. Consequently, more secure operation and a more reliable system is ensured. By applying different corrective actions as presented at the end of Chapter 2, it is observed that although generation rescheduling is an effective way of reducing line loadings in case of an outage, it might not be of any help in some severe contingencies. In those cases, load shedding is the only solution to reduce the stress on branches and hence prevent any further failures.

The steady state analysis results, presented in Chapter 3, reveal that increasing PV penetration levels can lead to alteration of the steady state voltage

magnitudes. At some penetration levels, over voltages are observed at transmission level buses. The majority of over voltages were observed in the case with 30% PV generation. Analytical studies conducted for a simplified system confirm the simulation results achieved for a larger system.

For the system considered, dynamic analyses conducted in Chapter 4 indicate that high PV penetration can have both detrimental and beneficial impacts on the transmission system. These impacts are observed by case studies carried out in this work. Simulation results reveal that, PV penetration levels, system topology, type of the disturbance as well as the location of a fault are all important factors in determining the impact of the high PV penetration on the system.

In almost all the case studies, bus voltage magnitudes are the most affected system parameters during the transients. It is observed that systems with high PV penetration levels achieve greater voltage dips as well as more oscillations, following the disturbances. These voltage dips have the potential to cause more severe problems in other loading conditions such as summer peak cases. Generator relative rotor angles have also shown higher transient peaks following some disturbances. Replacing conventional generators with photovoltaic systems and hence less inertia in the system is one reason for more rotor angle oscillations. Double line outages that have shown to be severe disturbances in the base case and lead to instability have shown to have improved performances with PV solar generations present in the system.

The sensitivity analyses pinpoint the fact that the eigenvalues are detrimentally impacted as the inertia of conventional generators is reduced. The negative sensitivities of the real part of the eigenvalue to inertia show that the eigenvalues move closer to the right half plane with a reduction in generator inertia and therefore result in degraded damping performance during system transients. Transient studies carried out for various PV penetration levels substantiate the results of small signal analysis together with eigenvalue sensitivity analysis. Based on the simulation results presented in this work, PV generation is found to have a detrimental impact on small signal stability of the studied system with increased penetration of PV systems. In view of the fact that this detrimental impact of PV penetration is caused by reduced system inertia, maintaining the critical generators in service can be helpful in mitigating the impact of poor damping resulted from high PV penetration. The critical generators can be identified by examining the sensitivity of the critical modes to the inertia of the generators.

Simulation results carried out in this work illustrate the fact that various dispatch ratios can have diverse effect on steady state as well as transient stability of the power systems. Therefore, in order to achieve a reliable system operation and maintain the stability of the systems during various disturbances it is essential to identify the optimal dispatch ratio of the conventional generating units while the system is operating with high PV penetration.

A measure of bus criticality or line criticality which in introduced in this work, effectively estimates the criticality of the system based on the historical

data achieved from contingency analysis. By calculating these indices, a linear regression based method estimated the optimal dispatch ratio as a function of the criticality indices. These methods provide a tool that can be applied to the power systems prior to addition of PV systems in order to identify the optimal dispatch ratios that cause less voltage instability or limit violations under various contingencies.

Based on simulation results presented in this dissertation and the conclusions stated above, the following steps can be taken towards improving system reliability with the application of smart grid technology.

- Use of condition monitoring to increase awareness of the weak points of the system and thus estimate the chance of failure.
- Circuit breakers and transformers indentified as critical components are the best candidates for condition monitoring. Therefore, the best place to apply condition monitoring is at the stressed branches.
- Corrective actions that are found based on offline system studies can be applied to the system in case of an impending failure or a sudden contingency. As a result of this action, overloading in other branches can be prevented. In case, generation rescheduling is not sufficient for decreasing the loadings of the branches, load shedding can be the only solution to the stressed system. However, sensitivity analysis should be conducted in order to determine the loads that are effective in alleviating a contingency.

- By identifying the potential impacts of high penetration of photovoltaic systems, more reliable preventive measures could be taken to alleviate these impacts on the future grids.
- To ensure the secure operation of the system at all times, systems should be equipped with sufficient reactive power reserves in the systems with high PV penetration levels.
- Prior to addition of increased PV generation to the systems, transmission planning methods such as contingency analysis should be conducted to study the effect of various dispatch ratios of the conventional generating units.
- Identifying the optimal dispatch ratio of the conventional generating units can effectively reduce the adverse impacts of high PV penetration on power system stability.

The main contributions of this dissertation are summarized in Table 7-1.

Table 7-1 Principal contributions of the dissertation

Category	Contribution
Smart grid technology	Application of contingency ranking methods to identify the optimal location of the condition monitoring systems
High PV penetration	Identification of impacts of high PV penetration on power system steady state bus voltages
	Identification of impacts of high PV penetration on power system transient stability
	Propose a method to analyze the impact of high PV penetration on small signal stability of the power systems
	Introduce a measure to estimate the severity of the system under various dispatch ratios of the conventional generating units and estimate the optimal dispatch ratio of these units

7.3 Future Work

The work presented in this dissertation could be extended to further investigate the effects of high PV penetration on the transmission system. Below are a few suggestions for the future work.

- Correlation of actual operating conditions already observed by historical data with the simulation results
- Study various disturbance scenarios with other loading conditions such as the summer peak case
- To further extend the method introduced for calculation of ODR to also include the transient behavior of the system in the ODR calculation
- To calculate the ODR as a combination of bus criticality indices, line overload indices, and transient behavior

REFERENCES

[1] U. S. Environmental Protection Agency, "Renewable portfolio standards fact sheet" 2009, available at: http://www.epa.gov/chp/state-policy/renewable_fs.html

[2] IEEE, "IEEE 1547 standard for interconnecting distributed resources with electric power systems," [online] Available: http://groupe.ieee.org/groups/scc21/1547/1547/index.html

[3] E. Gulachenski, E. J. Kern, W. Feero, and A. Emanuel, "Photovoltaic generation effects on distribution feeders, volume 1: description of the gardner, massachusetts, twenty-first century PV community and research program," *EPRI technical report EL-6754*, Palo Alto CA, 1990.

[4] N. Srisaen, A. Sangswang, "Effects of PV grid-connected system location on a distribution system," *in proc. IEEE Asia pacific conference on circuits and systems,* pp. 852-855, Dec. 2006.

[5] P. P. Barker, R.W. De Mello, "Determining the impact of distributed generation on power systems: part I radial distribution systems," *in proc. IEEE Power and Engineering Society Summer Meeting,* Seattle, WA, pp. 1645-1656, vol. 3, Jul. 2000.

[6] General Electric Co., "Reliable, low cost distributed generator/utility system interconnect 2001 annual report," *GE Corporate Research and Development*, NREL/SR-560-34634, August 2003, available at: http://www.nrel.gov/docs/fy03osti/34634.pdf

[7] Y. Liu, J. Bebic, B. Kroposki, J. de Bedout, W. Ren, "Distribution system voltage performance analysis for high – penetration PV," *in proc. IEEE Energy 2030 Conference,* Atlanta, GA, pp. 1-8, Nov. 2008.

[8] K. Turitsyn, P. Šulc, S. Backhaus, M. Chertkov, "Distributed control of reactive power flow in a radial distribution circuit with high photovoltaic penetration," *in proc. IEEE Power and Energy Society General Meeting,* Minneapolis, MN, pp. 1-6, Jul. 2010.

[9] J. W. Smith, W. Sunderman, R. Dugan, B. Seal, "Smart inverter volt/var control functions for high penetration of PV on distribution systems," *in*

proc. IEEE Power Systems Conference and Exposition, Phoenix, AZ, pp. 1-6, Mar. 2011.

[10] M. McGranaghan, T. Ortmeyer, D. Crudele, T. Key, J. Smith, P. Barker, "Renewable system interconnection study: advanced grid planning and operation," *Sandia National Laboratory report,* Feb. 2008.

[11] Y. Zhang, C. Mensah-Bonsu, P. Walke, S. Arora, J. Pierce, "Transient over-voltages in high voltage grid connected PV solar interconnection," *in proc. IEEE Power and Energy Society General Meeting, Minneapolis,* MN, pp. 1-6, Jul. 2010.

[12] L. Haifeng, J. Licheng, D. Le, A. A. Chowdhury, "Impact of high penetration of solar photovoltaic generation on power system small signal stability," *in proc. International Conference on Power System Technology,* pp. 1-7, Oct. 2010.

[13] S. Achilles, S. Schramm, J. Bebic, "Transmission system performance analysis for high-penetration photovoltaics," *NREL Report No. SR-581-42300*, Feb. 2008, available at: http://www.nrel.gov/docs/fy08osti/42300.pdf

[14] J. Woodcock, J. C. Wright, "Power transformer design enhancements made to increase operational life," *66th Annual International Conference of Double Clients,* April 1999.

[15] *IEC Loading Guide for Oil Immersed Power Transformers*, IEC 354 1991-09, 1991.

[16] "The smart grid: an introduction," *US Department of Energy,* 2008.

[17] Z. Jiang, F. Li, W. Qiao, H. Sun, H. Wan, J. Wang, Y. Xia, Z. Xu, P. Zhang, " A vision of smart transmission grids," *in proc. of IEEE Power and Energy Society General Meeting,* pp. 1-10, July 2009.

[18] G. Stefopoulos, F. Yang, G. J. Cokkinides, and A. P. Meliopoulos, "Advanced contingency selection methodology," *37th North American Power Symposium*, Oct. 2005.

[19] L. D. Arya, S. C. Choube, and D. P. Kothari, "Line outage ranking for voltage limit violations with corrective rescheduling avoiding masking," *Journal of Electrical Power and Energy Systems*, vol. 23, pp.837-846, 2001.

[20] Mohamed, A. Shaaban and A. Kahla, "A fast efficient accurate technique for circuit contingency evaluation," *International Journal of Electric Power Systems Research*, vol. 45, pp. 181-189, 1998.

[21] P. S. Meliopoulos, C. Cheng, " A new contingency ranking method," *in proc. of Energy and Information Technologies in the Southeast*, pp. 837-842, vol. 2, April 1989.

[22] G. C. Ejebe, B. F. Wollenberg, " Automatic contingency selection," *IEEE Transactions on Power Apparatus and Systems,* pp. 97-109, vol. PAS-98, no. 1, January 1979

[23] M. Abedi, M. Ehsan, Z. G. Jahromi, and M. M. Jamei, "Utilization of analytical hierarchy process in contingency ranking," *in proc. of Power System Conference and Exposition,* April 2009.

[24] S. Eftekharnejad, G.T. Heydt, and V. Vittal, "Implications of smart grid technology on transmission system reliability," *Power Systems Conference and Exposition,* March 2011, Phoenix, AZ.

[25] DSATools^{TM} version 11 user's manual, Power Tech. Lab., Vancouver BC, April 2011.

[26] M. Kezunovic, M. Knezev, Z. Djekic, "Automated circuit breaker monitoring," *PSERC Project Report*, 2007.

[27] J. L. Blackburn, "Protective relaying," *Marcel Dekker,* 1987.

[28] "Final report on results of second international enquiry into circuit breaker reliability," CIGRE Brochure 83.

[29] B. Das and C. Patvardhan, “Useful multi-objective hybrid evolutionary approach to optimal power flow,” *IEEE proc. of Generation, Transmission and Distribution*, vol. 150, no. 3, May 2003.

[30] Z. Qiu, G. Deconinck, R. Belmans, “A literature survey of optimal power flow problems in the electricity market context,” *in proc. of Power System Conference and Exposition,* Seattle, April 2009.

[31] J. A. Momoh, M. E. El-Hawary, and R. Adapa, “A review of selected optimal power flow literature to 1993 part I: nonlinear and quadratic programming approaches,” *IEEE Transactions on Power Systems.*, vol. 14, no. 1, pp. 96–104, Feb. 1999.

[32] H. W. Dommel and W. F. Tinney, “Optimal power flow solutions,” *IEEE Transactions on Power Apparatus and Systems*, vol. PAS-87, pp 1866-1876, October 1968.

[33] A. H. El Abiad, and F. J. Jaimes, “A method for optimum scheduling of power and voltage magnitude,” *IEEE Transactions on Power Apparatus and Systems*, vol. PAS-88, no.4, pp 413-422, April 1969.

[34] M. Sasson, “Combined use of the parallel and fletcher-powell non-Linear programming methods for optimal load flows,” *IEEE Transactions on Power Apparatus and Systems*, vol. PAS-88, no 10, pp 1530-1537, October 1969.

[35] M. Sasson, “Decomposition technique applied to the non-linear programming load flow method,” *IEEE Transactions on Power Apparatus and Systems*, vol. PAS-89, no.1, January 1970, pp 78-82.

[36] H. W. Dommel and W. F. Tinney, "Optimal power flow solutions," *IEEE Transactions on Power Apparatus and Systems*, vol. PAS-87, no 10, pp. 1866-1876, October 1968.

[37] G. F. Reid and L. Hasdorf, “Economic dispatch using quadratic programming,” *IEEE Transactions on Power Apparatus and Systems*, vol. PAS-92, pp. 2015-2023, 1973.

[38] F. Wollenberg and W. O. Stadlin "A real time optimizer for security dispatch," *IEEE Transactions on Power Apparatus and Systems*, vol. PAS-93, pp. 1640- 1649, 1974.

[39] G. C. Contaxis, B. C. Papadias, and C. Delkis, "Decoupled power system security dispatch," IEEE Transactions on Power Apparatus *Systems*, vol. PAS-102, pp 3049-3056, September 1983.

[40] S. N. Talukdar, T. C. Giras and V. K. Kalyan, "Decompositions for optimal power flows," *IEEE Transactions on Power Apparatus and Systems*, vol. PAS-102, no. 12, pp 3877-3884, December 1983.

[41] M. H. Rashed and D. H. Kelly "Optimal load flow solution using lagrangian multipliers and the hessian matrix," *IEEE Transactions on Power Apparatus and Systems*, vol. PAS-93., pp 1292-1297, 1974.

[42] H. H. Happ "Optimal power dispatch," *IEEE Transactions on Power Apparatus and Systems*, vol. PAS-93, pp 820-830, no. 3, May/June 1974.

[43] W. Wells, "Method for economic secure loading of a power system," *Proceedings of the Institute of Electrical Engineers*, vol. 115, no. 8, pp. 1190-1194, 1968.

[44] K. Y. Lee, Y. M. Park, and J. L. Ortiz, "Fuel cost minimization for both real and reactive power dispatches," *IEEE proc. of Generation, Transmission and Distribution*, vol. 131, no. 3, pp. 85-93, 1984.

[45] J. Carpentier, "Optimal power flows," *International Journal of Electric Power and Energy System*, vol. 1, pp. 3-15, 1979.

[46] J. Nanda, D. P. Kothari, and S. C. Sirvastava, "New optimal power-dispatch algorithm using Fletcher's quadratic programming method," *IEEE Proc. of Generation, Transmission and Distribution, vol. 136, no. 3, pp. 153-161,*1989.

[47] "WECC guide for representation of photovoltaic systems in large-scale load flow simulations," *prepared by WECC renewable energy modeling task force,* Available*:* http://www.wecc.biz/committees/StandingCommittees/PCC/TSS/MVWG/REMTF/Solar%20Documents/WECC%20PV%20Plant%20Power%20Flow%20Modeling%20Guidelines%20-%20August%202010.pdf

[48] A. Ellis, "PV system models for system planning and interconnection studies," *Sandia National Laboratories (SNL) report*, Oct. 2009.

[49] PSLF version 17.0 user's manual, General Electric International, Inc., Schenectady NY, Dec. 2006.

[50] P. Kundur, J. Paserba, V. Ajjarapu, G. Andersson, A. Bose, C. Cañizares, N. Hatziargyriou, D. Hill, A. Stankovic, C. Taylor, T. V. Custem, and V. Vittal, "Definition and classification of power system stability," *IEEE Trans. Power Syst.*, vol. 19, no. 2, pp. 1387–1401, May 2004.

[51] K. Clark, N. W. Miller, R. Walling, "Modeling of GE solar photovoltaic plants for grid studies," *GE Energy*, Schenectady NY, April 2010.

[52] P. Kundur, "Power system stability and control," EPRI Power System Engineering Series, New York, McGraw Hill, 1994.

[53] GE Energy, "Western wind and solar integration study: February 2008 – February 2010," NREL Report No. SR-550-47434, Golden CO, May 2010.

[54] S. Arabi, G.J. Rogers, D.Y. Wong, P. Kundur, M. G. Lauby, "Small signal stability program analysis of SVC and HVDC in AC power systems," *IEEE Trans. on Power Systems*, vol. 6, issue 3, pp. 1147–1153,1991.

[55] D. Gautam, V. Vittal, T. Harbour, "Impact of increased penetration of DFIG-based wind turbine generators on transient and small signal stability of power systems," *IEEE Trans. on Power Systems*, vol. 24, issue 3, pp. 1426–1434, Aug. 2009.

[56] H. Liu, L. Jin, D. Le, and A. A. Chowdhury, “Impact of high penetration of solar photovoltaic generation on power system small signal stability,” *in proc. International Conference on Power System Technology,* pp. 1-7, Oct. 2010.

[57] W. Du, H. F. Wang, and L. -Y. Xiao, "Power system small signal stability as affected by grid-connected photovoltaic generation," *European Trans. Electrical Power*, DOI: 10.1002/etep.598. B.

[58] Tamimi, C, Canizares, and K. Bhattacharya, “Modelling and performance analysis of large-scale photovoltaic generation on voltage stability and inter-area oscillations," IEEE PES General Meeting, Detroit, Michigan, USA, 2011.

[59] R Shah, et al, "Contribution of PV systems with ultracapcitor energy storage on inter-area oscillation," Proc. IEEE PES General Meeting, Detroit, Michigan, USA, 2011.

[60] P. Kundur, “Power system stability and control,” *EPRI Power System Engineering Series*, New York, McGraw Hill, 1994.

[61] T. Smed, “Feasible eigenvalue sensitivity for large power systems,” *IEEE Trans. Power Syst.*, vol. 8, no. 2, pp. 555–561, May 1993.

[62] J. F. Hauer, C. J. Demeure, and L. L. Scharf, “Initial results in Prony analysis of power system response signals,” *IEEE Trans. Power Syst.*, vol. 5, no. 1, pp. 80–89, February 1990.

[63] GE Energy, “Western wind and solar integration study: February 2008 – February 2010,” NREL report No. SR-550-47434, May 2010.

[64] North American Electric Reliability Corporation, "Standard BAL-001-0.1a: real power balancing control performance," 2008, available at: http://www.nerc.com/files/BAL-001-0_1a.pdf

[65] N. W. Miller, M. Shao, S. Venkataraman, "California ISO (CAISO) Frequency Response Study," *GE Energy*, Schenectady NY, November 2011.

[66] Donald Knuth, "The art of computer programming: fundamental algorithms," vol. 1, Massachusetts, Addison-Wesley, 1997.

[67] Christopher M. Bishop, "Pattern recognition and machine learning," vol. 4., No. 4., New York, springer, 2006.

APPENDIX A

TRANSFOMER BRANCHES ABOVE 115 KV

Table A-1 Transformer branches above 115 kV

Transformer	From	To	ID	Transformer	From	To	ID
1	1487	1488	1	36	546	545	2
2	1487	1489	1	37	546	545	2
3	1487	1490	1	38	1219	1206	2
4	558	555	1	39	1219	1206	3
5	558	556	1	40	1219	1206	4
6	558	557	1	41	1546	1545	1
7	558	1	1	42	1546	1545	2
8	1886	1885	4	43	1546	1545	3
9	1646	1644	1	44	1546	1545	4
10	182	185	1	45	1580	1579	1
11	183	185	1	46	1580	1579	2
12	184	185	1	47	1580	1579	3
13	942	941	1	48	1580	1579	4
14	942	941	2	49	1869	1870	2
15	942	1097	1	50	1869	1870	4
16	1082	1098	1	51	15605	1959	3
17	1451	1450	1	52	1960	1959	4
18	1643	1642	1	53	1960	1959	5
19	2036	2032	1	54	1959	1968	1
20	2036	2033	1	55	1959	1968	2
21	2387	2121	1	56	1959	1966	1
22	2180	1630	1	57	1959	1969	1
23	103	116	3	58	1959	1970	1
24	103	116	4	59	1980	1981	1
25	110	116	1	60	1980	1981	3
26	133	132	1	61	2231	2232	1
27	133	132	2	62	2231	2232	2
28	150	148	1	63	2231	2232	3
29	150	148	2	64	2231	2232	4
30	150	148	3	65	2340	2339	1
31	150	148	4	66	2340	2339	2
32	304	303	1	67	2386	2387	1
33	304	303	2	68	2386	2387	3
34	304	303	3	69	1959	1968	2
35	546	545	2	70	315	316	4
				71	659	660	1

APPENDIX B

IN SERVICE GENERATORS IN THE BASE CASE

Table B-1 Base case in service generators

Bus Number	Gen. Name	Pgen (MW)	Qgen (MW)	Bus Number	Gen. Name	Pgen (MW)	Qgen (MW)
1798	B2	21.00	3.00	810	E5	750.00	78.19
894	A13	180.00	24.26	619	O1	164.00	15.38
886	A5	115.00	16.87	2332	S1	6.00	2.92
892	A6	160.00	22.77	2332	S2	6.00	2.92
887	A7	115.00	16.82	2333	S3	6.00	2.92
888	A9	115.00	16.86	2333	S4	6.00	2.92
893	A10	160.00	22.76	2102	SS3	450.00	66.27
889	A11	115.00	16.88	2103	SS4	450.00	66.27
890	A12	115.00	16.83	2302	VV1	5.00	4.17
459	D1	110.00	-13.21	1085	HH6	110.00	18.00
469	D2	245.00	-4.65	1085	HH7	110.00	17.00
471	D3	260.00	-3.14	1088	HH9	50.00	10.00
473	D4	390.00	-4.77	1088	HH10	50.00	20.00
806	E1	170.00	8.26	1089	HH11	100.00	15.00
807	E2	170.00	8.23	1089	HH12	100.00	30.00
808	E3	220.00	10.71	1091	HH13	100.00	27.62
883	A1	115.00	16.85	930	GC5	31.00	-23.45
884	A2	115.00	16.87	930	GC6	31.00	-23.45
891	A3	160.00	22.80	931	GC7	115.00	-20.87
885	A4	115.00	16.83	931	GC8	115.00	-20.87
2468	K2	80	15.7	968	GR3	297.00	35.88
555	CC1	429.00	92.09	1967	W14	160.00	15.13
556	CC2	421.00	89.80	1969	W15	140.00	41.47
1488	BB1	805.00	62.90	1970	W16	130.00	57.37
2100	SS1	420.00	64.02	617	DV5	45.00	10.00
1914	I3	80.00	-26.00	1595	GP2	25.00	3.00
1203	W7	155.00	23.70	1596	GP3	25.00	2.00
1489	BB2	804.40	62.51	1075	HH1	100.00	20.00
2247	BB3	944.65	77.77	1076	HH2	100.00	22.00
1204	W6	84.00	13.33	1077	HH3	100.00	22.00
183	P2	90.00	23.71	1078	HH4	100.00	8.00
184	P3	160.00	37.70	1079	HH5	100.00	20.00
1566	G1	1410.00	29.06	1091	HH13	100.00	27.62
1567	G2	1407.00	29.06	1094	HH15	110.00	30.00
1568	G3	1410.00	29.06	1094	HH16	110.00	30.00
1913	I1	30.00	5.82	1096	HH17	110.00	30.00

Table B-2 Base case in service generators (continued)

Bus Number	Gen. Name	Pgen (MW)	Qgen (MW)	Bus Number	Gen. Name	Pgen (MW)	Qgen (MW)
1930	H1	110.00	-6.21	928	GC1	100.00	-3.93
1931	H2	100.00	-7.12	928	GC2	100.00	-3.93
2520	L4	24.00	-0.39	929	GC3	100.00	-20.12
2523	L5	25.00	-4.05	929	GC4	100.00	-20.12
2084	ST3	170.00	58.45	1377	C1	3.00	0.48
279	LY1	150.00	-12.71	809	E4	750.00	122.27
163	AC5	71.00	1.29	2521	L6	48.00	0.83
164	AC6	193.00	23.95	2522	L7	48.00	0.83
158	AC3	65.00	0.75	2139	N1	40.00	14.08
159	AC4	38.00	-4.44	2141	N2	40.00	14.00
156	AC1	7.90	0.56	620	O2	164.00	28.64
157	AC2	19.00	1.35	621	O3	249.00	41.37
165	AC7	193.00	24.04	591	U1	1.00	1.20
673	MM1	44.00	-1.49	2075	U2	1.00	0.70
2161	DD4	75.00	-0.15	613	DV1	45.00	10.00
2162	DD5	75.00	-0.06	614	DV2	45.00	10.00
2163	DD6	103.00	0.89	615	DV3	45.00	10.00
2164	DD1	125.00	2.72	616	DV4	45.00	10.00
2101	SS2	420.00	64.02	1594	GP1	25.00	4.00
1896	RD	51.00	0.00	1597	GP4	25.00	3.00
1022	LL1	6.50	-0.96	966	GR1	145.00	35.88
1023	LL2	6.50	-0.96	967	GR2	145.00	35.88
1024	LL3	6.50	-0.96	2083	ST2	170.00	58.45
1912	I2	30.00	5.65	1096	HH19	110.00	30.00
1968	W12	264.00	81.47	2082	ST1	170.00	58.45
1966	W13	160.00	60.04				

APPENDIX C

PHOTOVOLTAIC SYSTEM BUS LOCATIONS

Table C-1 Residential rooftop buses

Num	Capacity (kW)	Num	Capacity (kW)	Num	Capacity (kW)	Num	Capacity (kW)
31	5	495	86.1	350	755.1	959	18.6
99	76.9	608	81.5	363	66.8	972	12
193	14.5	653	52.5	372	34.1	1157	41.7
381	14.4	662	46.6	412	101.8	1319	38.5
625	62	686	47.1	426	102.2	1351	106.4
715	7	688	47	430	5.1	1452	166
788	19	696	6	432	65.9	1616	22.1
814	85.8	706	14	2095	96.9	1661	5
970	36.8	755	16	2117	62.1	1842	46.8
1071	6	877	76.8	2193	20.2	2042	70.1
1127	19.1	918	43	2334	13.3	2042	8.2
1150	75	1018	54.7	2356	18.2	518	4
1256	42	1119	40.1	2374	20.1	1269	86.1
1272	38.7	1166	9	125	10	1634	169.3
1293	24	1282	2	210	7	1973	33
1372	14	1355	94.7	227	13	1003	31.7
1392	4	1456	77.5	324	24.1	525	33.4
1428	46.3	1768	17	1562	5.7	488	92.3
1438	77.8	1781	51	1624	6	1743	39.7
1501	20	1856	184.4	2239	12.1	1613	186.7
1516	22	2007	55	2300	5	2440	6
1542	158.9	2123	132.8	2436	19.5	1033	12.4
1654	61.6	2209	22.8	2280	23	2346	4
236	8.3	242	92.1	727	23	772	15.2
2263	42.5	2178	35.9	791	50.5	2011	30
2128	28.9	2179	40.1	190	48.8	1864	3
1876	3	751	8	2224	25.1	534	0.81
1918	0.67	763	0.47	2417	0.61	1107	0.60
2205	0.62	1878	0.62	1508	0.28	2457	0.67
2165	0.64	956	0.73	538	0.68	1230	0.78
918	0.55	2351	0.87	1433	0.55	1310	0.57

Table C-2 Residential rooftop buses (continued)

Num	Capacity (kW)	Num	Capacity (kW)	Num	Capacity (kW)	Num	Capacity (kW)
1440	0.52	2090	0.26	307	0.17	1634	0.62
2342	0.37	1895	0.66	2125	0.39	1982	0.36
1881	0.18	882	0.22	1162	0.15	1509	0.76
995	0.34	1234	0.85	149	0.36	2111	0.27
2352	0.29	798	0.21	824	0.40	431	0.73
872	0.19	476	0.51	1983	0.35	1647	1.84
225	0.12	1324	0.25	792	0.51	2311	0.22
1329	0.30	2378	0.20	2001	0.51	836	0.22
559	0.12	1308	0.52	1179	0.26	926	0.58
1726	0.60	2091	0.36	120	0.93	2385	0.58
2010	0.07	2107	2.29	253	0.53	821	0.50
1027	1.05	2294	0.05	1328	0.27	2351	0.50
477	0.05	175	0.53	2433	0.56	2338	0.50
2166	0.17	801	0.49	674	0.79	2213	0.52
520	0.26	2208	0.42	1048	0.54	1083	0.88
345	0.39	1133	0.97	1555	0.88	2282	0.29
1430	0.05	1123	0.88	1537	0.28	1339	0.34
293	0.12	2000	0.03	2114	0.51	1062	0.26
161	0.77	659	0.88	1829	0.65	2181	0.36
2252	0.39	1758	1.37	2165	0.62	1558	0.64
						430	0.59

Table C-3 Utility scale PV buses

Bus Number	Utility Scale Unit Name	Voltage kV
659	PV1	69
315	PV2	69
1758	PV3	69
75	PV4	69
2386	PV5	69
103	PV6	69
995	PV7	69
1535	PV8	69
104	PV9	69
105	PV10	69
106	PV11	69
194	PV12	69

APPENDIX D

LIST OF DISPLACED GENERATORS FOR VARIOUS PV GENERATIONS

Table D-1 List of displaced generators for 10% PV penetration

Bus Number	Bus Name	Pgen (MW)	Qgen (MW)	Bus Number	Bus Name	Pgen (MW)	Qgen (MW)
459	D1	110	-13.21	884	A2	115	16.87
469	D2	245	-4.65	891	A3	160	22.8
471	D3	260	-3.14	885	A4	115	16.87
883	A1	115	16.85	886	A5	115	16.87
2139	N1	40	14.08	555	CC1	429	93
183	P2	90	23.71	556	CC2	421	90

Table D-2 List of displaced generators for 20% PV penetration

Bus Number	Bus Name	Pgen (MW)	Qgen (MW)	Bus Number	Bus Name	Pgen (MW)	Qgen (MW)
1970	W16	130.00	57.37	1203	W7	155.00	23.70
184	P3	160.00	37.70	1968	W12	264.00	81.47
2523	L5	25.00	-4.05	2141	N2	40.00	14.00
2520	L4	24.00	-0.39	2521	L6	48.00	0.83
892	A6	160.00	22.77	2522	L7	48.00	0.83
890	A12	90	23.71	556	CC2	421	90
894	A13	180.00	24.26	1912	I2	30.00	5.65

Table D-3 List of displaced generators for 30% PV penetration

Bus Number	Bus Name	Pgen (MW)	Qgen (MW)	Bus Number	Bus Name	Pgen (MW)	Qgen (MW)
1930	H1	110.00	-6.21	2100	SS1	420.00	64.02
1931	H2	100.00	-7.12	2101	SS2	420.00	64.02
887	A7	115.00	16.82	1075	HH1	100.00	20.00
888	A9	115.00	16.86	1076	HH2	100.00	22.00
930	GC5 & GC6	31.00	-23.45	1077	HH3	100.00	22.00
1022	LL1	6.50	-0.96	1078	HH4	100.00	8.00
1023	LL2	6.50	-0.96	1079	HH5	100.00	20.00
1089	HH11 & HH12	100.00	15.00	1085	HH6 & HH7	110.00	17.00
966	GR1	145.00	35.88	1088	HH9 & HH10	50.00	10.00
967	GR2	145.00	35.88				

Table D-4 List of displaced generators for 40% PV penetration

Bus Number	Bus Name	Pgen (MW)	Qgen (MW)	Bus Number	Bus Name	Pgen (MW)	Qgen (MW)
473	D4	390.00	-4.77	158	AC3	65.00	0.75
806	E1	170.00	8.26	164	AC6	193.00	23.95
807	E2	170.00	8.23	165	AC7	193.00	24.04
808	E3	220.00	10.71	2163	DD6	103.00	0.89
1896	RD	51.00	0.00	2164	DD1	125.00	2.72
1966	W13	160.00	60.04	1913	I1	30.00	5.82
157	AC2	19.00	1.35	1204	W6	84.00	13.33
2468	K2	80	15.7				

Table D-5 List of displaced generators for 50% PV penetration

Bus Number	Bus Name	Pgen (MW)	Qgen (MW)	Bus Number	Bus Name	Pgen (MW)	Qgen (MW)
1967	W14	160.00	15.13	810	E5	750.00	78.19
2084	ST3	170.00	58.45	968	GR3	297.00	35.88

APPENDIX E

CATEGORY OF THE GENERATORS USED FOR VARIOUS DISPATCH RATIOS

Table E-1 Dispatched generators in the base case

Bus Num	ID	Power MW	Bus Num	ID	Power MW
14911	1	170	15146	1	90
14912	1	170	15147	1	160
14913	1	220	15981	1	804.4
14914	1	750	15982	1	803.43
14915	1	750	16500	1	420
16501	1	420	16519	1	450
16518	1	450			

Table E-2 Base generators in the base case

Bus Num	ID	Power MW	Bus Num	ID	Power MW
15983	1	In	19307	1	In
84839	1	In	19311	1	In
19001	1	In	19312	2	In
19002	1	In	19313	3	In
19003	1	In	19323	2	In
19004	1	In	16709	3	In
19005	1	In	14931	1	In
19006	1	In	14932	1	In
19007	1	In	14933	1	In
19008	1	In	79150	1	In
19009	1	In	79150	2	In
19305	1	In	79151	3	In
19306	1	In	79151	4	In
79153	7	In	79152	5	In
79153	8	In	79152	6	In

Table E-3 Displaced generators in the base case

Bus Num	ID	Power MW	Bus Num	ID	Power MW
14800	1	115	14902	1	260
14801	1	115	14903	1	390
14802	1	160	14941	1	110
14803	1	115	14942	1	100
14804	1	115	14943	1	30
14805	1	160	14944	1	30
14806	1	115	14945	1	80
14807	1	115	14964	1	24
14808	1	160	14965	1	25
14809	1	115	14969	1	48
14810	1	115	14970	1	48
14811	1	180	14990	1	40
14813	1	21	14991	2	40
14820	1	3	15140	1	164
14900	1	110	15141	1	164
14901	1	245	15142	1	249
15188	2	6	16507	1	75
15188	3	6	16508	1	75
15189	6	6	16509	1	103
15189	7	6	16514	1	44
15476	1	1	17024	1	7.9
15737	1	1	17025	1	19
15918	1	84	17026	1	65
15919	1	155	17027	1	38
15926	1	264	17028	1	71
15927	1	160	17029	1	193
15928	1	160	17030	1	193
15929	1	140	19023	1	100
15930	1	130	19024	1	100
15971	1	429	19025	1	100
15972	1	421	19026	1	100
16503	1	125	19027	1	100
19033	N3	100	19028	A1	110
19033	N4	100	19028	A2	110
19034	N5	110	19031	A8	50
19034	N6	110	19031	A9	50
19035	N7	110	19032	N1	100
19035	N8	110	19032	N2	100
19317	1	170	19319	3	170
19318	2	170			

APPENDIX F

PROGRAM TO CREATE POWER FLOW SCNERAIOS

```
#include <iostream>
#include <math.h>
#include <string>
#include <fstream>
#include <iomanip>

using namespace std;
int main()
{
		ofstream outputFile;
		ifstream inputFile;
		ifstream dataFile;
		ifstream inFile;
		const int count=20;
		const int gen_displaced=79; //to be assigned
		const int gen_dispatched=13; //to be assigned
		double Pgen_num[gen_displaced];
		string Pgen_id[gen_displaced];
		double Pgen2_num[gen_dispatched];
		string Pgen2_id[gen_dispatched];
		double Pgen_displace[gen_displaced][count+1];
		double Pgen_dispatch[gen_dispatched][count+1];


		inputFile.open("displacednames.txt");
		if (!inputFile)
			cout << "Error opening data1 file\n";
		else
		{
			for (int i=0;i<gen_displaced;i++)
			{
				inputFile>>Pgen_num[i];
				inputFile>> Pgen_id[i];

	//cout<<"Pgen_num["<<i<<"]="<<Pgen_num[i]<<endl;
			}

		}
		inputFile.close();
		dataFile.open("displaced_runs.txt");
		if (!dataFile)
			cout << "Error opening data2 file\n";
		else
		{
			for (int i=0;i<gen_displaced;i++)
```

```
                        {
                                for (int j=0;j<=count;j++)
                                {
                                        dataFile >> Pgen_displace[i][j];
                                }
                        }

                dataFile.close();
                }
//procedure for dispatched generators

inFile.open("dispatchednames.txt");
                if (!inputFile)
                        cout << "Error opening data3 file\n";
                else
                {
                        for (int i=0;i<gen_dispatched;i++)
                        {
                                inFile>>Pgen2_num[i];
                                inFile>> Pgen2_id[i];
                        }

                }
                inFile.close();

                dataFile.open("dispatched_runs.txt");
                if (!dataFile)
                        cout << "Error opening data4 file\n";
                else
                {
                        for (int i=0;i<gen_dispatched;i++)
                        {
                                for (int j=0;j<=count;j++)
                                {
                                        dataFile >> Pgen_dispatch[i][j];
                                }
                        }

                dataFile.close();
                }

int run=0;
for (int run=0;run<=count;run++)
{
```

```
	if(run==0)
		outputFile.open("Macro_Create0.txt");

	else if(run==1)
		outputFile.open("Macro_Create1.txt");
	else if(run==2)
		outputFile.open("Macro_Create2.txt");
	else if(run==3)
		outputFile.open("Macro_Create3.txt");
	else if(run==4)
		outputFile.open("Macro_Create4.txt");
	else if(run==5)
		outputFile.open("Macro_Create5.txt");
	else if(run==6)
		outputFile.open("Macro_Create6.txt");
	else if(run==7)
		outputFile.open("Macro_Create7.txt");
	else if(run==8)
		outputFile.open("Macro_Create8.txt");
	else if(run==9)
		outputFile.open("Macro_Create9.txt");
	else if(run==10)
		outputFile.open("Macro_Create10.txt");
	else if(run==11)
		outputFile.open("Macro_Create11.txt");
	else if(run==12)
		outputFile.open("Macro_Create12.txt");
	else if(run==13)
		outputFile.open("Macro_Create13.txt");
	else if(run==14)
		outputFile.open("Macro_Create14.txt");
	else if(run==15)
		outputFile.open("Macro_Create15.txt");
	else if(run==16)
		outputFile.open("Macro_Create16.txt");
	else if(run==17)
		outputFile.open("Macro_Create17.txt");
	else if(run==18)
		outputFile.open("Macro_Create18.txt");
	else if(run==19)
		outputFile.open("Macro_Create19.txt");
	else
		outputFile.open("Macro_Create20.txt");

	//outputFile.open("Macro_Create.txt");
```

```
		outputFile<<"[PSAT 10.0 Macro]"<<endl;
		outputFile<<"MacroRecordBy:Number"<<endl;

		for (int j=0;j<gen_displaced;j++)
		{
			if(Pgen_displace[j][run]==0)

	outputFile<<"ModifyData:Generator;"<<Pgen_num[j]<<";"<<Pgen_i
d[j]<<";Status;Out\n"<<"Solve"<<endl;
			else

	outputFile<<"ModifyData:Generator;"<<Pgen_num[j]<<";"<<Pgen_i
d[j]<<";MW Output;"<<Pgen_displace[j][run]<<endl;
		}

		for (int j=0;j<gen_dispatched;j++)
		{

	outputFile<<"ModifyData:Generator;"<<Pgen2_num[j]<<";"<<Pgen
2_id[j]<<";MW Output;"<<Pgen_dispatch[j][run]<<endl;
		}
	//get the status of the other generators

	const int NUMBER_BASE=32;
	double base_num[NUMBER_BASE];
	string base_id[NUMBER_BASE],base_status[NUMBER_BASE];
	double base_pgen[NUMBER_BASE];
	ifstream baseFile;

	baseFile.open("base_gens.txt");
	if (!baseFile)
			cout << "Error opening data5 file\n";
		else
		{

	for (int i=0;i<NUMBER_BASE;i++)
	{
		baseFile>> base_num[i];
		baseFile>> base_id[i];
		baseFile>> base_status[i];
		baseFile>> base_pgen[i];

	outputFile<<"ModifyData:Generator;"<<base_num[i]<<";"<<base_id
[i]<<";Status;"<<base_status[i]<<endl;
```

```
        outputFile<<"ModifyData:Generator;"<<base_num[i]<<";"<<base_id
[i]<<";MW Output;"<<base_pgen[i]<<endl;
        }
        baseFile.close();
        }
//out of service gens
        const int NUMBER_OUT=102;
        double out_num[NUMBER_OUT];
        string out_id[NUMBER_OUT],out_status[NUMBER_OUT];
        double out_pgen[NUMBER_OUT];
        ifstream outFile;

        outFile.open("out_service_gens.txt");
        if (!outFile)
                        cout << "Error opening others file\n";
                else
                {
        for (int i=0;i<NUMBER_OUT;i++)
        {
                outFile>> out_num[i];
                outFile>> out_id[i];
                outFile>> out_status[i];
                outFile>> out_pgen[i];
        outputFile<<"ModifyData:Generator;"<<out_num[i]<<";"<<out_id[i]
<<";Status;"<<out_status[i]<<endl;

        outputFile<<"ModifyData:Generator;"<<out_num[i]<<";"<<out_id[i]
<<";MW Output;"<<out_pgen[i]<<endl;
        }
        outFile.close();
        }
        outputFile <<"Solve"<<endl;
        outputFile <<"Solve"<<endl;
        outputFile <<"SavePowerflowAs:\"C:\\Documents and
Settings\\seftekha\\Desktop\\run"<<run<<".pfb"<<endl;
        outputFile.close();
}
                return 0;
}
```